UNCLASSIFIED
SECURITY CLASSIFICATION OF THIS PAGE

(2)

REPORT DOCUMENTATION PAGE

Form Approved
OMB No. 0704-0188

1a. REPORT SECURITY CLASSIFICATION UNCLASSIFIED	1b. RESTRICTIVE MARKINGS
2a. SECURITY CLASSIFICATION AUTHORITY 2b.	3. DISTRIBUTION/AVAILABILITY OF REPORT Approved for Public Release; Distribution Unlimited
4. **AD-A232 798**	5. MONITORING ORGANIZATION REPORT NUMBER(S) AFOSR-TR- 91 0137
6a. NAME OF PERFORMING ORGANIZATION Dept of Civil Engineering University of Michigan 6b. OFFICE SYMBOL (If applicable)	7a. NAME OF MONITORING ORGANIZATION AFOSR/NA
6c. ADDRESS (City, State, and ZIP Code) 2366 G. G. Brown Bldg. Ann Arbor, MI 48109-2125	7b. ADDRESS (City, State, and ZIP Code) Bldg. 410 Bolling AFB, DC 20332-6448
8a. NAME OF FUNDING/SPONSORING ORGANIZATION AFOSR 8b. OFFICE SYMBOL (If applicable) NA	9. PROCUREMENT INSTRUMENT IDENTIFICATION NUMBER AFOSR-88-0166
8c. ADDRESS (City, State, and ZIP Code) Bldg. 410 Bolling AFB, DC 20332-6448	10. SOURCE OF FUNDING NUMBERS PROGRAM ELEMENT NO: 6.1102F PROJECT NO: 2302 TASK NO: C1 WORK UNIT ACCESSION NO:

DTIC
ELECTE
MAR 08 1991
S E D

11. TITLE (Include Security Classification) (U)
Load Transfer Mechanisms in Anchored Geosynthetic Systems

12. PERSONAL AUTHOR(S)
Hryciw, Roman D.

13a. TYPE OF REPORT	13b. TIME COVERED	14. DATE OF REPORT (Year, Month, Day)	15. PAGE COUNT
Final	FROM 3/15/88 TO 9/14/90	20 December, 1990	~~59~~ 218

16. SUPPLEMENTARY NOTATION

17. COSATI CODES			18. SUBJECT TERMS (Continue on reverse if necessary and identify by block number)
FIELD	GROUP	SUB-GROUP	Anchored Geosynthetics

19. ABSTRACT (Continue on reverse if necessary and identify by block number)

The success of an anchored geosynthetic system (AGS) depends on the satisfactory transfer of load between the surface-deployed geosynthetic and anchors (typically ribbed reinforcing rods) driven into the slope; between the geosynthetic and soil and between the anchors and soil. A study was performed to evaluate the load transfer mechanisms at these interfaces in an AGS. Additionally, a critical evaluation of the AGS concept was made, system weaknesses were identified, design guidelines were recommended and possible improvements were suggested.

A model was developed for predicting the pullout resistance of plane ribbed inclusions. The model considered the contribution of both frictional and passive resistance components of pullout resistance. Optical observation

20. DISTRIBUTION/AVAILABILITY OF ABSTRACT	21. ABSTRACT SECURITY CLASSIFICATION
☒ UNCLASSIFIED/UNLIMITED ☐ SAME AS RPT ☐ DTIC USERS	UNCLASSIFIED
22a. NAME OF RESPONSIBLE INDIVIDUAL Major Steven C. Boyce	22b. TELEPHONE (Include Area Code) (202) 767-6963
	22c. OFFICE SYMBOL AFOSR/NA

DD Form 1473, JUN 86 Previous editions are obsolete. SECURITY CLASSIFICATION OF THIS PAGE
UNCLASSIFIED

of sand around the ribs was made to determine the behavior of soil around the moving ribs during pullout. A carbowax solidification technique was developed to facilitate identification of failure surfaces. Experimental results verified the model and guidelines for optimum rib spacing on anchors were established. Pullout tests on actual anchors were also performed in a large triaxial testing tank constructed for the project. Significant degradation of interface friction was observed with cycling indicating that redriving of anchors may be detrimental to an AGS, especially in well graded sands.

Solutions were developed for the pullout problem of long slender elastic anchors in cohesionless soil. Both rigid body translation and elastic deformation of the anchor are significant components of the pullout stiffness. Inadequate pullout stiffness may cause loss of tension in the geosynthetic rendering the AGS ineffective. In light of these findings, a threaded anchor and nut system was established to be the most effective geosynthetic-anchor connector.

A theoretical study also disclosed that the optimum anchor orientation for stabilization of infinite slopes depends on several factors including slope angle and in-situ stresses. It typically ranges from 20° to 30° from the normal to the slope with the anchor driven upslope.

An experimental study was conducted to confirm that the soil-geosynthetic interface friction angle may be correctly predicted from the residual or critical state friction angle of the sand as suggested by others in previous studies. Equations were developed for the load transfer at curved soil-fabric interfaces. An experimental study verified that the increases in soil stress with distance from the anchor may be predicted by the developed equations.

TABLE OF CONTENTS

LIST OF FIGURES

1.0 INTRODUCTION

Anchored geosynthetics are a recently developed earth reinforcement system in which a geotextile, geonet or geogrid is placed directly on an exposed soil and anchored to the ground by small diameter deformed metal rods, typically reinforcing rods. These "ribbed inclusions" are driven into the soil in a grid pattern through reinforced openings in the geosynthetic material. Prior to driving the final 10 to 25% of the required length, the geosynthetic is pinned to the rod. The final driving then pulls the geosynthetic along with the rod thereby tensioning the geosynthetic and compressing the soil.

Anchored geosynthetic systems were first introduced by Koerner (1986). His conceptualization of the system and free-body diagrams of the various components are shown in Figure 1. In general, the role of the geosynthetic is to place the encompassed soil in compression thereby increasing the normal stresses on a potential failure surface. The anchor's task is to maintain the geosynthetic in tension while obtaining frictional pullout resistance from the surrounding soil. The success of an anchored geosynthetic system therefore depends on the satisfactory transfer of load between the geosynthetic material and the anchors; between the geosynthetic and soil and between the anchors and soil. A research program was therefore conducted to investigate the load transfer mechanisms in anchored geosynthetic systems.

While anchored geosynthetics provided the primary impetus for the study, many of the findings bear directly on several fundamental issues in reinforced soil systems including the interaction of soils with high strength and stiffness ribbed inclusions, soil-fabric interaction, orientation of surface loads and anchors for optimum slope stabilization and development of solutions for the pullout mechanics of elastic anchors in frictional soils.

Koerner, R. M. amd Robbins, J. C. (1986) "In-Situ Stabilization of Slopes Using Nailed Geosynthetics," Proc. of the Third Intl. Conf. on Geosynthetics, Vienna, Austria pp. 395-400.

2.0 RESEARCH OBJECTIVES

1. To determine the load transfer mechanisms between scils and plane ribbed inclusions. This objective included development of appropriate experimental systems and methodologies to facilitate observation of grain movements in the intrarib region and development of failure surfaces.

2. To conduct a comprehensive laboratory investigation of the effects of normal stress, void ratio and rib spacing on pullout resistance of ribbed inclusions.

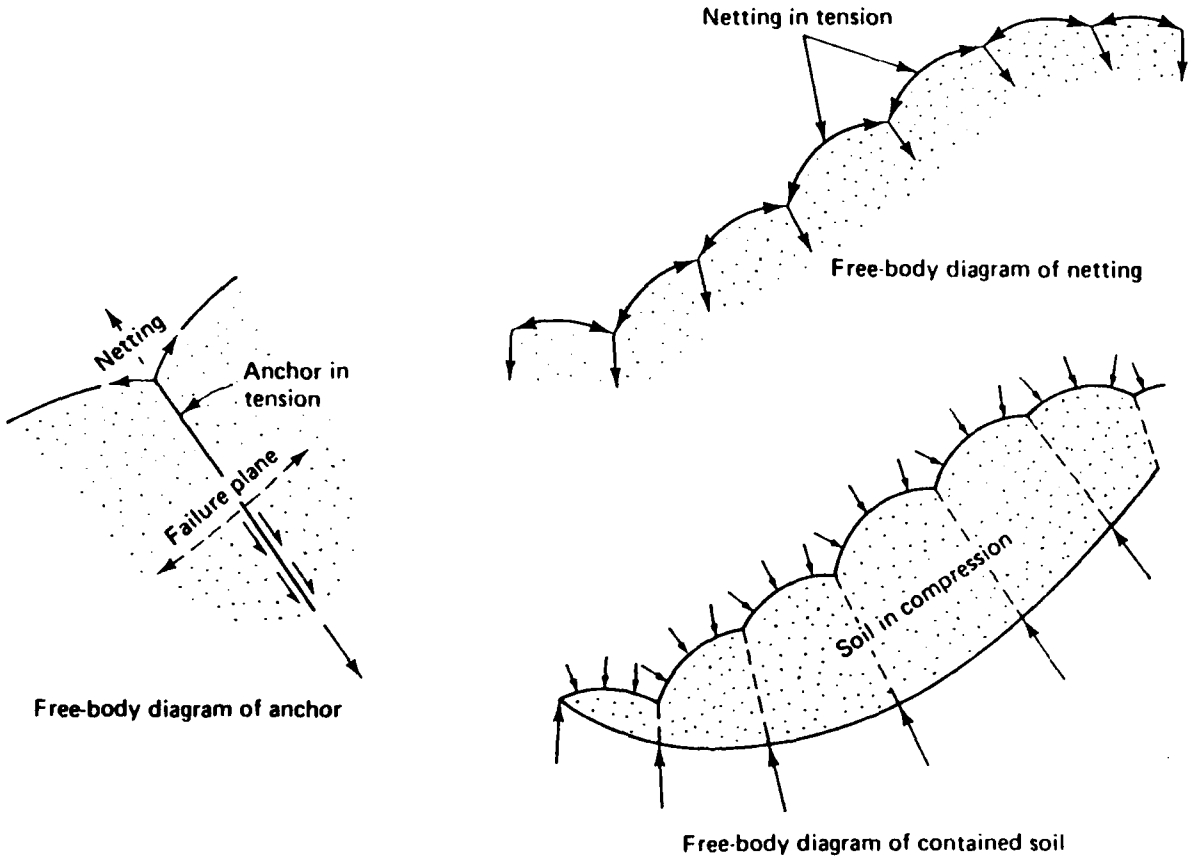

Fig. 1 Conceptualization of an Anchored Geosynthetic System (from Koerner, 1986)

3. To develop an analytical model, based on the load transfer mechanisms found in objective #1, for the residual pullout resistance of plane ribbed inclusion in cohesionless soils.

4. To verify the analytical model by laboratory testing.

5. To perform a parametric study of the model variables to assess their relative importance to pullout resistance.

6. To determine optimum rib spacings on plane inclusions to maximize pullout resistance.

7. To study the pullout resistance of actual axisymmetric anchors in two different soils under typical confining stresses and to develop rational explanations for the observed behavior.

8. To study the load transfer mechanisms between anchors and geosynthetics. Specifically, to determine if existing standard tests are appropriate for evaluation of required fabric strengths for anchored geosynthetic systems.

9. To study the friction characteristics of soil-geosynthetic interfaces.

10. To study the mechanics of load transfer from geosynthetics to soils along curved interfaces and to develop guidelines for estimating the increases in stress along potential failure surfaces.

11. To develop approximate closed form solutions for the normal stresses on anchors in infinite slopes.

12. To develop closed form solutions for the pullout stiffness of elastic anchors in slope stabilization systems

13. To evaluate the importance of anchor installation methods and anchor-fabric connection types in maintaining system integrity.

14. To develop a methodology for determining the factor of safety of infinite slopes stabilized by anchored geosynthetics

15. To develop a procedure for determining optimum anchor orientations for maximizing increases in slope stability.

16. To suggest practical and effective improvements to the existing method of stabilizing slopes by anchored geosynthetics.

3.0 PUBLICATIONS

Papers published or in review:

[1] Hryciw, R. D. and Irsyam, M. (1990) "Shear Zone Characterization in Sands by Carbowax Impregnation", ASTM Geotechnical Testing Journal, Volume 12, Number 1, pp. 49-52.

[2] Hryciw, R. D. (1991) "Anchor Design for Slope Stabilization by Surface Loading" accepted by the Journal of the Geotechnical Engineering Division of ASCE.

[3] Vitton, S. J. and Hryciw, R. D. (1991) "Soil-Anchor Interaction in Anchored Geosynthetic Systems," accepted for the Geotechnical Engineering Congress to be held at the University of Colorado at Boulder.

[4] Irsyam, M. and Hryciw, R. D. "Friction and Passive Resistance in Soil Reinforced by Plane Ribbed Inclusions," submitted to Geotechnique, in review.

[5] Hryciw, R. D. and Irsyam, M. "Pullout Stiffness of Elastic Anchors in Slope Stabilization Systems," submitted to the Canadian Geotechnical Journal, in review.

Papers in preparation or planned:

[6] Vitton, S. J. and Hryciw, R. D. "Load Transfer Mechanisms in Anchored Geosynthetic Systems" planned.

[7] Hryciw, R. D. and Irsyam, M. "An Experimental Study of Pullout Resistance of Plane Ribbed Inclusions in Sand" in preparation.

[8] Hryciw, R. D. "Load Transfer At Curved Soil-Fabric Interfaces" in preparation.

[9] Irsyam, M. and Hryciw, R. D. "Behavior of Sand Particles Around Ribbed Inclusions" in preparation.

[10] Hryciw, R. D. and Irsyam, M. "Pullout Mechanics of Elastic Rods in Cohesionless Soil" in preparation.

[11] Irsyam, M. and Hryciw, R. D. "Passive Resistance of Soil to Plane and Axisymmetric Ribbed Inclusions" planned.

4.0 SIGNIFICANT ACCOMPLISHMENTS

The significant accomplishments presented in this section will be keyed to the research objectives listed in Section 1.0 of the report. Many of the accomplishments have been documented in technical papers which are attached as Appendix A. The present report serves as an executive summary of these accomplishments. Lists of references are provided with each technical paper and are not repeated herein. However additional references are provided with each section of the report as needed.

4.1 LOAD TRANSFER MECHANISMS BETWEEN SOIL AND PLANE RIBBED INCLUSIONS

To determine the load transfer mechanisms between soils and "ribbed inclusions", the movement of soil particles in the vicinity of the inclusions must be visually studied. Since such observation is virtually impossible for axisymmetric anchors, a study was conducted of plane ribbed inclusions in soils. The parameters investigated included soil density, grain size, grain angularity, normal stress, rib spacing and rib geometry as shown in Figure 2. In most tests, a square rib with dimensions 2.5 mm by 2.5 mm was used.

A complete description of the testing system is presented in technical papers [1] and [4]. A schematic of the direct shear testing system is shown in Figure 3. Visual observation of individual grain movements was facilitated by video monitoring of the intrarib region through plexiglass walls. A carbowax solidification technique was also adopted for identifying failure surfaces [4] and for determination of void ratios in intrarib regions [1].

4.1.1 Conclusions From Visual Observations

a) At small displacements, prior to mobilization of peak strength, significant movement of sand grains occurs at large distances from the ribbed inclusion, possibly as far as 15 grain diameters and beyond. In dense sands, as peak strength is approached, initial failure planes develop extending from the rib corners at 30 to 50 degree angles from the horizontal. With increasing relative displacement, the failure surface drops toward the horizontal.

b) After achieving peak pullout resistance, a failure surface becomes fully developed and a steady state of plastic shear flow occurs. This is accompanied by stabilization of the pullout resistance at a constant post-peak residual strength.

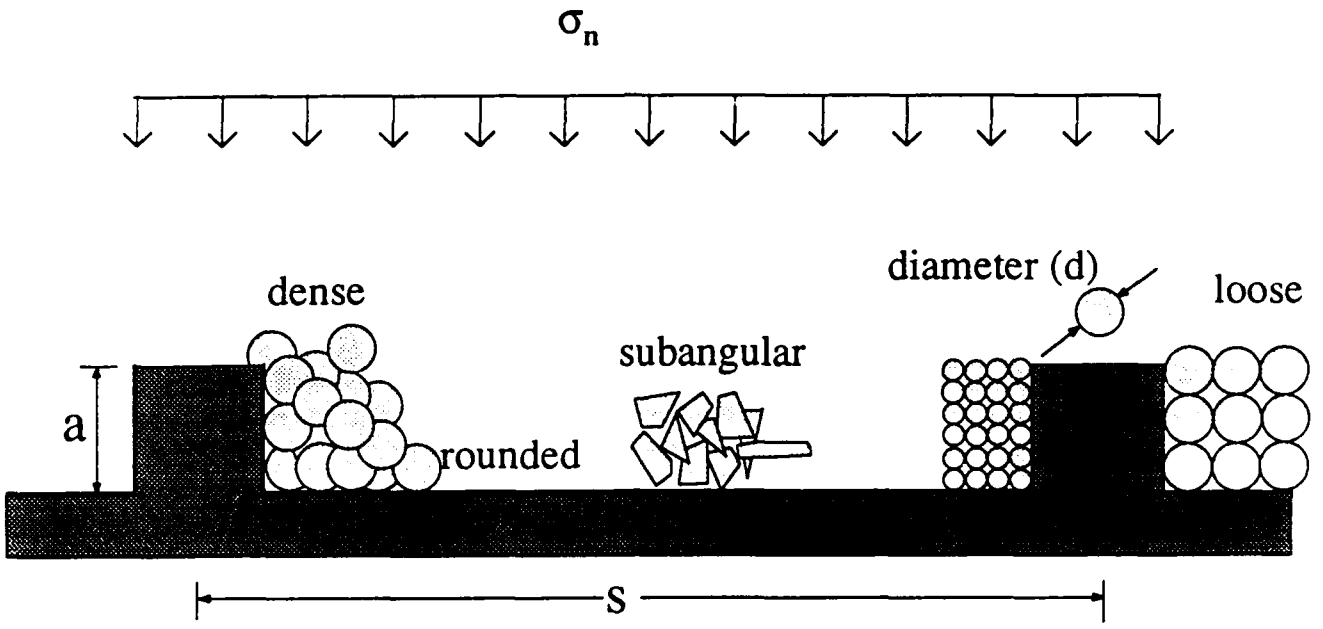

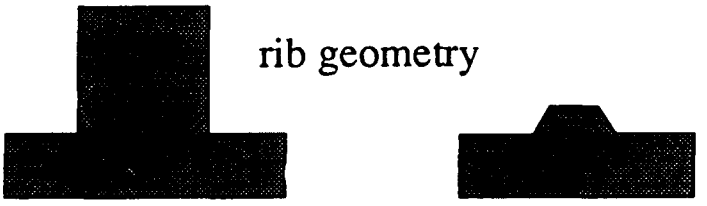

PARAMETRIC STUDY

Fig. 2 Parameters Investigated in Plane Direct Shear

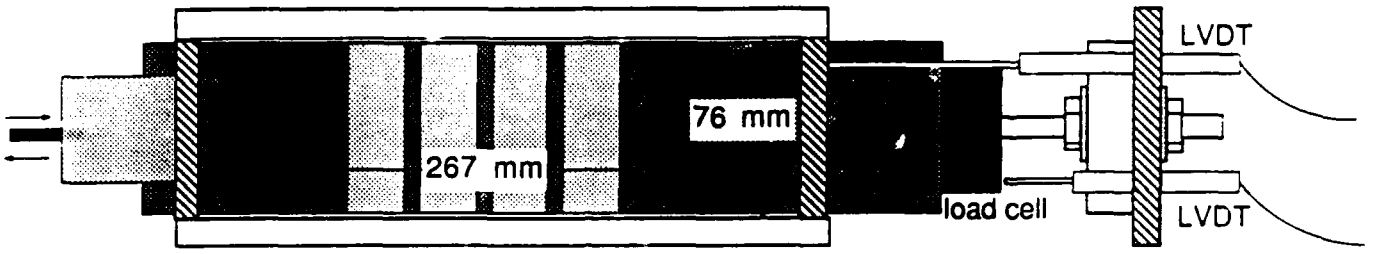

TOP VIEW - LOADING PLATE REMOVED

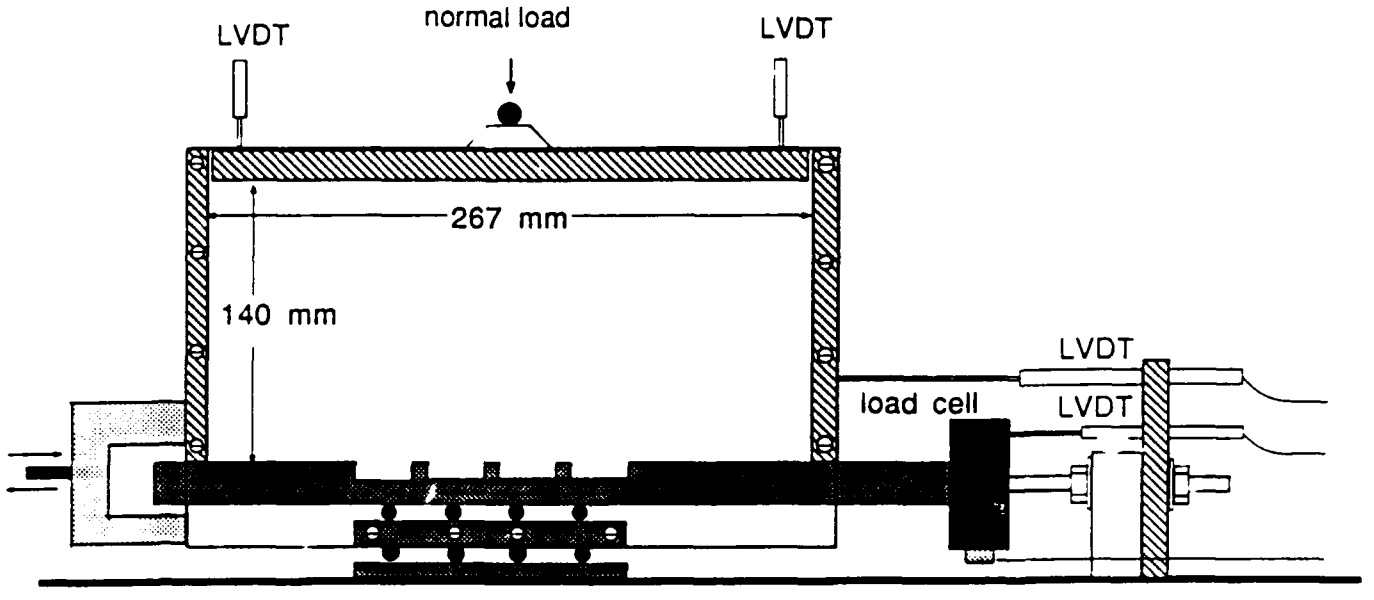

SIDE VIEW

Fig. 3 Direct Shear Testing Apparatus

c) Displacement vectors for select grains of a medium dense sand and rib spacings of 15 mm (0.6 in.) and 33 mm (1.3 in.) are shown in Figure 4. The displacement vectors represent the movement occurring subsequent to an initial displacement of one rib spacing. Distinct differences between failure patterns for the two rib spacings were observed. For small spacings, the failure surface approaches a plane parallel to the plate (Figure 4a). For larger rib spacings, the failure surface exhibits a pronounced curvature as shown in Figure 4b.

d) For large rib spacings, a loose grain structure develops behind the ribs [1]. This zone is approximately given by area ABC in Figure 5 where BC is approximately equal to one rib height, H_r. A compressive soil arch develops between the top of the rib and the base of the plate as shown. At the front face of each rib, a zone of lower void ratio develops. Optical monitoring has shown that once residual strength develops, the sand grains in the region EFG essentially move as a rigid plug ahead of the rib. The distance EF is approximately equal to $2H_r$. The relative motion of sand grains above the surface ABCDHA' is large and opposite to the direction of plate movement. In the area bounded by DEGA'H the relative motion of grains is also opposite to that of the plate, however the velocity is very small by comparison to that of grains above ABCDHA'.

e) An additional plane ribbed inclusion was prepared simulating the size, spacing and shape of rib on a typical 0.95 cm diameter deformed rod currently used for anchoring geosynthetics. The displacement vectors are shown in Figure 6. The trapezoidal shape and relatively small spacing of ribs resulted in a failure surface located approximately two rib heights above the rib. Clearly, the size, shape and, or spacings of ribs on existing anchors are far from optimum for developing full passive resistance.

4.1.2 Conclusions From Carbowax Solidification

The shapes of the failure surfaces obtained by carbowax solidification were very similar to the results obtained by optical monitoring of individual grain movements. Since the carbowax procedure is much quicker than monitoring the individual movement of sand grains, a greater number of parameters could be investigated. Specifically, carbowax solidification was used to study the effect of rib spacing, grain shape, grain size and void ratio on the failure surface. Illustrations of all of the carbowax solidification tests are included as Appendix B to this report. The conclusions may be summarized as follows:

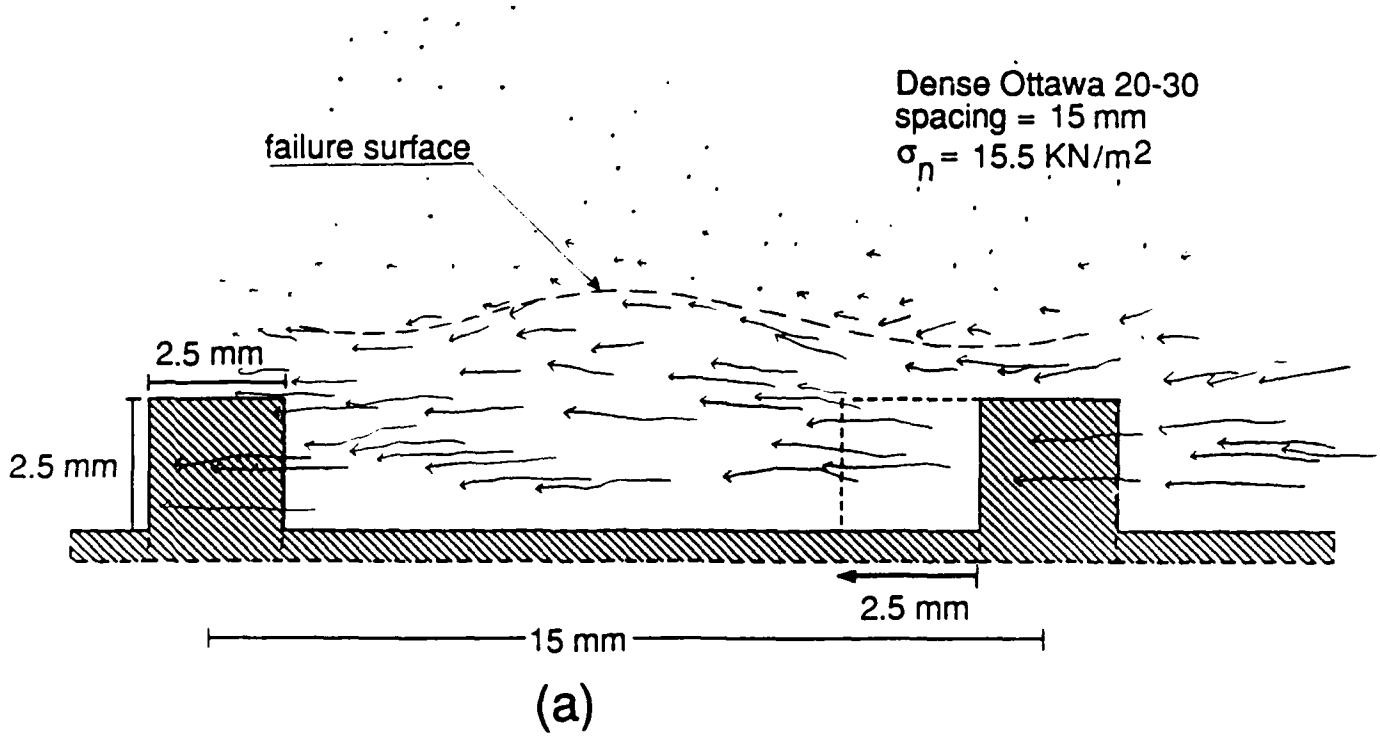

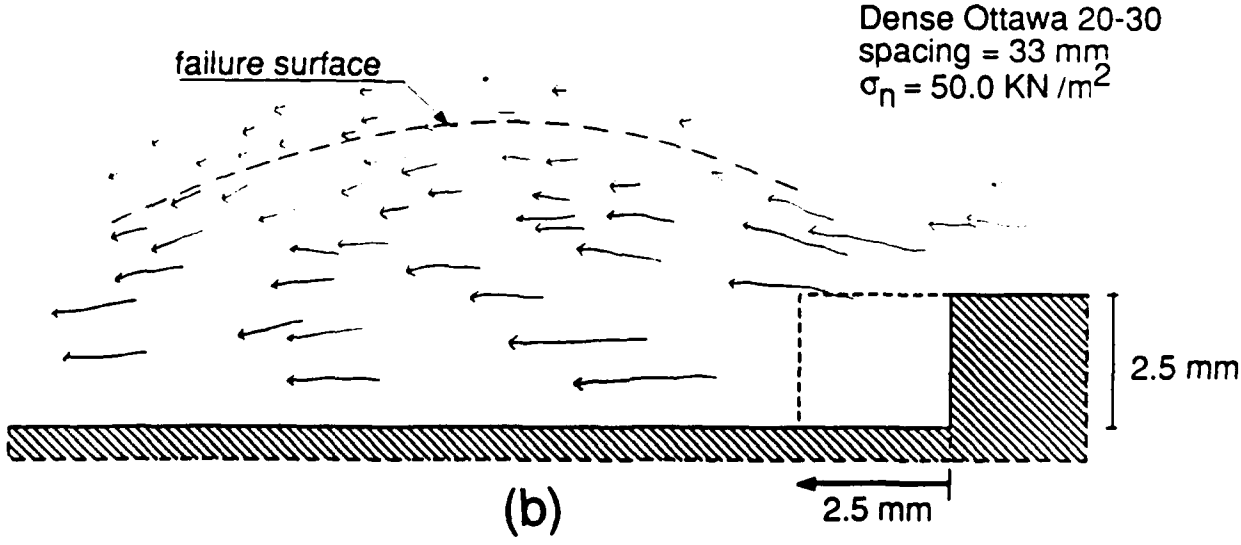

Fig. 4 Displacement of Sand Grains Around Moving Ribbed Inclusions

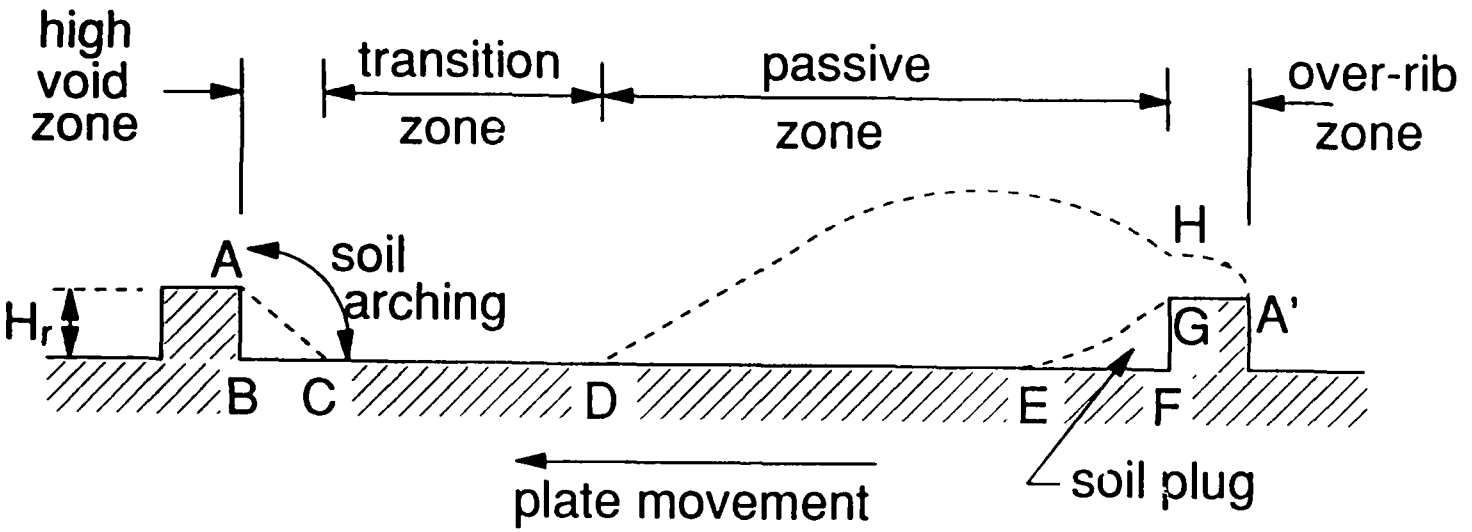

Fig. 5 Characteristic Zones Around Ribbed Inclusions

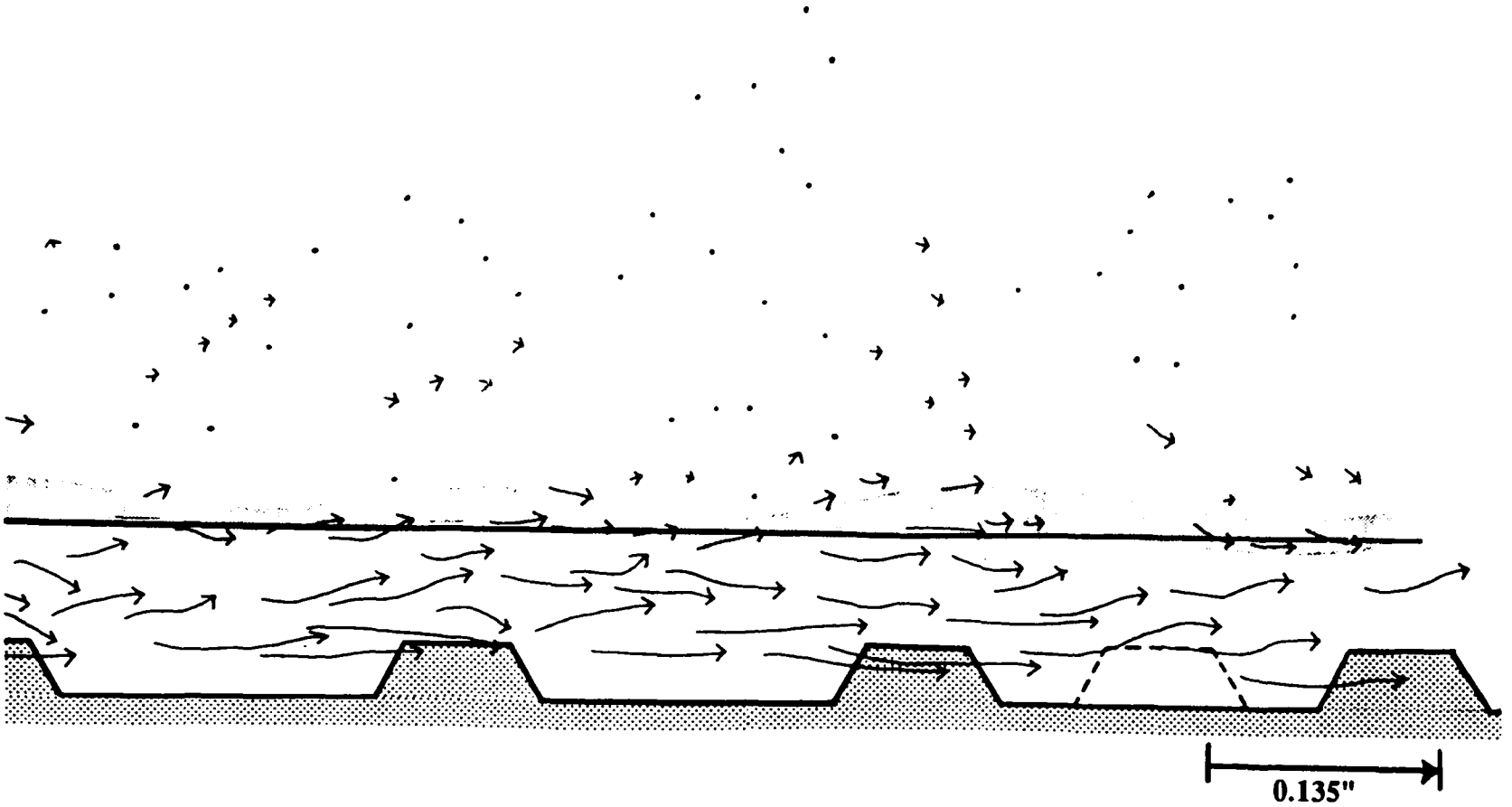

Displacement vectors of grains on a ribbed plate

Ottawa 20-30

dense (e=0.52)

σ_n = 2.25 psi

rib shape = trapezoid

Fig. 6 Displacement of Sand Grains Around Ribs on Typical Reinforcing Rods

4.1.2.1 Spacing Effects

a) For relatively large rib spacings, (at least 33 mm) the failure plane consists of three distinct regions as shown in Figure 5. That is, a passive zone, a transition zone and a high void region.

b) For small rib spacings (5 mm) the shearing resistance is entirely due to planer friction. This friction is partially along a sand-sand interface and partially along the sand/top-of-rib interface.

c) For intermediate spacings (15 mm) a transition condition occurs which includes partial development of a passive zone and sand-to-sand friction.

4.1.2.2 Density Effects

a) The effect of initial void ratio on the failure surface is more pronounced for spacings of 33 mm than for 15 mm. This is due to the entrapment of grains in the intrarib zone at small spacings.

b) In dense sands the distance GH in Figure 4 is greater than it is in loose sands. The result is a larger passive zone and accordingly higher pullout resistances.

4.1.2.3 Grain Size Effects

For the two soil sizes tested, Ottawa 20-30 and Ottawa 40-50, there was no observed difference in the failure shape. It is presumed that the failure shapes for finer materials would be the same. However, for coarser sands and gravels the grain sizes will approach the rib dimension and the failure surface would certainly be different.

4.1.2.4 Grain Shape Effects

Angular materials exhibited a larger and higher passive zone. This is a clear manifestation of the higher friction angles associated with grain interlocking. The implication is that the optimum rib spacing will be greater as will be discussed in Section 4.6.

4.2 EXPERIMENTAL INVESTIGATION OF PULLOUT RESISTANCE OF PLANE RIBBED INCLUSIONS.

A comprehensive laboratory study was conducted to investigate the effects of normal stress, soil void ratio and rib spacing on the peak and residual strengths of ribbed inclusions in sands. The results of this investigation were previously documented in the first annual report to AFOSR. The major conclusions are repeated here and the test results are attached as Appendix C.

4.2.1 Peak Strength

The conclusions regarding peak strengths, τ_{peak} are:

a) Dense sands yield higher τ_{peak} than loose sands.

b) Increases in σ_n results in a nonlinear increase in τ_{peak} (and therefore a decrease in the apparent friction angle) for both dense and loose sands.

c) The optimum rib spacing for dense sands was 33 mm or greater. For loose sands it was approximately 15 mm.

4.2.2 Residual Strength

The conclusions regarding residual strengths, τ_{res} are:

a) The initial void ratio had less of an effect on τ_{res} than it did on τ_{peak}.

b) Increases in σ_n results in a nonlinear increase in τ_{res} (and therefore a decrease in the apparent friction angle) for both dense and loose sands.

c) The effect of rib spacing was less significant to τ_{res} than it was to τ_{peak}

d) The differences between peak and residual strengths were smaller for loose sands than for dense sands.

4.3 ANALYTICAL MODEL FOR PULLOUT RESISTANCE OF PLANE RIBBED INCLUSIONS

The pullout resistance model was presented in reference [4]. It focuses on large rib spacings where a full passive zone develops. This situation is most desirable as it will result in greater pullout resistances than at smaller spacings. The total pullout resistance per rib spacing will consist of both a frictional component as well as passive soil resistance:

$$F = F_f + F_p \quad \text{.....(1)}$$

where F=pullout resistance per rib spacing, F_f=frictional component and F_p=passive resistance component. The frictional component was determined to be given by:

$$F_f = (s-2H_r)\sigma_n \tan\delta_b \quad \text{.....(2)}$$

where s=rib spacing, H_r=rib height (and width), σ_n'=effective normal stress, δ_b=soil-rib friction angle.

Optical observations revealed that the sand grains in the region bounded by GA'H in Figure 5 are moving at small relative velocities compared to the grains above A'H. As such, the grains in the region GA'H effectively act as an extension of the rib and thus increase the height of the wall against which passive resistance develops. The distance GH in Figure 5 is defined as H_s, the height of the soil component of the passive wall. H_s for Ottawa 20-30 and Ottawa 40-50 were very similar. However, it is believed that if a greater range of particle sizes had been investigated, H_s would have been found to be a function of grain size and shape. It is also likely that H_s is somewhat related to the rib width (distance GA').

Analytical solutions for pullout resistance of ribbed inclusions in soil were obtained using the Sokolovski method as summarized in an appendix to reference [4]. The region ahead of each rib may be divided into five distinct boundary problems as shown in Figure 7. Region I is a Cauchy problem; regions II and IV are Goursat problems and regions III and V are mixed problems. To establish the slipline network for this problem, the following parameters must be prescribed: the soil friction angle, ϕ, the base plate friction angle, δ_b, the rib wall friction angle, δ_r, the soil wall friction angle, δ_s, the rib height, H_r and the soil wall height, H_s.

For an assumption of weightless soil, closed form solutions for the passive stresses along the rib wall and along the soil wall were determined. The expression for pressure along the rib wall is:

$$p_r = \sigma_n' \frac{\sin\Delta_b \sin(\Delta_r+\delta_r)}{\cos\delta_b \sin(\Delta_b-\delta_b) \sin\Delta_r} e^{2(\pi/2-\theta_b-\theta_r)\tan\phi} \quad \text{.....(3)}$$

$$\text{where} \qquad \Delta_b = \sin^{-1}\left[\frac{\sin\delta_b}{\sin\phi}\right]; \quad \text{.....(4)}$$

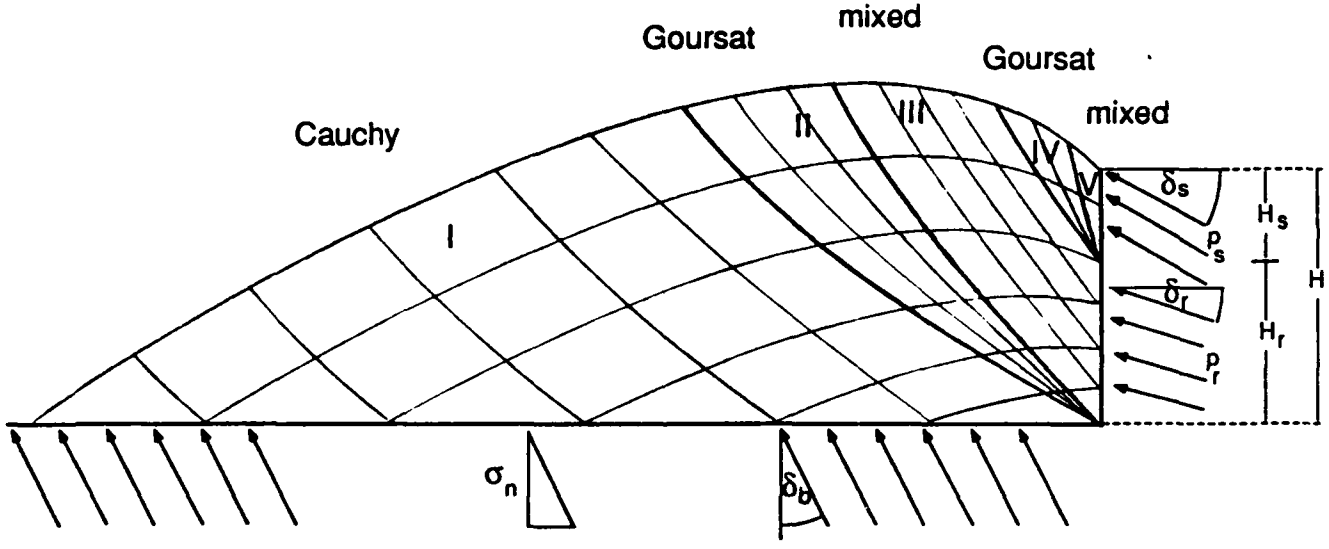

Fig. 7 Passive Soil Resistance Model

$$\theta_b = \left[\frac{\pi}{4} - \frac{\phi}{2}\right] + \frac{1}{2}\left[\Delta_b - \delta_b\right]; \quad \text{.....(5)}$$

$$\Delta_r = \sin^{-1}\left[\frac{\sin \delta_r}{\sin \phi}\right] \quad \text{.....(6)}$$

$$\theta_r = \left[\frac{\pi}{4} + \frac{\phi}{2}\right] - \frac{1}{2}\left[\Delta_r + \delta_r\right] \quad \text{.....(7)}$$

and σ_n'=effective normal stress. The expression for pressure along the soil wall is:

$$p_s = \sigma_n' \frac{\sin \Delta_b \sin(\Delta_s + \delta_s)}{\cos \delta_b \sin(\Delta_b - \delta_b) \sin \Delta_s} e^{2[(\pi/2 - \theta_b - \theta_r) + (\theta_r - \theta_s)]\tan\phi}$$

.....(8)

where $$\Delta_s = \sin^{-1}\left[\frac{\sin \delta_s}{\sin \phi}\right] \quad \text{.....(9)}$$

and $$\theta_s = \left[\frac{\pi}{4} + \frac{\phi}{2}\right] - \frac{1}{2}\left[\Delta_s + \delta_s\right] \quad \text{.....(10)}$$

The total horizontal force acting per unit width on the combined rib and soil wall due to passive resistance is then:

$$F_p = p_r H_r \cos \delta_r + p_s H_s \cos \delta_s \quad \text{.....(11)}$$

The passive resistance model for plane ribbed inclusions is being extended to cylindrical axisymmetric ribbed inclusions. This work will be completed by July, 1991.

4.4 VERIFICATION OF MODEL FOR PULLOUT RESISTANCE OF PLANE RIBBED INCLUSIONS

4.4.1. Pullout Resistance

To predict pullout resistances by equation (1), ϕ, δ_b, δ_r, δ_s, H_r, H_s, s and σ_n must be known, estimated or determined. To determine ϕ, direct shear tests were performed on dense and loose Ottawa 20-30 sand. The dense condition corresponded to a relative density between 90% and 100% (void ratio 0.51 - 0.53), while the loose condition corresponded to a relative density between 30% and 40% (void ratio 0.62 - 0.64). The corresponding friction angles were $\phi = 33°$ and $\phi = 29°$ respectively.

Direct shear tests were also performed on a smooth aluminium plate to determine δ_b'. It was found to be 23° for dense Ottawa 20-30 and 21° for loose Ottawa 20-30. It is also reasonable to assume that $\delta_r \cong \delta_b$.

The height of ribs, H_r was maintained at 2.5 mm (0.1 in.) in all tests and the rib spacing, s was 33 mm. The height of the sand grain wall above the ribs, H_s was obtained from optical and carbowax observations. For the soils tested, H_s was found to be approximately equal to H_r and $0.8H_r$ for the dense and loose Ottawa sands respectively.

Since δ_s cannot be directly measured nor optically observed it must be estimated. Realistically, we should expect δ_s to be intermediate between δ_r and ϕ. Therefore it was assumed to be 30° for the dense and 27° for the loose conditions. With these parameter values, the apparent friction angles were computed to be 47° and 38.5° for the dense and loose Ottawa sands. A detailed procedure of this analysis is given in [4]. Experimental direct shear test results are shown in Figure 8 along with the predicted apparent friction angles. Clearly, the model is in very good agreement with the observed behavior.

4.4.2 Failure Shape

The Sokolovski method was also used to predict the failure shape around the rib. As can be seen in the Figure 9, the stress characteristic lines, s_1, are close to the experimental results from the optical monitoring and carbowax solidification observations for both dense and loose conditions. It seems, therefore, that the Sokolovski method is well capable of predicting the failure surface.

A method of velocity characteristics for predicting failure shapes was also considered but was significantly less successful as seen in Figure 9. A critical analysis of the discrepancies is given in reference [4].

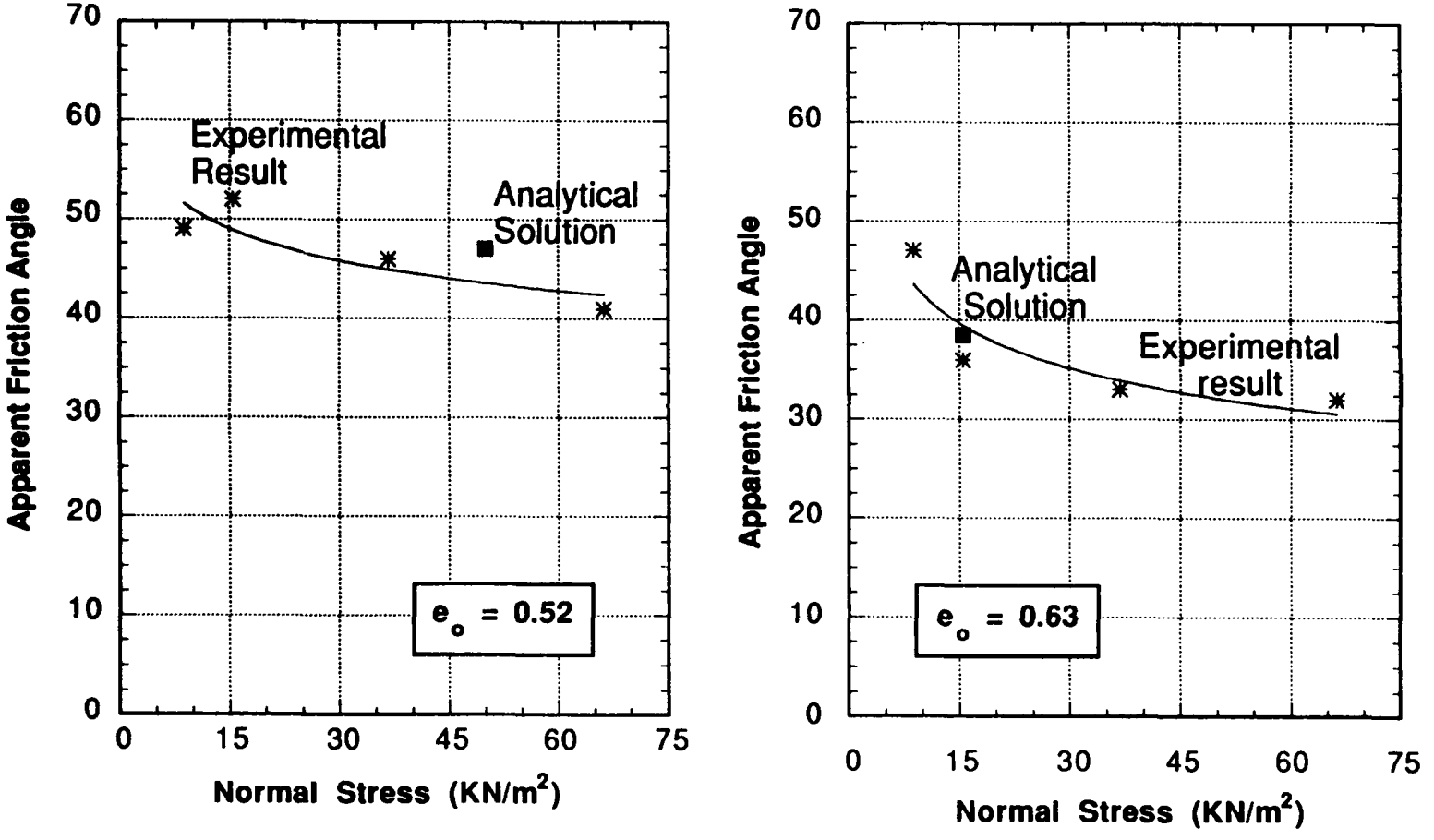

Fig. 8 Comparison of Model with Experimental Test Results

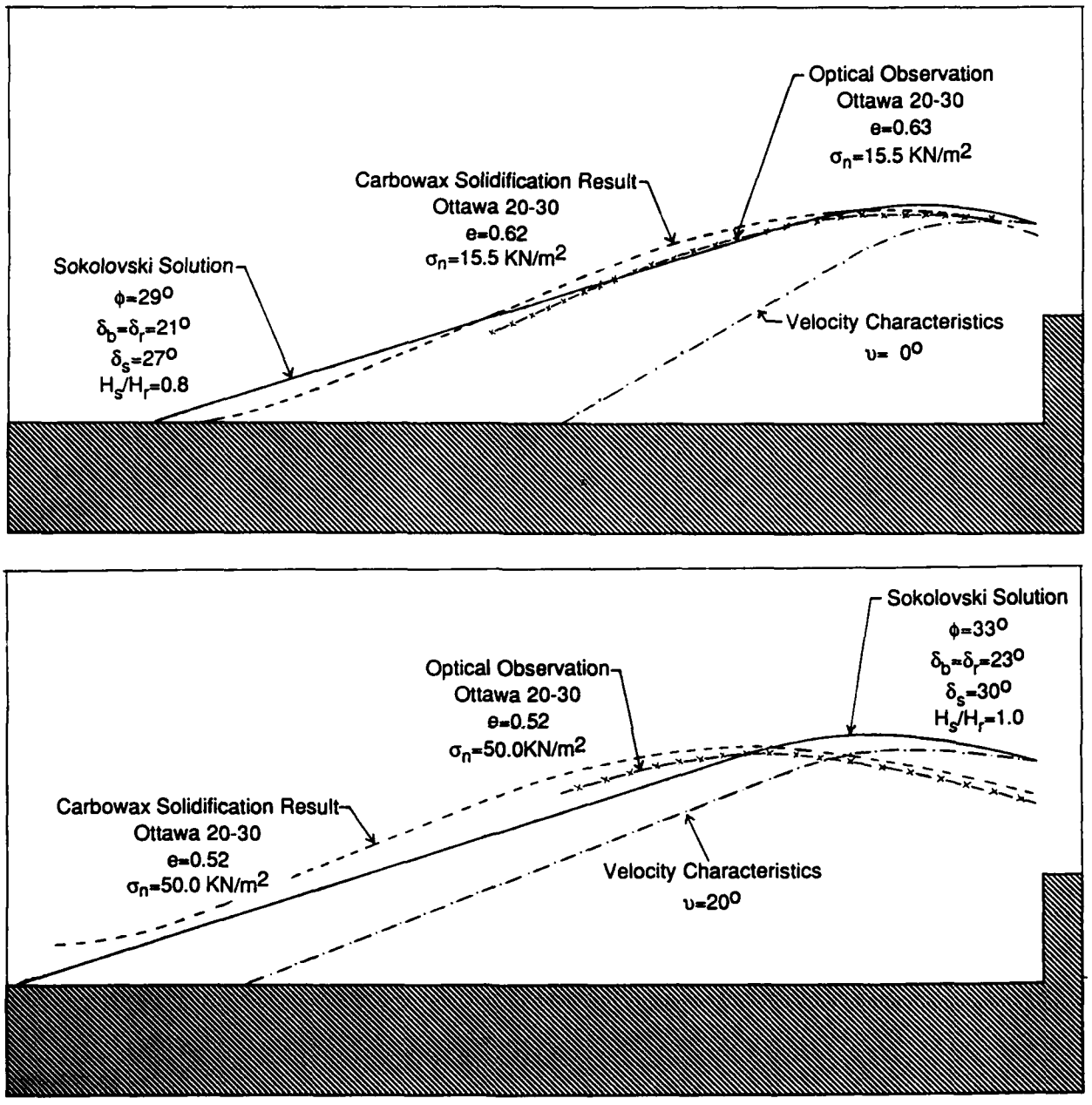

Fig. 9 Comparison of Observed Failure Shapes with Predictions by Sokolovski Procedure and Method of Velocity Characteristics

4.5 PARAMETRIC STUDY OF MODEL FOR PULLOUT RESISTANCE OF PLANE RIBBED INCLUSIONS

A sensitivity analysis was performed to evaluate the relative importance of the various parameters on F_p. The results of the analysis are presented as charts in Appendix D. They illustrate that F_p is very sensitive to H_s and ϕ but not very sensitive to δ_s, δ_r and δ_b.

4.6 OPTIMUM RIB SPACING

The dual mechanism (friction and passive resistance) of load transfer between soil and ribbed inclusions implies that pullout resistance is a function of the rib spacing. Thus, an optimum rib spacing must exist. To optimize the pullout resistance, the spacing should be such as to maximize the number of fully developed passive zones per length of reinforcement. Stated otherwise, the transition zone shown in Figure 5 should be kept to a small distance, optimally a point. The present study reveals, both analytically and experimentally, that the optimum spacing is 10 H_r for loose Ottawa 20-30 sand; approximately 13 H_r for dense Ottawa 20-30 sand; 13 H_r for loose Glazier Way Sand and greater than 13 H_r (possibly as high as 16 H_r) for dense Glazier Way Sand where H_r was maintained at 2.5 mm.

For rib spacings smaller than optimum, the transition zone will be absent, a full passive zone will fail to develop, the grains between adjacent ribs will be trapped and the shear surface will be above the ribs as shown in Figure 4a. The pullout resistance will be primarily due to soil-soil friction with some indeterminate contribution from a partially developed passive zone. As s becomes even smaller, say $s=2H_r$, all passive resistance disappears and pullout resistance decreases even further. Furthermore, the frictional resistance becomes partially due to soil-soil friction and partially due to friction between the soil and the tops of the ribs. In the limit, as s approaches H_r, the pullout resistance approaches $P_f=\sigma_n' \tan \delta_b$.

Conversely, If the rib spacing is increased beyond optimum, the size of the transition zone increases while the number of passive zones per unit length of reinforcement decreases. Therefore, total pullout resistance decreases. As the spacing becomes very large, the total pullout resistance approaches F_f. Figure 10 illustrates the relative contributions of F_p and F_f to pullout resistance. At optimum spacing, the relative contribution of F_p is maximum while that of F_f is minimum.

Based on the plasticity model presented in Section 4.3, a parameteric study of the optimum rib spacing was performed. The results of this study are presented in Appendix E.

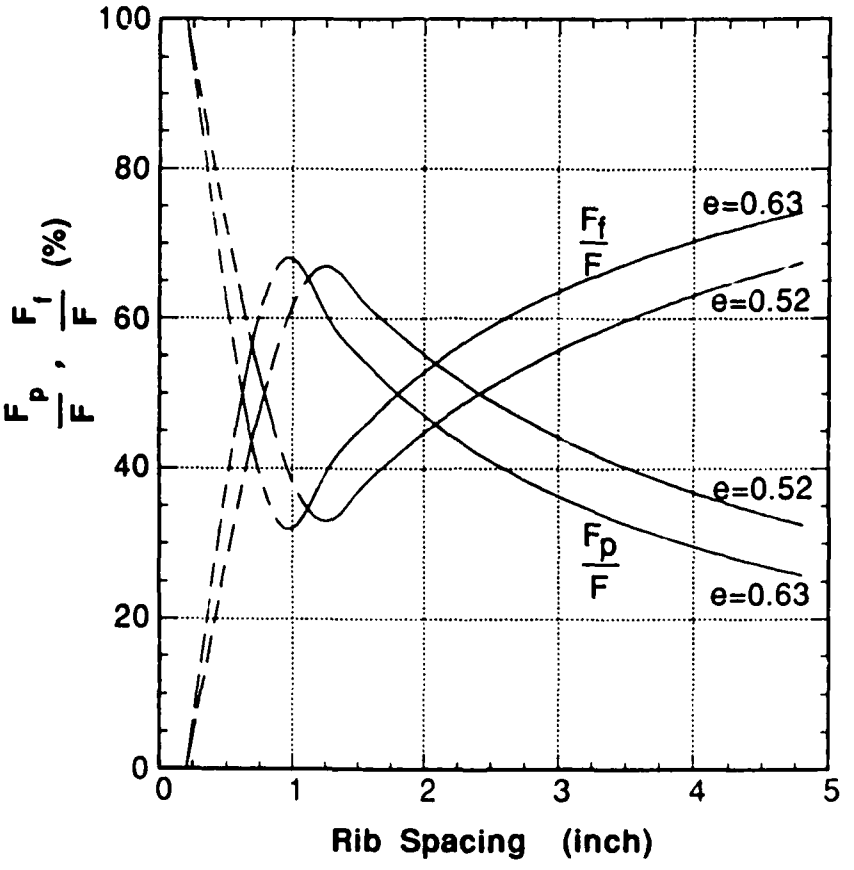

Fig. 10 Relative Contributions of Friction and Passive Resistance to Pullout Resistance

4.7 ANCHOR PULLOUT RESISTANCE

To study the behavior of actual anchors in soils, a relatively large triaxial testing apparatus shown in Figure 11 was designed and constructed. The sample preparation and reaction systems are shown in Figure 12. To simulate free field conditions, the ratio of tank to anchor diameter was designed to exceed 40.

Although in actual field installations the anchors are driven into the soil, in these tests the soil was deposited around the anchors in order to observe the development of peak resistance. However, prior to pullout, the anchors were always displaced downward until a constant residual resistance was developed prior to pullout. The anchors were also extended through the base of the testing device to eliminate tip resistance effects. In several tests, anchors were strain gauged to check if load takeout was uniform along the length of the anchor. A typical result, shown in Figure 13 confirmed this to be the case. Additional details of the testing system and experimental investigation are provided in reference [3].

Both Ottawa 20-30 and Glacier Way sands were tested at isotropic confining stresses of 5 to 15 psi. Testing results are documented in Table 1 of reference [3]. The following conclusions were presented and are repeated here:

In all tests, high peak strength values were observed. In dense sands, the peak apparent friction coefficients were similar to those observed in other studies of ribbed strips. In dense sands, a relatively high post peak residual load was maintained as shown in Figure 14 while loose sands exhibited a large decrease in strength. It is believed that increases in normal stress due to dilation in the dense sand were responsible for this behavior.

On the first load reversal, an approximate 50% decrease in apparent interface friction was observed for dense sands. It is postulated that this was due to the loss of the dilation induced normal stresses and possibly the development of circumferential sand arches around the anchor.

Significant degradation of interface friction occurred with cycling, especially in non-uniform subangular sand where particle segregation and reorientation was occurring. Particle coating by iron oxide from the anchor may also contribute to the loss of interface friction.

Upon each load reversal, a zone of negligible resistance to pullout was observed as shown in Figure 14. This was due to the development of the high void regions behind the ribs (Figure 5).

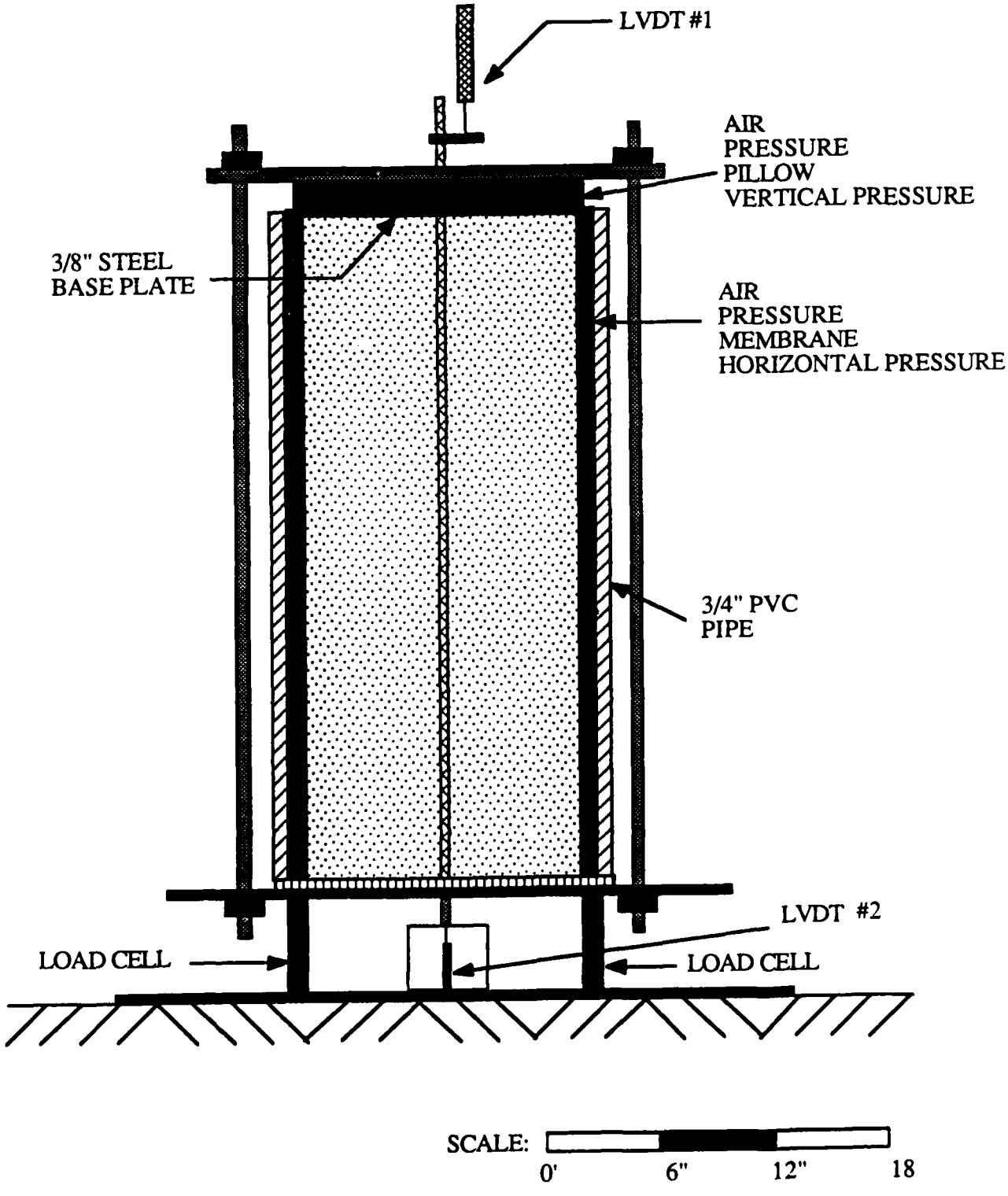

Fig. 11 Triaxial Tank for Anchor Pullout Testing

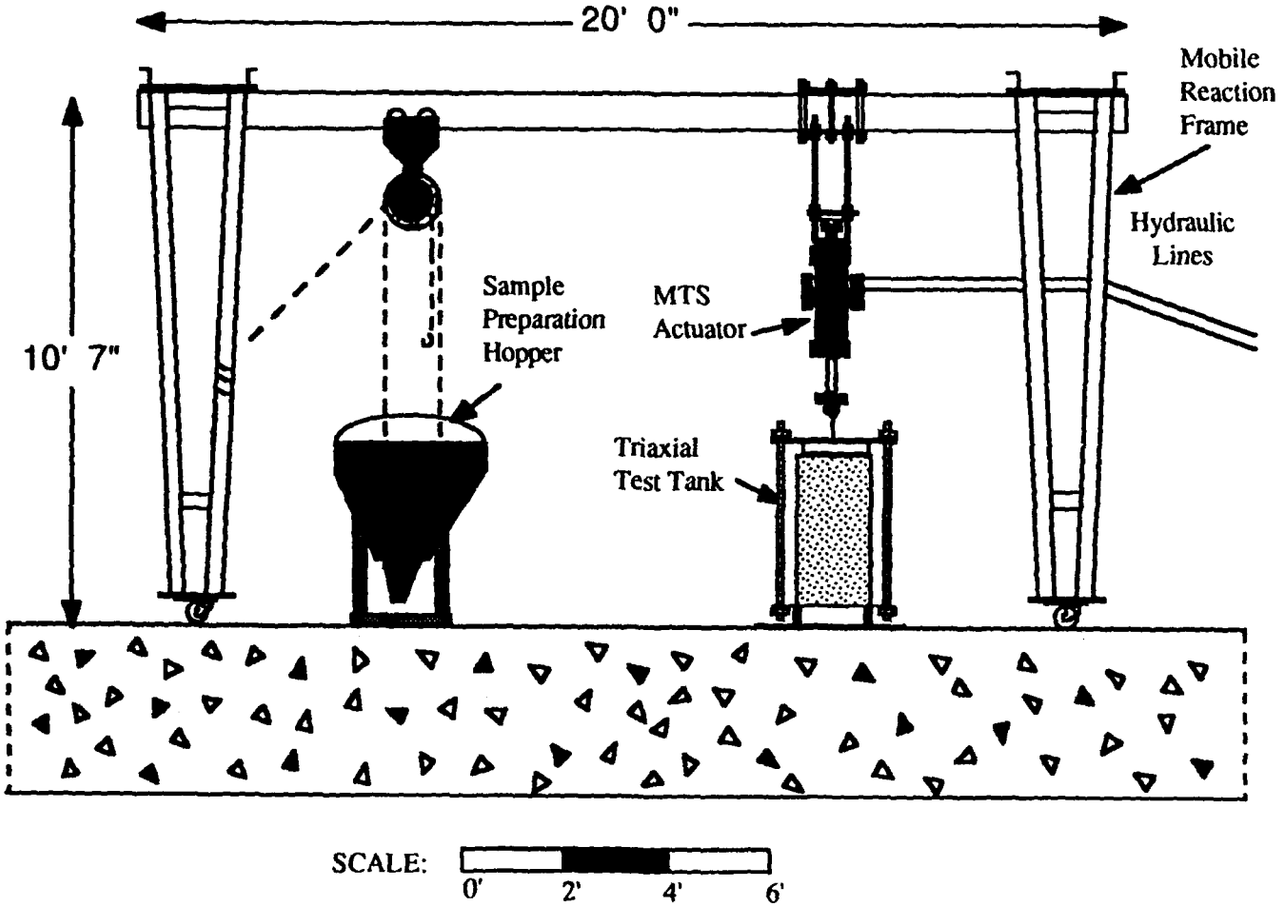

Fig. 12 Sample Preparation and Reaction System

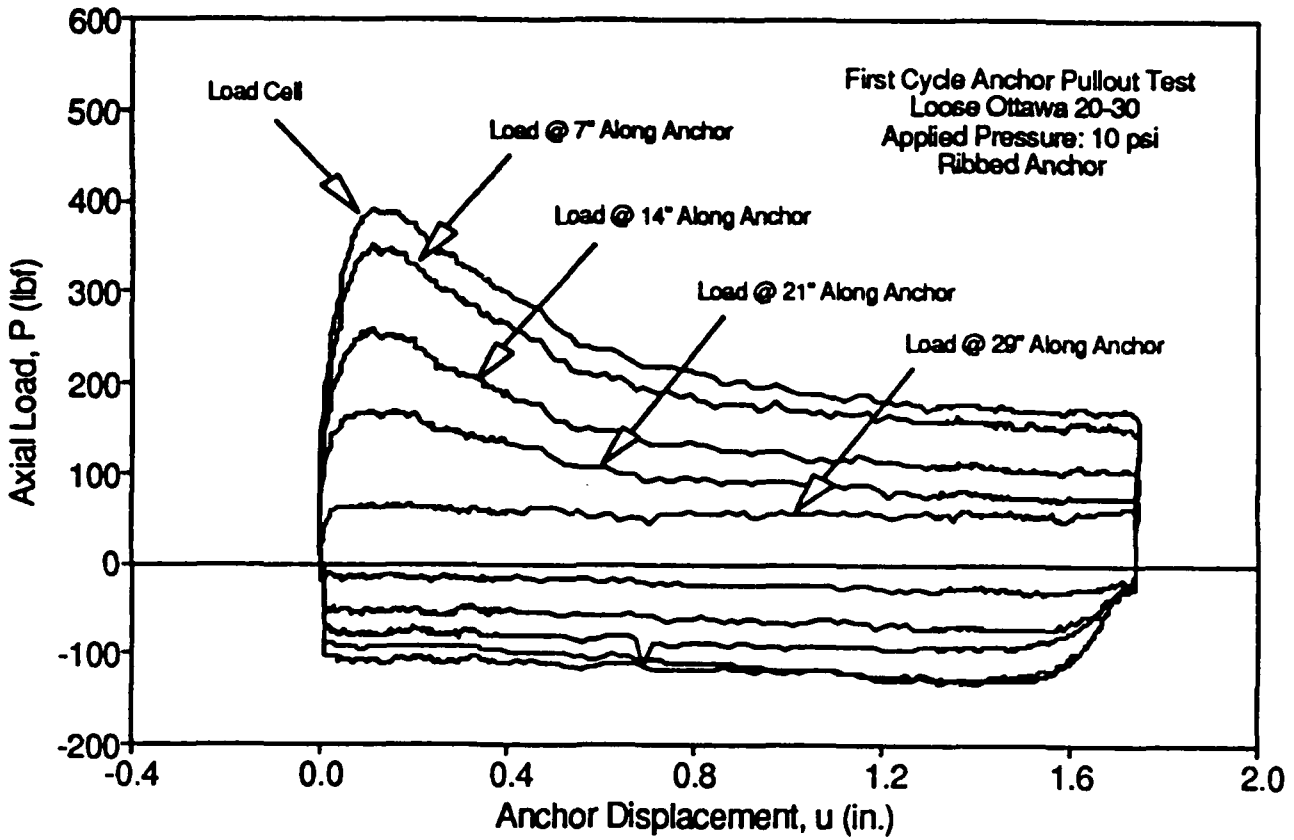

Fig. 13 Typical Load Takeout Results From Instrumented Anchors

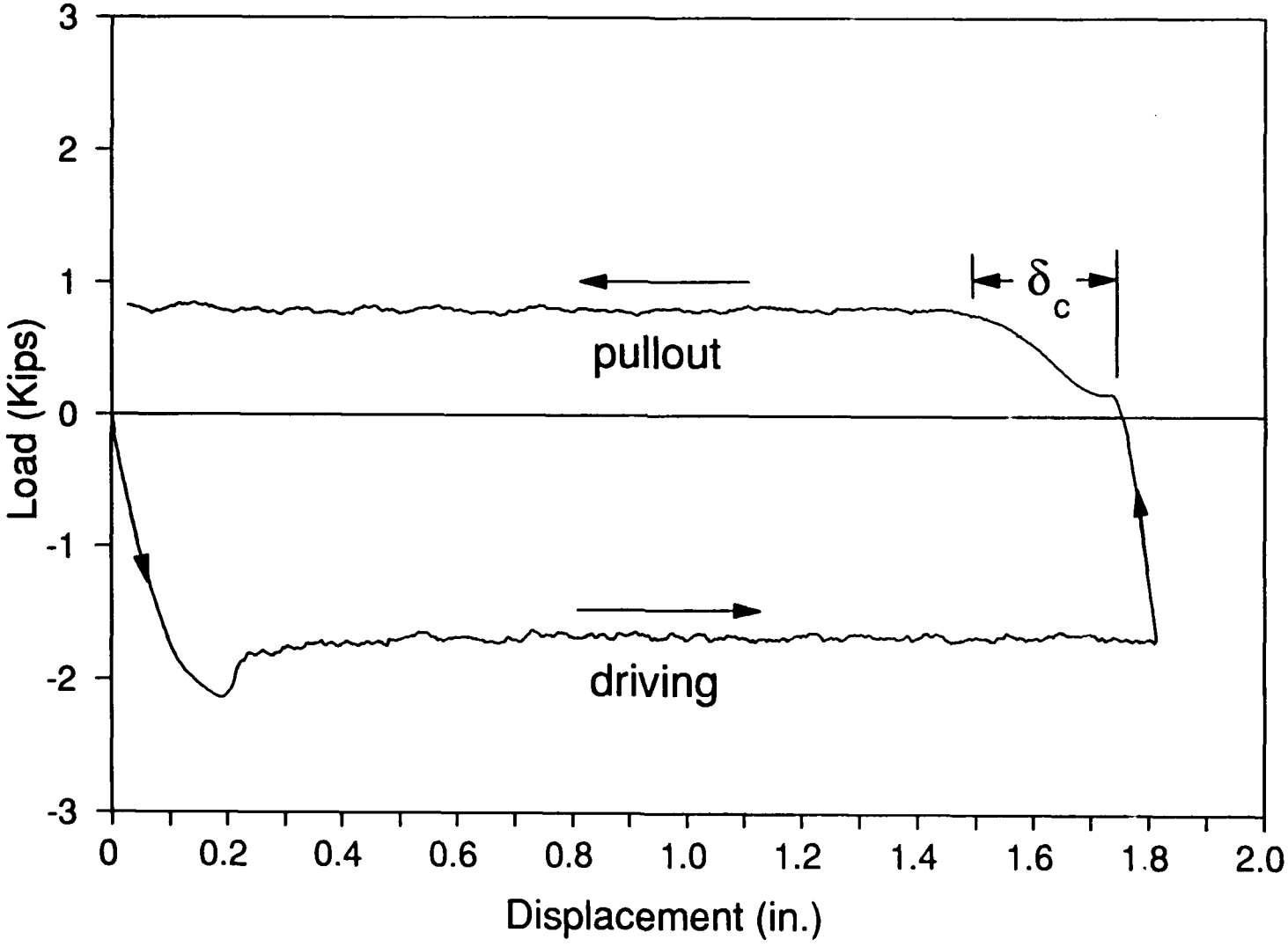

Fig. 14 Typical Load Versus Displacement Relationship for Driving and Pullout of Ribbed Anchors. Ottawa 20-30, 0.95 cm. (3/8 in.) dia. deformed rod, 69 kN/m^2 (10 psi) isotropic confinement.

The lengths of theses zones corresponded to the D_{50}'s of the two soils. However, it is reasonable to assume that the rib geometry would also affect the length of these zones. Peak pullout resistance was developed after one rib spacing of displacement or 0.25 in.

4.8 LOAD TRANSFER BETWEEN ANCHORS AND GEOSYNTHETICS

In an anchored geosynthetic system, the maximum loads in the fabric must be carried at the anchor connection. Therefore, tests were performed to determine if the strength of the fabric at the connection could be estimated from standard width-width tensile strength tests (ASTM-4595). A 5.1 cm diameter connector was used and the geosynthetics were held in a 56 cm. aluminum ring. Tests were performed under strain controlled conditions. The results indicated that the width-width tensile strength may be used with appropriate corrections as follows.

In non-woven fabrics a uniform stress generally develops and failure occurs almost simultaneously around the perimeter of the connection. Therefore, the ultimate load for the anchor-fabric connection, $T_{o\ max}$ may be expressed as

$$T_{o\ max} = \sigma_t \sin(\theta_o)\ \pi d \ \ldots\ldots\ldots\ldots\ldots\ldots (12)$$

where σ_t = width-width tensile strength of the fabric, θ_o = angle between the fabric and a plane normal to the anchor at the connection and d = diameter of the anchor connection.

In woven fabrics, the fiber stiffnesses and strengths are greater in the warp (machine) direction than in the weft (cross) direction. Therefore, the load is carried primarily by fibers in the warp direction and only over a width equal to the connection diameter. Therefore, the ultimate load carrying capacity of the fabric connection may be expressed:

$$T_{o\ max} = \sigma_{tw} \sin(\theta_o)\ fd \ \ldots\ldots\ldots\ldots\ldots\ldots (13)$$

where σ_{tw}=tensile strength of the fabric in the warp direction and f is a factor which depends on the fixity of the fabric to the anchor connector. If the connector is such that tensile stresses are easily transmitted across the connector f=1 should be used. If the fabric is gripped very securely by the connector so that tensile stresses are not transmitted across the connector, then failure should develop simultaneously on opposite sides of the connector and f=2 should be used.

In recognition of the tensile stress concentrations around an anchor, R. M. Koerner at Drexel University has developed a geonet termed "spider netting" with reinforced openings for carrying higher loads. This material was not tested for the present study but it offers a great hope for improving the effectiveness of anchored geosynthetic systems.

4.9 SOIL-GEOSYNTHETIC INTERFACE FRICTION

Anchor driving pulls and stretches the geosynthetic over the soil surface. O'Rourke et al. (1990) have pointed out that when slippage occurs along an interface, the interface becomes a plane of zero extension. Jewell and Wroth (1987) showed that slippage on a plane of zero extension occurs under the condition:

$$\sin \phi_{ps}' = \frac{\tan \delta}{\cos \psi \ [1 + (\tan \delta) \tan \psi]} \quad \ldots\ldots\ldots\ldots\ldots\ldots\ldots\ldots (14)$$

where ϕ_{ps}' = effective plane strain friction angle, ψ = angle of dilation and $\tan \delta = \tau'/\sigma_n'$ the ratio of shear to normal stress on the sliding surface. Since displacement will clearly be such that residual or constant volume interface friction will develop, ϕ_{ps}' may be replaced by ϕ_{cv}' and $\psi = 0$ in equation 14. This produces:

$$\tan \delta = \sin \phi_{cv} \quad \ldots\ldots\ldots\ldots\ldots\ldots\ldots\ldots\ldots\ldots\ldots\ldots\ldots\ldots (15)$$

Equation 15 defines a limiting stress condition approached by relatively soft and, or rough materials (such as most geosynthetics) for which failure occurs by rolling of the particles along the interface and creation of a parallel shear surface through the sand mass. Therefore equation (15) is conceptually applicable to the fabrics used in anchored geosynthetics.

Equation (15) suggests that δ is not a function of the initial soil density nor the fabric material, but only a function of ϕ_{cv}' which in turn is only dependent on soil mineralogy (Bolton, 1986). This is a particularly useful observation since ϕ_{cv}' for most sands falls within a narrow range of values from 33° for quartz to 40° for feldspar (Bolton, 1986) Accordingly, δ for most situations would range from 29° to 33°.

To verify equation (15) for use in anchored geosynthetic systems, two soils (Ottawa 20-30 and Glazier Way sand) and two fabrics (a Trevia 1155 nonwoven and a Nicolon 1500NC woven) were

tested. The soil/fabric interfaces tests were performed using an 45.7 cm x 30.5 cm (18 in. x 12 in.) shear box. Shearing was in the long direction. Separate direct shear tests were also conducted to determine ϕ_{cv}'. The test results were as follows:

	Trevia 1155 (nonwoven)	Nicolon 1500NC (woven)
Ottawa 20-30	$\phi_{cv}' = 31.0°$ $\delta_{calc} = 27.3°$ $\delta_{peak} = 26.7°$ $\delta_{res} = 25.0°$	$\phi_{cv}' = 31.0°$ $\delta_{calc} = 27.3°$ $\delta_{peak} = 27.2°$ $\delta_{res} = 26.4°$
Glazier Way	$\phi_{cv}' = 38.0°$ $\delta_{calc} = 31.5°$ $\delta_{peak} = 31.0°$ $\delta_{res} = 30.6°$	$\phi_{cv}' = 38.0°$ $\delta_{calc} = 31.5°$ $\delta_{peak} = 31.4°$ $\delta_{res} = 30.2°$

The results clearly confirm that equation (15) offers an excellent method for evaluating the soil-geosynthetic interface friction.

References

Bolton, M. D. (1986) "The Strength and Dilatancy of Sands," Geotechnique, Vol. 36, No. 1, pp. 65-78.

Jewell, R. A. and Wroth, C. P. (1987) "Direct Shear Tests on Reinforced Sand," Geotechnique, Vol. 37, No. 1, pp. 53-68.

O'Rourke, T. D., Druschel, S. J. and Netravali, A. N. (1990) "Shear Strength Characteristics of Sand-Polymer Interfaces," Jour. Geotech. Engnrg.Div., ASCE, Vol. 116, No. 3, pp. 451-469.

4.10 LOAD TRANSFER FROM GEOSYNTHETIC TO SOIL

The stresses transferred from the geosynthetic to the soil at a given point on the interface are only a function of the tension in the fabric and its local curvature. If the tension at the anchoring point, the complete deformed shape of the geosynthetic and the friction characteristics between the fabric and soil are known, the distribution of stresses between the soil and geosynthetic can be determined. Solutions for both plane and axisymetric situations are presented. A simplified procedure for estimating the stresses at depth is also presented in recognition of the overlapping of pressure bulbs from individual anchorage points.

4.10.1 PLANE ANALYSIS

For the case of plane (2-D) geosynthetic curvature as shown in Figure 15, the incremental decrease in fabric tension is given by:

$$T_2 = \frac{2 - (\Delta\theta)\tan(\delta)}{2 + (\Delta\theta)\tan(\delta)} T_1 \quad \text{.....(16)}$$

or, equivalently

$$T_2 = T_1 \, e^{-\Delta\theta \tan(\delta)} \quad \text{.....(17)}$$

where T_1 = tension per unit width of fabric at point 1 Figure 15,
T_2 = tension per unit width of fabric at point 2,
$\Delta\theta$ = change in fabric curvature between points 1 and 2,
δ = soil-fabric interface friction.

The normal stress between soil and fabric acting over the increment $\Delta\theta$ is then given by

$$\sigma_n = \frac{(T_2 + T_1)}{2} \frac{\Delta\theta}{\Delta s} \quad \text{.....(18)}$$

where Δs is the incremental curvilinear distance between points 1 and 2. Recognizing that $\Delta s/\Delta\theta$ is the radius of curvature (r), the normal stress at any point in the interface may be expressed as:

$$\sigma_n = \frac{T}{r} \quad \text{.....(19)}$$

A complete derivation of equations 16-19 will be given in reference [8].

Once the normal stress distribution has been determined, the forces acting normal (y-direction) and parallel (x-direction) to the slope may be determined. These expressions are given by:

$$F_y = \sigma_n \Delta s[\sin(\theta) - \cos(\theta)\tan(\delta)] \quad \text{.....(20)}$$

and

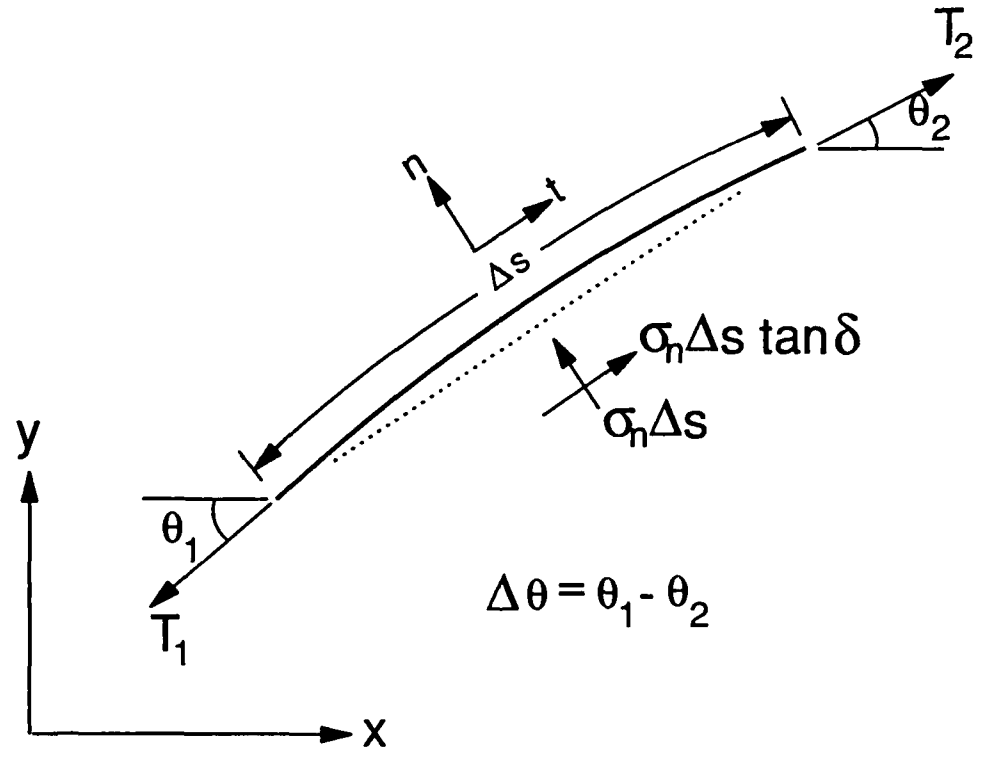

Fig. 15 Load Transfer Between Geosynthetic and Soil over an Incremental Fabric Length

$$F_x = \sigma_n \Delta s[\cos(\theta)+\sin(\theta)\tan(\delta)] \quad \text{.....(21)}$$

By static equilibrium the following equations must also hold

$$\frac{T_o}{2} \sin \theta_o = \int_0^{S/2} F_y \, dx \quad \text{.....(22)}$$

$$\frac{T_o}{2} \cos \theta_o = \int_0^{S/2} F_x \, dx \quad \text{.....(23)}$$

where T_o=total tensile force applied to the fabric at the anchor connection, θ_o=the angle between the fabric and the slope surface at the connection and S=slope distance between anchor points. Ideally, to maximize the load transferred to the soil θ_o should be as close to 90° as possible. To achieve this condition requires driving the anchor connection into the soil at least 0.5 m.

4.10.2 AXIALLY SYMMETRIC PROBLEM

For square or triangular anchor patterns, an axially symmetric analysis is required. A cylindrical coordinate system is employed. The expression for tension decrease along the interface is similar to that for the plane case:

$$T_{c2} = \frac{2 - (\Delta\theta)\tan(\delta)}{2 + (\Delta\theta)\tan(\delta)} T_{c1} \quad \text{.....(24)}$$

or

$$T_{c2} = T_{c1} \, e^{-\Delta\theta \tan(\delta)} \quad \text{.....(25)}$$

where $\Delta\theta$ and δ are identical to the plane case. However, T_c is the total tensile load acting on a concentric ring of the fabric (rather than the tension per unit width). The relationship between T and T_c is given by:

$$T = T_c/2\pi r \quad \text{.....(26)}$$

where r= radial distance from the anchor. The normal stress is once again given by equation 19.

An important observation and resulting assumption was made regarding the fabric in deriving the equations for axially symmetric situation. As fabric elements are pulled toward the anchor point during driving, they will "pleat" in order to occupy the shrinking circumferences. Neither compression nor tension develops in the circumferential direction. Thus, a T_θ was not required in the equilibrium equations for the axisymmetric element.

4.10.3 EXPERIMENTAL INVESTIGATIONS

To validate the models for transfer of loads from fabric to soil a series of full scale geosynthetic anchorage tests were performed. The Glazier Way sand was tested with both woven and non-woven geosynthetics. The fabrics were held in a rigid 3 m (10 ft.) diameter ring, thereby approximately simulating the conditions developed with a 3 m anchor spacing. The fabric/anchor connector was 5.1 cm (2 in.) in diameter. Loading was applied by a hydraulic actuator buried beneath the soil surface. Vertical deformations and normal stresses were measured with distance from the anchor. Complete details of these experiments will be provided in reference [6]. The main conclusions were:

1. Based on the deformed fabric shapes and δ=30.5° as discussed in Section 4.9, equations (19), (25) and (26) do correctly predict the increases in normal stress. Figures 16 and 17 show the deformed fabric shapes for the woven and non-woven fabrics as well as the location of stress gages. A comparison of measured and calculated values at peak load are given below:

Trevia 1155 (Nonwoven)	Gage 11 (psi)	Gage 720 (psi)
Measured	9.1	1.5
Calculated	9.2	0.7-3.0

Nicolon 1500NC (Woven)	Gage 715 (psi)	Gage 498 (psi)	Gage 720 (psi)
Measured	25	8	3
Calculated	24	6	2

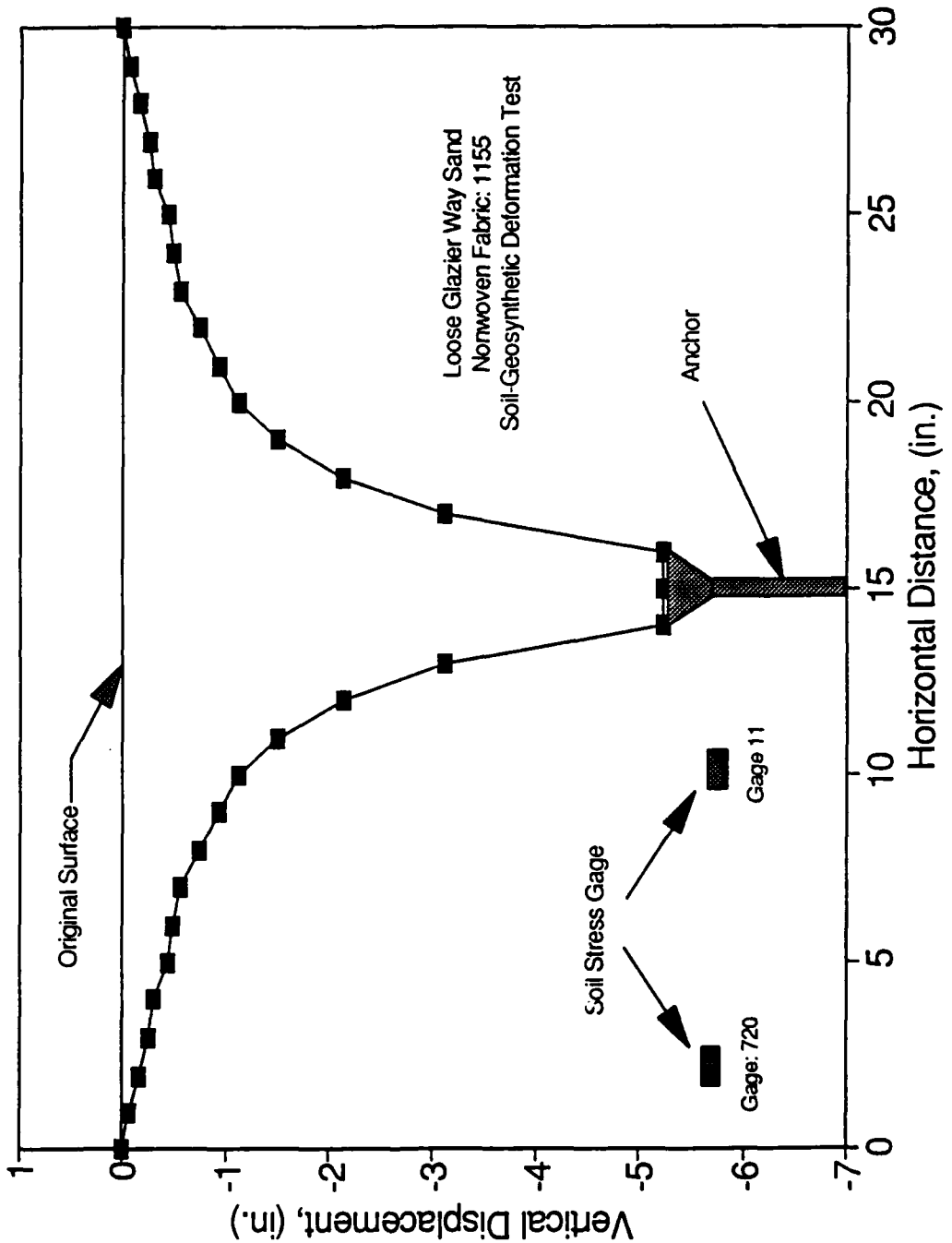

Fig. 16 Deformed Shape of Non-woven Geosynthetic at Peak Load

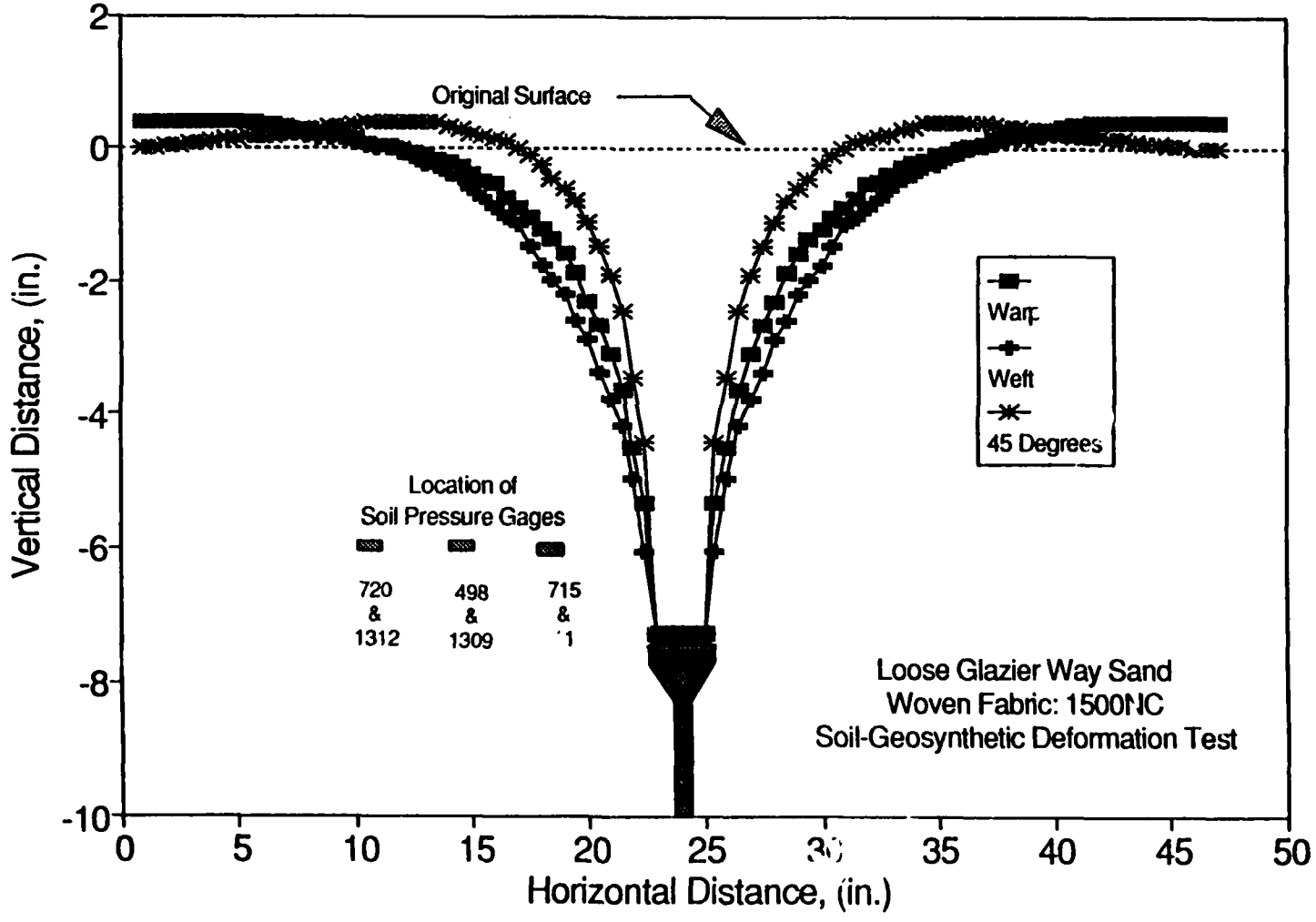

Fig. 17 Deformed Shape of Woven Geosynthetic at Peak Load

2. Soil deformation occurred to a distance of 0.46 m (18 in). However, significant fabric curvature was only observed to a distance of 0.20 m (8 in.). It is emphasized that the soil surface was originally flat.

3. Load-anchor displacement curves for both fabrics are shown in Figures 18 and 19. The deformations in both fabrics were highly plastic. As a result, very little upward displacement of the anchor was required to cause loss of fabric tension. This behavior has very important implications to the required anchor pullout stiffnesses and anchor/fabric connection mechanisms as will be discussed in Sections 4.12 and 4.13.

4. The deformation of the non-woven fabric was axisymmetric. However in the woven fabric, the load is carried almost exclusively by the fibers specifically attached to the anchor/fabric connector. The result is essentially equivalent to application of two perpendicular strip loads of width equal to the diameter of the anchor/fabric connector. This concentrated strip loading causes a plastic deformation of the soil and bulging of the fabric in the diagonal directions as seen in Figure 16. The bulging in turn develops some fabric tension in each of the four quadrants and a small normal stress as seen in Figure 20.

5. The non-woven fabric exhibits almost complete stress relaxation after tensioning. As such, it's use as an anchored geosynthetic is discouraged. The woven fabric also exhibits large stress relaxation when loaded beyond approximately 60% of the yield strength. At lower stress levels stress relaxation is not as severe as shown in Figures 20 and 21. Nevertheless, stress relaxation is a major concern and requires further research.

4.10.4 SIMPLIFIED SOLUTIONS FOR LOAD TRANSFER

While the solutions presented in section 4.10.1 and 4.10.2 provide insight into the distribution of actual load transferred between tensioned anchors and the soil, the experimental results indicated that significant curvature of the soil-fabric interface only develops to a distance of approximately 0.2 m from the anchor. This distance can easily be increased to 0.3 m or greater by excavating small conical depressions at anchor locations prior to installation. As such, for estimation of stress increases within a slope, the load transferred from a geosynthetic can be approximated by:

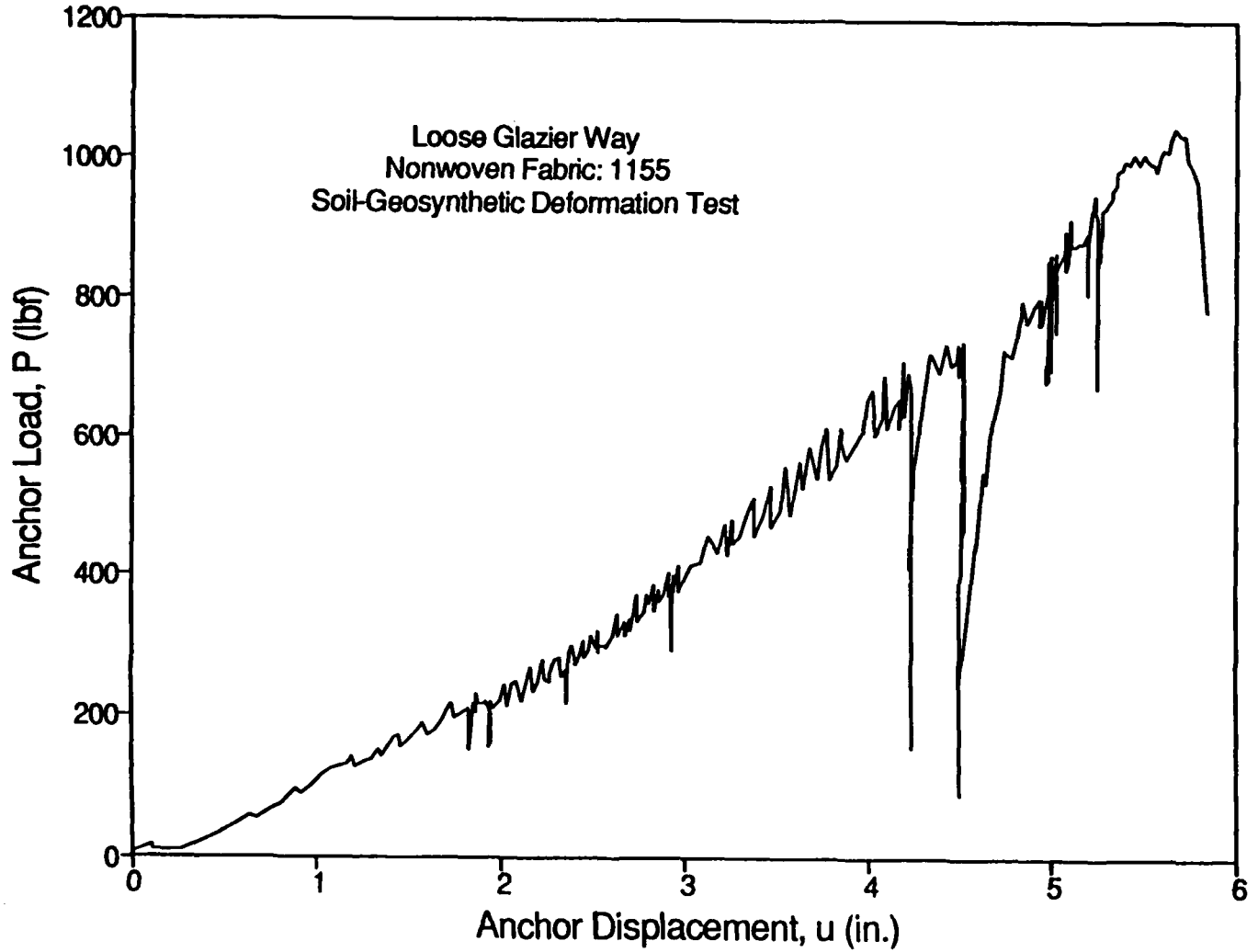

Fig. 18 Load-Deformation Relationship, Nonwoven Fabric

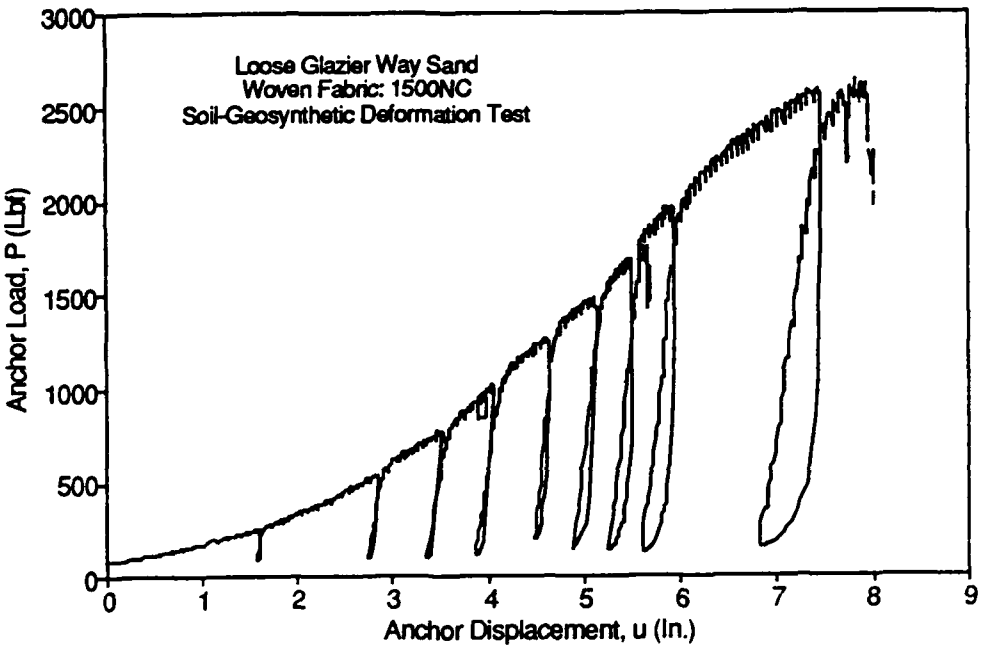

Fig. 19 Load-Deformation Relationship, Woven Fabric

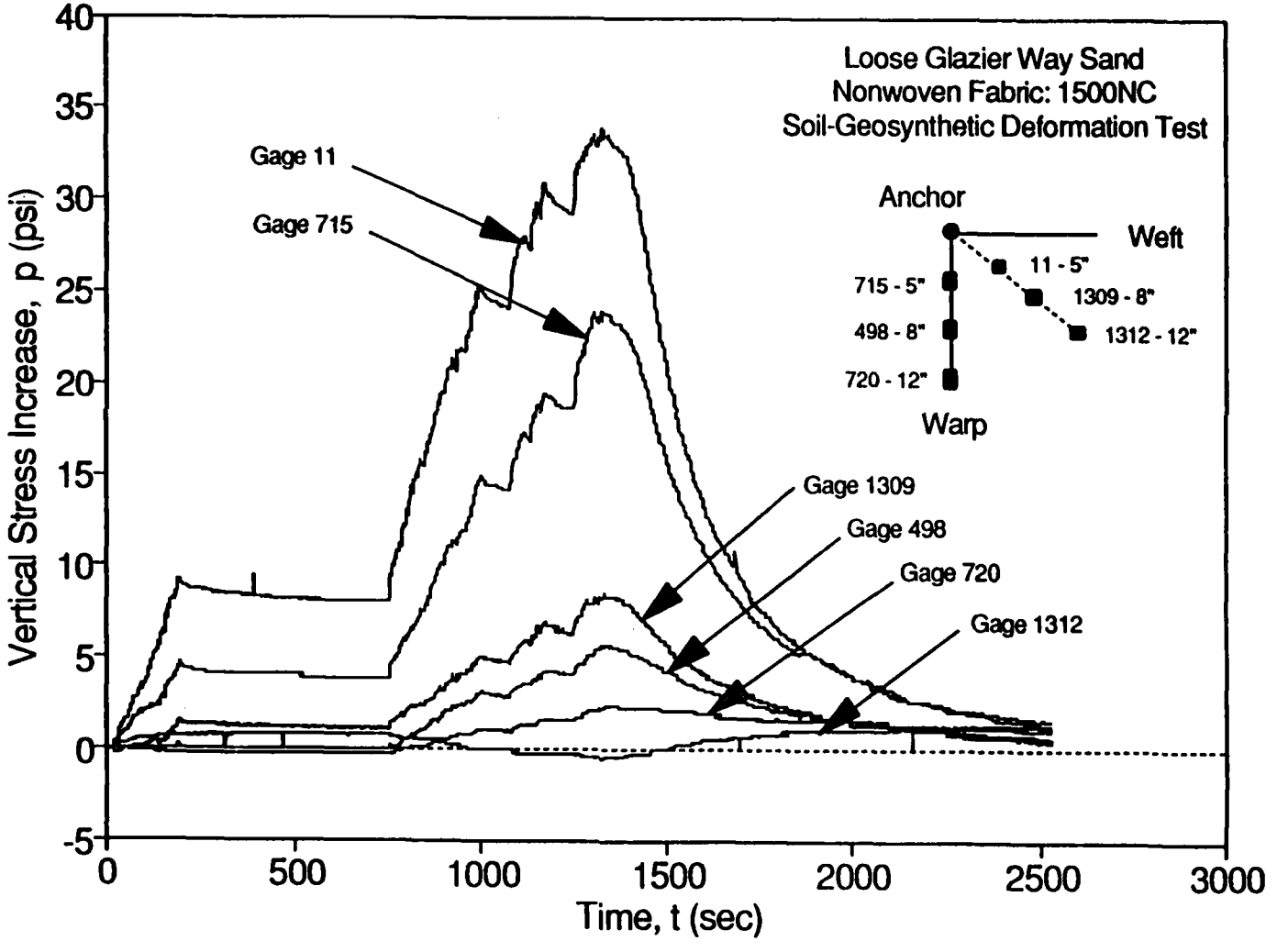

Fig. 20 Stress-Time Relationship, Nonwoven Fabric

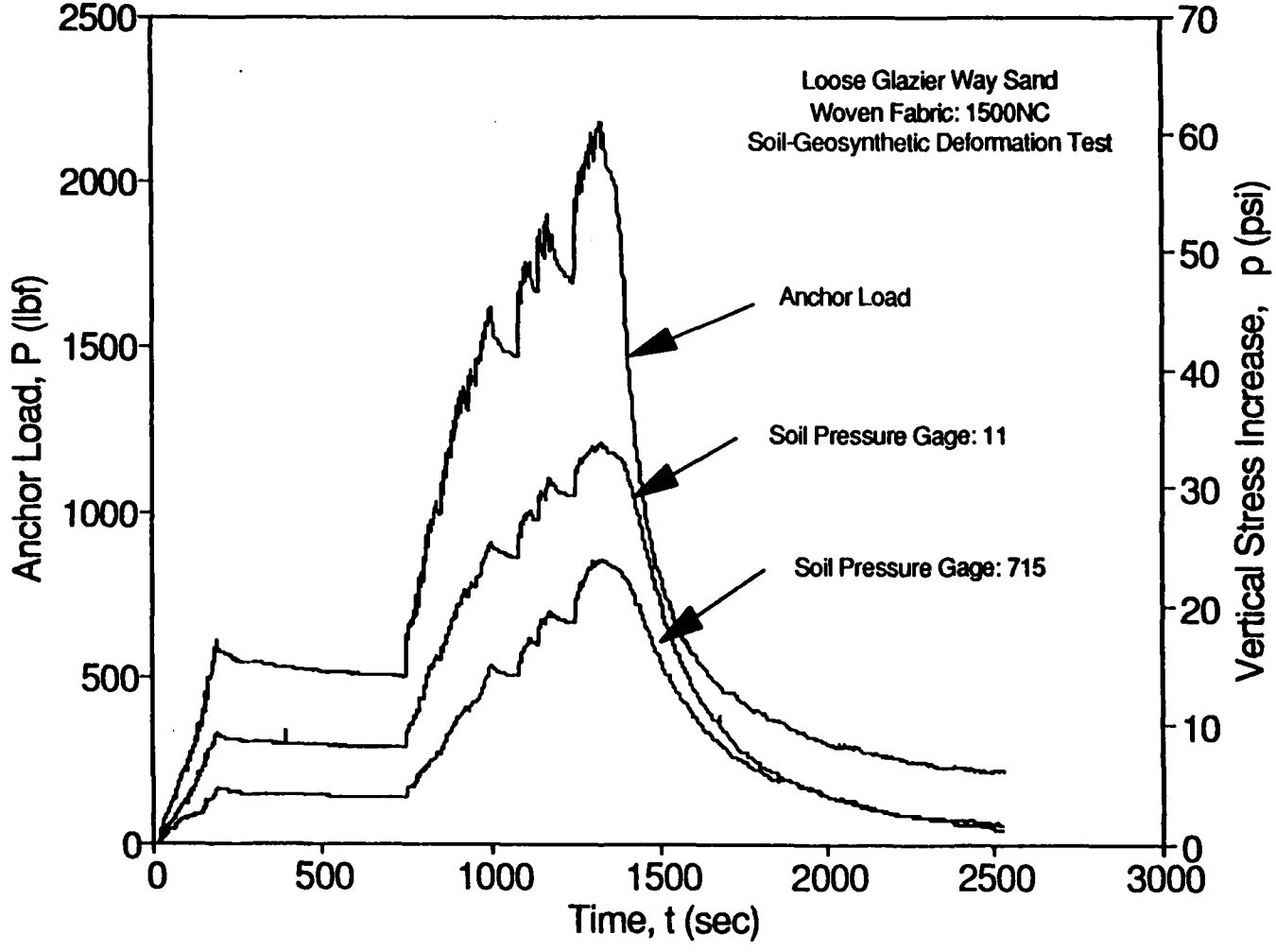

Fig. 21 Stress-Time Relationship, Woven Fabric

$$q = \frac{T_o}{\pi r_{eff}^2} \quad \text{.....(27)}$$

where r_{eff}= effective radius of loading which may conservatively be assumed to be 0.3 m. and T_o=the total vertical load applied to the soil. Due to the coalescence of pressure bulbs from adjacent anchors, for typical anchor spacings of 1.5 to 2.5 m the variations in pressure increases on a potential sliding surface parallel to the slope at a depth of 0.75 times the anchor spacing will be less than 10%. Therefore for a simplified stability analysis, is may be assumed that the anchored geosynthetic system exerts a uniform pressure of:

$$q = \frac{T_o}{S^2} \quad \text{.....(28)}$$

at the slope surface.

4.10.5 EROSION CONTROL

Since the radius of significant fabric curvature is only approximately 0.3 m, much of the soil between anchor points at depths less than S/2, is subject to very little increase in stress. While the overall stability of the slope may not suffer, the soil in these regions remains particularly susceptible to surficial sloughing and erosion. Figure 22(a) illustrates that for a square anchor spacing a relatively wide erosion channel of width S_e may form beneath the stretched but uncurved fabric.

By offsetting alternate anchor rows as shown in Figure 22(b) into a triangular anchor pattern, the width of a direct downslope erosion channel can be considerably reduced. However, meandering erosion channels as shown by line 'aa' could form. If in addition to offsetting alternate rows, the spacing between rows is reduced as shown in Figure 22(c), a meandering erosion channel must follow a more tortuous path and therefore soil loss may be arrested. Further study is needed to develop row spacing criteria as a function of the soils erosion susceptibility.

Finally, "pre-plowing" across a slope is recommended as a way to both enhance curvature and provide erosion cutoffs. By plowing into the soil and mounding it on the upslope and downslope sides of the furrow, the zone of fabric curvature would be enlarged. Anchors would be installed in the furrow as shown in Figure 23. Since the geosynthetic would coform to the shape of the furrow an effective erosion cut-off would also be established.

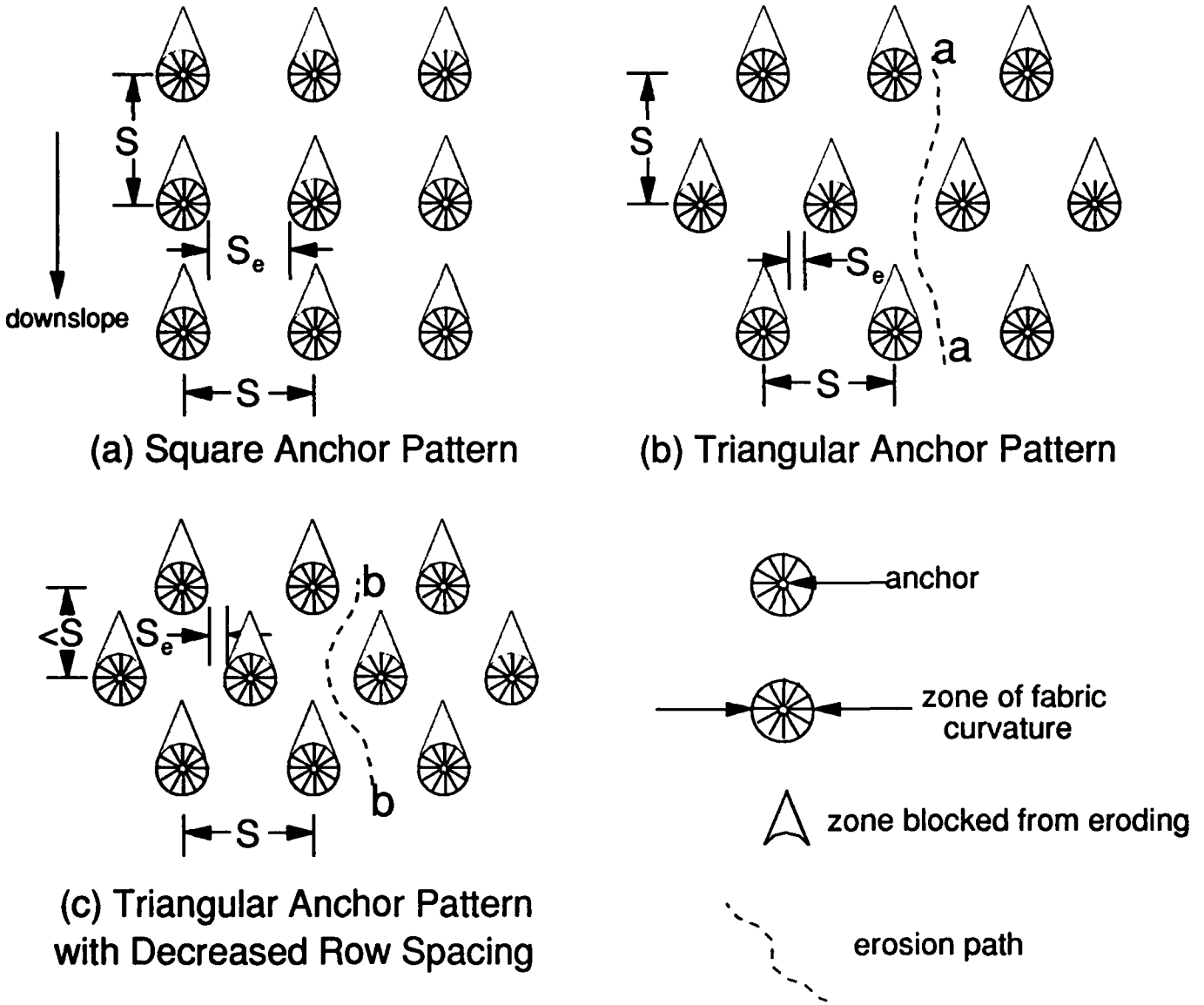

Fig. 22 Anchor Patterns

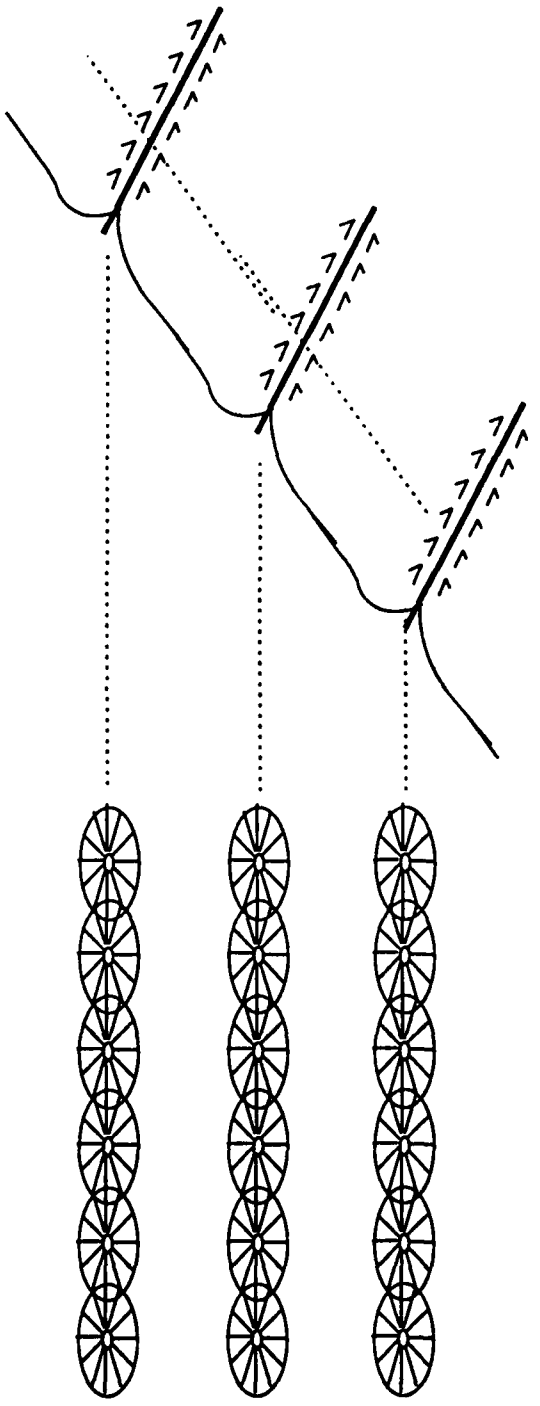

Fig. 23 Preplowing Across Slope and Installation of Anchors in Rows for Erosion Control.

4.11 NORMAL STRESSES ON ANCHORS IN INFINITE SLOPES

A procedure was developed for estimating the normal stresses on anchors in infinite slopes based on existing elasticity solutions. The procedure is detailed in reference [5]. The average normal stress on an anchor at a distance z from the surface shown in Figure 24 is given by:

$$\sigma_n = F_n \gamma z \quad \text{.....(29)}$$

where γ=soil unit weight and F_n = a stress factor given by:

$$F_n = \frac{K_X+2K_Y+1}{4}\cos(\theta+\beta) + \frac{K_X-1}{4}\cos(\theta+\beta)\cos 2(\theta+\beta) +$$

$$\frac{1+2\nu}{2}\sin(\theta+\beta)\tan\beta + \frac{\theta+\beta}{\pi}\cos(\theta+\beta)\sin 2(\theta+\beta)\tan\beta \quad \text{.....(30)}$$

where K_X and K_Y are coefficient of horizontal earth pressure in directions perpendicular and parallel to the slope, ν=Poissons's ratio, θ=angle between the anchor axis and the face of the slope and β=slope angle.

4.12 PULLOUT STIFFNESS OF ELASTIC ANCHORS IN INFINITE SLOPES

The pullout stiffness, defined as the pullout force (T_o) divided by the displacement of the top of the anchor (δ_o) is an important parameter in the design of anchored geosynthetic systems. Inadequate pullout stiffness may result in a loss of fabric tension. Anchors are typically long slender driven reinforcing rods. Thus, both elastic axial extension and rigid body translation are significant components of the total upward anchor displacement. Solutions for the pullout stiffness were developed and are presented in reference [5], therefore, only the key equations are presented here.

The governing differential equation for pullout stiffness is:

$$EA\frac{d^2\delta(z)}{dz^2} - C\,\tau(z) = 0 \quad \text{.....(31)}$$

where E= Young's modulus, A=anchor cross-sectional area, δ=displacement, C=perimeter of shearing surface and τ_z=shear stress on the anchor.

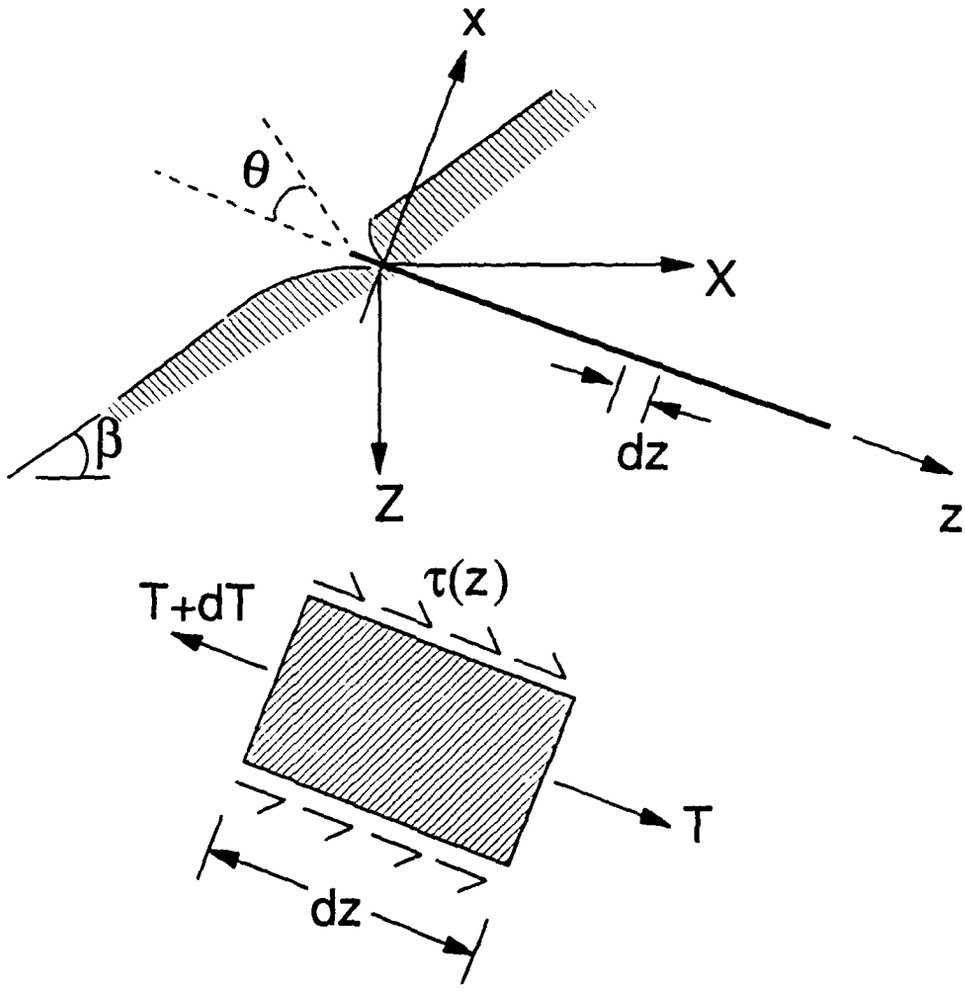

Fig. 24 Forces on an Anchor Element During Pullout

The laboratory tests on both plane ribbed inclusions and actual anchor segments revealed that the mobilized interface shear strength between soil and a predriven anchor increases linearly as the relative displacement increases from zero to a critical relative displacement, δ_c. Beyond this critical displacement the shear strength remains constant. Thus, $\tau(z)$ is given by:

$$\tau(z) = \frac{\delta}{\delta_c} \tau_{max} \quad \text{when } \delta \leq \delta_c \qquad \ldots\ldots(32)$$

and

$$\tau(z) = \tau_{max} \quad \text{when } \delta \geq \delta_c. \qquad \ldots\ldots(33)$$

Solution of the governing differential equation and equilibrium conditions provided expressions for δ_o and T_o. The pullout stiffness of an anchor was thus found to be given by:

$$\frac{T_o}{\delta_o} = AE\Phi \quad \text{when} \quad T_o \leq T_{cr} \qquad \ldots\ldots(34)$$

and

$$\frac{T_o}{\delta_o} = \frac{-AE\left[\frac{1}{2}\lambda L_c^2 + \left[\frac{\Psi_6\Phi - \Psi_4}{\Psi_1 - \Psi_2\Phi}\right]\right]}{\left[1 + \frac{1}{3}\lambda L_c^3 + \frac{\Psi_6\Phi - \Psi_4}{\Psi_1 - \Psi_2\Phi} L_c\right]} \quad \text{when} \quad T_o > T_{cr} \qquad \ldots\ldots(35)$$

where

$$\lambda = \frac{CF_n\gamma\nu^*}{EA\delta_c},$$

ν^* = apparent coefficient of friction

T_{cr} = pullout force which causes an anchor displacement of δ_c at the surface

L_c = the distance along the anchor at which $\delta = \delta_c$ (when $T > T_{cr}$)

$$\Phi = \frac{\sum_{n=1}^{\infty} \frac{\lambda^n L^{3n-1}}{R(n)}}{1 + \sum_{n=1}^{\infty} \frac{\lambda^{n_L} 3n}{S(n)}}$$

$$\Psi_1 = 1 + \sum_{n=1}^{\infty} \frac{\lambda^{n_{L_c}} 3n}{P(n)} \qquad \Psi_2 = L_c + \sum_{n=1}^{\infty} \frac{\lambda^{n_{L_c}} 3n+1}{Q(n)}$$

$$\Psi_3 = \sum_{n=2}^{\infty} \frac{\lambda^{n_{L_c}} 3n-2}{U(n)} \qquad \Psi_4 = \sum_{n=1}^{\infty} \frac{\lambda^{n_{L_c}} 3n-1}{R(n)}$$

$$\Psi_5 = \sum_{n=2}^{\infty} \frac{\lambda^{n_{L_c}} 3n-1}{V(n)} \qquad \Psi_6 = 1 + \sum_{n=1}^{\infty} \frac{\lambda^{n_{L_c}} 3n}{S(n)}$$

where $P(n) = (3n)(3n-1)(3n-3)(3n-4)\ldots(3)(2)$
$Q(n) = (3n+1)(3n)(3n-2)(3n-3)\ldots(4)(3)$
$R(n) = (3n-1)(3n-3)(3n-4)\ldots(3)(2)$
$S(n) = (3n)(3n-2)(3n-3)\ldots(4)(3)$
$U(n) = (3n-3)(3n-4)\ldots(3)(2)$
$V(n) = (3n-2)(3n-3)\ldots(4)(3)$

The first derivative, or the incremental pullout stiffness of an anchor will also play an important role in system integrity as will subsequently be discussed in Section 4.14. It is given by

$$\frac{\partial T_o}{\partial \delta_o} = AE\Phi \qquad \text{when} \quad T_o \leq T_{cr} \qquad \ldots\ldots(36)$$

and

$$\frac{\partial T_o}{\partial \delta_o} = AE\delta_c \left[\lambda L_c - \left[\frac{(\Psi_1 - \Psi_2\Phi)\Psi_3 - (\Psi_4 - \Psi_6\Phi)\Psi_4 - [(\Psi_1 - \Psi_2\Phi)\Psi_5 - (\Psi_4 - \Psi_6\Phi)\Psi_6]\Phi}{(\Psi_1 - \Psi_2\Phi)^2} \right] \right]$$

$$\text{when} \quad T_o > T_{cr}. \qquad \ldots\ldots(37)$$

4.13 ANCHOR INSTALLATION, ANCHOR-FABRIC CONNECTIONS AND SYSTEM INTEGRITY

Three different mechanical systems for attaching geosynthetics to the anchors in anchored geosynthetic systems are shown in Figure 25. Each of the systems imparts a different loading sequence to the anchor and geosynthetic.

The spring steel collar permits only unidirectional movement of the geosynthetic with respect to the anchor. The geosynthetic is tensioned by driving or pushing on the collar assembly. Once the installation force is removed, the collar fingers lock on the underside of the reinforcing rod ribs and the tensioned geosynthetic imparts an uplift to the anchor. The resulting rigid body translation and elastic extension of the anchor combine to produce the load-displacement curve for the anchor shown in Figure 26(a). The upward movement of the anchor connection in turn causes partial stress relaxation in the fabric. If the installation load is removed from the collar slowly enough so that oscillations of load between the anchor and geosynthetic do not occur, the system will come to equilibrium at point "E" in Figure 26(a).

A second possible tensioning system consists of a threaded anchor and nut as shown in Figure 25(b). A ball bearing plate may be used beneath the nut to prevent the transfer of torque to the geosynthetic. Since the tension in the geosynthetic and anchor develop simultaneously, as shown in Figure 26(b), the geosynthetic is never stretched beyond its designed tension. The critical design criteria for this type of connection is that the incremental stiffness of the anchor ($dT_o/d\delta_o$) must be greater than the stiffness of the geosynthetic for loads up to the design T_o. In current practice, anchors are driven through reinforced openings in the fabric to approximately 90% of the required anchorage depth. The geosynthetic is then fastened to the anchor by a pin inserted through the anchor as shown in Figure 25(c) and driven or pushed to its final depth. The application of stress to the anchor causes, in addition to the rigid body displacement, an elastic shortening of the rod. Therefore, upon removal of the driving force, elastic rebound must precede the tensioning and stretching of the anchor (Fig. 24c). The resulting displacements of the anchor, δ_o, will be greater than in either the spring collar or threaded anchor and nut systems thereby rendering this system least attractive for maintaining tension in the fabric.

Example problems are presented in reference [5] to illustrate the use of pullout concepts to design. They demonstrate that a threaded anchor and nut connection requires a significantly shorter anchor length to develop the required pullout stiffness and are therefore preferred over spring steel connections or the current practice of tensioning by driving on the anchors.

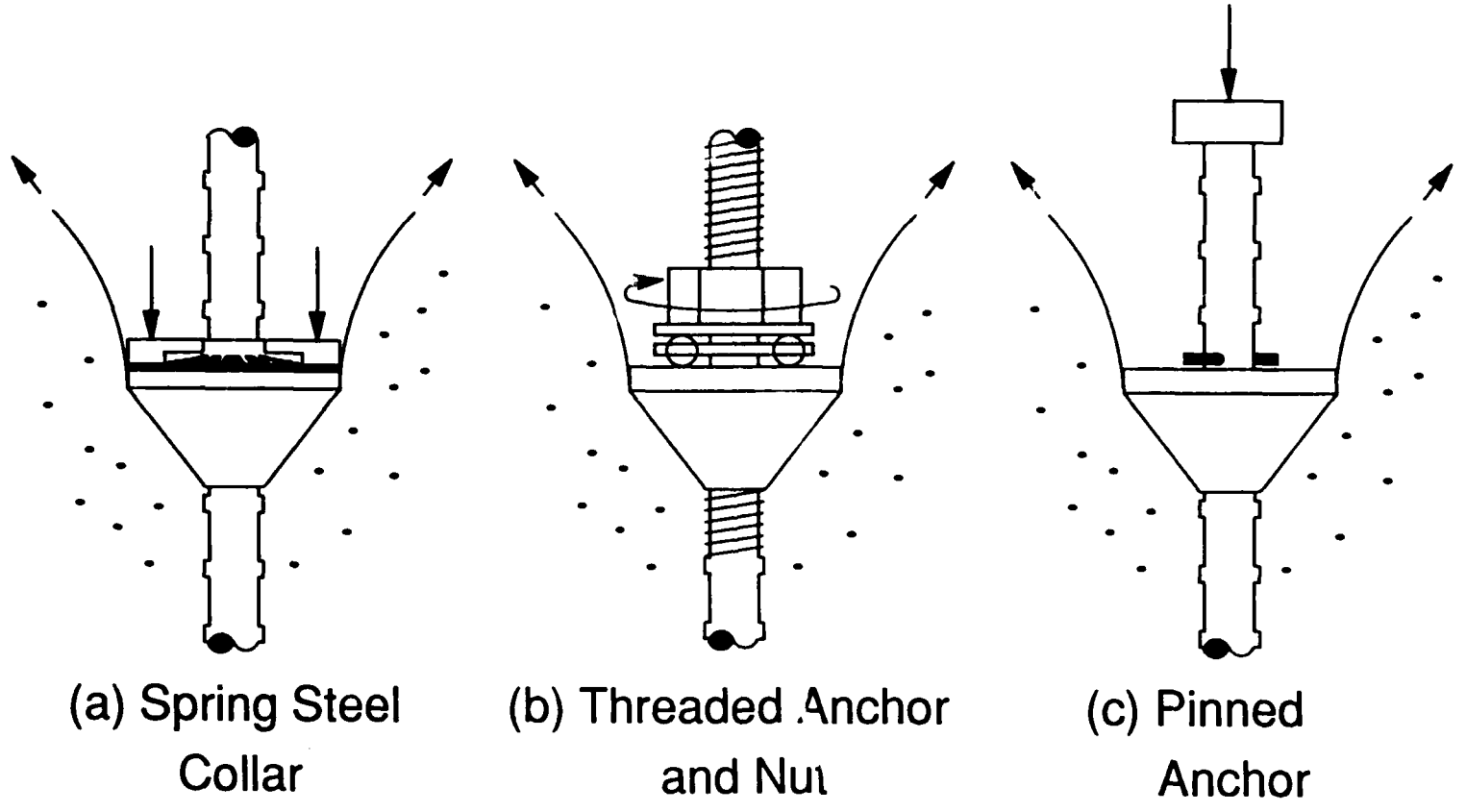

Fig. 25 Anchor Connector Types

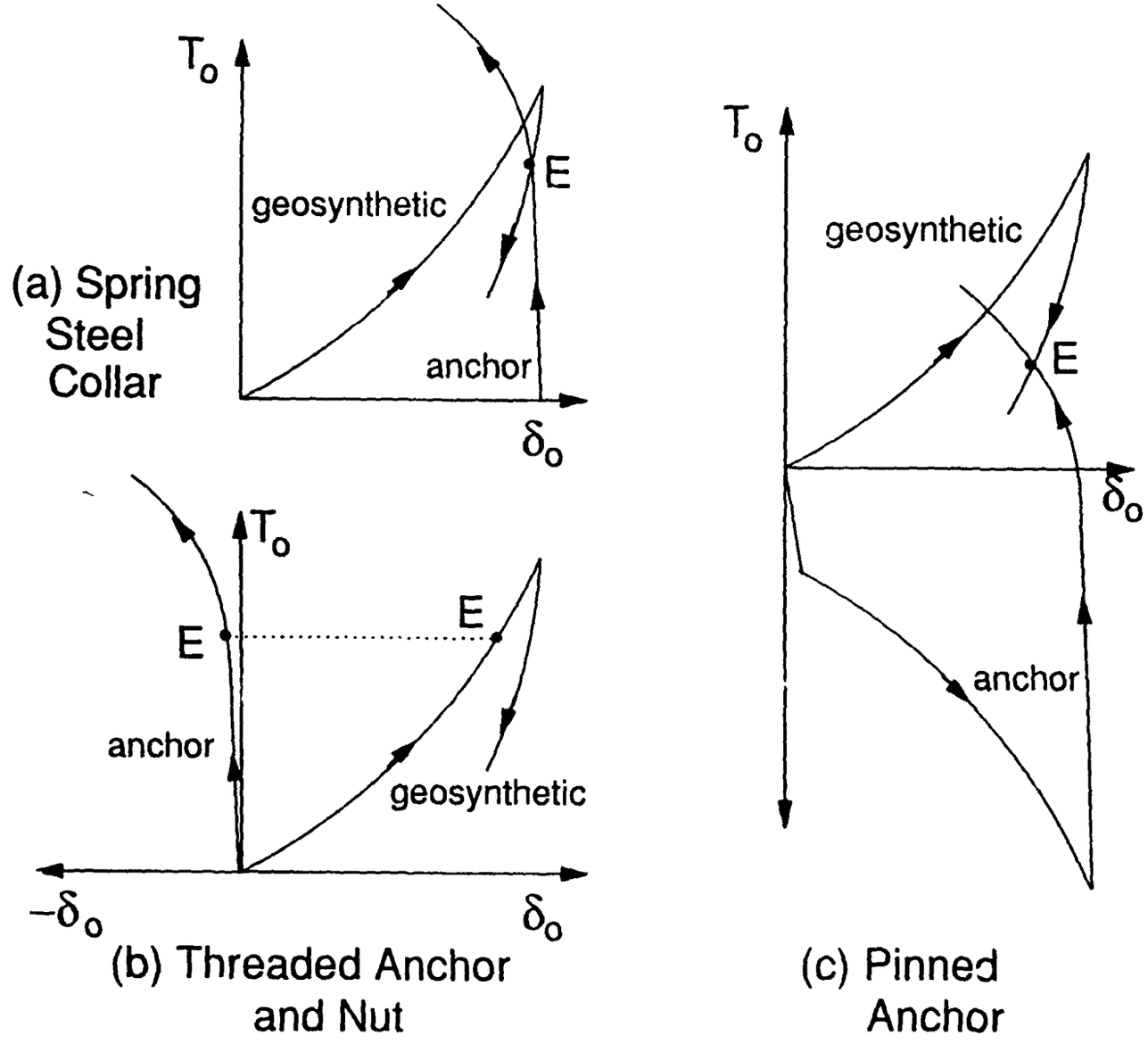

Fig. 26 Load Transfer Between Anchors and Geosynthetics

4.14 STABILIZATION OF INFINITE SLOPES BY ANCHORED GEOSYNTHETICS

The factor of safety against sliding for infinite slopes is quantified by the ratio of forces resisting shear to the driving forces on a potential sliding surface as shown in Figure 27a. For cohesionless, dry soils on infinite slopes with no external loads, the expression takes the form:

$$F_o = \frac{W \cos \beta \tan \phi}{W \sin \beta} = \frac{\tan \phi}{\tan \beta} \quad \ldots\ldots\ldots\ldots\ldots\ldots\ldots\ldots\ldots\ldots\ldots\ldots (38)$$

where F_o=factor of safety (prior to stabilization), W=the weight of the slice shown in Figure 27a, β=slope angle and ϕ= angle of internal friction of the soil. If external loads of magnitude T_o are applied in a square pattern of spacing s x s at an angle θ to the slope normal as shown in Figure 27b, eq. 38 may be modified as:

$$F = \frac{(W \cos \beta + T_o \cos \theta) \tan \phi}{W \sin \beta - T_o \sin \theta} \quad \ldots\ldots\ldots\ldots\ldots\ldots\ldots\ldots\ldots\ldots\ldots\ldots (39)$$

The factor of safety ratio (FSR) is defined as F/F_o and is given by:

$$FSR = \frac{\tan \beta \ (W \cos \beta + T_o \cos \theta)}{W \sin \beta - T_o \sin \theta} \quad \ldots\ldots\ldots\ldots\ldots\ldots\ldots\ldots\ldots\ldots\ldots\ldots (40)$$

For an anchor installed normal to the slope (θ=0) equation 40 reduces to

$$FSR - 1 = \frac{T_o}{W \cos \beta} \quad \ldots\ldots\ldots\ldots\ldots\ldots\ldots\ldots\ldots\ldots\ldots\ldots\ldots\ldots\ldots\ldots (41)$$

Since FSR-1 is the percentage increase in F_o and $W=\gamma z$, equation (41) reveals that the effectiveness of stabilizing infinite slopes by application of surface loads decreases as $(z \cos \beta)^{-1}$ for any applied surface load.

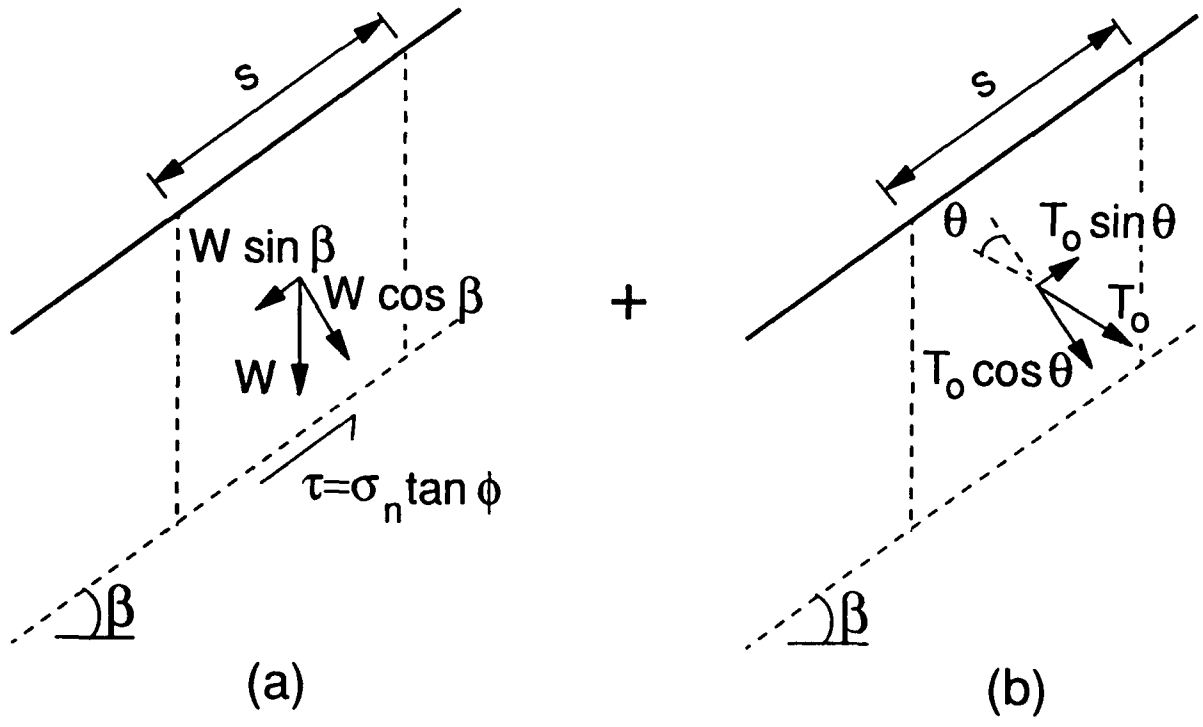

Fig. 27 Loads on Element of an Infinite Slope. (a) Soil Weight, (b) Applied Load

4.15 OPTIMUM ANCHOR ORIENTATION IN INFINITE SLOPES

A theoretical study was performed to determine the optimum orientation of anchors for development of surface loads for stabilization of slopes. Complete details of the study are given in reference [2]. Three cases as shown in Figure 28 were analyzed.

CASE I. Surface Loading without anchorage

For the hypothetical case of a surface load without anchorage, the optimum orientation for a load resultant is between 0° and 20° up from horizontal depending on the slope angle, β and the ratio $\xi = T_o/W$. An excellent approximation for θ_{opt} was given by:

$$\theta_{opt} = 90 - \beta + 60\xi \quad \ldots\ldots\ldots\ldots\ldots\ldots\ldots\ldots\ldots\ldots (42)$$

However, in most practical cases, the load can be oriented as much as 20° below optimum without significantly affecting the gain in factor of safety.

CASE II Surface Loading With End Anchorage

Since the end of a grouted anchor must be located beyond the potential sliding surface, the length requirement increases with θ. However, this increase is gradual from $\theta = 0$ to $\approx 40°$. Therefore, as a rule of thumb, $\theta \approx 45°$ strikes a practical compromise between length requirements and increases in F_n.

CASE III SURFACE LOADING WITH FRICTION ANCHORAGE

For surface loads developed through friction anchors, the optimum anchor angle and ξ/F_n were presented as a function of FSR, β and K. In general, both θ_{opt} and ξ/F_n increase with FSR and decrease with β and K. Tables of θ_{opt} and the corresponding $(\xi/F_n)_{min}$ were prepared and are given in [2]. However, a simplified linear expression for θ_{opt} is found to be given by:

$$\theta_{opt} = 47.5° - 0.7(\beta) - 9.0(K) + 8.0(FSR) \quad \ldots\ldots\ldots\ldots\ldots\ldots (43)$$

An example problem in [2] illustrated the importance of anchor orientation on the increase in slope stability.

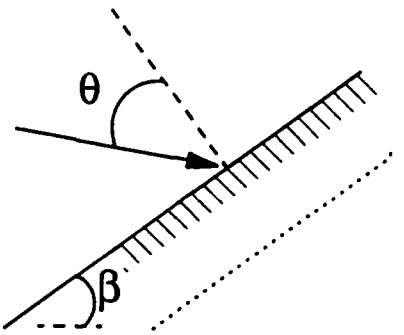

Case I Surface Load, No Anchorage

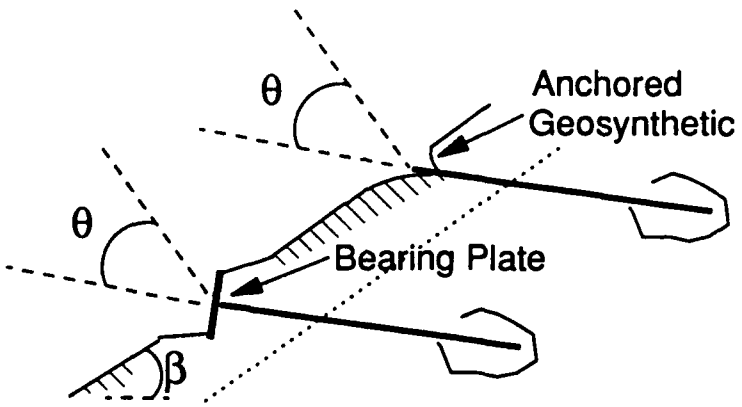

Case II End Anchorage

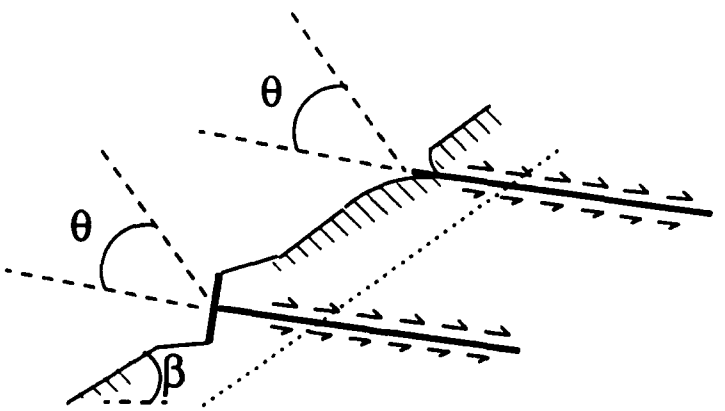

Case III Skin Friction Anchorage

Fig. 28 Types of Anchorage for Stabilization of Slopes by Surface Loading

4.16 PRACTICAL RECOMMENDATIONS FOR ANCHORED GEOSYNTHETIC SYSTEMS

1. Anchored Geosynthetic Systems are most effective for stabilization of shallow failure surfaces, typically 1 to 3 m in depth. For a uniform load applied normal to an infinite slope, the percentage increase in factor of safety is proportional to $(z \cos \beta)^{-1}$ where z is depth and β is the slope angle.

2. If an AGS is installed without "shaping" the soil at anchor locations, effective fabric curvature will only extend to a radius of approximately 0.2 to 0.3 m. As such, the fabric does not apply a uniform stress at the slope surface. However, due to coalescence of pressure bulbs, at a depth of 0.75 times the anchor spacing, the variation in normal stress on a plane parallelling the slope face varies by less than 10%.

3. To enhance fabric curvature and control erosion, anchors could be installed into preplowed furrows across the slope rather than in square or triangular spacings.

4. The use of ribbed cylindrical inclusions as anchors could greatly enhance the pullout resistance of anchors. However, the trapezoidal shape and relatively small spacing between ribs on common reinforcing rods does not permit development of full passive resistance in the soil. The optimum rib spacing for 2.5 mm x 2.5 mm square ribs on plane inclusions was found to range from 20 mm to 35 mm depending on the friction angle of the soil and the height of a "soil wall" above the ribs.

5. An undesirable aspect of ribbed anchors is that considerable loss in pullout resistance develops with cycling, especially in well graded angular and subangular sands. Therefore, the redriving of anchors to retension the geosynthetic is discouraged. The use of vibratory hammers for initial installation is useful in that the vibration will tend to densify loose sands and will also preclude the development of distinct shear surfaces during installation.

6. The geosynthetic must meet two performance criteria. First, the material must possess some ability to rebound ellastically during unloading. If the straining is highly plastic, even small upward movement of the anchor, or soil creep, will cause an unacceptable loss of tension in the fabric. Secondly, the geosynthetic must posses good stress relaxation qualities.

7. The pullout stiffness of anchors must be considered in evaluating the ability of the anchors to maintain fabric tension. Both rigid body translation and elastic deformation of the anchor are significant components of the upward displacement of the anchors.

8. A threaded anchor and nut connection is recommended over other fabric-anchor connectors for two reasons. First, the need for anchor redriving is eliminated, therefore, degradation of pullout resistance with cycling of the anchor-soil interface is eliminated. Secondly, during installation, the anchor and geosynthetic would be stressed simultaneously. Thus, the anchor will not experience a sudden application of load and uplift resulting in stress release and loss of tension in the fabric. The governing criteria for threaded anchor and nut connections is the incremental pullout stiffness rather than the pullout stiffness.

9. The optimum anchor orientation in infinite slopes is a function of the slope angle, the in-situ stresses and the desired percentage increase in factor of safety. Typically, anchors should be installed upslope at 20° to 30° from the slope normal.

5.0 PROFESSIONAL PERSONNEL ASSOCIATED WITH THE PROJECT.

Roman D. Hryciw, Asst. Prof. of Civil Engineering, served as the principal investigator (PI). He directed the research program, oversaw budgets and served as thesis advisor for the doctoral students working on the project.

Donald H. Gray, Professor of Civil Engineering, assisted with review of research results and publications. He also served on the doctoral committees of both Ph.D. candidates.

Masyhur Irsyam, Research Assistant, was instrumental in meeting objectives 1-6 and 12. His doctoral dissertation, tentatively titled "Pullout Resistance of Ribbed Inclusions In Cohesionless Soil," is scheduled for completion in 1991.

Stanley J. Vitton, Research Assistant, was instrumental in meeting objectives 7-10. His doctoral dissertation, tentatively titled "A Laboratory Investigation of Load Transfer Mechanisms in Anchored Geosynthetic Systems," is also scheduled for completion in 1991.

APPENDIX A

Completed Publications

Authorized Reprint 1990 from Geotechnical Testing Journal, March, 1990

TECHNICAL NOTE

Roman D. Hryciw[1] *and Masyhur Irsyam*[2]

Shear Zone Characterization in Sands by Carbowax Impregnation

REFERENCE: Hryciw, R. D. and Irsyam, M., **"Shear Zone Characterization in Sands by Carbowax Impregnation,"** *Geotechnical Testing Journal*, GTJODJ, Vol. 13, No. 1, March 1990, pp. 49–52.

ABSTRACT: A procedure is presented for determining the void ratio distribution of very small zones in soil by carbowax impregnation. If the wax is injected slowly, complete filling of voids occurs and volume measurements become unnecessary. Thus, even irregularly shaped volumes can easily be characterized. The technique was employed in determining the void ratio distribution in the intrarib region of a ribbed inclusion in sand during direct cyclic shearing. The measured void radios supported magnified video observations.

KEYWORDS: carbowax impregnation, void ratio, cyclic shear test, shear zone, soil structure, soil reinforcement, ribbed inclusions, sand, shear tests

Ethylene glycol, commonly known as Carbowax, has been used in geotechnical research for preparation of thin sections for fabric analysis under a microscope [*1*]. A soil specimen is partially immersed in melted Carbowax, thereby allowing the wax to flow into the soil pores while displacing the original pore water or air. One of the specimen surfaces must be exposed to the surface to allow the displaced air or water to flow from the specimen. Once in the pores, the wax is allowed to cool and solidify before cutting the specimen. The time required for wax impregnation depends on the soil's permeability and can last for several days in a clay. Carbowax is solid at room temperatures but melts at 60°C, and its specific gravity is 1.20.

Although Carbowax has been primarily used for preparing thin sections, it can also be used to determine the soil's void ratio. If the Carbowax is slowly introduced into a sand specimen from the bottom, it will displace the water or air uniformly upward, resulting in complete filling of the voids. Assuming full saturation, the void ratio becomes

$$e = \frac{V_w}{V_s} = \frac{W_w/G_w}{W_w/G_s} \tag{1}$$

where

e = void ratio,
V_w = volume of wax,
V_s = volume of solids,
W_w = weight of wax,
W_s = weight of solids,
G_w = specific gravity of wax, and
G_s = specific gravity of solids.

The weight of wax, W_w, cannot be determined directly. However, since Carbowax is miscible in water, W_w can be determined by obtaining the total specimen weight, then melting and washing the wax away with hot water and subtracting the remaining weight of solids from the total sample weight. Equation 1 can therefore be written

$$e = \frac{W_t - W_s}{W_s} \frac{G_s}{G_w} \tag{2}$$

where

W_t = total specimen weight.

The most attractive feature of carbowax impregnation for determining e is that no measurement of specimen volume is required. Therefore the void ratio of even very small, irregularly shaped volumes of soil can be found. This makes the procedure ideal for determining the void ratio distributions in localized areas of soil specimens such as in shear zones. The present paper discusses a carbowax impregnation procedure adopted by the authors to monitor changes in void ratio in the intrarib zone of a rigid ribbed inclusion in soil.

Soil-Ribbed Inclusion Interaction

Several different soil reinforcement and stabilization systems, including Reinforced Earth® [*2,3*], Anchored Earth® [*4*], geogrids [*5*], welded wire [*6*], soil nails [*7*], and the deformed rebar used in anchored geosynthetic systems [*8*], rely on the passive resistance of soil against "ribs" to provide a significant compo-

[1]Assistant professor, Department of Civil Engineering, University of Michigan, Ann Arbor, MI 48109-2125.
[2]Graduate student research assistant, Department of Civil Engineering, University of Michigan, Ann Arbor, MI 48109-2125.

0149-6115/90/0003-0049$02.50

nent of the overall pullout resistance. A study of the pullout resistance of rigid ribbed inclusions was thus undertaken.

Planer ribbed inclusions were tested in a 26.7 by 14.0 by 7.6-cm direct shear box (Fig. 1). To simulate the driving, pullout, and redriving sequences of the anchors in anchored geosynthetic systems, cyclic shearing was required.

The ribbed inclusions were installed in the central portion of a rigid plate. Loads in the plate were measured by a 2.2-kN load cell rigidly affixed to a vertical reaction plate. Four LVDTs were employed to record the horizontal motion of the shear box and vertical dilation or contraction of the soil. The load cell and LVDT readings were recorded by a microcomputer-based data acquisition system.

The direct shear box was constructed with plexiglass walls to facilitate visual observations of grain structure during testing. A videotape camera was used to enlarge the intrarib zone on a large monitor. Sand grains were colored to allow the movement of individual grains to be followed during a test.

The shearing resistance versus relative displacement for a typical test is shown in Fig. 2. The soil was an Ottawa 20-30 sand prepared at a void ratio of 0.51; the normal stress on the ribbed plate was 48.3 kPa; and the ribs were 2.5 mm high, 2.5 mm wide, and spaced 33.0 mm apart. Figure 3 shows the displacement vectors for select sand grains during three increments of relative displacement: 0 to 2.5 mm, 2.5 mm to 5.1 mm, and 5.1 mm to 7.6 mm.

Several important observations could be made concerning changes in soil fabric and the resulting effects on shearing resistance. At small displacements, prior to mobilization of peak strength, significant movement of sand grains occurs above the rib elevation. As peak strength is approached, initial failure planes develop extending from the rib corner at 30 to 50° angles from the horizontal. With increasing relative displacement (2.5 to 5.1 mm), the failure plane drops toward the horizontal. This drop in the shearing plane is accompanied by development of a postpeak residual strength. Eventually, a distinct failure plane develops along a line connecting the tops of the ribs.

A very distinct grain structure also develops in the intrarib zone. The front face of each rib imparts a "bulldozing" action on the soil grains, thereby compressing the soil skeleton and creating a zone of lower void ratio as shown in Fig. 3. At the back face of each rib, a loose grain structure develops.

The development of a loose zone at the back face has important implications for the "pullout stiffness" of an anchor. Once the direction of relative motion between soil and ribbed inclusion is reversed, the motion of the ribs is into the loose zone. It would follow that the amount of displacement required to mobilize the residual shear strength during reverse motion would depend on the compressibility and extent of this loose zone. Figure 2 reveals that on reverse motion, the maximum strength was not mobilized until approximately 13 mm of movement.

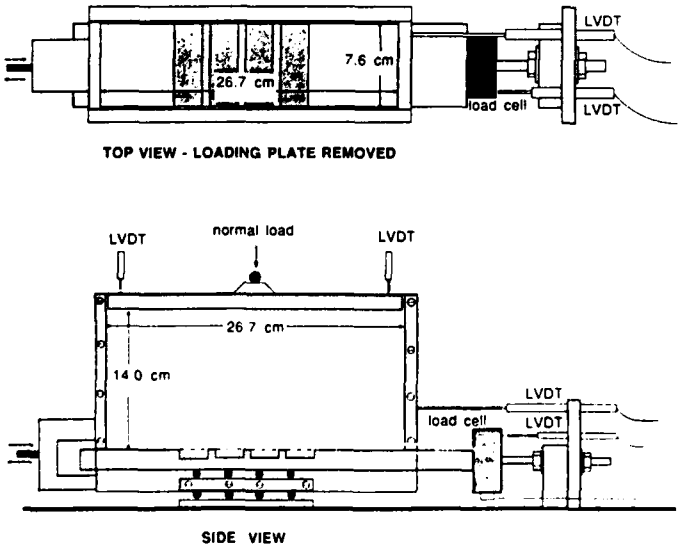

FIG. 1—*Modified direct shear device for testing ribbed inclusions.*

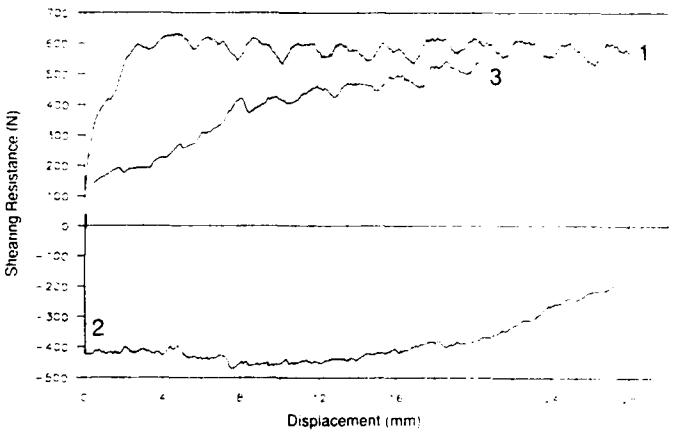

FIG. 2—*Typical shearing resistance versus relative displacement. Ottawa 20-30 sand; e = 0.51; rib size = 2.5 by 2.5 mm; rib spacing = 33 mm; normal stress = 48.3 kPa.*

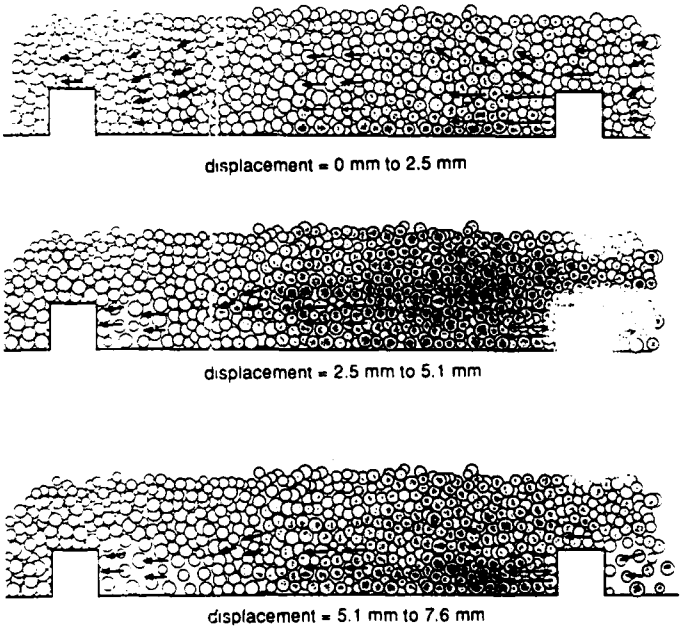

FIG. 3—*Displacement vectors for select sand grains obtained by video monitoring.*

Void Ratio Determination by Carbowax Impregnation

To verify and quantify the visual observations, actual measurement of void ratio in the intrarib zone would be required. A grain-counting procedure through the plexiglass walls was considered whereby the number of grains per unit area would provide an index parameter for void ratio. However, this approach was determined to be unacceptable for several reasons. First, the plexiglass walls afforded only a limited view of the 7.6-cm-wide specimen, therefore the specimen volume would be rather small and possibly not representative. Secondly, the plexiglass walls themselves create boundary effects that may produce a different soil fabric at the walls than in the specimen's interior. Thirdly, the counting procedure itself would be somewhat subjective because most grains were only partially visible. Finally, a procedure would still have to be developed for estimating the void ratio from the grain count.

A carbowax impregnation procedure was therefore adopted. The wax was injected through a 1.6-mm hole in the base of the ribbed inclusion as shown in Fig. 4. A heated hypodermic needle proved very useful for this task. Copper tubes carried hot water through the plate during impregnation to keep the plate warm and prevent rapid cooling of the wax. Once sufficient wax was injected to fill the pores in the intrarib zone, flow through the copper tubes was turned off and the wax was allowed to cool and solidify. After the wax hardened, the ribbed plate was removed from the testing apparatus and the soil was trimmed using a miniature power drill and a sanding adapter until a relatively flat surface, parallel to the plate but only 2 to 3 grain diameters above the ribs, remained.

To determine the distribution of void ratio at 7 to 8 equally spaced increments between adjacent ribs, the sand-wax matrix was carefully excavated using dental picks. Each specimen was approximately 2.5 by 2.5 by 76.2 mm (476 mm^3). The excavating was performed in a transparent closed container to prevent loss of sand or wax. Each sample was transferred to a miniature 19-mm-diameter sieve and weighed. Hot water was then poured over the sample to melt the wax. After drying, the remaining solids were weighed and the void ratio was computed by Eq 2.

The test was repeated three times under identical initial conditions. Each test was terminated at a different point on the load-displacement curve. These points, labelled 1, 2, and 3, are shown on Fig. 2, and the corresponding void ratio distributions are presented in Fig. 5.

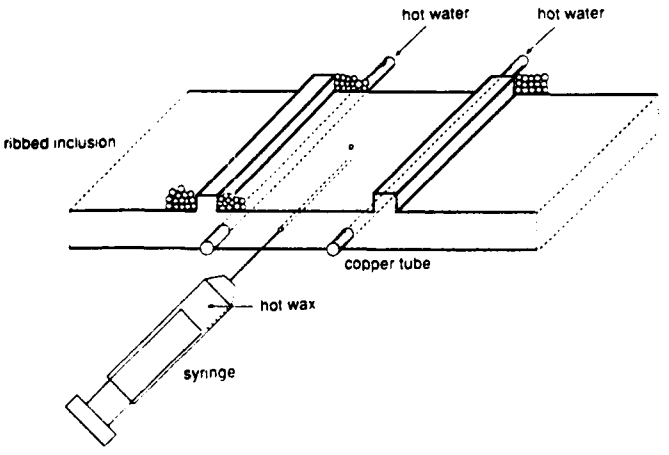

FIG. 4—*Carbowax impregnation through base of ribbed inclusion.*

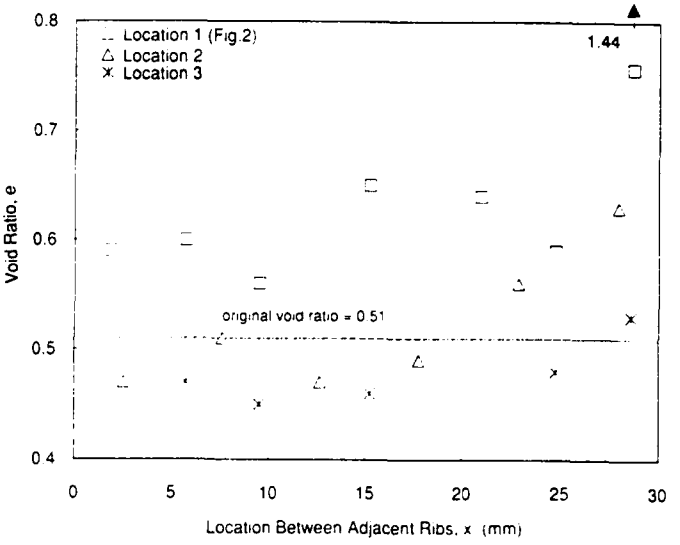

FIG. 5—*Void ratio distribution in the intrarib region during cyclic shear.*

The results indicate that the initial medium-dense soil first dilates during development of the shear plane. An extremely loose soil structure develops at the back of the rib, as confirmed by visual observations. Reversing the relative motion and returning to the zero position causes the soil to densify as grains fall by gravity into the loose zone between the ribs. The void ratio continues to decrease during a second forward motion, but the changes are not as significant as they were from the initial state to point 1 or from point 1 to point 2. Continued relative motion would probably not significantly alter the void ratio.

Conclusions

Carbowax impregnation was shown to be a useful method for determining the void ratio distribution in very small sand specimens or in very small localized areas such as in shear zones. The technique could of course be adopted for large homogeneous specimens as well, but less time-consuming techniques are available for such tasks. The carbowax procedure was adopted for determining the void ratio distribution in the intrarib region of a rigid ribbed plate in a direct shear test. The computed void ratios confirmed visual observations of an extremely loose zone developing at the back of a rib during initial forward motion of the plate.

The success of carbowax impregnation suggests that the procedure could be adopted to other research efforts where local soil structure or changes in soil structure must be assessed and quantified. In addition to determining the soil structure in shear zones, other areas of application may include quantifying soil piping and clogging in filters and compression of loose soil beneath loaded areas or around penetration testing devices.

Acknowledgements

This study was part of a research program supported and funded by the Air Force Office of Scientific Research under Grant No. AFOSR-88-0166.

References

[1] Mitchell, J. K. *Fundamentals of Soil Behavior*, John Wiley and Sons, Inc., New York, 1976.

[2] Schlosser, F. and Elias, V., "Friction in Reinforced Earth," *Proceedings*, ASCE Symposium on Reinforced Earth, Pittsburgh, Pa, 1978, ASCE, New York, pp. 735–763.

[3] Schlosser, F. and Vidal, H., "Reinforced Earth," *Bulletin de Liaison des Laboratoires Routiers-Ponts et Chaussees*, No. 41, November 1969.

[4] Murray R. T., "Studies of the Behavior of Reinforced and Anchored Earth," Ph.D. Thesis, Heriot-Watt University, Edinburgh, Scotland.

[5] Jewell, R. A., Millilgan, G. W. E., Sarsby, R. W., and Dubois, D., "Interaction Between Soil and Geogrids," *Proceedings*, Symposium on Polymer Grid Reinforcement in Civil Engineering, Science and Engineering Research Council and Netlon Limited, March 1984.

[6] Peterson, M. L., "Pullout Resistance of Welded Wire Mesh Embedded in Soil," M.S. thesis, Utah State University, Logan, Utah, 1980.

[7] Juran, I., Shafiee, S., Schlosser, F., Humbert, P., and Guenot, A., "Study of Soil-Bar Interaction the Technique of Soil Nailing," *Proceedings*, 8th European Conference on Soil Mechanics and Foundation Engineering, Helsinki, Finland, 1983.

[8] Koerner, R. M. and Robins, J. C., "In-Situ Stabilization of Soil Slopes Using Nailed Geosynthetics," *Proceedings*, Third International Conference on Geotextiles, Vienna, Austria, 1986.

ANCHOR DESIGN FOR SLOPE STABILIZATION BY SURFACE LOADING

by Roman D. Hryciw[1]

ABSTRACT

The increase in slope stability by application of discrete surface loads depends in part on the orientation of the load. For stabilization systems such as anchored geosynthetics, the load orientation cooresponds to the angle of anchor installation. A theoretical study was performed to determine the optimum orientation of such anchors to maximize the increase in slope stability. Three cases were analyzed: a hypothetical surface load without anchorage, surface load with grouted end anchorage and surface load with driven friction anchors. The last case involves the most interesting analytical solution since the optimum anchor orientation is a function of the slope geometry, the in-situ stresses and the desired increase in factor of safety. The required length and spacing of anchors depend, in addition to the above factors, on the anchor diameter, the internal friction angle of the soil, the soil-anchor interface friction, the strength of the geosynthetic and the depth of the potential failure surface. A simplified equation is given for the anchor orientation and a design chart is presented for determining spacing and length requirements. An example problem illustrates the importance of proper anchor orientation.

KEYWORDS: Slope Stability, Slope Stabilization, Soil Mechanics, Tiebacks, Anchored Geosynthetics, Soil Anchors

[1] Asst. Prof., University of Michigan, Ann Arbor, MI 48109

INTRODUCTION

Relatively shallow soils on hazardous slopes may be stabilized by application of discrete loads at the slope face. The word "discrete" is used to distinguish such loads from the continuous support provided by retaining structures. The loads are usually developed by anchorage of steel rods within the soil mass and tensioning at the surface against a bearing plate, concrete pad (Pearlman, personal communication), tensioned geosynthetic (Koerner, 1984, 1985, 1986) or geogrid (Greenwood, 1985). The anchorage is achieved by either grouting the rods below the potential sliding surface or, if the rods are driven, by frictional resistance to pullout along the length of the rod. Greenwood (1985) has used driven duck-billed anchors for stabilization of a soft clay by geogrids. Bearing plates with end anchorage are closely related to tiebacks for retaining walls.

While the natural inclination is to install anchors normal to the slope in order to intersect potential failure surfaces with minimum anchor lengths, this orientation is far from optimum for increasing slope stability. The present paper will analyze the optimum orientation and length requirements for the anchors. The three cases shown in Figure 1 will be studied. In Case I, a surface loading comes from sources external to the soil mass being stabilized. Although this case is somewhat hypothetical, it will illustrate the importance of load orientation and serves as a necessary intermediate step for cases II and III. In Case II, end anchorage is considered. Here, the anchored end must be

installed beyond the potential sliding zone and with sufficient soil cover to prevent pullout. In the third and analytically most interesting case, anchorage is achieved by frictional resistance to pullout along the length of the anchor.

Surface loading is most attractive for stabilization of shallow failure surfaces to a depth of approximately 10 ft (3 m). With increasing depth, an applied surface load becomes a smaller fraction of the total load on a failure surface. To stabilize deep failure surfaces, the surface load requirements would be such as to necessitate a large bearing pad area and thus a continuous retaining structure would become more attractive.

When the length of a failure surface is greater than approximately twenty times its depth, an infinite slope analysis may be performed (Gonsior et al., 1974). Since discrete surface loads would primarily be used for stabilization of shallow failure surfaces, an infinite slope analysis was implemented in the present study. Soils were assumed to be cohesionless and uniform throughout the slope. A limiting equilibrium approach was taken for stability analysis.

Several other assumptions are made. The bending stiffness of the anchors is neglected and therefore the load resultant acts parallel to the axis of the anchor. The anchor spacing to diameter ratios are typically too large (>100) to develop a coherent soil mass. Therefore, while the presence of an anchor increases the shear resistance in the immediate vicinity of the anchor, the shearing resistance of anchors does not contribute

significantly to the overall stability of the slope. This is fundamentally different from "soil nailing" where the spacing to diameter ratios are less than 25 and the shearing and bending resistances play crucial roles in the stabilization. The other principle difference between soil nailing and ground anchorage is that while anchors are stressed, soil nails are not except for slight tensioning to provide adequate seating of shotcrete or other facing elements.

Finally, the assumption is made that loads are distributed uniformly at the surface. While this is clearly not the case, the validity of the assumption increases as the ratio of depth to spacing increases. As a rule of thumb, if the depth is greater than the spacing, the surface loading can be assumed to be uniformly distributed.

CASE I SURFACE LOADING

The factor of safety against sliding for infinite slopes is quantified by the ratio of forces resisting shear to the driving forces on a potential sliding surface as shown in Figure 2a. For cohesionless, dry soils on infinite slopes with no external loads, the expression takes the form:

$$F_o = \frac{W \cos \beta \tan \phi}{W \sin \beta} = \frac{\tan \phi}{\tan \beta} \quad \text{.....(1)}$$

where F_o=factor of safety (prior to stabilization), W=the weight of the slice shown in Figure 2a, β=slope angle and ϕ= angle of internal friction of the soil. If external loads of

magnitude T_o are applied in a square pattern of spacing s x s at an angle θ to the slope normal as shown in Figure 2b, eq. 1 may be modified as:

$$F = \frac{(W \cos \beta + T_o \cos \theta)\tan \phi}{W \sin \beta - T_o \sin \theta} \quad \ldots\ldots\ldots\ldots\ldots\ldots\ldots\ldots\ldots\ldots (2)$$

Taking the derivative of eq. 2 with respect to θ and setting it to zero yields:

$$\frac{dF}{d\theta} = 0 = \frac{W \cos \theta_{opt} \cos \beta - W \sin \theta_{opt} \sin \beta + T_o}{(W \sin \beta - T_o \sin \theta_{opt})^2} \quad \ldots\ldots\ldots (3)$$

where θ_{opt} = the θ at which F is maximized. Since (W sin β - T_o sin θ_{opt}) cannot go to infinity the only solution for eq. 3 is

$$0 = W \cos \theta_{opt} \cos \beta - W \sin \theta_{opt} \sin \beta + T_o \quad \ldots\ldots\ldots\ldots\ldots\ldots (4)$$

or

$$\xi = \frac{T_o}{W} = \sin \theta_{opt} \sin \beta - \cos \theta_{opt} \cos \beta \quad \ldots\ldots\ldots\ldots\ldots\ldots (5)$$

Although eq. 5 cannot be written explicitly for θ_{opt}, when $10° < \beta < 50°$ and $0 < \xi < 0.5$ an excellent approximation is found by:

$$\theta_{opt} = 90 - \beta + 60\xi \quad \ldots\ldots\ldots\ldots\ldots\ldots\ldots\ldots\ldots\ldots\ldots\ldots\ldots\ldots (6)$$

Eq. 6 is good to within ±0.5° of the exact solution found by eq. 5. It is interesting to note that as ξ approaches 0, θ_{opt} tends to 90-β, that is, a horizontal load. As ξ increases, the optimum load orientation moves upward from horizontal.

Equation 2 may also be written as:

$$F = \frac{\tan \beta \ (W \cos \beta + T_o \cos \theta)}{W \sin \beta - T_o \sin \theta} \quad \ldots\ldots\ldots\ldots\ldots\ldots\ldots\ldots\ldots\ldots (7)$$

or

$$FSR = \frac{F}{F_o} = \frac{\sin \beta + \xi \cos \theta \tan \beta}{\sin \beta - \xi \sin \theta} \quad \ldots\ldots\ldots\ldots\ldots\ldots\ldots\ldots\ldots\ldots (8)$$

where FSR = the ratio of the new factor of safety after stabilization to the original factor of safety.

Equation 8 is presented graphically in Figure 3. To increase slope stability by a factor of FSR, one would read across from the FSR axis to the optimum curve. This point represents the minimum ξ and the corresponding required orientation.

It is important to note in figure 3 that ξ is rather insensitive to θ near the optimum for most practical applications where FSR $\leq$ 1.3 is required. In fact, θ can vary by $\pm 20^\circ$ from the optimum without appreciably increasing the required ξ.

CASE II SURFACE LOADING WITH END ANCHORAGE

For end anchored bolts, or tiebacks, the grouted portion must lie beyond the potential failure surface. Referring to Fig. 4, for an anchor oriented at angle θ to the slope normal, to stabilize a potential sliding surface at depth z, the anchor length requirement would be:

$$L = \frac{\cos \beta}{\cos \theta} z \quad \ldots\ldots\ldots\ldots\ldots\ldots\ldots\ldots\ldots\ldots\ldots\ldots\ldots\ldots\ldots\ldots (9)$$

plus an additional grouted length L_b which depends on soil conditions (Weatherby and Nicholson, 1982). The requirement for L is illustrated in Figure 5. Clearly, the shortest anchor would correspond to θ=0°. However, θ=0° also requires the greatest ξ. Fortunately, L/z increases very gradually as θ increases from 0° to ≈40°. Combined with the previous observation that ξ does not increase appreciably until θ is more than 20° below it's optimum, we find the best orientation for anchors considering both ξ and L/z to be between θ=30° and 50°.

A second requirement for end anchorage is that the grouted end be under sufficient soil cover, z_{min} to develop adequate pullout resistance. As a rule of thumb, z_{min}=15 ft (4.6 m) is commonly recommended (Weatherby and Nicholson, 1982). If $z>z_{min}$ this criteria is automatically satisfied. If $z<z_{min}$, L must be increased or θ must be decreased. Acceptable combinations of L and θ may be found by multiplying the L/z value given in Figure 5 by z_{min}.

While it would be difficult to theoretically optimize the anchor orientation since material and installation costs would contribute to the final selection of θ, a sensitivity analysis could be performed utilizing Fig. 5 to assist in the final selection of anchor length, orientation and tensioning load.

CASE III SURFACE LOADING WITH FRICTION ANCHORAGE

The third case, that of frictional anchorage is analytically the most complicated due to the dependence of pullout resistance

on anchor length. A second cartesian coordinate system x'y'z' is adopted in which the z'-axis is colinear with the anchor and with origin at the ground surface as shown in Fig. 6. The stresses in an infinite slope may be determined by combining the elasticity solutions for infinite triangular loads (Gray, 1936) with the stresses beneath a horizontal surface as illustrated in Figure 7. The stresses at any point within an infinite slope are thus given by:

$$\sigma_z = \gamma z + \gamma x \tan\beta \quad \text{.....(10a)}$$

$$\sigma_x = K_x \gamma z + \gamma x \tan\beta \quad \text{.....(10b)}$$

$$\sigma_y = K_y \gamma z + 2\gamma\nu x \tan\beta \quad \text{.....(10c)}$$

$$\tau_{xz} = \gamma z \tan\beta \frac{(2\alpha-\pi)}{\pi} \quad \text{.....(10d)}$$

$$\tau_{yx} = \tau_{yz} = 0 \quad \text{.....(10e)}$$

where K_x and K_y = coefficients of lateral earth pressure in the x and y directions, γ= unit weight of soil and ν=Poisson's ratio.

If x'=0 and y'=0, corresponding to the anchor axis, we have:

$$\alpha = \frac{\pi}{2} + \theta + \beta \quad \text{.....(11a)}$$

$$x = z' \sin(\theta+\beta) \quad \text{.....(11b)}$$

and

$$z = z' \cos(\theta+\beta) \quad \text{.....(11c)}$$

Combining eqs. 10 and 11 yields:

$$\sigma_z = \gamma z' \cos(\theta+\beta) + \gamma z' \sin(\theta+\beta)\tan\beta \quad \text{.....(12a)}$$

$$\sigma_x = K_x \gamma z' \cos(\theta+\beta) + \gamma z' \sin(\theta+\beta)\tan\beta \quad \text{.....(12b)}$$

$$\sigma_y = K_y \gamma z' \cos(\theta+\beta) + 2\gamma\nu z' \sin(\theta+\beta)\tan\beta \quad \text{.....(12c)}$$

$$\tau_{xz} = 2\gamma z' \cos(\theta+\beta)\tan\beta \frac{(\theta+\beta)}{\pi} \quad \text{.....(12d)}$$

The stress normal to the anchor in the xz-plane is given by:

$$\sigma_{x'} = \frac{\sigma_x + \sigma_z}{2} + \frac{\sigma_x - \sigma_z}{2} \cos 2(\theta+\beta) + \tau_{xy} \sin 2(\theta+\beta) \quad \text{.....(13a)}$$

while the stress normal to the anchor in the yz-plane is

$$\sigma_{y'} = \sigma_y \quad \text{.....(13b)}$$

The average normal stress on the anchor at z′ is then:

$$\sigma_n = \frac{\sigma_{x'} + \sigma_{y'}}{2} \quad \text{.....(14)}$$

Assuming that $K_x = K_y = K$ and that $\nu = 0.25$, equations 12, 13 and 14 may be combined to give:

$$\sigma_n = F_n \gamma z' \quad \text{.....(15)}$$

where F_n = a stress factor given by:

$$F_n = \frac{1}{4}\left[(1+3K)\cos(\theta+\beta) + 3\tan\beta\sin(\theta+\beta) + (K-1)\cos(\theta+\beta)\cos 2(\theta+\beta) + \frac{4(\theta+\beta)}{\pi}\cos(\theta+\beta)\tan\beta\sin 2(\theta+\beta)\right] \quad \text{.....(16)}$$

Examples of the relationship between F_n, K, θ and β are shown in Figure 8.

The maximum load, T_o that could be applied at the surface is the pullout resistance of the anchor, or

$$T_o = \int_0^L 2\pi r\ \tau_{max}\ dz' \quad \text{.......................................(17)}$$

where r=anchor radius, L=anchor length and

$$\tau_{max} = \sigma_n \tan\delta \quad \text{.......................................(18)}$$

where δ=the interface friction angle between anchor and soil. Combining eqs. 15, 17 and 18 and performing the integration yields

$$T_o = \pi r \tan(\delta) F_n \gamma L^2 \quad \text{.......................................(19)}$$

Returning to equation 8, we may solve for ξ to find:

$$\xi = \frac{T_o}{W} = \frac{(FSR-1)\ \sin\beta}{\cos\theta\ \tan\beta + (FSR-1)\sin\theta} \quad \text{..........................(20)}$$

If anchor points are installed in a square pattern, s x s, we find:

$$\xi = \frac{T_o}{W} = \frac{\pi r \gamma \tan(\delta) F_n L^2}{z \gamma s^2 \cos\beta} \quad \text{.................................(21)}$$

It is interesting to note that ξ is independent of the soil unit weight. Eq. 21 can also be rearranged as:

$$\frac{L}{s} = \left[\frac{z \cos\beta}{\pi r \tan\delta} \frac{\xi}{F_n} \right]^{1/2} \quad \text{.....(22)}$$

The optimum anchor orientation would clearly be the one that achieved a desired FSR at minimum L/s. For a given set of variables r, δ, z and β, this requires minimizing ξ/F_n. While low values of ξ occur at $\theta \simeq 50°$ to 70° (figure 3), high F_n's occur when $\theta \simeq 0°$ to 20° (figure 8). Therefore the minimum ξ/F_n, hereafter termed $(\xi/F_n)_{min}$, will lie in between these ranges. Since ξ is a function of β, θ and FSR while F_n is a function of β, θ and K, an itterative procedure is required to arrive at θ_{opt} and $(\xi/F_n)_{min}$. For convenience, a summary of θ_{opt} and $(\xi/F_n)_{min}$ are therefore provided in Tables 1 and 2 for various K, β and FSR.

Inspection of Table 1 reveals that θ_{opt} is almost linearly related to K, β and FSR for typical ranges of these variables. A remarkably good linear expression for θ_{opt} is given by:

$$\theta_{opt} = 47.5° - 0.7\beta - 9K + 8FSR \quad \text{.....(23)}$$

where θ_{opt} and β are in degrees. The standard deviation of the difference between the exact θ_{opt} and that given by eq. 23 is only 0.33° and the maximum difference is less than 1°. Thus, equation 23 may be used with a high degree of confidence for determining the optimum anchor orientation.

Table 2 shows that for $25° < \beta < 40°$, $(\xi/F_n)_{min}$ is not very sensitive to β. Since the required L/s is related to $\sqrt{(\xi/F_n)_{min}}$, it is notable that the difference between the actual $\sqrt{(\xi/F_n)_{min}}$

and the average $\overline{(\xi/F_n)_{min}}$ for $25°<\beta<40°$ is less than 3%. Therefore, Figure 9 shows the average $(\xi/F_n)_{min}$ for $25°<\beta<40°$ as a function of K and FSR. For $\beta>40°$, Table 1 must be used.

DESIGN EXAMPLE

A $\beta=30°$ slope with 7 ft (2.1 m) of loose sand ($\phi=31°$, $\gamma=100$ pcf (15.7 kN/m^3)) is to be stabilized by an anchored geosynthetic. The maximum load that can be transferred at each geosynthetic-anchor connection is limited by the strength of the geosynthetic, in this example we will use 2500 lbs. (11.1 kN). The anchors will be driven #4 reinforcing bars. The assumed coefficient of lateral earth pressure is 0.6 and $\delta=35°$ (δ is actually greater than ϕ because of the passive resistance of the soil to ribs on a deformed reinforcing rod). An F of 1.3 is desired. The optimum anchor orientation and required L must be determined.

From the statement of the problem:

$$FSR = \frac{F}{F_o} = F\,\frac{\tan\beta}{\tan\phi} = 1.3\,\frac{\tan 30°}{\tan 31°} = 1.25$$

By eq. 23 (or Table 1):

$$\theta_{opt} = 47.5-0.7(30)-9(0.6)+8(1.25) = 31.1° \text{ say } 31°$$

From fig. 9 or Table 2 for $\beta=30°$, FSR=1.25 and K=0.6 we find $(\xi/F_n)_{min}=0.133$. Then by eq. 22:

$$\frac{L}{s} = \left[\frac{z\cos\beta}{\pi r\tan\delta}\ \frac{\xi}{F_n}\right]^{1/2}$$

$$= \left[\frac{(7\text{ ft.})\cos(30°)}{\pi(0.5/12\text{ ft.})\tan(35°)}(0.133)\right]^{1/2} = 2.97$$

From eq. 21 (or fig. 3) for θ_{opt}=31° we have ξ=0.110. Since ξ also =T_o/W and $W=z\gamma s^2\cos\beta$, the maximum anchor spacing is computed as:

$$s = \left[\frac{T_o}{z\gamma\xi\cos\beta}\right]^{1/2} = \left[\frac{2500\text{ lbs}}{(7\text{ ft.})(100\text{ pcf})(0.110)\cos(30°)}\right]^{1/2} = 6.1\text{ ft.}$$

For an anchor spacing of 6.1 ft (1.9 m), the required length will be (6.1)(2.97)=18.1 ft (5.5 m).

The implications of installing 18.1 ft anchors at θ other than θ_{opt} for stabilization of this slope are illustrated in Fig. 10. Notice should be taken that if 18.1 ft anchors were driven perpendicular to the slope (θ=0), the FSR would only be 1.13 while at θ_{opt} FSR= 1.25. For $\theta<\theta_{opt}$, to achieve the FSR represented by the dashed line in fig. 10, T_o would have to be greater than the allowable 2,500 lbs., therefore, the solid line indicates the FSR for T_o maintained at 2,500 lbs.

It should also be noted that the anchor length requirement can be reduced by decreasing the anchor spacing. For a 5.0 ft (1.5 m) spacing the required anchor length at θ_{opt} would be only (5.0)(2.97)=14.9 ft (4.5 m).

CONCLUSIONS

A theoretical study was performed to determine the optimum orientation of anchors for development of surface loads for stabilization of slopes. For the hypothetical case of a surface load without anchorage, the optimum orientation for a load resultant is between 0° and 20° up from horizontal depending on the slope angle, β and the ratio $\xi = T_o/W$. An excellent approximation for θ_{opt} was given by equation 6. However, in most practical cases, the load can be oriented as much as 20° below optimum without significantly affecting the gain in factor of safety.

The last observation has important implications for the second case analyzed, that of end anchorage. Since the grouted end must be located beyond the potential sliding surface, the length requirement increases with θ. However, this increase is gradual from $\theta = 0$ to $\simeq 40°$. Therefore, as a rule of thumb, $\theta \cong 45°$ strikes a practical compromise between length requirements and increases in F. If z is less than the soil cover requirement, z_{min}, a lower θ or higher L may be needed.

For surface loads developed through friction anchors, the optimum anchor angle and ξ/F_n were presented as a function of FSR, β and K. In general, both θ_{opt} and ξ/F_n increase with FSR and decrease with β and K. Tables of θ_{opt} and the corresponding $(\xi/F_n)_{min}$ were prepared. A simplified linear expression for θ_{opt} was given by equation 23. An example problem illustrated the importance of anchor orientation on the increase in slope stability.

Acknowledgements

This study was part of a research program supported and funded by the Air Force Office of Scientific Research under Grant No. AFOSR-88-0166.

Appendix I. ——References

Gonsior, M.J., Hartsog, W.S. and Martin, G.L. (1974) "Failure Surfaces in Infinite Slopes", USDA Forest Service Research Paper INT-150, 33 pp.

Gray, H. (1936) "Stress Distribution in Elastic Solids", Proc. of the First International Conference on Soil Mechanics and Foundation Engineering, Harvard University, Cambridge Mass., vol. II, 157-168.

Greenwood, J. R. (1985) "Geogrids and Anchors for Slope Stabilization-Simple Method of Analysis," Discussion, Proceedings of the 11th International Conference on Soil Mechanics and Foundation Engineering, Vol. 5, pp. 2770-2771.

Koerner, R. M. (1984) "In-Situ Soil Slope Stabilization Using Anchored Nets," Low Cost & Energy Saving Construction Materials Conference Proceedings, Rio De Janiero, Brazil, 465-478.

Koerner, R. M (1985) "Slope Stabilization Using Anchored Geotextiles and/or Geogrids," Proc. Special Geotechnical Engineering for Roads and Bridges, Harrisburg, PA.

Koerner, R. M. and Robins, J. C. (1986) "In-Situ Stabilization of Soil Slopes Using Nailed Geosynthetics," Proc. of the Third International Conference on Geotextiles, Vienna, Austria, 395-400.

Pearlman, S. (1990). Personal Communication, Nicholson Construction Co., Bridgeville, PA.

Weatherby, D. E. and Nicholson, P. J. (1982) "Tiebacks Used For Landslide Stabilization", Proc. of ASCE Sessions on Application of Walls to Landslide Control Problems, Las Vegas, NV. April 29, pp. 44-60.

Appendix II. ——Notation

F = factor of safety
F_n = normal stress factor
F_o = original factor of safety
FSR = F/F_o
K = coefficient of lateral earth pressure
L = anchor length
L_{req} = required anchor length
r = anchor radius
s = anchor spacing
T_o = applied surface load per slice
x,y,z = cartesian coordinate system (z=down)
$x'y'z'$ = cartesian coordinate system (z' coincides with anchor)
W = weight of slice

β = slope angle
γ = soil unit weight
δ = soil-anchor friction angle
ϕ = angle of internal friction of soil
θ = angle of anchor to slope normal
θ_{opt} = optimum anchor angle
ξ = T_o/W.
σ = stress
σ_n = average normal stress on the anchor
τ_{max} = maximum shearing resistance between soil and anchor

TABLE 1. Optimum Anchor Orientations, θ_{opt}

K	FSR	θ_{opt}				
		β=25°	β=30°	β=35°	β=40°	β=45°
0.4	1.0	35.4	31.6	27.6	23.6	19.6
0.4	1.1	36.1	32.4	28.4	24.6	20.5
0.4	1.2	36.6	33.0	29.3	25.4	21.5
0.4	1.3	37.2	33.6	30.0	26.2	22.4
0.4	1.4	37.7	34.2	30.6	26.9	23.4
0.4	1.5	38.0	34.6	31.1	27.7	23.9
0.6	1.0	33.1	29.1	25.6	21.7	17.9
0.6	1.1	33.9	30.2	26.5	22.7	19.0
0.6	1.2	34.5	30.9	27.4	23.6	19.9
0.6	1.3	35.0	31.6	28.0	24.4	20.7
0.6	1.4	35.5	32.1	28.8	25.2	21.6
0.6	1.5	35.9	32.7	29.4	25.9	22.3
0.8	1.0	31.0	27.3	23.7	19.9	16.2
0.8	1.1	31.8	28.4	24.6	20.9	17.2
0.8	1.2	32.5	29.1	25.5	21.9	18.2
0.8	1.3	33.0	29.8	26.3	22.8	19.1
0.8	1.4	33.6	30.4	27.1	23.6	20.0
0.8	1.5	34.1	31.0	27.7	24.3	20.8
1.0	1.0	29.0	25.5	21.9	18.2	14.6
1.0	1.1	29.9	26.5	23.0	19.3	15.6
1.0	1.2	30.7	27.3	23.8	20.3	16.7
1.0	1.3	31.3	28.0	24.7	21.2	17.7
1.0	1.4	31.9	28.7	25.5	22.0	18.6
1.0	1.5	32.4	29.3	26.1	22.8	19.3

TABLE 2. ξ/F_n at Optimum Anchor Orientation

K	FSR	$\left[\frac{\xi}{F_n}\right]_{min}$				
		β=25°	β=30°	β=35°	β=40°	β=45°
0.4	1.0	0	0	0	0	0
0.4	1.1	0.061	0.062	0.060	0.057	0.050
0.4	1.2	0.116	0.117	0.114	0.108	0.975
0.4	1.3	0.164	0.168	0.165	0.156	0.142
0.4	1.4	0.208	0.214	0.211	0.201	0.185
0.4	1.5	0.248	0.256	0.254	0.243	0.225
0.6	1.0	0	0	0	0	0
0.6	1.1	0.056	0.057	0.056	0.053	0.048
0.6	1.2	0.106	0.109	0.108	0.102	0.093
0.6	1.3	0.151	0.156	0.155	0.148	0.136
0.6	1.4	0.192	0.199	0.199	0.192	0.177
0.6	1.5	0.228	0.239	0.240	0.232	0.216
0.8	1.0	0	0	0	0	0
0.8	1.1	0.051	0.053	0.052	0.050	0.046
0.8	1.2	0.098	0.101	0.101	0.097	0.089
0.8	1.3	0.139	0.146	0.146	0.141	0.131
0.8	1.4	0.177	0.186	0.188	0.182	0.170
0.8	1.5	0.211	0.223	0.227	0.221	0.208
1.0	1.0	0	0	0	0	0
1.0	1.1	0.047	0.049	0.049	0.047	0.044
1.0	1.2	0.090	0.095	0.095	0.092	0.085
1.0	1.3	0.128	0.136	0.138	0.134	0.125
1.0	1.4	0.163	0.174	0.177	0.173	0.163
1.0	1.5	0.195	0.209	0.214	0.211	0.199

LIST OF FIGURES

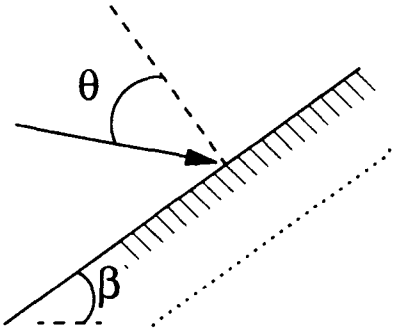

Case I Surface Load, No Anchorage

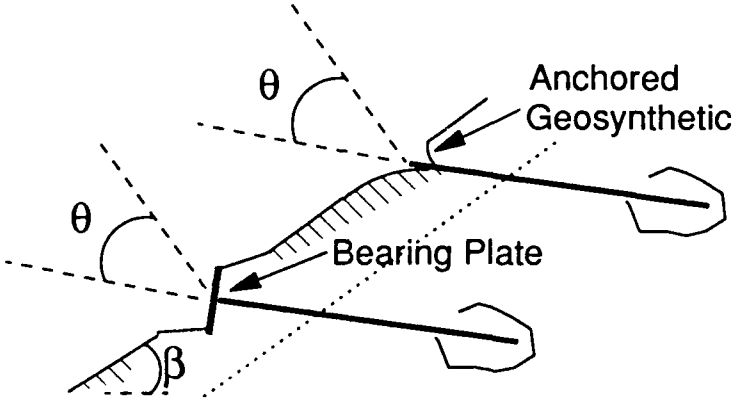

Case II End Anchorage

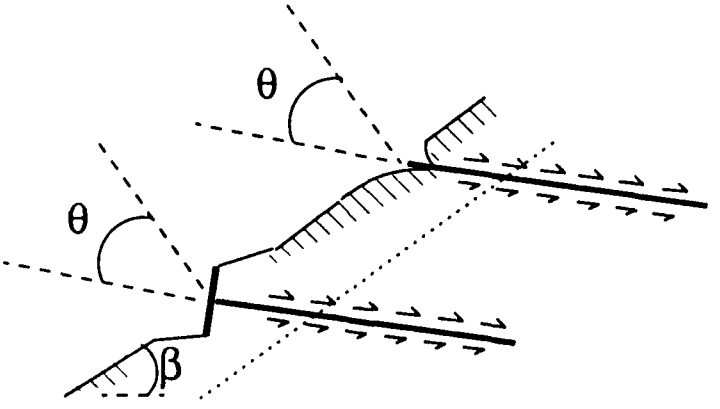

Case III Skin Friction Anchorage

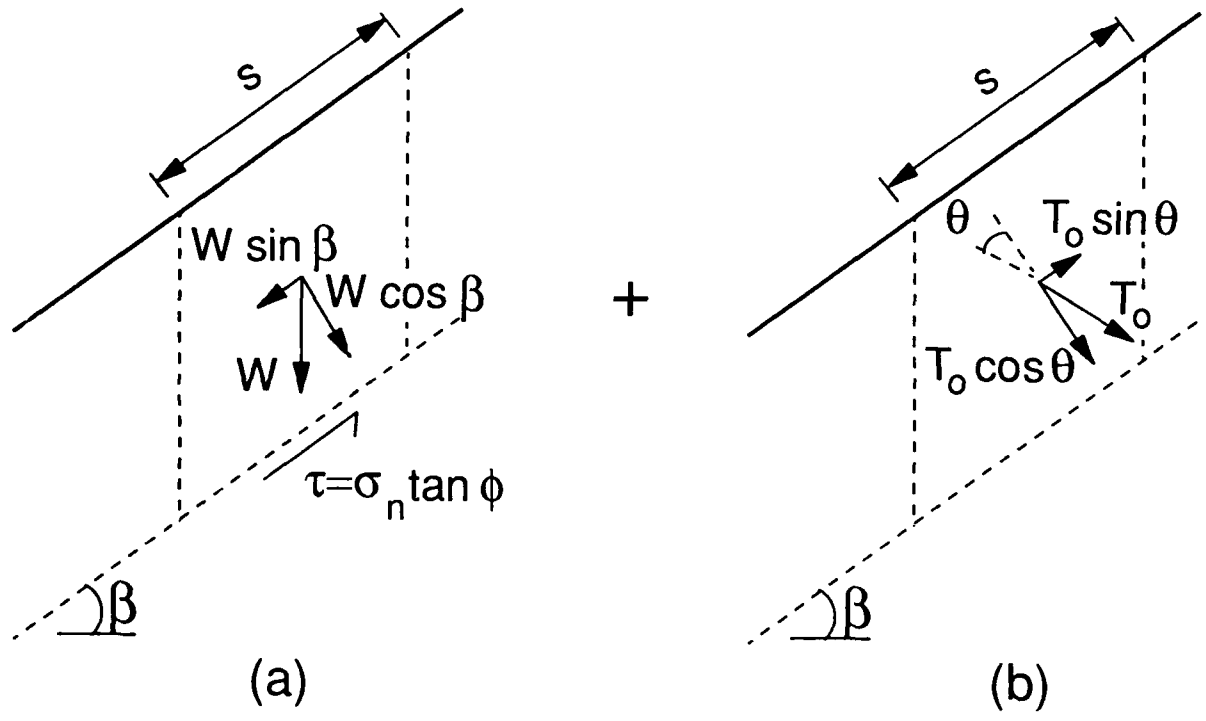
s
W sin β
W cos β
W
τ=σ n tan ϕ
β
(a)
+
s
θ
T o sin θ
T o
T o cos θ
β
(b)

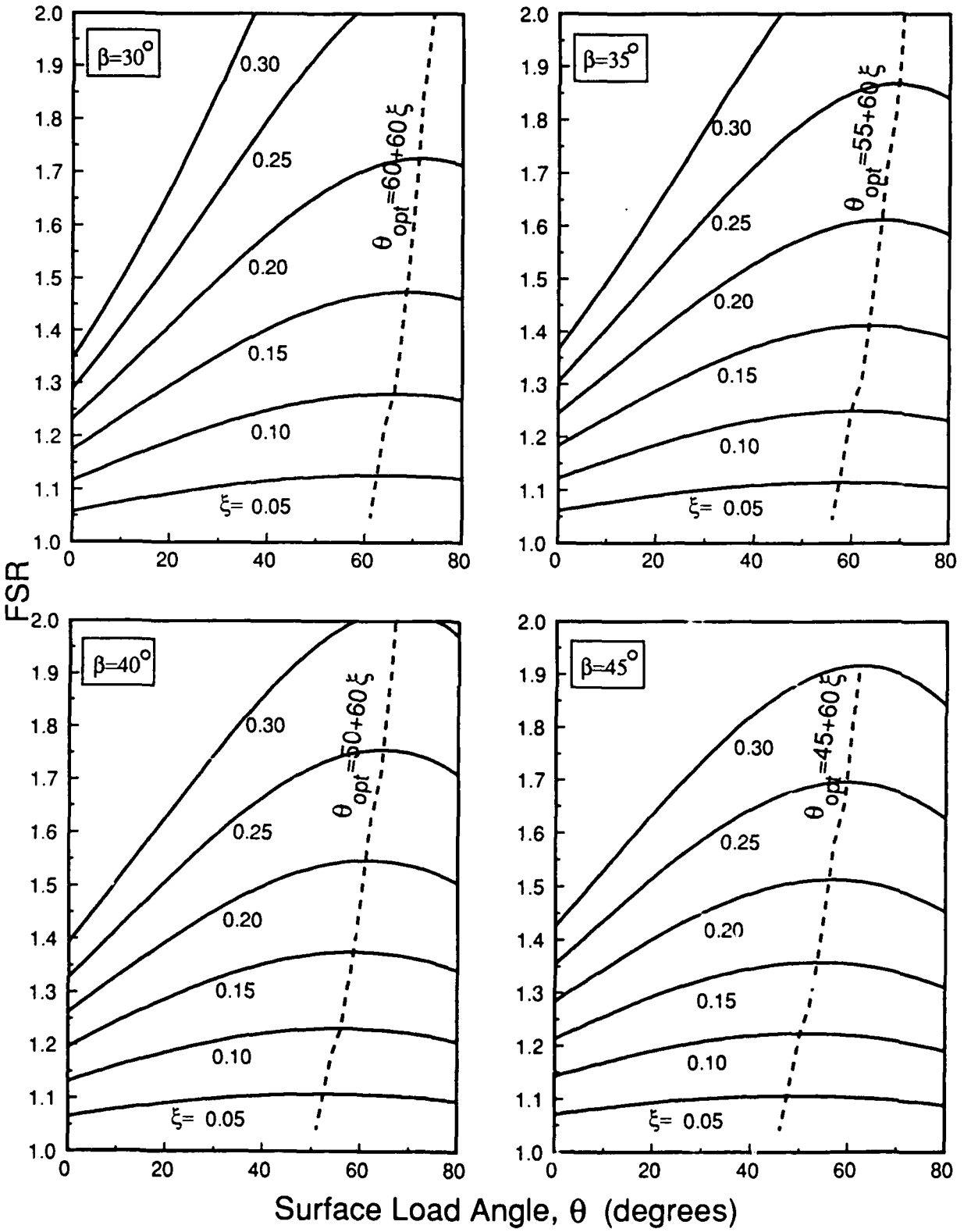
β=30°
β=35°
β=40°
β=45°
0.30
0.25
0.20
0.15
0.10
ξ= 0.05
θopt=60+60ξ
θopt=55+60ξ
θopt=50+60ξ
θopt=45+60ξ
FSR
Surface Load Angle, θ (degrees)
1.0
1.1
1.2
1.3
1.4
1.5
1.6
1.7
1.8
1.9
2.0
0
20
40
60
80

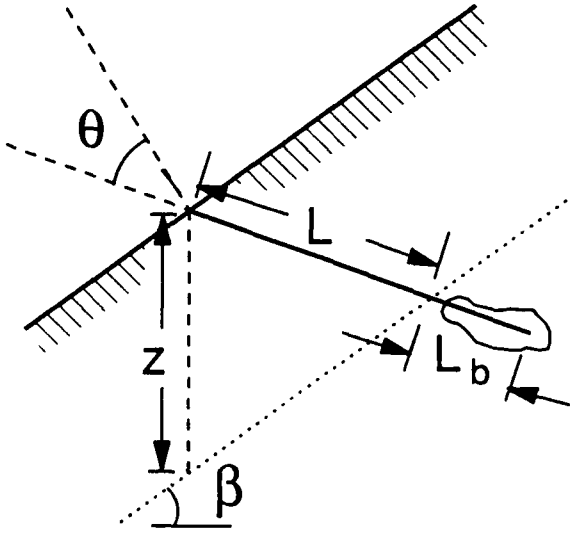
θ
L
z
L_b
β

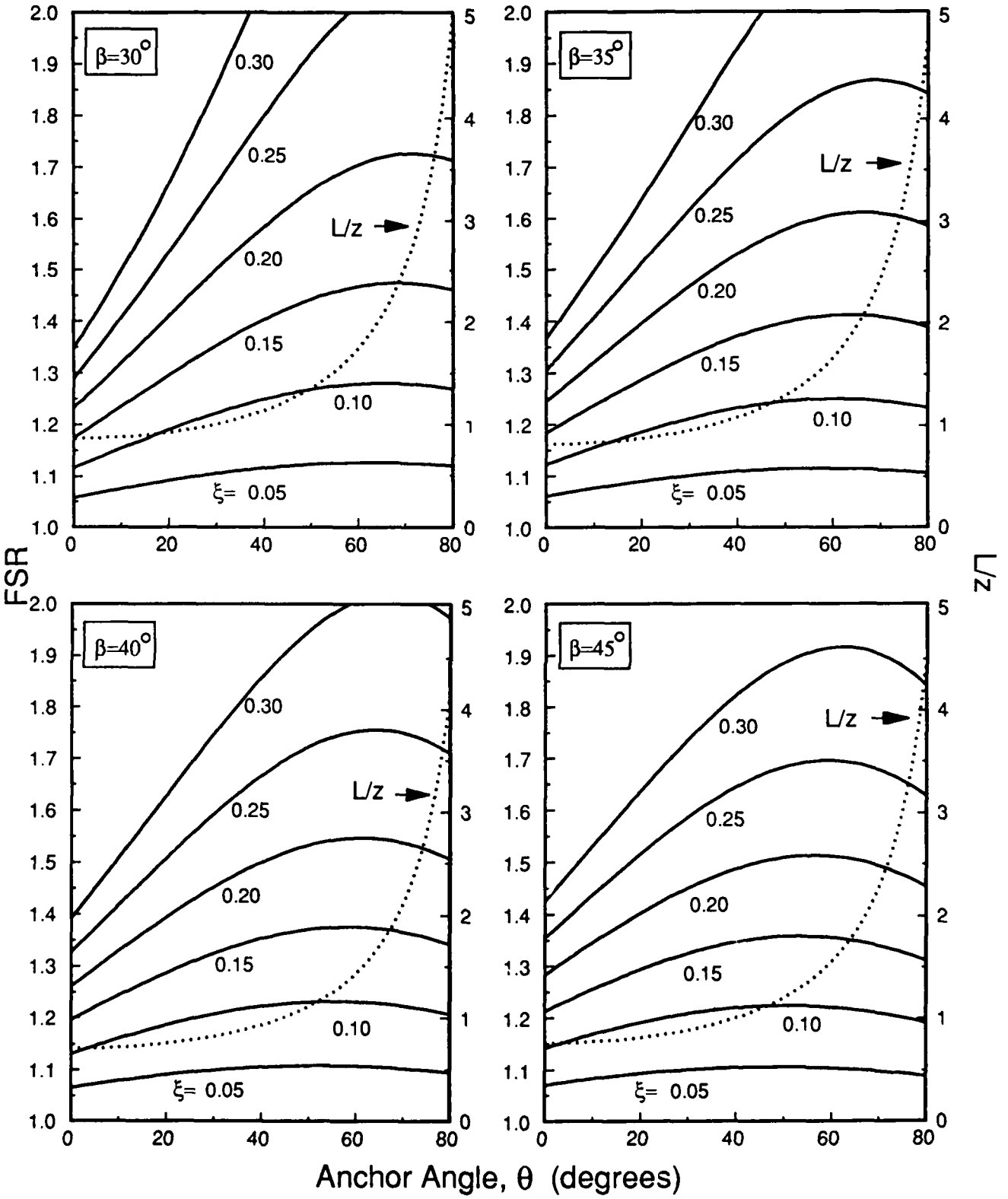
β=30°
β=35°
β=40°
β=45°
0.30
0.25
0.20
0.15
0.10
ξ= 0.05
L/z
FSR
L/z
Anchor Angle, θ (degrees)

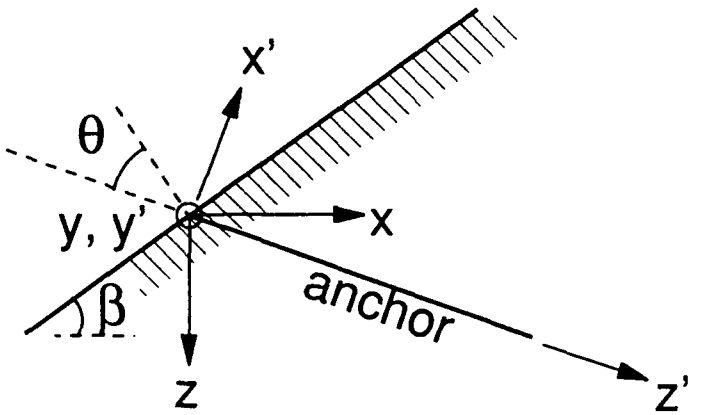
x'
θ
y, y'
x
anchor
β
z
z'

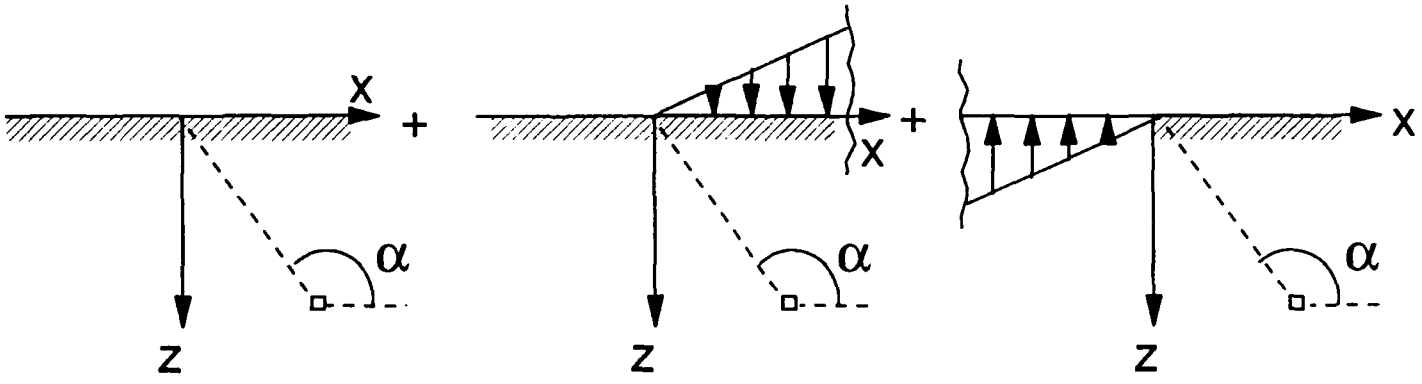
x
+
α
z
x
+
α
z
x
α
z

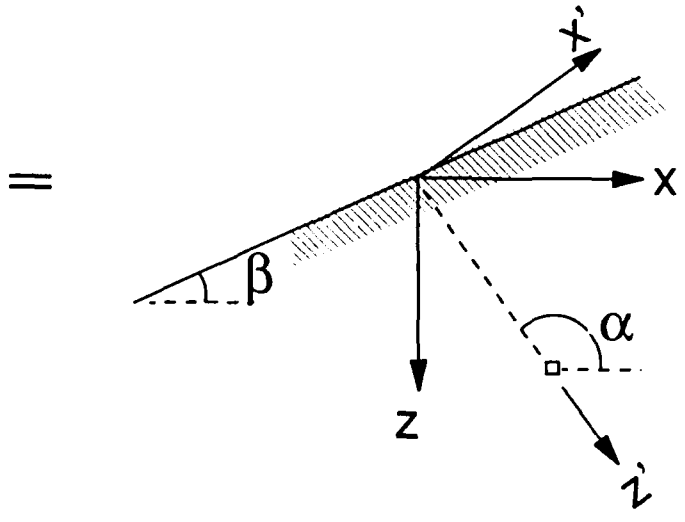
=
x'
x
β
α
z
z'

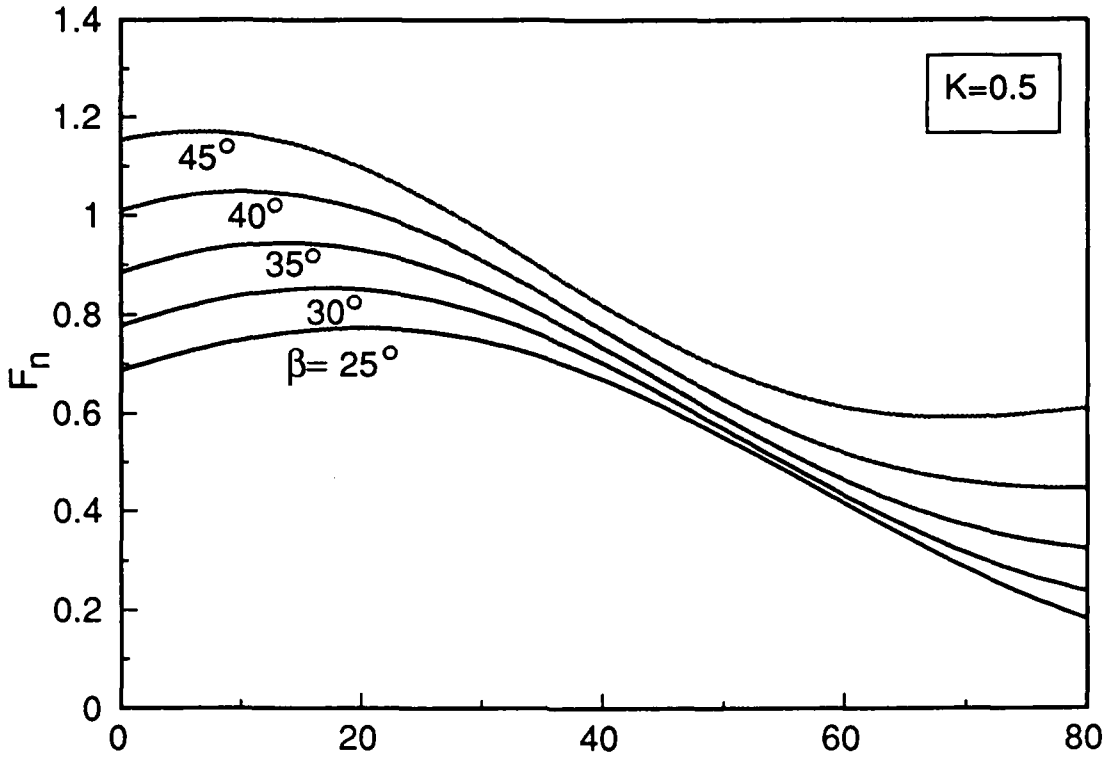
K=0.5
45°
40°
35°
30°
β= 25°
F_n
1.4
1.2
1
0.8
0.6
0.4
0.2
0
0
20
40
60
80

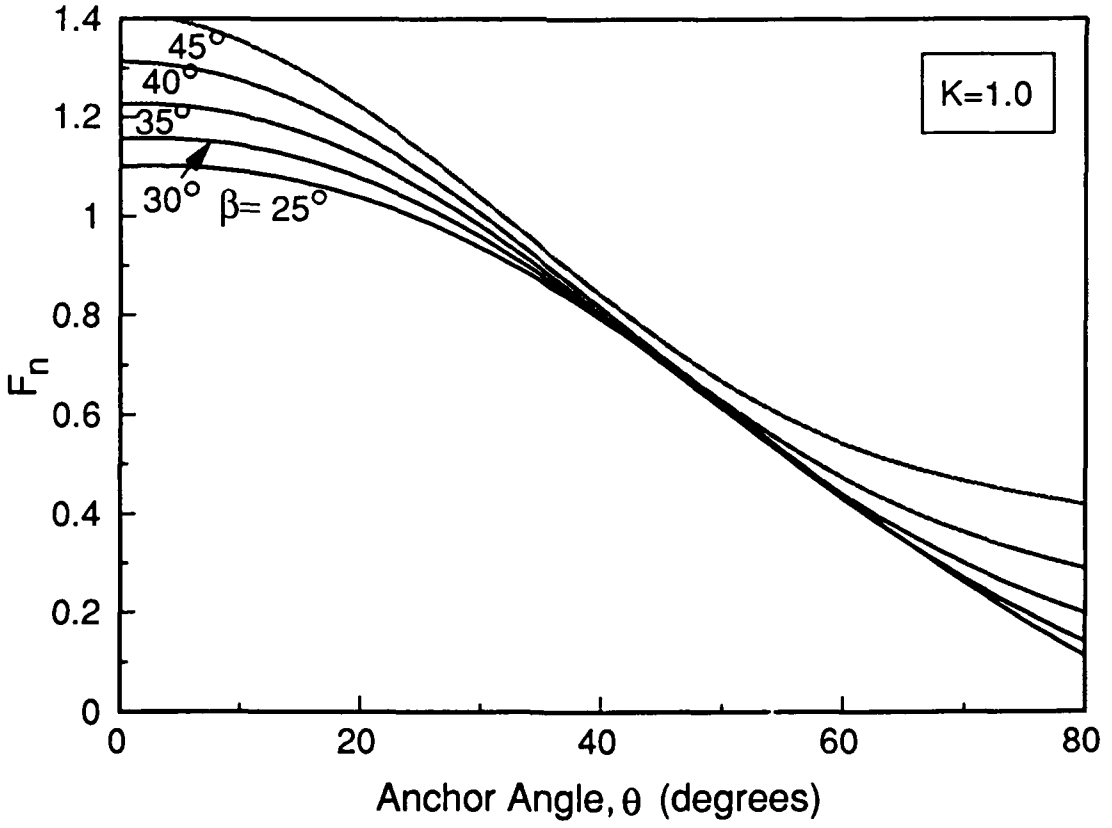
K=1.0
45°
40°
35°
30°
β= 25°
F_n
1.4
1.2
1
0.8
0.6
0.4
0.2
0
0
20
40
60
80
Anchor Angle, θ (degrees)

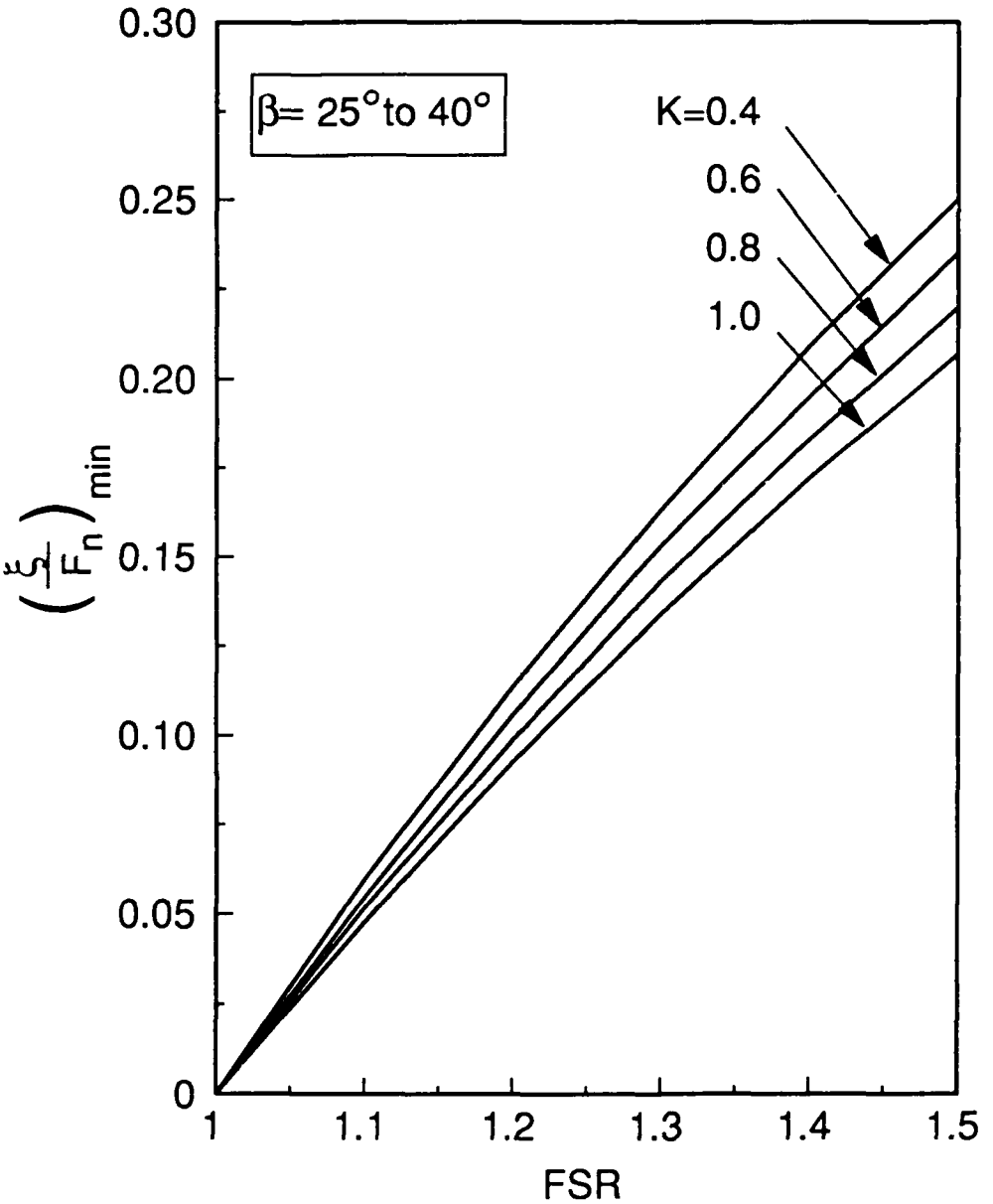
β= 25°to 40°
K=0.4
0.6
0.8
1.0
0.30
0.25
0.20
0.15
0.10
0.05
0
1
1.1
1.2
1.3
1.4
1.5
FSR
$\left(\frac{\xi}{F_n}\right)_{min}$

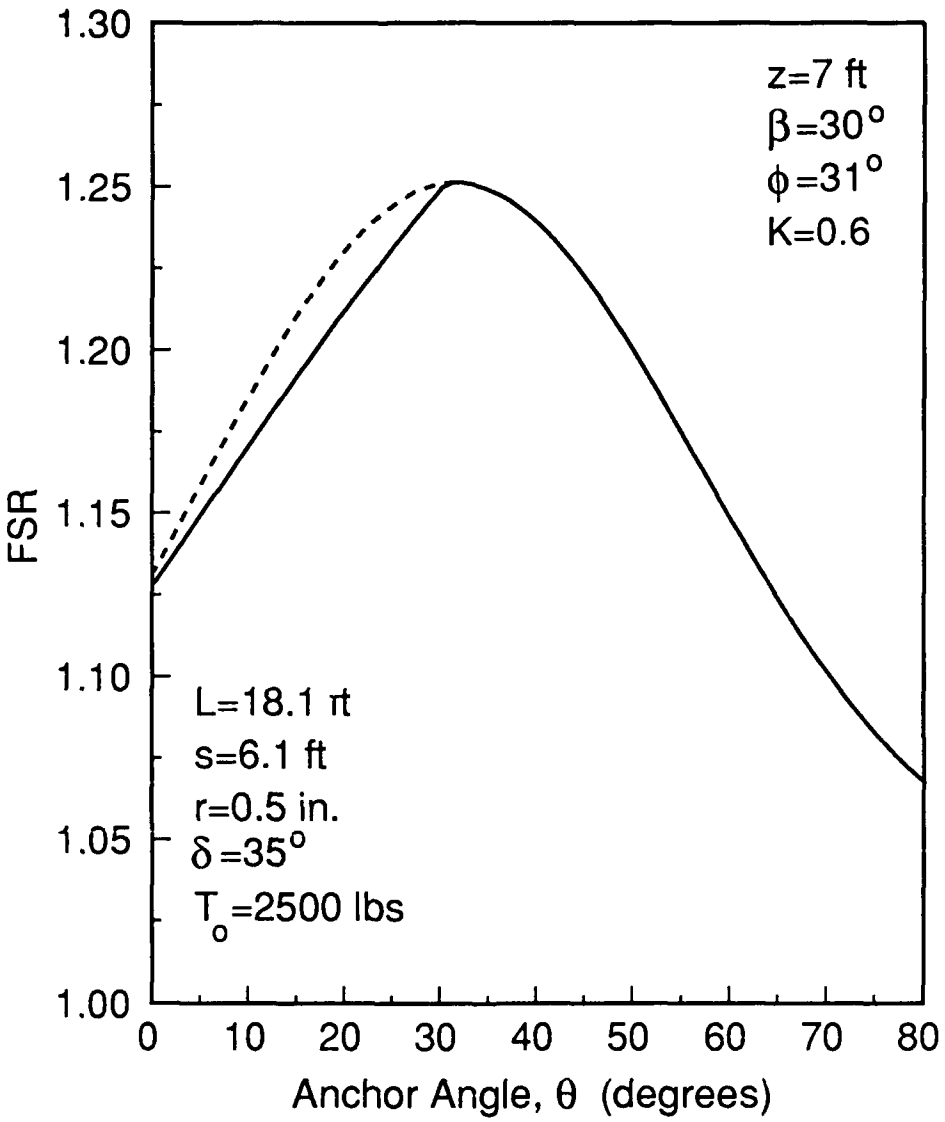
1.30
1.25
1.20
1.15
1.10
1.05
1.00
FSR
z=7 ft
β=30°
φ=31°
K=0.6
L=18.1 ft
s=6.1 ft
r=0.5 in.
δ=35°
T_o=2500 lbs
0
10
20
30
40
50
60
70
80
Anchor Angle, θ (degrees)

SAND-ANCHOR INTERACTION IN ANCHORED GEOSYNTHETIC SYSTEMS

S.J. Vitton[1], M.ASCE and R.D. Hryciw[2], M.ASCE

ABSTRACT: A series of ribbed anchor pullout tests was conducted in sand to study the behavior of anchors used in anchored geosynthetic systems (AGS). A large triaxial testing tank was constructed and used to investigate the effects of confining stress. Two dissimilar sands were tested in loose and dense conditions. Large displacement two-way cyclic loading tests were conducted to simulate the loading history of the anchor. The initial peak load resistance for dense sands corresponded to pullout results observed in earth reinforcement. However, significant loss in pullout resistance occurs upon load reversal. Continued cycling resulted in large degradation of both the driving and pullout resistance. Possible mechanisms that may contribute to the load loss are presented.

INTRODUCTION

Anchored geosynthetic systems (AGS) were developed by Koerner (6,7) for in-situ stabilization of soil slopes that are at or near failure. These systems combine a surface deployed geosynthetic with an anchoring system of driven reinforcing rods. The anchors are driven through reinforced openings in the geosynthetic to a depth sufficient to achieve anchorage. The geosynthetic is then fastened to the anchor and the anchor is driven an additional distance, thereby tensioning the geosynthetic and creating a curved geosynthetic-soil interface. This tensioning and curvature imparts compressive stress to the soil and a pullout load to the anchor. The stress transferred to the soil increases the shear resistance along potential failure surfaces, thereby increasing stability. Soil consolidation and stress relaxation in the geosynthetic may require anchor redriving after the initial installation.

A major factor in the success or failure of an AGS is the ability of the anchors to resist pullout. Therefore, an investigation was conducted to develop an understanding of soil-anchor interaction during pullout as well as during driving and redriving of the anchors. The present paper presents the results of this investigation and discusses possible load transfer mechanisms between sands and anchors in AGS.

---

[1]Assistant Professor, Dept. of Civil Engineering, The University of Alabama, Tuscaloosa, AL 35487-0205

[2]Assistant Professor, Dept. of Civil Engineering, The University of Michigan, Ann Arbor, MI 48109-2125

Background The procedure for installing an AGS is outlined by Koerner (5). Small diameter, ribbed steel rods (rebar) typically 1/2 in. (1.3 cm) in diameter or larger are used as anchors. The anchors are driven into the soil using a vibropercussion, pneumatic or similar type of hammer. The anchors are driven to approximately 75 to 90% of their designed depth, connected to the geosynthetic and then driven the remaining distance, thereby tensioning the fabric and exerting a pullout load on the anchor.

For smooth anchors the main load transfer mechanism is interface skin friction. The coefficient of interface friction (μ) typically ranges from (0.5 to 0.8)tanϕ', where ϕ' is the angle of internal friction (8). The value of μ increases with surface roughness. However, beyond a critical roughness the failure develops through the sand. Uesugi, et al. (14,15,16) have shown that the height of the shear zone is about five times D_{50}, where D_{50} is the diameter corresponding to 50% finer in the particle-size distribution curve. Further increase in the surface roughness beyond the critical roughness does not increase interface friction. Therefore, an upper limit for μ is tanϕ'. Since ϕ' itself, is a function of the test boundary conditions and other effects including induced and inherent anisotropy, some questions remain as to which ϕ' value to use for estimating μ. A lower limit would be the residual or constant volume friction angle of the sand, ϕ'_{cv}. Since, large relative motion between anchors and sand will occur in AGS, the use of ϕ'_{cv} in the present study is particularly appropriate.

For ribbed anchors the load transfer mechanisms are far more complicated than in smooth anchors and may include passive resistance of the soil against the ribs. For the ribbed reinforcement used in reinforced soil systems, Mitchell and Villet (8) state that "proven theoretical means for computing the relative contributions (of friction and passive resistance) are not available, and actual data are very limited ... accordingly, the most reliable values of friction coefficient are obtained by direct measurement." As a consequence, in situations where both side friction and passive soil resistance occur an apparent friction coefficient μ^*, is used. Schlosser and Elias (12) indicate that the values of μ^* for a dense sand vary from 0.5 for smooth reinforcements to over 6.0 for ribbed reinforcements. It should also be noted that for dense sands the greater the confining stress is the more restricted dilation of the sand becomes. The result of this is a decrease in the apparent coefficient of friction (12).

Hryciw and Irsyam (3) have studied the pullout resistance of plane ribbed inclusions in sand. They found that a very distinct grain structure develops between the ribs during shearing. The front face of each rib compress the soil skeleton thereby developing a zone of passive resistance while leaving a loose zone at the back face of each rib. Hryciw (2) has shown that for 0.1 in. x 0.1 in. (2.5 mm x 2.5 mm) square ribs, a spacing of approximately 1.3 in. (3.3 cm) maximizes the pullout resistance of ribbed inclusions in dense sand. As the spacing increases beyond 1.3 in. (3.3 cm), the amount of slippage along the sand-inclusion interface increases. For spacing less than 1.3 in. (3.3 cm) a full passive zone does not develop and the shear surface is entirely through the sand mass rather than along the soil-anchor interface (4).

EXPERIMENTAL INVESTIGATION

Testing System To study the load transfer mechanisms between a rebar-anchor and sand under large displacement cyclic loading, a large triaxial testing tank was

designed and constructed. The inside diameter is 16.7 in. (42.4 cm) and the height is 36 in. (91.4 cm). Horizontal and vertical confining stresses can be applied independently to the soil through latex rubber membranes built into the sides and the top platen. The triaxial testing tank is illustrated in Figure 1.

An MTS 22 Kip (98 kN) closed loop servo-controlled hydraulic actuator was used for controlled compressive and tensile loading of the anchor. All tests were displacement controlled. An IBM-PC, with a digital to analog card, provided program control. A 5000 lbf (22 kN) load cell measured anchor load. Displacement of the anchor was measured with a $\pm$ 4 in. ($\pm$10.2 cm) LVDT.

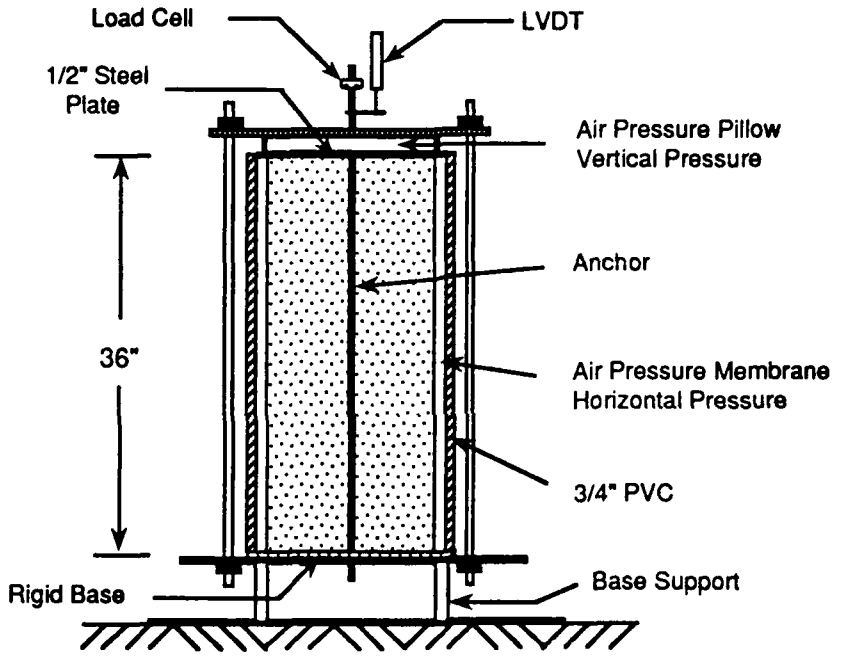

Figure 1. Triaxial test tank for anchor pullout tests.

Soil Description Two sands were tested: an Ottawa 20-30 sand and a glacial outwash sand termed Glazier Way Sand. The Ottawa 20-30 sand is a coarse, poorly graded (SP), subrounded quartz sand, while the Glazier Way sand is a fine to medium, poorly graded (SP) brown subangular sand containing quartz, feldspar, limestone and mafic minerals. The following parameters characterize the two sands:

Ottawa 20-30 Sand	Glazier Way Sand
D_{10} = 0.60 mm	D_{10} = 0.13 mm
D_{50} = 0.72 mm	D_{50} = 0.32 mm
C_u = 1.1	C_u = 2.9
e_{min} = 0.51	e_{min} = 0.40
e_{max} = 0.70	e_{max} = 0.76

Model Anchors Number 3, grade 60, Laclede steel rebar was used for the model anchors. A cross-section of the anchor is shown in Figure 2. The outside diameter of the rebar's ribs is 0.40 in. (10.2 mm), the diameter of the shaft is 0.35 in. (9.0 mm), while the spacing of the anchor ribs is 0.25 in. (6.4 mm). The nominal dimension of 3/8 in. (9.5 mm) was used for computation of interface friction. As shown in Figure 1, the test tank is designed to allow the anchor to extend through the bottom of the tank. A smooth 3/8 in. rod was drilled and pressed onto the anchor base so that a rib-free section of the anchor could pass through a teflon sleeve built into the base of the platform, thus preventing the release of sand from the bottom of the test tank.

Boundary Effects The top and sides of the tank are controlled stress boundaries and the applied confining stress remained constant throughout each test. The tank to anchor diameter ratio was greater than 40 to insure simulation of free field conditions. The base was rigid. A stress boundary at the base would have been more representative of in-situ conditions and it is believed that the rigid base did affect the test results to some degree as will be subsequently discussed.

Soil Placement In actual field installation the anchors are driven into the soil. However, to gain a basic understanding of rib behavior in sand, including development of peak resistance, test samples were prepared by first placing an anchor in the triaxial tank and then preparing the sand around it. Testing was performed at loose and dense soil conditions. Loose Ottawa 20-30 sand and Glazier Way sand were prepared with a 2 in. (5.1 cm) PVC pipe. The pipe was filled with sand and slowly raised allowing the sand to flow out in a loose condition. Relative densities were measured to be below 10% for the Ottawa 20-30 sand and between 10 and 15% for the Glazier Way sand. Two methods had to be used to prepare dense samples. An air pluviating system was used for the Ottawa 20-30 sand and relative densities were measured to be between 95 and 100%. Dense Glazier Way sand was prepared in 1.5 in. (3.8 cm) lifts with vibratory compaction. Relative densities for both dense Ottawa 20-30 and dense Glazier Way sand for the anchor pullout tests were measured to be approximately 95%.

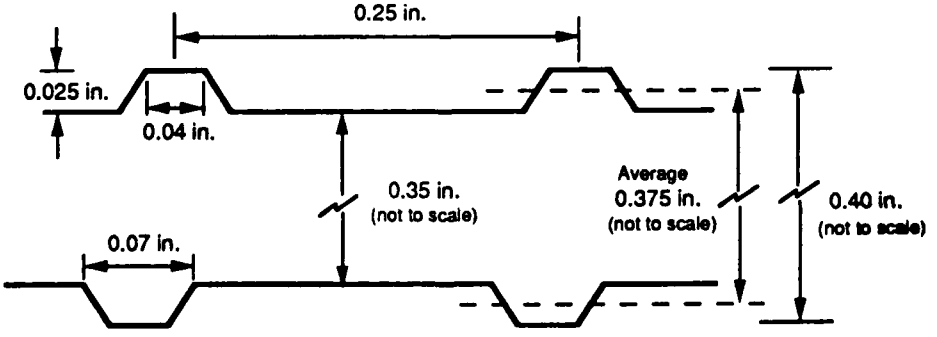

Figure 2. Cross-section of the rebar-anchor.

Soil Loading and Testing After the anchor and soil had been placed into the test tank an effective isotropic confining pressure, σ_o' of 5, 10 or 15 psi (34, 69, 103 kN/m^2) was applied. Tests were conducted in displacement control using a constant anchor displacement rate of 0.0023 in./s (0.06 mm/s). The first loading cycle was a "push" or compressive loading of the anchor to simulate driving conditions. In all of the pullout tests, the anchor was displaced downward 1.75 in. (44 mm) and then 1.75 in. back to its starting position. Hereafter, the subscript *peak* is used for the highest or peak load reached on the first cycle of loading, *res* is used for the post peak residual load and *pull* is used for the residual load upon anchor pullout.

RESULTS

1. The load versus displacement curves for tests conducted at $\sigma_o' = 5$ psi are shown in Figure 3. Corresponding curves for 10 and 15 psi showed the same features, although as would be expected, the loads increased with increasing confining stress. Due to laboratory constraints, samples were not all cycled the same number of times. A summary of all test results is given in Table 1. The initial loading in all tests resulted in a relatively high peak load, P_{peak}, as the anchor was displaced from its at-rest position. The apparent coefficient of friction, μ^* corresponding to the P_{peak} values are plotted in Figure 4 against μ^* values at similar normal stresses σ_n reported by Schlosser and Elias (12) for ribbed strips.

2. After achieving P_{peak}, continued displacement results in establishment of a residual load, P_{res}. In dense sand P_{peak} was followed by a fairly high P_{res}. It is interesting to note that the uniform subrounded Ottawa 20-30 sand quickly dropped from P_{peak} to P_{res}, while the less uniform subangular Glazier Way sand had a gradual reduction of load from P_{peak} to P_{res}. Several tests were conducted in which the first direction of anchor movement was upward. These tests revealed identical behavior, therefore the high residual strength in dense sand is not attributable to the rigid base of the triaxial tank. In loose sand P_{peak} was followed by a significant load reduction before a constant P_{res} was established.

3. In both dense and loose tests, a constant residual load was allowed to develop prior to reversing the loading to simulate anchor pullout. On pullout no distinct peak load was observed and P_{pull} remained relatively constant throughout the pullout range as is seen in Figure 3. On the first cycle, significant load loss occurred from P_{res} to P_{pull} for the tests in dense sand. The ratio P_{pull}/P_{res} for dense sand tests was 0.55 ($\pm$0.05). For loose sands the loss was considerably less with an average P_{pull}/P_{res} of 0.86 ($\pm$0.15).

4. Upon load reversals, a zone of negligible resistance to anchor movement was observed; the length of this zone was approximately 0.015 in. (0.38 mm) for Glazier Way sand and 0.03 in. (0.76 mm) for Ottawa 20-30 sand. This zone of negligible resistance developed only after several cycles in loose sands. It is interesting to note that the lengths of these zones were approximately equal to D_{50} for each sand. However, it is reasonable to presume that the rib dimensions would also affect the length of these zones.

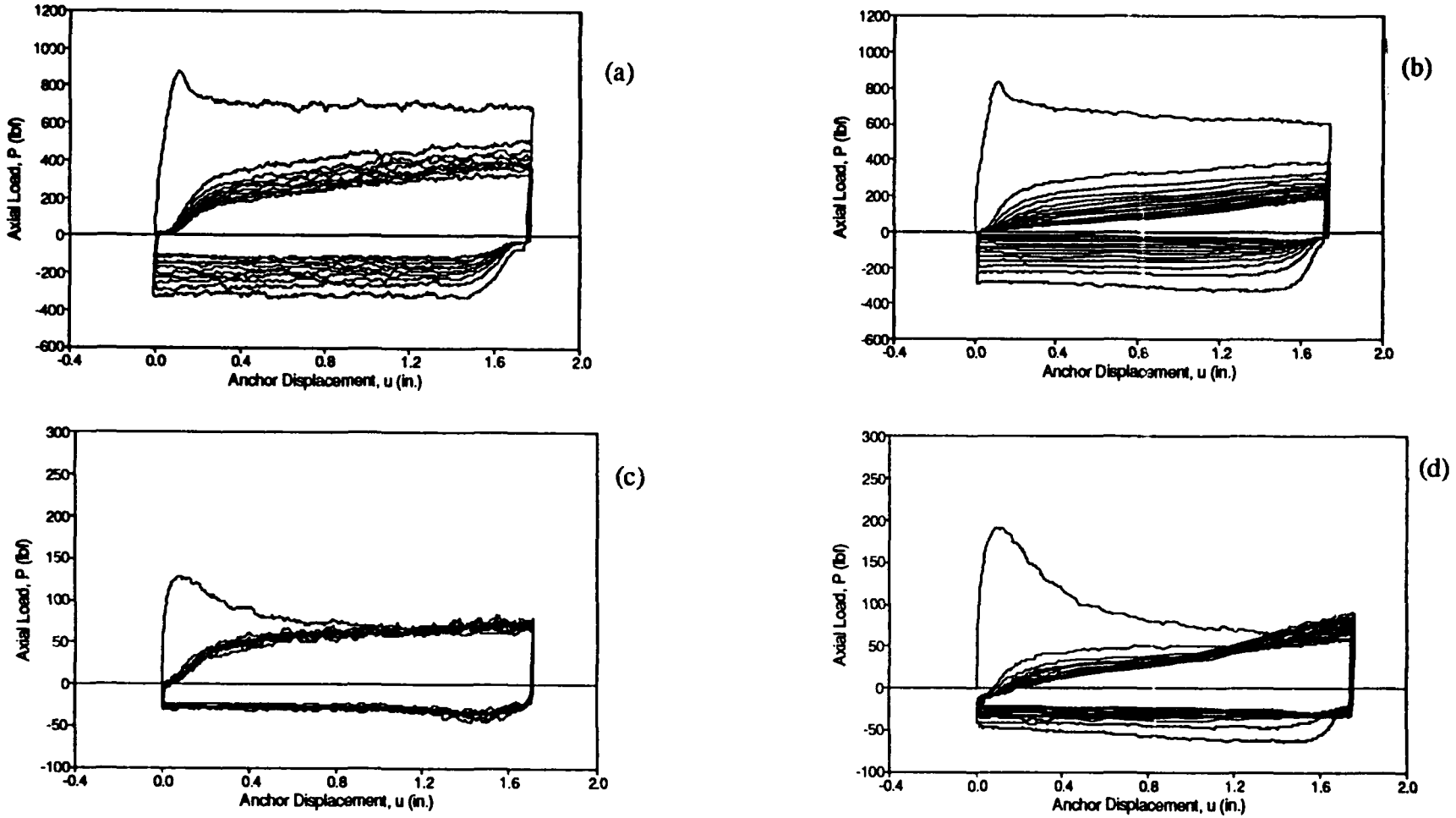

Figure 3. Two-way cyclic load-displacement test at 5 psi, (a) dense Ottawa 20-30 sand, (b) dense Glazier Way sand, (c) loose Ottawa 20-30 sand, dense Glazier Way sand.

5. After each load reversal, the displacement to reach full strength mobilization in both dense and loose sand was approximately 0.25 in. (6.4 mm) or one rib spacing. Smooth anchors required considerably less displacement, about 0.12 in. (3 mm) to mobilize the full interface friction.

6. In dense sand, severe degradation of the interface friction occurred with cycling as shown in Figure 5 for Glazier Way sand. The degradation was greater for Glazier Way than for Ottawa 20-30 sand. In fact, after ten cycles the average μ^* for Glazier Way sand was 0.25 or $0.32\tan\phi'_{cv}$, where $\phi'_{cv}=38°$. For Ottawa 20-30 sand, after ten cycles the average μ^* was 0.64 or $1.06\tan\phi'_{cv}$, where $\phi'_{cv}=31°$.

Table 1 Summary of Anchor Pullout Tests

Sand Type	σ_o (psi)	Total Cycles N	First Cycle						Last Cycle	
			P_{peak} (lbf)	P_{res} (lbf)	P_{pull} (lbf)	μ^* peak	μ^* res	μ^* pull	P_{pull} (lbf)	μ^* pull
Ott-L	5	8	128	70	44	0.60	0.33	0.21	31	0.15
Ott-L	10	10	277	115	103	0.65	0.27	0.24	56	0.13
Ott-L	15	6	462	235	224	0.73	0.37	0.35	170	0.27
GW-L	5	22	190	60	64	0.90	0.28	0.30	30	0.14
GW-L	10	18	393	172	136	0.93	0.41	0.32	30	0.07
GW-L	15	18	585	217	175	0.92	0.34	0.28	25	0.04
Ott-D	5	12	880	700	325	4.15	3.30	1.53	113	0.53
Ott-D	10	5	1770	1358	820	4.17	3.20	1.93	575	1.36
Ott-D	15	12	2500	1950	1137	3.93	3.07	1.79	472	0.74
GW-D	5	15	826	600	320	3.90	2.83	1.51	43	0.20
GW-D	10	14	1423	934	500	3.36	2.20	1.18	51	0.12
GW-D	15	7	1925	1355	767	3.03	2.13	1.21	250	0.39

Ott-L = Ottawa 20-30 Loose Sand GW-L = Glazier Way Loose Sand
Ott-D = Ottawa 20-30 Dense Sand GW-D = Glazier Way Dense Sand

7. Loose Ottawa 20-30 sand maintained an average μ^*_{pull} of 0.18 or $0.30\tan\phi'_{cv}$ with cycling. Degradation of the side friction did not occur and in fact a slight increase in interface friction resulted with cycling. The loose Glazier Way sand, on the other hand, exhibited significant degradation of side friction with cycling resulting in an average μ^*_{pull} of 0.08 or $0.10\tan\phi'_{cv}$ after an average 19 cycles.

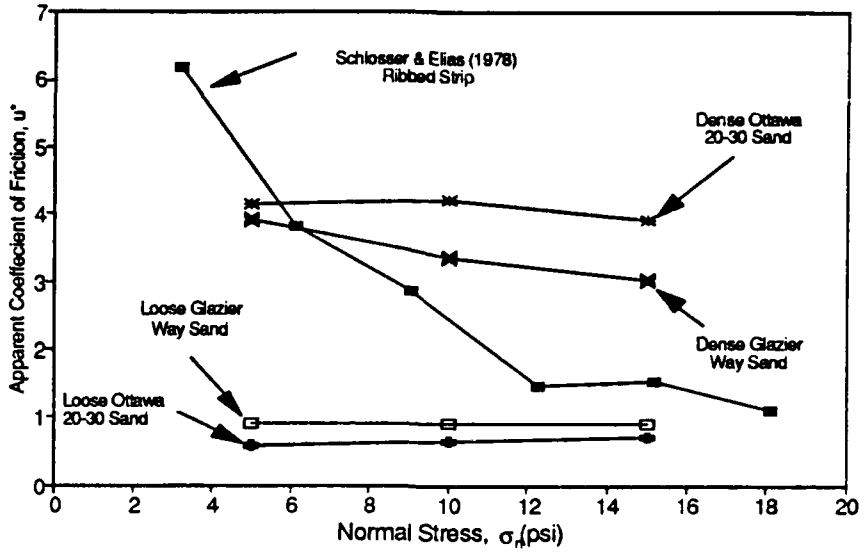

Figure 4. Apparent coefficient of friction versus normal stress including data published by Schlosser & Elias (12).

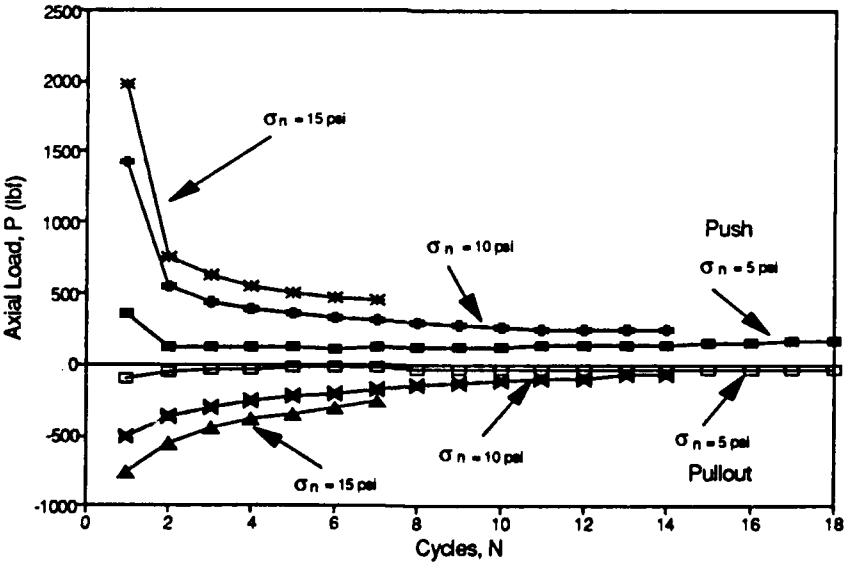

Figure 5. Load degradation with cycling for dense Glazier Way sand at 10 psi.

8. A visual inspection of the sand around the anchor was made after testing. For the Ottawa 20-30 sand, a 0.6 in. (15 mm) diameter zone of black sand grains surrounded the anchor. The sand particles were blackened by the abrasion of the iron oxide surface of the rebar-anchor. Consequently, a polishing of the rebar anchor was occurring while the iron oxide was coating the Ottawa sand particles.

   Polishing of the rebar-anchor occurred in the Glazier Way sand as well. This resulted in the light brown sand turning light gray. The extent of this gray zone was difficult to determine. A major difference between the Glazier Way and Ottawa sand in the zone around the anchor was that the Glazier Way sand was noticeably finer and more uniform in particle size than the surrounding sand.

9. On all downward loading cycles, the load gradually increased with displacement until load reversal. It is believed that the rigid base of the testing tank was responsible for this behavior.

DISCUSSION

1. It is not possible to study the micro-mechanics of soil-rib interaction in an axisymmetric test configuration. However, in a related study, Irsyam (4) traced the movements of sand grains and monitored the development of failure surfaces around plane ribbed inclusions. While a distinct passive zone was observed for 0.1 in. x 0.1 in. square ribs spaced 1.3 in. apart, no such passive zone was observed for the rib shape and spacing shown in Figure 2 and used in the present study. Therefore, the rebar-anchor behaves merely as a rough surface.

2. Preliminary tests were performed on smooth rods of 3/8 in. (9.5 mm) diameter. The computed values of μ^*_{peak} were fairly consistent with results presented by Schlosser and Elias (12) for smooth strips and Uesugi et al. (14) for smooth plates. When ribbed anchors were tested, μ^*_{peak} for dense sand was similar to values observed by Schlosser and Elias for ribbed strips. Although passive resistance has been cited as a possible mechanism for high μ^*_{peak} values for ribbed inclusions (8), this mechanism was not a factor for the anchors in the present study as discussed above. Two alternative explanations are therefore offered for the high computed μ^*_{peak} for dense sand. First, the tank to anchor diameter was sufficiently large to simulate free field conditions and therefore allow stress concentrations to develop normal to the anchors due to sand dilation. Second, unlike for plane strips, the surface area used for computation of μ^*_{peak} for cylindrical anchors does not correspond to the actual area of the shearing surface. Irsyam (4) has shown that the development of μ^*_{peak} is accompanied by grain movement as far away as 0.75 in. (19 mm) from the interface. For plane inclusions, the area of a potential "shearing surface" does not change with distance from the interface. For cylindrical inclusions, the area of a shearing surface could be far larger than the interface area computed from the nominal anchor diameter.

3. After μ_{res} has been reached a distinct shear zone, approximately five grain diameters in height develops during post peak shear as observed by Irsyam (4). Therefore, the reduction of μ^*_{peak} to μ_{res} is probably due to a reduction in the total area of the shear surface. However, the normal stresses due to dilation may continue to increase since a majority of the volumetric increase occurs between μ^*_{peak} to μ_{res}.

4. The pullout load, P_{pull} on the first cycle was consistently lower than P_{res}. This probably resulted from the loss of the dilational induced normal stress increases that developed during the initial push. This is confirmed by Irsyam's (4) visual observation of sand grain movement towards the ribbed surface upon load reversal. The inward movement of grain is also likely to facilitate the development of circumfential arching thereby further reducing the normal stresses.

   A loss of interface friction upon load reversal was also observed by Rao and Venkatesh (11) in their study of uplift behavior of piles in sand. They observed decreases in skin friction of up to 80% from the initial driving skin resistance and found that the decrease in pullout resistance was associated with increasing surface roughness.

5. Although degradation of interface friction with cycling has been reported by numerous researchers (1,9,13), the degradation seen in the test results for ribbed anchors is considerably more rapid and severe, especially for Glazier Way sand. It is believed that load degradation for dense sands occurs due to the reduction of the shear zone surrounding the anchor with cycling. Additional mechanisms causing significant loss of load in the non-uniform subangular Glazier Way sand are particle segregation and reorientation. As the anchor is cycled the larger grains are pushed away from the shear surface by the ribs, while smaller grains move towards it. The agglomeration of fine particles around the ribs results in poor interlocking of grains with the ribs and the reorientation of particles results in decreased interlocking between particles. Neither mechanism would occur to any significant measure in the uniform subrounded Ottawa 20-30.

   Another mechanism that could account for the loss of interface friction is the coating of sand grains with iron oxide from the abrasion of the anchor. Oda et al. (10) have reported that sand grains coated with talcum powder suffered a 50% reduction in overall friction angle.

CONCLUSIONS

A study of the interaction of sand with ribbed anchors was performed. The tests were conducted in a large triaxial tank. To simulate driving conditions, the anchors were driven past the peak load until a constant residual load developed. For dense sand the residual load was relatively close to the peak load, while for loose sand the residual load value was considerably lower.

The most significant observation, however, was the loss of pullout resistance with cycling. On the first load reversal in dense sand a decrease in pullout resistance of approximately 45% occurred. For both dense and loose sand severe interface friction degradation then followed with continued cycling. The only

exception to the degradation of interface friction was for loose Ottawa 20-30 sand which did not degrade but actually increased to some degree. For all load reversals in both dense and loose sand the displacement to mobilize full shear resistance was 0.25 in. or one rib spacing. Proposed mechanisms responsible for side friction degradation are the loss of the increased normal stress on the anchor due to initial dilation, development of circumferential arching, particle segregation, and particle coating.

ACKNOWLEDGMENTS

This study was part of a research program supported and funded by Air Force Office of Scientific Research under Grant No. AFOSR-88-0166 to the University of Michigan. The authors thank Mr. Masyhur Irsyam for contributing the results of his study of grain movements to the discussion of the ribbed anchor pullout tests.

REFERENCES

1. DV Holmquist and H Matlock, Resistance-Displacement Relationships for Axially-Loaded Piles in Soft Clay, Proc. Offshore Tech. Conf., Houston, Texas, 1976, OTC2474.
2. RD Hryciw, Load Transfer Mechanisms in Anchored Geosynthetic, University of Michigan Report to AFOSR on Grant No. 88-0166, 1990.
3. RD Hryciw and M Irsyam, Shear Zone Characterization in Sands by Carbowax Impregnation, ASTM, Geotechnical Testing Journal, March, 1990. pp. 49-52.
4. M Irsyam, Load Transfer Mechanisms in Anchored Geosynthetic Systems, thesis to be submitted to the University of Michigan, Ann Arbor, MI, in partial fulfillment of the requirements for the degree of Doctor of Philosophy.
5. RM Koerner, Designing with Geosynthetics, Prentice-Hall, Englewood-Cliffs, NJ, 1986, pp 118-123.
6. RM Koerner, Slope Stabilization Using Anchored Geotextiles: Anchored Spider Netting, Proceedings Spec. Engineering for Roads and Bridges Conference, PennDot, 1984, Harrisburgh, PA.
7. RM Koerner and JC Robbins, In-situ Stabilization of Slopes Using Nailed Geosynthetics, Proceedings of the Third International Conference on Geotextiles, Vienna, Austria, April 7-11, 1986.
8. JK Mitchell and WCB Villet, Reinforcement of Earth Slopes and Embankments, National Cooperative Highway Research Program Report 290, Transportation Research Board, national Research Council, Washington DC, June, 1987, pp.22-31.
9. HG Poulos, Cyclic Axial Response of Single Pile, J. Geotech. Engrg. Div., ASCE, 107(GT1), Jan. 1981, pp. 41-58.
10. M Oda, K Junichi, and S. Nemat-Nasser, Experimental Micromechanical Evaluation of the Strength of Granular Materials: Effects of Particle Rolling, Mechanics of Granular Materials: New Models and Constitutive Relations, Elsevier, Amsterdam, 1983, pp. 21-29.
11. KSS Rao and KH Venkatesh, Uplift Behavior of Short Piles in Uniform

Sand, Soils and Foundation, Vol. 25, No. 4, Dec. 1985, pp. 1-7.
12. F Schlosser and V Elias, Friction in Reinforced Earth, Proc. ASCE Symposium on Earth Reinforcement, Pittsburgh, PA, 1978, pp. 735-761.
13. JP Turner and FH Kulhawy, Drained Uplift Capacity of Drilled Shafts Under Repeated Axial Loading, J. Geotech. Engrg., ASCE, Vol 116 No. 3, March 1990, pp. 470-491.
14. M Uesugi, and H Kishida, Frictional Resistance at Yield Between Dry Sand and Mild Steel, Vol. 26, No. 4, Dec. 1986, pp. 139-149.
15. M Uesugi, H Kishida and Y Tsubakihara, Behavior of Sand Particles in Sand-Steel Friction, Soils and Foundations, Vol. 28, No. 1, Mar. 1988, pp. 107-118.
16. M Uesugi, H Kishida and Y Tsubakihara, Friction Between Sand and Steel Under Repeated Loading, Soils and Foundations, Vol. 29, No. 3, Sept. 1989, pp. 127-137.

FRICTION AND PASSIVE RESISTANCE IN SOIL REINFORCED BY PLANE RIBBED INCLUSIONS

By Masyhur Irsyam[1] and Roman D. Hryciw[2]

ABSTRACT

A theoretical analysis, supported by laboratory investigations, of stress transfer between soil and ribbed reinforcement has been performed to evaluate the individual contributions of friction and passive resistance to overall pullout resistance. The laboratory experiments consisted of direct shear pullout tests of rigid ribbed inclusions with various rib spacings. Optical monitoring and a carbowax solidification technique assisted in identifying failure surfaces. A plasticity model, based on Sokolovski's method, was developed for a fully developed passive component of the pullout resistance. A parametric study revealed the significance of each of the model parameters. The optimum rib spacing is one which allows the maximum number of full passive zones to develop per rib spacing. For a rib height and width of 2.5 mm, the optimum spacings were found to be 25 mm for loose and 33 mm for dense Ottawa sands.

---

[1] Research Assistant, Univ. of Michigan, Ann Arbor, MI, USA
[2] Asst. Prof. of Civil Engrg. Univ. of Michigan, Ann Arbor, MI, USA

INTRODUCTION

The transfer of stress between soils and various soil reinforcement systems involves two basic mechanisms,- friction and, or passive resistance. In systems such as welded wire and Anchored Earth, passive resistance is the primary mechanism. In others, such as smooth steel strips, smooth rods or sheets, friction dominates. In reinforcement by ribbed strips, deformed rods and geogrids both mechanisms are active but the relative contribution of each mechanism has hitherto been indeterminate (Mitchell and Villet, 1987).

A study of the pullout resistance of plane rigid ribbed inclusions in cohesionless soils was thus undertaken. Rather than focusing on a specific reinforcement type, the inclusions represented a simple generic form of reinforcement consisting of a rigid base plate with ribs protruding vertically from the plate at various spacings. Both friction and passive resistance mechanisms were anticipated to develop.

The investigation included laboratory direct shear testing accompanied by optical monitoring of failure patterns. A carbowax solidification technique for determining failure shapes was also developed. The present paper presents a plasticity model for the pullout resistance of ribbed inclusions. Model predictions are compared to experimental results. The relative contributions of passive resistance and friction to the overall pullout resistance are assessed. Finally, conclusions and practical recommendations for optimum rib spacing are made.

EXPERIMENTAL CONFIGURATION

Pullout tests were conducted in a 267 mm x 140 mm x 76 mm direct shear box shown in Figure 1. Various interchangeable ribbed inclusions were installed in the central portion of a rigid base plate. Loads in the plate during shear were measured by a 2.2 kN load cell. Four LVDTs monitored the horizontal motion of the shear box and the vertical dilation or contraction of the soil. The load cell and LVDT readings were recorded by a microcomputer based data acquisition system.

The direct shear box was constructed with plexiglass walls to facilitate visual observation of grain structure during testing. A video camera was used to view an enlargement of the intrarib zone on a large monitor. Sand grains were colored to allow the movement of select individual grains to be followed during a test.

In addition to optical monitoring of individual grains, a carbowax solidification technique was developed for identifying shear surfaces. Hot wax was injected through a 1.6 mm hole in the base of the ribbed inclusion as shown in Figure 2. Copper tubes carried hot water through the plate during injection to keep the plate warm and prevent wax solidification. Injection continued until the intrarib region shown in Figure 3a was saturated. The soil was then sheared while maintaining the wax in a liquid state. After one rib spacing of relative displacement, cold water was passed through the copper tubes to cool and solidify the wax. The solidified sand mass revealed the shape of

the failure surface as shown in Figure 3(b). Hryciw and Irsyam (1990) also used carbowax impregnation to determine void ratios in the intrarib region.

The shearing resistance versus relative displacement for a typical test is shown in Figure 4. For this test, the soil was an Ottawa 20-30 sand prepared at a void ratio of 0.51, the normal stress on the ribbed plate was 48.3 kPa, the ribs were 2.5 mm high, 2.5 mm wide and spaced 33.0 mm apart. Complete results of the experimental program which studied the effects of normal stress, density and rib spacing on pullout resistance have been presented by Hryciw (1990) and Irsyam (1991).

OBSERVATIONS FROM OPTICAL MONITORING AND CARBOWAX SOLIDIFICATION

At small displacements, prior to mobilization of peak strength, significant movement of sand grains occurs at large distances from the ribbed inclusion, possibly as far as 15 grain diameters and beyond. In dense sands, as peak strength is approached, initial failure planes develop extending from the rib corners at 30 to 50 degree angles from the horizontal. With increasing relative displacement, the failure surface drops toward the horizontal. After one rib spacing of relative displacement, a failure surface is fully developed and a steady state of plastic shear flow is occurring. This is accompanied by stabilization of the pullout resistance at a constant post-peak residual strength. Displacement vectors for select grains of a medium dense sand and rib spacings of 15 mm (0.6 in.) and 33 mm

(1.3 in.) are shown in Figure 5. The displacement vectors represent the movement occurring subsequent to an initial displacement of one rib spacing. Distinct differences between failure patterns for the two rib spacings were observed. For small spacings, the failure surface approaches a plane parallel to the plate (Figure 5(a)). For larger rib spacings, the failure surface exhibits a pronounced curvature as shown in Figure 5(b).

For large rib spacings, a loose grain structure develops behind the ribs (Hryciw and Irsyam, 1990). This zone is approximately given by area ABC in Figure 6 where BC is approximately equal to one rib height, H_r. A compressive soil arch develops between the top of the rib and the base of the plate as shown. At the front face of each rib, a zone of lower void ratio develops. Optical monitoring has shown that once residual strength develops, the sand grains in the region EFG essentially move as a rigid plug ahead of the rib. The distance EF is approximately equal to $2H_r$. The relative motion of sand grains above the surface ABCDHA' is large and opposite to the direction of plate movement. In the area bounded by DEGA'H the relative motion of grains is also opposite to that of the plate, however the velocity is very small by comparison to that of grains above ABCDHA'.

Plastic shear flow may be geometrically idealized by sliding of infinitesimally close laminae parallel to a shear surface. The shear surface may represent a discontinuity of displacements of laminae as shown in Figure 7(a) or it may represent a shear

band of finite width over which the relative displacements of parallel laminae change most rapidly (i.e. shear strain is greatest) as shown in Figure 7(b).

Because of the particulate nature of sand, an actual failure surface denoted by S'S' in Figure 7(c), undulates about an idealized shear plane SS. For shearing to occur, grains on opposite sides of the failure surface must ride over one another. As such, the actual micro-movement of individual grains generally does not parallel SS nor S'S'. However, when the entire assembly of particles is considered, the average motion is parallel to the idealized shear surface SS. As such, SS is considered as a statistical shear surface through the soil fabric.

In light of the previous discussion, shear surfaces may be constructed from the displacement vectors of sand grains as shown by the dashed lines in Figure 5. For a rib spacing of 15 mm (0.6 in.), a wavy shear surface was observed which could be characterized as having a wavelength of one rib spacing, peaks at midpoints between adjacent ribs and troughs bottoming several grain diameters above the front face of each rib. For large rib spacings, a full passive soil wedge develops at the bulldozing face of each rib. Although the entire zone between adjacent ribs could not be captured optically, it was evident that the failure surface dipped below the tops of the ribs and in some cases scraped the base of the plate.

The shapes of the failure surfaces obtained by carbowax solidification were very similar to the results obtained by

optical monitoring of individual grain movements. Typical test results are shown in Figure 8. For a rib spacing of 15 mm (0.6 in.), the entire failure surface was above the ribs. For a spacing of 33 mm (1.3 in.), curved failure surfaces initiated above the tops of the ribs, touched the base plate and continued to the rear face of the previous rib. While void ratio appeared to have no effect for a rib spacing of 15 mm (0.6 in.), some difference was observed between originally loose and dense sands at the 33 mm (1.3 in.) spacing. Irsyam (1991) also conducted tests at a rib spacing of 5 mm (0.2 in.). He found that at such small spacings the grains become trapped between the ribs. The failure surface in such cases was flat, horizontal and immediately above the ribs.

THE PULLOUT RESISTANCE MODEL.

For relatively large rib spacings, (at least 33 mm) the failure plane consists of three distinct regions as shown in Figure 6. That is, a passive zone, a transition zone and a high void region. For small rib spacings (5 mm) the shearing resistance is entirely due to planer friction. This friction is partially along a sand-sand interface and partially along the sand/top-of-rib interface. For intermediate spacings (15 mm) a transition condition occurs which includes partial development of a passive zone and sand-to-sand friction. The pullout resistance model presented hereafter focuses on large rib spacings where a full passive zone develops. This situation is most desirable as

it will result in greater pullout resistances than at smaller spacings. The total pullout resistance of a ribbed inclusion will consist of both a frictional component as well as passive soil resistance:

$$F = F_f + F_p \quad \text{.....(1)}$$

where F=pullout resistance, F_f=frictional component and F_p=passive resistance component.

Frictional Component

To compute the contribution of friction to pullout resistance, two assumptions are made. First, although the normal stress distribution behind each rib is not uniform because of soil arching (Figure 6) and stress redistribution, it will be assumed that the net effect is a total frictional resistance equivalent to that of a uniform normal stress acting over the region.

At the front face of each rib, sand grains to a distance of approximately two rib heights, as shown in Figure 6, moved with the plate. As such, no friction between grains and the base plate was considered in this region. The total contribution of friction to pullout resistance then can be computed by:

$$F_f = (s-2H_r)\sigma_n \tan\delta_b \quad \text{.....(2)}$$

where s=rib spacing, H_r=rib height (and width), σ_n'=effective normal stress, δ_b=soil-rib friction angle.

Passive Resistance Component

To develop the solutions for passive resistance, the loads normal to the ribbed inclusions are assumed to be uniformly distributed. The problem is then statically determinate. It was previously indicated that the sand grains in the region bounded by GA'H in Figure 6 are moving at small relative velocities compared to the grains above A'H. As such, the grains in the region GA'H effectively act as an extension of the rib and thus increase the height of the wall against which passive resistance develops. The total height of the wall, H is thus:

$$H = H_r + H_s \quad \text{.....(3)}$$

where H_s= the height of soil contributing to the passive wall (distance GH in Figure 6). A distinction between H_r and H_s must be made because their respective friction angles with the soil ahead of the ribs will be different. Irsyam (1991) found that H_s for Ottawa 20-30 and Ottawa 40-50 were very similar. However, it is believed that if a greater range of particle sizes had been investigated, H_s would have been found to be a function of grain size and shape. It is also likely that the H_s is somewhat related to the rib width (distance GA').

Sokolovski's Method

Analytical solutions for pullout resistance of ribbed inclusions in soil were obtained using the Sokolovski method (Sokolov-

ski, 1960, 1965). Details of Sokolovski's method are given in Appendix A. The method enables a statically admissible stress distribution to be determined from known boundary conditions. An associated flow rule is obeyed. The solution is obtained by requiring both equilibrium and yield conditions to be satisfied at all points in the domain. Since optical observation and carbowax impregnation results indicated that the sand in the region of the ribbed plate undergoes significant deformation, the Sokolovski yield requirement is certainly met.

The region ahead of each rib may be divided into five distinct boundary problems as shown in Figure 9. Region I is a Cauchy problem; regions II and IV are Goursat problems and regions III and V are mixed problems. To establish the slipline network for this problem, the following parameters must be prescribed: the soil friction angle, ϕ, the base plate friction angle, δ_b, the rib wall friction angle, δ_r, the soil wall friction angle, δ_s, the rib height, H_r and the soil wall height, H_s.

The orientation of the sliplines and the magnitude of the stresses may be obtained by a finite difference procedure. However, the solution procedure can be greatly simplified by recognizing that the weight of the soil in the intrarib region contributes very little to the overall stresses. Assuming that the soil is weightless, Irsyam (1991) derived the closed form solutions for the passive stresses along the rib wall and along the soil wall. The expression for pressure along the rib wall is:

$$p_r = \sigma_n' \frac{\sin \Delta_b \sin(\Delta_r+\delta_r)}{\cos \delta_b \sin(\Delta_b-\delta_b) \sin \Delta_r} e^{2(\pi/2-\theta_b-\theta_r)\tan \phi} \quad \ldots\ldots\ldots(4)$$

where $$\Delta_b = \sin^{-1}\left[\frac{\sin \delta_b}{\sin \phi}\right]; \quad \ldots\ldots\ldots(5)$$

$$\theta_b = \left[\frac{\pi}{4} - \frac{\phi}{2}\right] + \frac{1}{2}\left[\Delta_b-\delta_b\right]; \quad \ldots\ldots\ldots(6)$$

$$\Delta_r = \sin^{-1}\left[\frac{\sin \delta_r}{\sin \phi}\right] \quad \ldots\ldots\ldots(7)$$

$$\theta_r = \left[\frac{\pi}{4} + \frac{\phi}{2}\right] - \frac{1}{2}\left[\Delta_r+\delta_r\right] \quad \ldots\ldots\ldots(8)$$

and σ_n'=effective normal stress.

The expression for pressure along the soil wall is:

$$p_s = \sigma_n' \frac{\sin \Delta_b \sin(\Delta_s+\delta_s)}{\cos \delta_b \sin(\Delta_b-\delta_b) \sin \Delta_s} e^{2[(\pi/2-\theta_b-\theta_r)+(\theta_r-\theta_s)]\tan\phi}$$

$$\ldots\ldots\ldots(9)$$

where $$\Delta_s = \sin^{-1}\left[\frac{\sin \delta_s}{\sin \phi}\right] \quad \ldots\ldots\ldots(10)$$

and $$\theta_s = \left[\frac{\pi}{4} + \frac{\phi}{2}\right] - \frac{1}{2}\left[\Delta_s+\delta_s\right] \quad \ldots\ldots\ldots(11)$$

The total horizontal force acting on the combined rib and soil wall due to passive resistance is then:

$$F_p = p_r H_r \cos \delta_r + p_s H_s \cos \delta_s \quad \ldots\ldots\ldots\ldots\ldots\ldots\ldots\ldots (12)$$

A sensitivity analysis was performed to evaluate the relative importance of the various parameters on F_p. Figure 10 illustrates that while F_p is very sensitive to H_s and ϕ, δ_s is relatively insignificant. It was also found that F_p is relatively insensitive to δ_r and δ_b.

Method of Velocity Characteristics

The associated flow rule, which is enforced in Sokolovski's method, requires that the dilatancy angle, ν be equal to the soil friction angle, ϕ. However, ν is commonly less than ϕ and there appears to be no basic reason for assuming $\nu=\phi$ for soils (Davis, 1968). Cox (1963) showed that by varying ν, the plastic deformation or velocity pattern may be considerably altered, although the failure loads may be identical. Thus, in order to account for the effects of dilation in sands during shear, the plastic deformations were also analyzed by the method of velocity characteristics. The pattern of velocity characteristics can easily be drawn from the stress characteristics since the former must everywhere intersect the latter at an angle $(\phi-\nu)/2$ (derivation in Appendix B).

COMPARISON OF THEORETICAL AND EXPERIMENTAL RESULTS

Pullout Resistance

To predict pullout resistances by equation (1), ϕ, δ_b, δ_r, δ_s, H_r, H_s, s and σ_n must be known, estimated or determined. To

determine ϕ, direct shear tests were performed on dense and loose Ottawa 20-30 sand. The dense condition corresponded to a relative density between 90% and 100% (void ratio 0.51 - 0.53), while the loose condition corresponded to a relative density between 30% and 40% (void ratio 0.62 - 0.64). The corresponding friction angles were ϕ = 33° and ϕ = 29° respectively.

Direct shear tests were also performed on a smooth aluminium plate to determine δ_b'. It was found to be 23° for dense Ottawa 20-30 and 21° for loose Ottawa 20-30. It is also reasonable to assume that $\delta_r \cong \delta_b$.

The height of ribs, H_r was maintained at 2.5 mm (0.1 in.) in all tests and the rib spacing, s was 33 mm. The height of the sand grain wall above the ribs, H_s was obtained from optical and carbowax observations. For the soils tested, H_s was found to be approximately equal to H_r and $0.8H_r$ for the dense and loose Ottawa sands respectively.

The soil wall friction angle, δ_s, cannot be directly measured nor optically observed. As such, it must be estimated. Realistically, we should expect δ_s to be intermediate between δ_r and ϕ. Therefore (remembering that F_p is not very sensitive δ_s), it was assumed to be 30° for the dense and 27° for the loose conditions.

With the above discussed parameter values, equation (11) predicts $F_p = 9.41\ H_r\ \sigma_n$ per rib spacing for dense Ottawa sand and $F_p = 6.14\ H_r\ \sigma_n$ per rib spacing for loose Ottawa sand. Since

s=33 mm and H_r=2.5 mm were maintained constant, equation (2) may be written F_f=11 H_r σ_n tanδ_b. As such, we find F_f=4.67 H_r σ_n for dense sand and 4.22 H_r σ_n for the loose sand. Then by equation (1), F=14.08 H_r σ_n and F=10.36 H_r σ_n per rib spacing for dense and loose Ottawa sand respectively. Since the rib spacing was 13 H_r, the pullout resistances per unit length of plate are F=1.08 σ_n' and F=0.80 σ_n'. The corresponding apparent friction angles are 47° and 38.5° for the dense and loose Ottawa sands. Experimental direct shear test results are shown in Figure 11 along with the predicted apparent friction angles. Clearly, the model is in very good agreement with the observed behavior.

Failure Shape

The Sokolovski method was also used to predict the failure shape around the rib. As can be seen in the Figure 12, the stress characteristic lines, s_1, are close to the experimental results from the optical monitoring and carbowax solidification observations for both dense and loose conditions. It seems, therefore, that the Sokolovski method is also capable of predicting the failure surface.

The Method of Velocity Characteristics was less successful at predicting the failure shapes. An angle of dilation, ν, of 20° was assumed for the dense sand as suggested by James and Bransby (1971). If we assume that after one rib-spacing of initial displacement the loose sand reaches a critical state (i.e., ν= 0°), the velocity characteristics will everywhere

intersect the stress characteristics at a 6.5° angle for the dense sand and at 14.5° for the loose sand. The resulting velocity characteristic lines, k, are shown in Figure 12. Unlike the stress characteristics, the velocity characteristics are not in a good agreement with the experimental results nor with Sokolovski's solution.

The failure of the velocity characteristics to correctly predict failure shapes may be explained be the inherent assumption of coaxiality whereby the directions of maximum and minimum stretching coincide with the directions of maximum and minimum stress respectively. As a result, the principal axes of the strain or strain increment tensor will coincide with the corresponding axes of the stress tensor. In non-coaxial situations, the principal stress axes are rotated through some angle with respect to the principal axes of the plastic strain increment.

The displacement vectors of sand grains from optical observation as well as the failure surfaces from carbowax solidification were obtained after a plate movement of 38 mm (1.5 in.). With this much displacement, the failure surfaces are fully developed and continued shearing occurs with particle overriding or rolling. Mandl and Luque (1970) have argued that in fully developed shear flow of perfectly isotropic granular material the internal kinematic constrains, which are associated with the overriding mode of motion, cause the principal axes of strain rate to deviate from the corresponding principal axes of stress, that is, a condition of non-coaxiality exists. Their argument was based on

both a macroscopic and a microscopic scale. Therefore, it seems likely that the discrepancies between the method of velocity characteristics and the experimental result are caused by the non-coaxiality of stress and strain increments.

The idea of non-coaxiality in plastic deformation of isotropic granular material is not new; it was introduced as a consequence of a macro-kinematical hypothesis by DeJong (1959), Geniev (1958), and later Mandl and Luque (1970). In addition to the fact that sand mass is not a continuum but consists of individual grains, DeJong even states that we cannot relate principal strain rate and stress direction in a unique way; in fact the degree of non-coaxiality between strain rate and stress within certain bounds is completely indeterminate (Mandl and Luque, 1970).

PRACTICAL SIGNIFICANCE OF RIB SPACING

The dual mechanism (friction and passive resistance) of load transfer between soil and ribbed inclusions carries an important practical significance. That is, it indicates that the pullout resistance is a function of the rib spacing. Thus, an optimum rib spacing must exist. To optimize the pullout resistance, the spacing should be such as to maximize the number of fully developed passive zones per length of reinforcement. Stated otherwise, the transition zone shown in Figure 6 should be kept to a small distance, optimally a point. The present study reveals,

both analytically and experimentally, that the optimum spacing ranges from 10 H_r for loose sand to 13 H_r for dense sand where H_r was maintained at 2.5 mm.

For rib spacings smaller than optimum, the transition zone will be absent, a full passive zone will fail to develop, the grains between adjacent ribs will be trapped and the shear surface will be above the rib heights as shown in Figure 5(a). The pullout resistance will be primarily due to soil-soil friction with some indeterminate contribution from a partially developed passive zone. As s becomes even smaller, say $s=2H_r$ as studied by Irsyam (1991), all passive resistance disappears and pullout resistance decreases even further. Furthermore, the frictional resistance becomes partially due to soil-soil friction and partially due to friction between the soil and the tops of the ribs. In the limit, as s approaches H_r, the pullout resistance approaches $P_f=\sigma_n' \tan \delta_b$.

Conversely, If the rib spacing is increased beyond optimum, the size of the transition zone increases while the number of passive zones per unit length of reinforcement decreases. Therefore, total pullout resistance decreases. As the spacing becomes very large, the total pullout resistance approaches F_f. Figure 13 illustrates the relative contributions of F_p and F_f to pullout resistance. At optimum spacing, the relative contribution of F_p is maximum while that of F_f is minimum.

CONCLUSIONS

An analytical model was developed for predicting the pullout resistance of rigid plane ribbed inclusions in sand. The model accounts for both frictional resistance and resistance due to passive earth pressure on the ribs. For a fully developed passive zone, a closed form solution for the passive resistance component, F_p of the total pullout resistance was developed based on Sokolovski's method. Predicted and observed values for the apparent friction angle agreed very well. Excellent agreement was also observed between the predicted shape of the failure surface and that observed by optical observation and carbowax solidification techniques. The optimum rib spacing is one that allows the greatest number of full passive soil zones to develop per length of reinforcement. At rib spacings both smaller and larger than optimum, the frictional component F_f becomes a larger component of the total pullout resistance. For a rib height of 2.5 mm (0.1 in.) the optimum spacings were found to be 25 mm (1.0 in.) for loose Ottawa Sand and 33 mm (1.3 in.) for dense Ottawa sand.

ACKNOWLEDGEMENTS

This study was part of a research program supported and funded by the United States Air Force Office of Scientific Research under Grant No. AFOSR-88-0166. Financial support for Mr. Irsyam's graduate studies were provided by IUC-ITB/MUCIA-World Bank XVII.

APPENDIX A SOKOLOVSKI'S METHOD

Sokolovski's method for solution of plane problems is developed from two basic assumptions. First, equilibrium conditions must hold. This requirement is given by the equations:

$$\frac{\partial \sigma_z}{\partial z} + \frac{\partial \tau_{xz}}{\partial x} = \gamma \quad \text{.....(13a)}$$

$$\frac{\partial \tau_{zx}}{\partial z} + \frac{\partial \sigma_x}{\partial x} = 0 \quad \text{.....(13b)}$$

$$\tau_{zx} = \tau_{xz} \quad \text{.....(13c)}$$

The second condition requires that the soil mass be at yield throughout and the strength is given by the Mohr-Coulomb criteria:

$$(\sigma_x - \sigma_z)^2 + 4\tau_{xz}^2 = (\sigma_x + \sigma_z)^2 \sin^2\phi \quad \text{.....(14)}$$

The state of stress at any point can be completely defined by two quantities, the mean principle stress, σ_m and the orientation of the principal stresses. If Ψ is defined as the angle between the major principal stress (σ_1) direction and vertical as shown in Figure 14, it may be shown that at limiting equilibrium:

$$\sigma_x = \sigma_m (1 - \sin\phi \cos 2\Psi) \quad \text{.....(15a)}$$

$$\sigma_z = \sigma_m (1 + \sin\phi \cos 2\Psi) \quad \text{.....(15b)}$$

$$\tau_{xz} = \sigma_m \sin\phi \sin 2\Psi \quad \text{.....(15c)}$$

Combining equations (15) into equations (13), results in a system of hyperbolic equations:

$$(1-\sin\phi \cos 2\Psi)\frac{\partial \sigma_m}{\partial x} + \sin\phi \sin 2\Psi \frac{\partial \sigma_m}{\partial z} + 2\sigma_m \sin\phi \sin 2\Psi \frac{\partial \Psi}{\partial x} +$$

$$2\sigma_m \sin\phi \cos 2\Psi \frac{\partial \Psi}{\partial z} = 0 \quad \text{.....(16a)}$$

$$\sin\phi \sin 2\Psi \frac{\partial \sigma_m}{\partial x} + (1+\sin\phi \cos 2\Psi) \frac{\partial \sigma_m}{\partial z} + 2\sigma_m \sin\phi \cos 2\Psi \frac{\partial \Psi}{\partial x} -$$

$$2\sigma_m \sin\phi \sin 2\Psi \frac{\partial \Psi}{\partial z} = \gamma \quad \text{.....(16b)}$$

The stresses are statically determinate and solutions may be obtained using the method of characteristics as described by Hill (1950). The entire field is uniquely described by two families of characteristic curves s_1 and s_2. One member from each family of characteristics passes through any point. Equations 16a and 16b express the variation of x, z, σ and Ψ along one of the characteristics.

The characteristic lines, also commonly known as slip lines represent critical surfaces along which limiting shear stress conditions hold. The s_1 characteristics are found at an angle υ clockwise from the major principal stress (σ_1) direction while the s_2 characteristics are at angle υ counterclockwise from σ_1. The angle υ is equal to $(\pi/4-\phi/2)$. Thus, the acute angle between s_1 and s_2 is always $(\pi/2-\phi)$. The orientations of the characteristics with respect to the x-z axes are given by:

$$\frac{dx}{dz} = \tan(\Psi-\upsilon) \quad \text{for the } s_1 \text{ characteristics .....(17a)}$$

and $$\frac{dx}{dz} = \tan(\Psi+\upsilon) \quad \text{for the } s_2 \text{ characteristics .....(17b)}$$

APPENDIX B VELOCITY CHARACTERISTICS

If u and v are the displacement components in the x and z directions respectively, we have the following relationships between velocities and strain rates:

$$\dot{\epsilon}_x = -\frac{\delta \dot{u}}{\delta x} \quad \text{.....(18a)}$$

$$\dot{\epsilon}_z = -\frac{\delta \dot{v}}{\delta z} \quad \text{and} \quad \text{.....(18b)}$$

$$\dot{\gamma}_{xz} = -\frac{\delta \dot{u}}{\delta z} - \frac{\delta \dot{v}}{\delta x} \quad \text{.....(18c)}$$

where $\dot{\epsilon}_x$= plastic strain rate in the x direction, ϵ_z= plastic strain rate in the z direction and γ_{xz}=plastic shear strain rate in the xz plane. Contractions are positive by convention.
If the major principal stress and strain directions are at angle Ψ to the z-axis, then

$$\dot{\epsilon}_z - \dot{\epsilon}_x = \dot{\gamma}_{xz} \cot 2\Psi \quad \text{.....(19)}$$

The principal plastic strain rates are given by:

$$\dot{\epsilon}_1 = \frac{1}{2}\{\dot{\epsilon}_x + \dot{\epsilon}_z + \sqrt{[(\dot{\epsilon}_x - \dot{\epsilon}_z)^2 + \dot{\gamma}_{xz}^2]}\} \quad \text{.....(20a)}$$

$$\dot{\epsilon}_3 = \frac{1}{2}\{\dot{\epsilon}_x + \dot{\epsilon}_z - \sqrt{[(\dot{\epsilon}_x - \dot{\epsilon}_z)^2 + \dot{\gamma}_{xz}^2]}\} \quad \text{.....(20b)}$$

An additional relationship between principal plastic strain rates is given by:

$$\frac{\dot{\epsilon}_3}{\dot{\epsilon}_1} = \tan^2\left[\frac{\pi}{2} + \frac{\upsilon}{2}\right] \quad \text{.....(21)}$$

Combining equations (20) and (21) with (19) yields:

$$\dot{\epsilon}_z + \dot{\epsilon}_x = -\dot{\gamma}_{xz} \sin\upsilon \csc 2\Psi \quad \text{.....(22)}$$

The system of equations resulting from substitution of equation (18) into (19) and (22) are hyperbolic, analogously to those for stress and are given by:

$$\frac{\partial u}{\partial x} + \cot 2\Psi \frac{\partial u}{\partial z} + \cot 2\Psi \frac{\partial v}{\partial x} - \frac{\partial v}{\partial z} = 0 \quad \text{.....(23a)}$$

$$\frac{\partial u}{\partial x} + \sin\upsilon \csc 2\Psi \frac{\partial u}{\partial z} + \sin\upsilon \csc 2\Psi \frac{\partial v}{\partial x} + \frac{\partial v}{\partial z} = 0 \quad \text{.....(23b)}$$

The entire field is then described by two families of characteristic curves, k_1 and k_2 that are commonly known as velocity characteristics. The orientations of the characteristics with respect to the x-z axes are given by:

$$\frac{dx}{dz} = \tan(\Psi - \xi) \quad \text{for the } k_1 \text{ characteristics} \quad \text{.....(24a)}$$

and $$\frac{dx}{dz} = \tan(\Psi + \xi) \quad \text{for the } k_2 \text{ characteristics} \quad \text{.....(24b)}$$

where $\xi = (\pi/4 - \upsilon/2)$. Figure 14 shows the orientation of the velocity characteristics with respect to the σ_1 direction. The k_1 characteristics are found at an angle of $(\phi - \nu)/2 + \upsilon$ clockwise from the σ_1 direction while the k_2 characteristics are at the same angle but counterclockwise from σ_1.

APPENDIX C REFERENCES

Cornforth, D. H., (1964) "Some Experiments on the Influence of Strain Condition on the Strength of Sand," Geotechnique 14, No. 2, pp. 143-167.

Cox, A. D. (1963) "The Use of Non-Associated Flow Rules in Soil Plasticity," R.A.R.D.E. Rep. (B) 2/63.

Davis, E. H. (1968) "Theories of Plasticity and the Failure of Soil Masses," Soil Mech. Selected Topics, Butterworth, London, pp. 341-380.

DeJong, G. D. (1959) Statics and Kinematics in the Failure Zone of a Granular Material, Delft: Uitgererij Waltman.

Geniev, G. A. (1958) "Problems of the Dynamics of a Granular Medium," Akad. Stroit. Archit., SSSR, Moscow.

Hill, R. (1950) The Mathematical Theory of Plasticity, Oxford, Clarendon Press.

Hryciw, R. D. and Irsyam, M. (1990) "Shear Zone Characterization in Sands by Carbowax Impregnation," Geotechnical Testing Journal of ASTM, Vol. 13, No. 1, PP. 49-52.

Hryciw, R. D. (1990) "Load Transfer Mechanisms in Anchored Geosynthetic Systems," University of Michigan Research Report on AFOSR Grant Number 88-0166.

Irsyam, M. (1991) "Pullout Mechanics of Ribbed Inclusions in Sand," a dissertation submitted to the University of Michigan in partial fulfillment for the degree, Doctor of Philosophy.

James, R.G. and Bransby, P. L. (1970) "Experimental and Theoretical Investigations of a Passive Earth Pressure Problems," Geotechnique 20, No. 1, pp. 17-37.

Mandl, G. and Luque, R. F. (1970) "Fully Developed Plastic Shear Flow of Granular Materials," Geotechnique 21, No. 3, pp. 277-307.

Mitchell J. K. and Villet, W. C. B. (1987) "Reinforcement of Earth Slopes and Embankments," National Cooperative Highway Research Program Report 290, Transportation Research Board of the National Research Council, Washington, D.C., 323 pp.

Sokolovski, V. V. (1960) Statics of Soil Media, London: Butterworth.

Sokolovski, V. V. (1965) Statics of Granular Media, Oxford: Pergamon.

LIST OF FIGURES

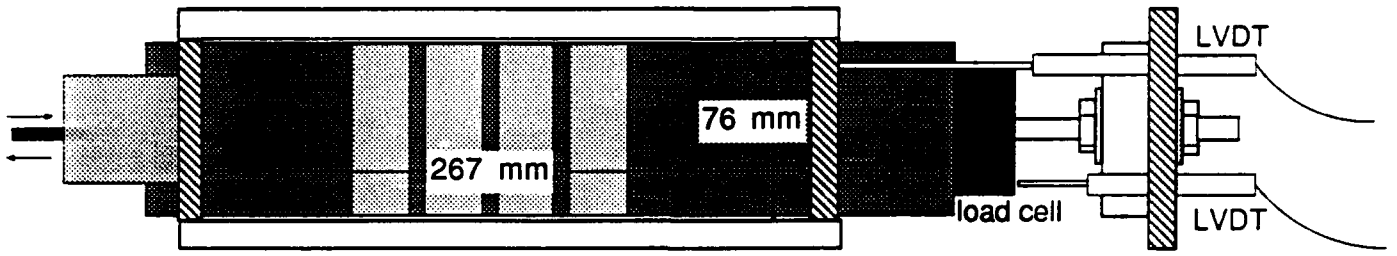

TOP VIEW - LOADING PLATE REMOVED

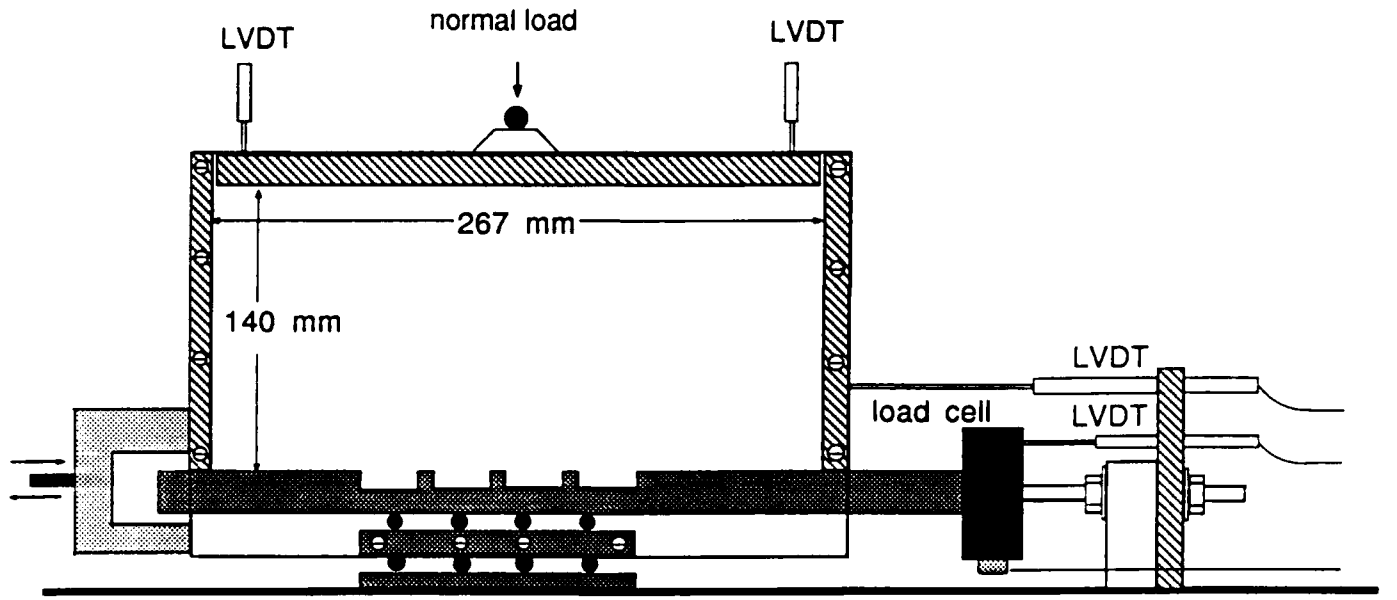

SIDE VIEW

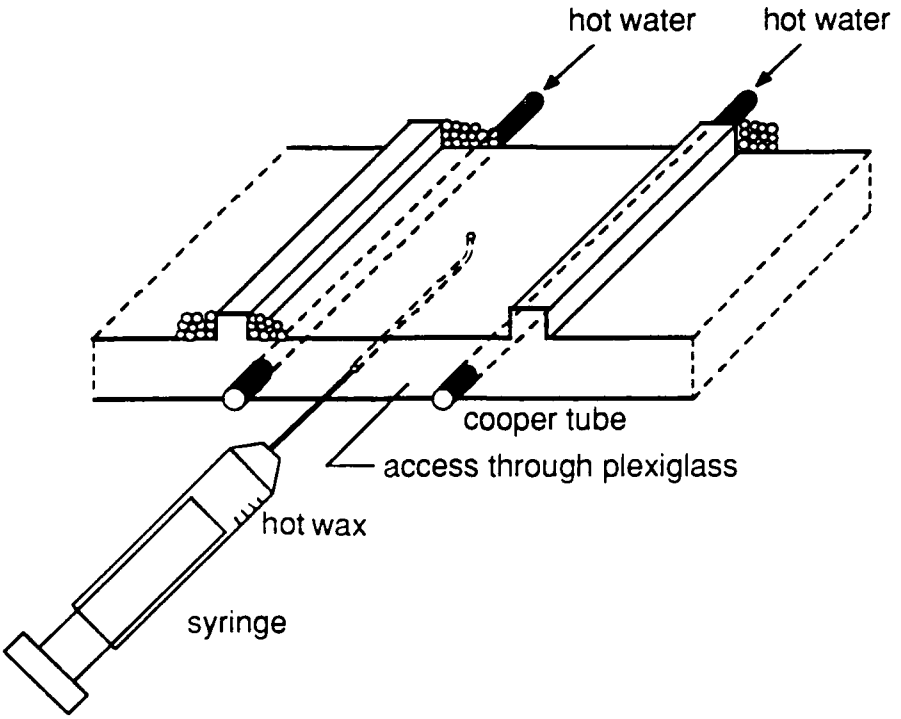
hot water
hot water
cooper tube
access through plexiglass
hot wax
syringe

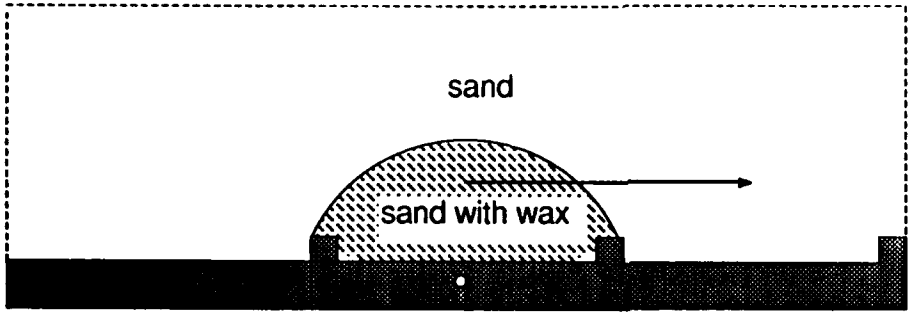

(a) Before Shearing

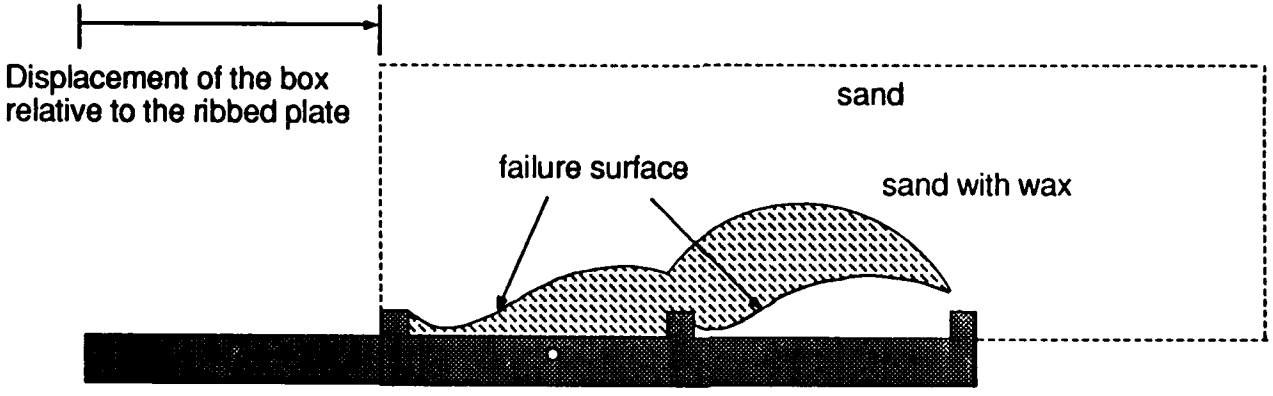

(b) After Shearing

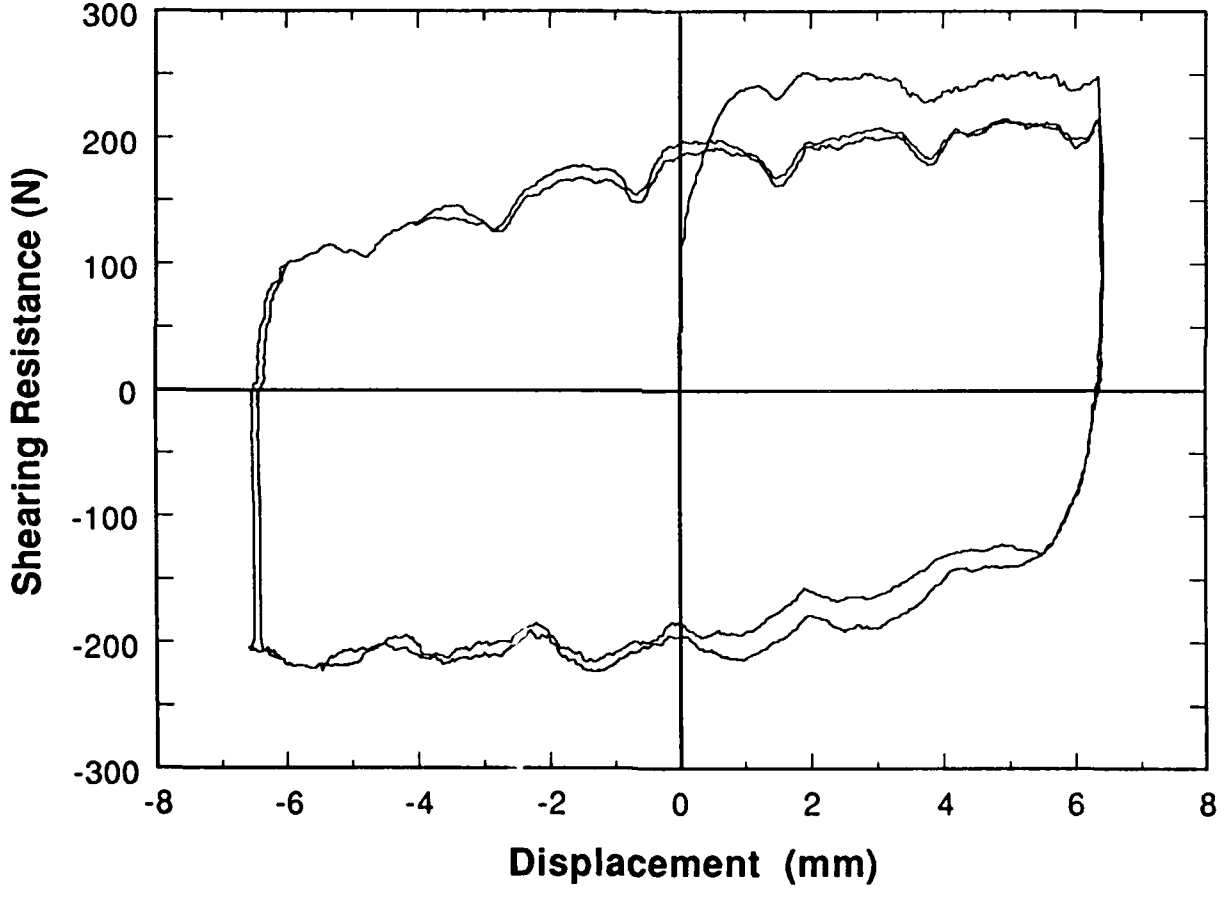
300
200
100
0
-100
-200
-300
-8
-6
-4
-2
0
2
4
6
8
Shearing Resistance (N)
Displacement (mm)

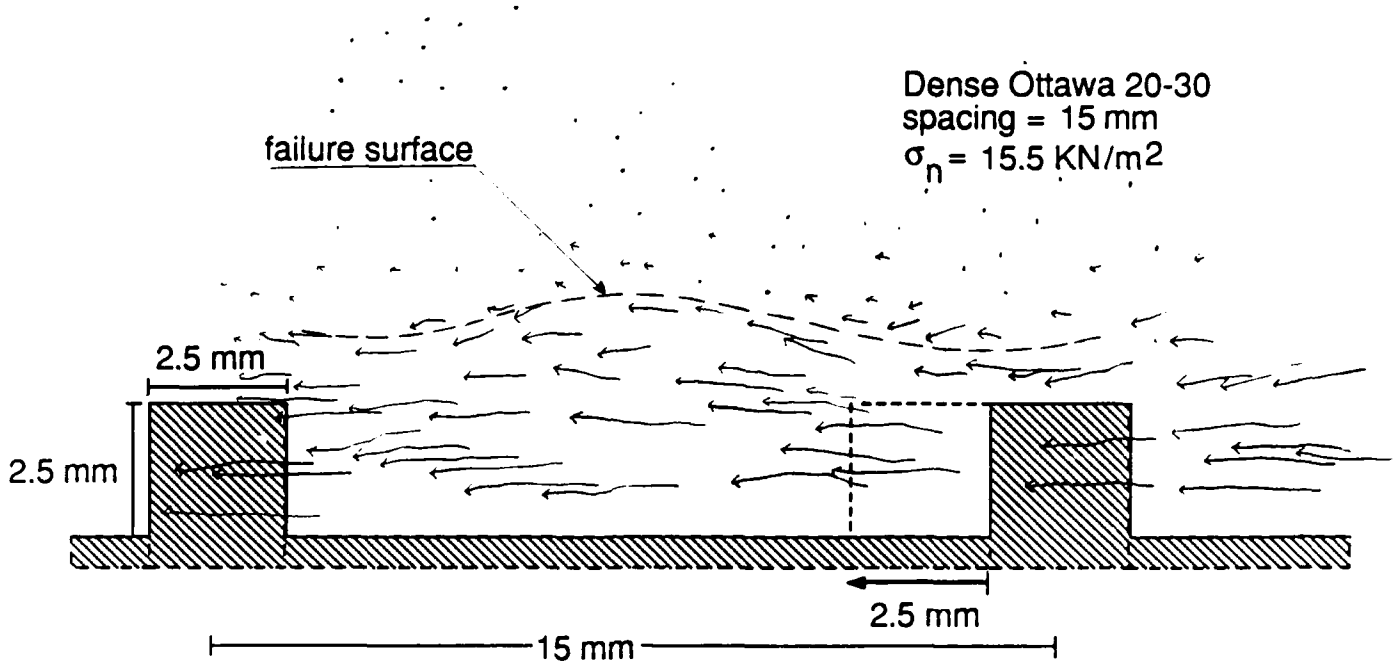
Dense Ottawa 20-30
spacing = 15 mm
σ_n = 15.5 KN/m2
failure surface
2.5 mm
2.5 mm
2.5 mm
15 mm

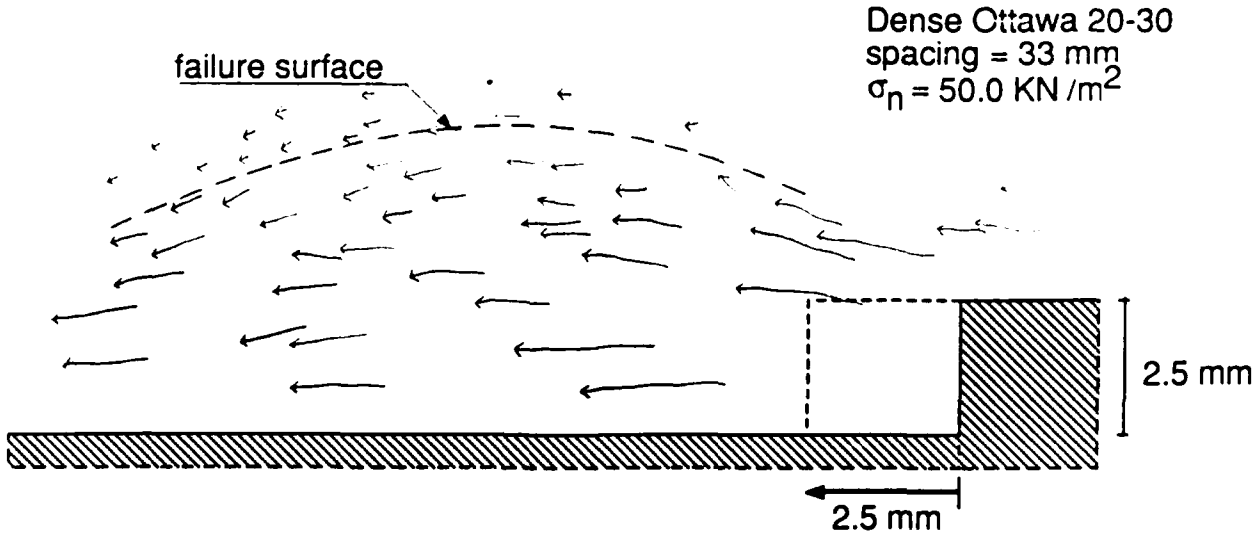
Dense Ottawa 20-30
spacing = 33 mm
σ_n = 50.0 KN /m2
failure surface
2.5 mm
2.5 mm

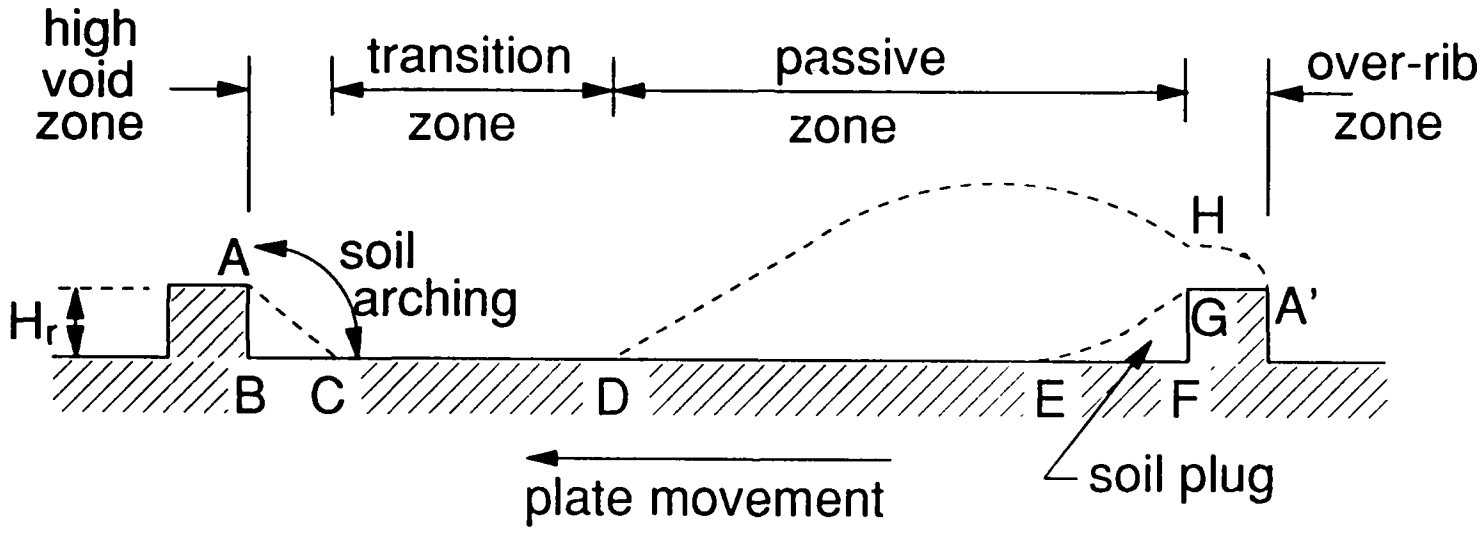
high
void
zone
transition
zone
passive
zone
over-rib
zone
H
A
soil
arching
H_r
G
A'
B
C
D
E
F
plate movement
soil plug

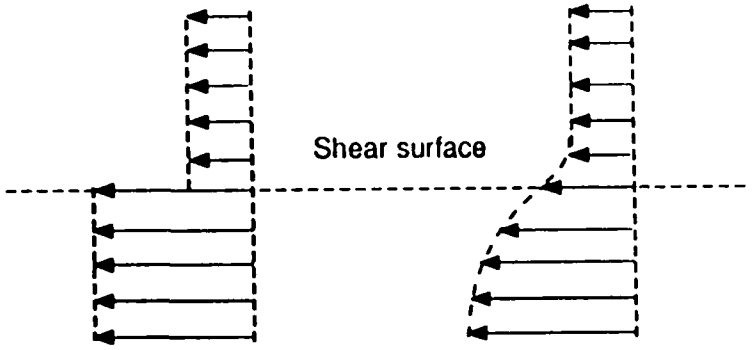

(a) (b)

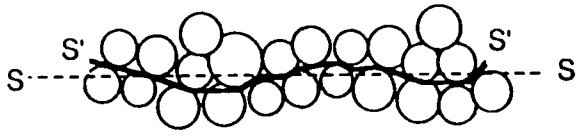

Macro-shear plane SS and overriding surface S'S'

(c)

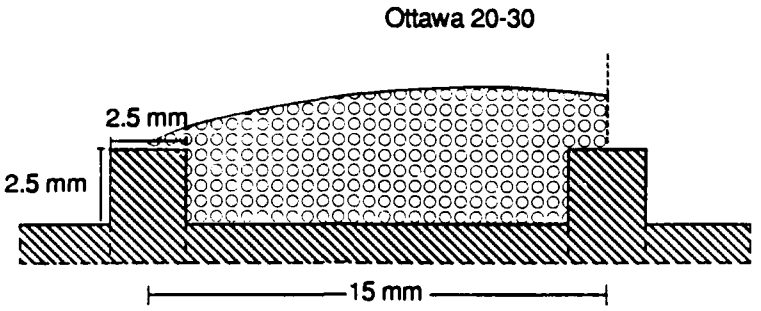
Ottawa 20-30
2.5 mm
2.5 mm
15 mm

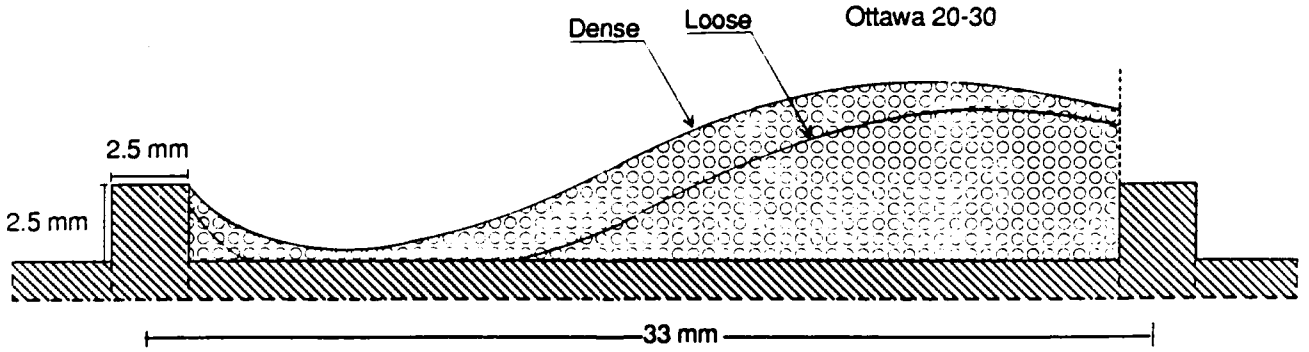
Dense
Loose
Ottawa 20-30
2.5 mm
2.5 mm
33 mm

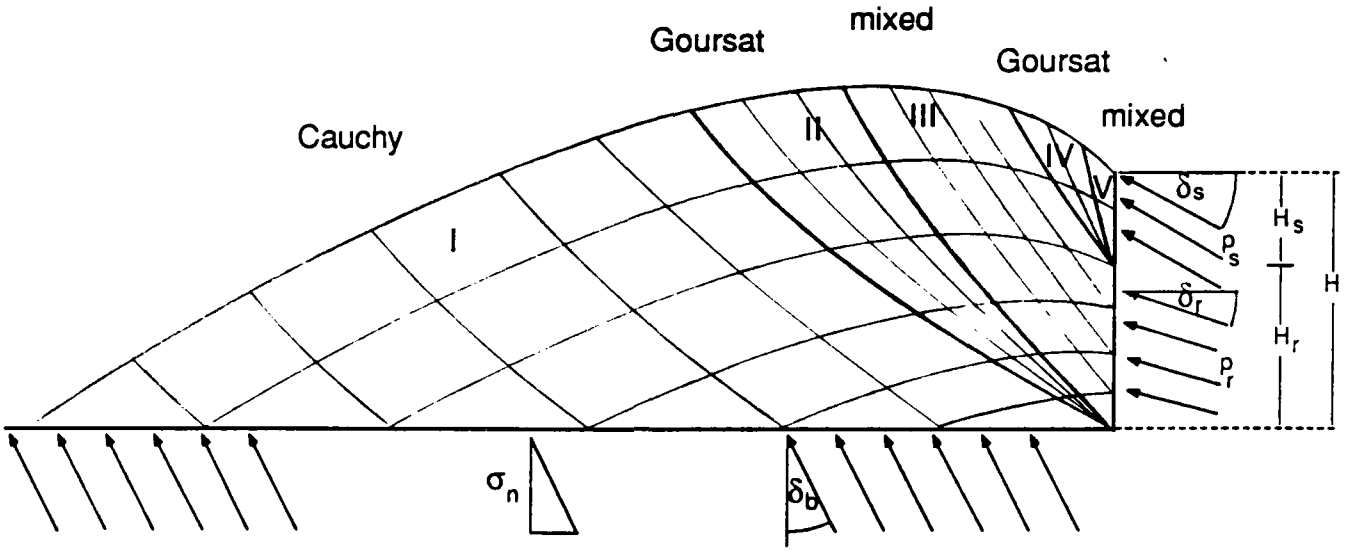
Goursat
mixed
Goursat
Cauchy
mixed
I
II
III
IV
V
δ_s
p_s
δ_r
p_r
H_s
H_r
H
σ_n
δ_b

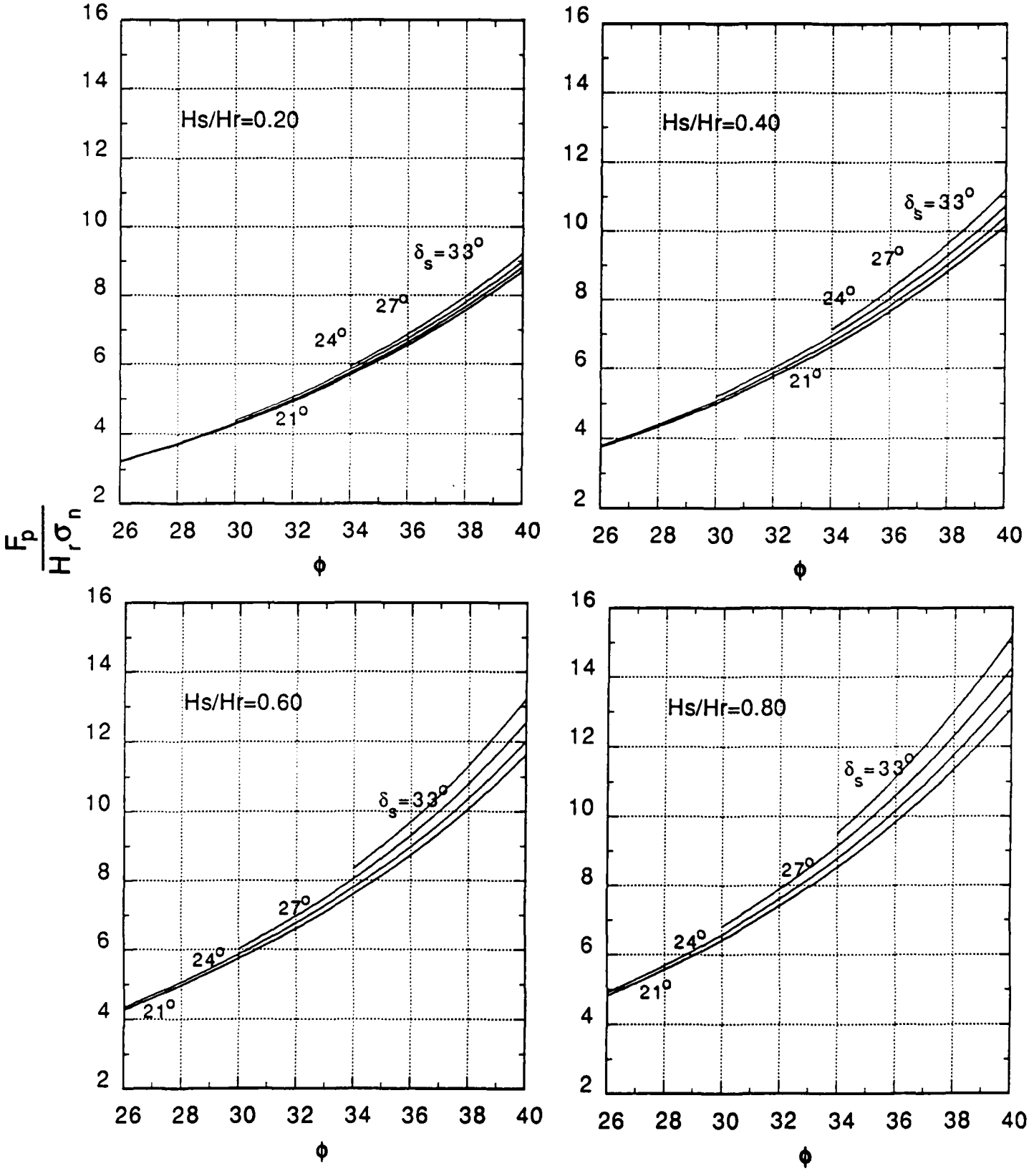
Hs/Hr=0.20
Hs/Hr=0.40
Hs/Hr=0.60
Hs/Hr=0.80
δ_s=33°
27°
24°
21°
$\frac{F_p}{H_r \sigma_n}$
ϕ
16
14
12
10
8
6
4
2
26
28
30
32
34
36
38
40

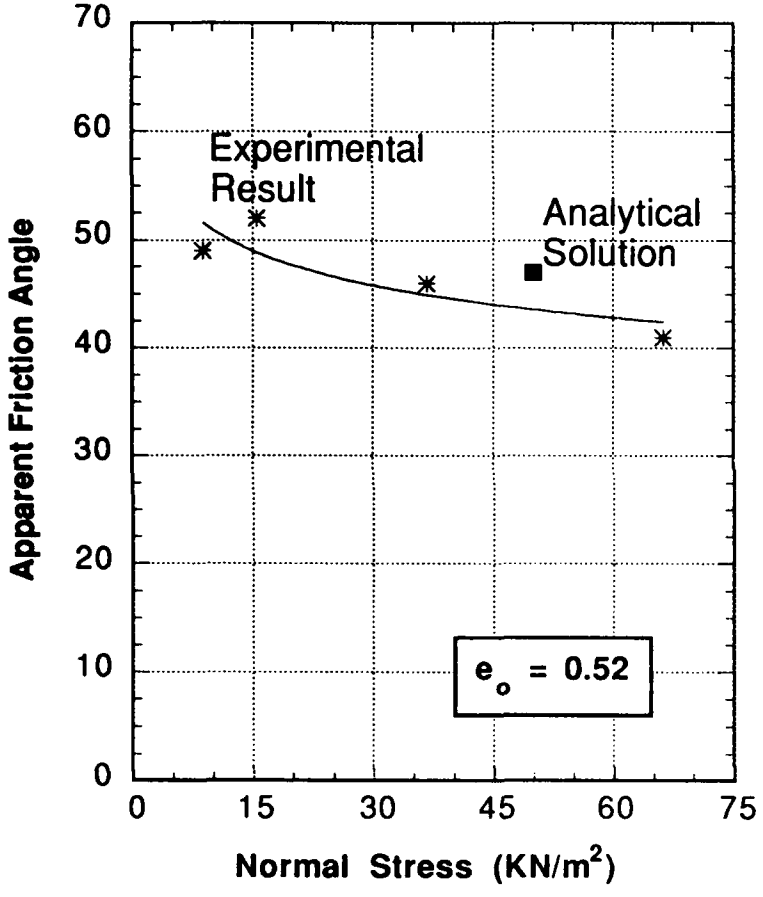
Apparent Friction Angle
70
60
50
40
30
20
10
0
0
15
30
45
60
75
Normal Stress (KN/m²)
Experimental Result
Analytical Solution
e_o = 0.52

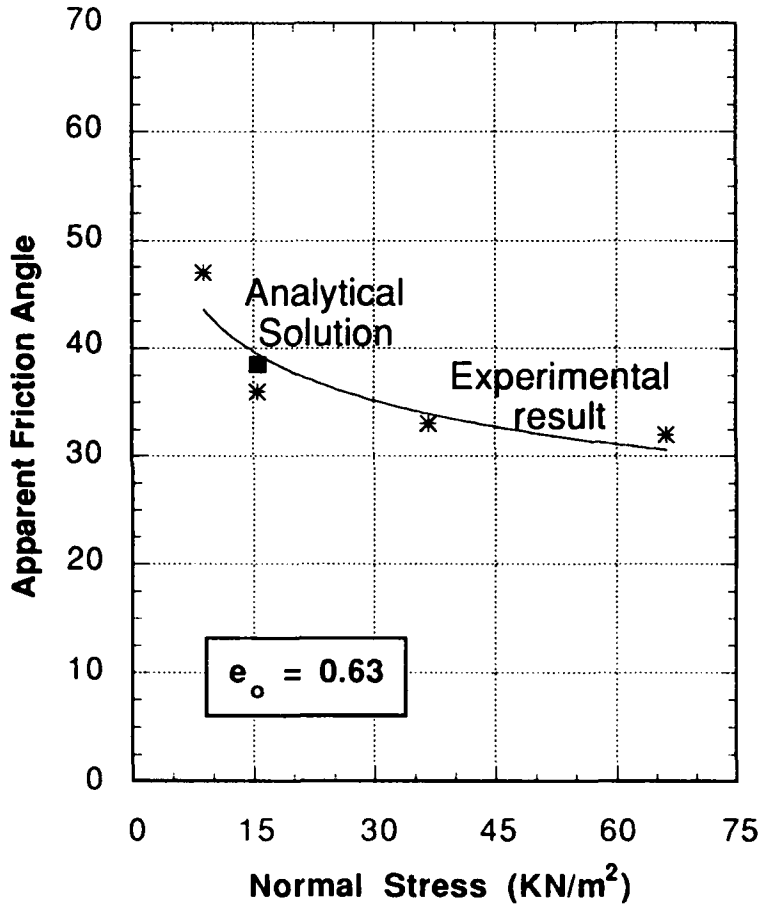
Apparent Friction Angle
70
60
50
40
30
20
10
0
0
15
30
45
60
75
Normal Stress (KN/m²)
Analytical Solution
Experimental result
e_o = 0.63

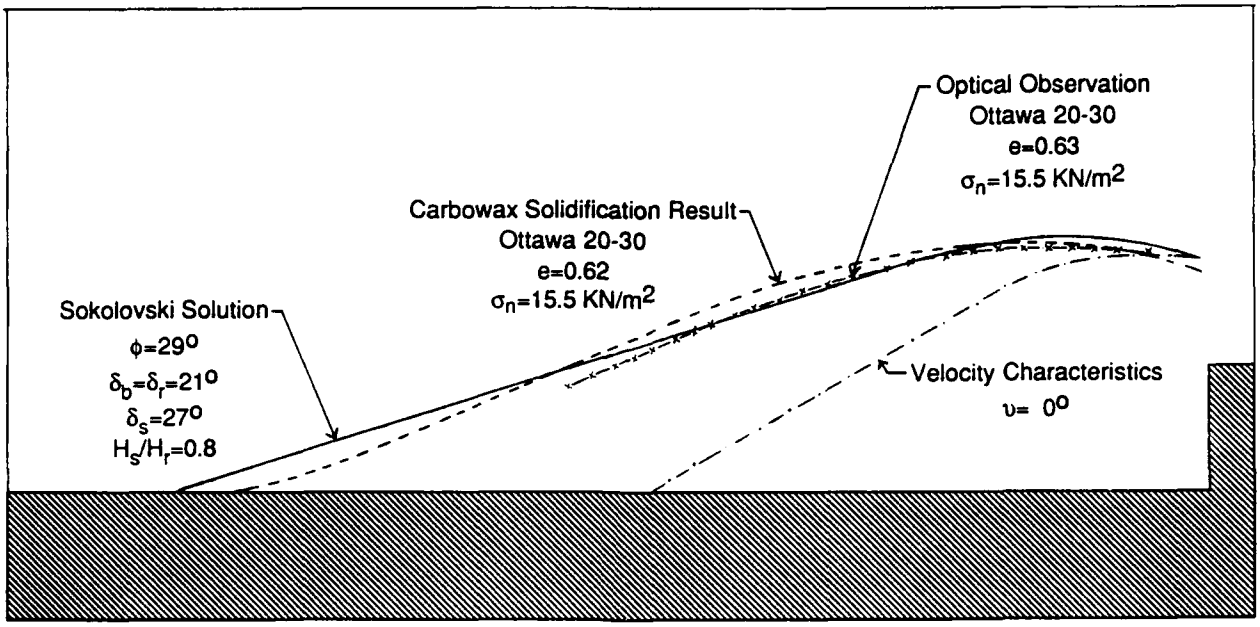
Optical Observation
Ottawa 20-30
e=0.63
σ_n=15.5 KN/m^2
Carbowax Solidification Result
Ottawa 20-30
e=0.62
σ_n=15.5 KN/m^2
Sokolovski Solution
ϕ=29^o
δ_b=δ_r=21^o
δ_s=27^o
H_s/H_r=0.8
Velocity Characteristics
υ= 0^o

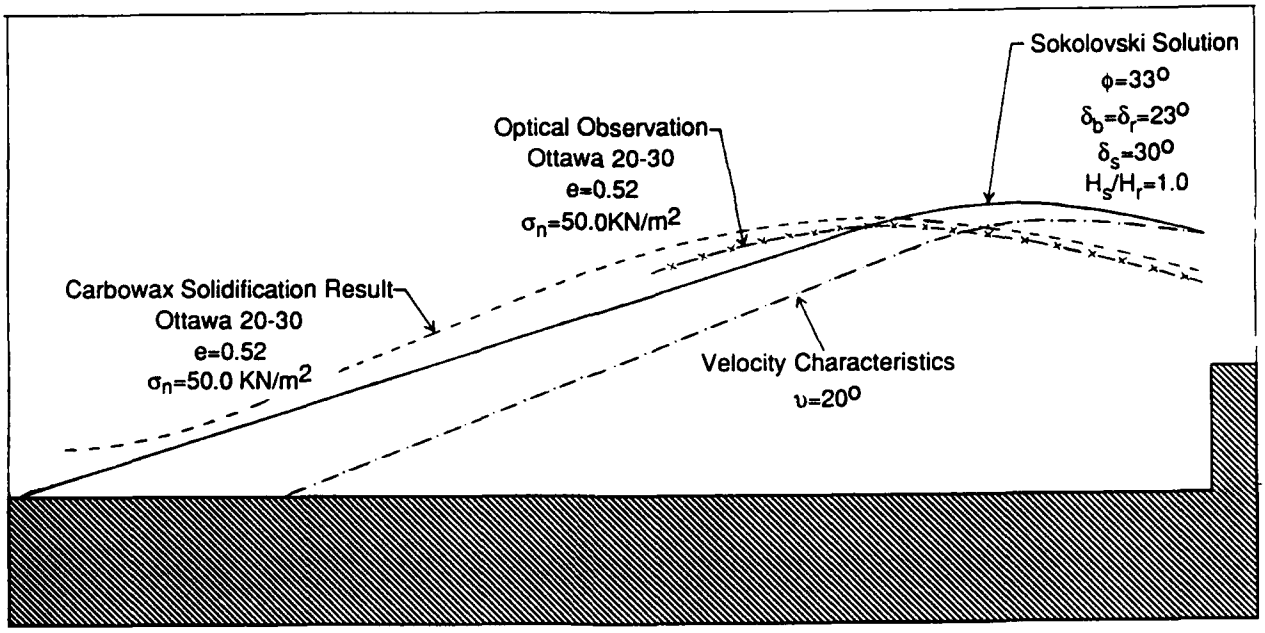
Sokolovski Solution
ϕ=33^o
δ_b=δ_r=23^o
δ_s=30^o
H_s/H_r=1.0
Optical Observation
Ottawa 20-30
e=0.52
σ_n=50.0KN/m^2
Carbowax Solidification Result
Ottawa 20-30
e=0.52
σ_n=50.0 KN/m^2
Velocity Characteristics
υ=20^o

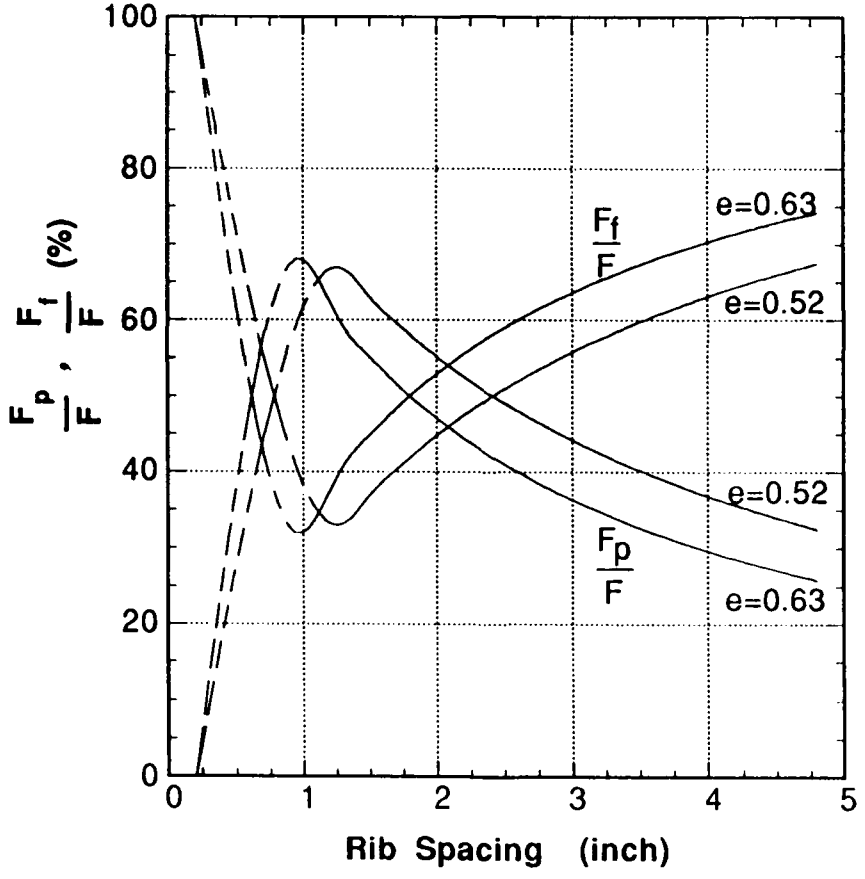
100
80
60
40
20
0
0
1
2
3
4
5
$\frac{F_p}{F}$, $\frac{F_f}{F}$ (%)
Rib Spacing (inch)
$\frac{F_f}{F}$
$\frac{F_p}{F}$
e=0.63
e=0.52
e=0.52
e=0.63

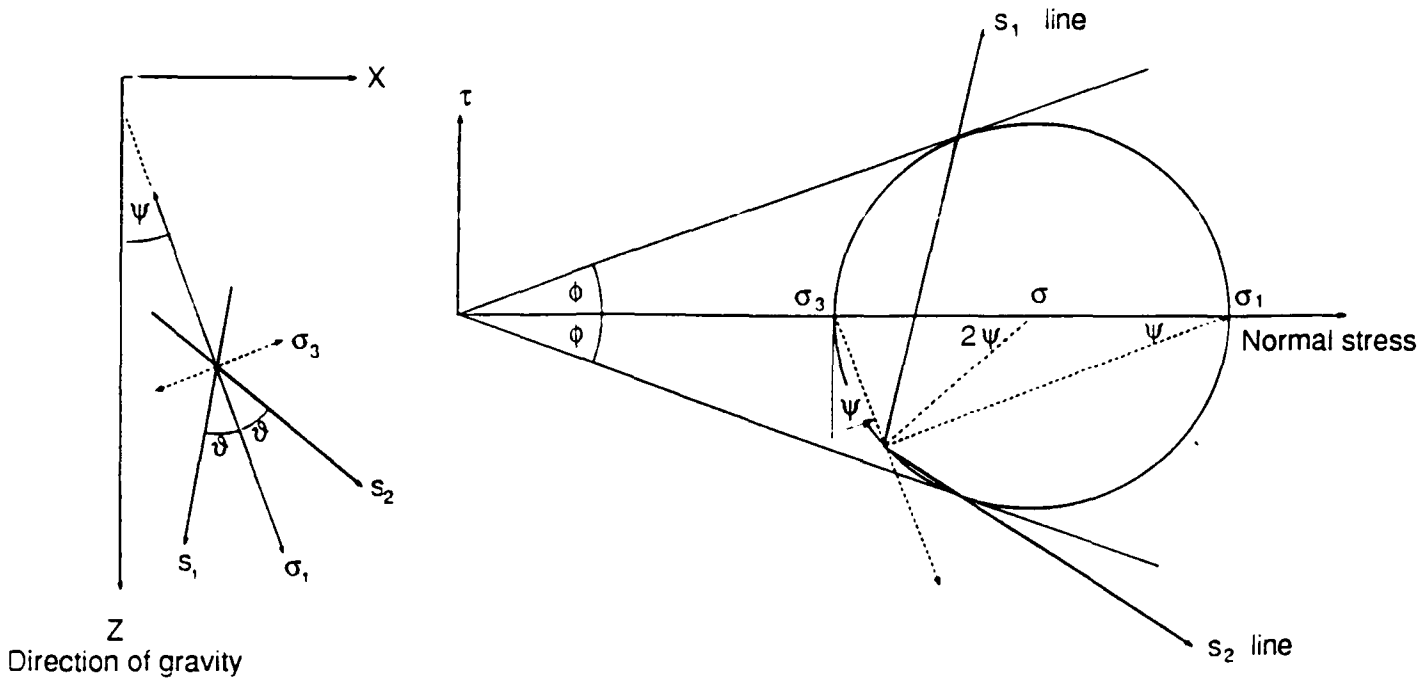
X
ψ
σ3
ϑ
ϑ
s2
s1
σ1
Z
Direction of gravity
s1 line
τ
ϕ
ϕ
σ3
σ
σ1
2ψ
ψ
ψ
Normal stress
s2 line

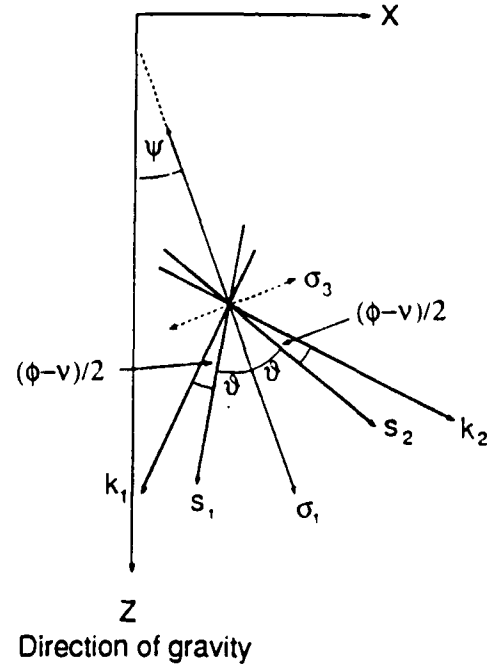
X
ψ
σ3
(ϕ−ν)/2
(ϕ−ν)/2
ϑ
ϑ
s2
k2
k1
s1
σ1
Z
Direction of gravity

PULLOUT STIFFNESS OF ELASTIC ANCHORS IN SLOPE STABILIZATION SYSTEMS

Roman D. Hryciw[1] and Masyhur Irsyam[2]

ABSTRACT

The success of slope stabilization systems which rely on the transfer of loads to the slope from anchored and tensioned geosynthetics, geonets or geogrids depends in large part on the pullout stiffness of the anchors. Pullout stiffness is defined as the ratio of load to displacement at the top of the anchor. Inadequate pullout stiffness may prevent the development of required system tension. Anchors are typically long slender driven reinforcing rods. Thus, both elastic axial extension and rigid body translation are significant components of the total upward anchor displacement. The mobilized interface shear strength between soil and a predriven anchor increases linearly as the relative displacement increases from zero to a critical relative displacement. Beyond this critical displacement the shear strength remains constant. Solutions are presented for the loads, displacements and interface shear stresses on elastic anchors installed in infinite slopes. Equations are then developed for the pullout stiffness and it's first derivative, the incremental pullout stiffness. An example problem demonstrates that the stiffness requirements are most easily met by utilizing a threaded anchor and nut for connecting the surface fabric to the anchor.

[1] Asst. Prof., Univ. of Michigan, Ann Arbor, MI 48109-2125
[2] Research Asst., Univ. of Michigan, Ann Arbor, MI 48109-2125

INTRODUCTION

Methods have recently been developed for stabilization of slopes by anchored and tensioned geosynthetics; geonets (Koerner, 1984, 1985, 1986) and geogrids (Greenwood, 1985). The anchors are typically 0.5 to 1.0 in. (13 to 25 mm) driven reinforcing rods. A geosynthetic or other material is draped over the slope face and fastened to the anchors by one of several mechanical systems shown in Figure 1. Tensioning of the geosynthetic compresses the soil thereby producing a curved soil-geosynthetic interface. The tensile stress distribution in the fabric and the deformed shape determine the magnitude and distribution of loads transferred to the soil. Hryciw (1990) has shown that the increase in stability of an infinite slope may be maximized by orienting the anchors at an optimum angle to the slope which depends on the slope angle, the in-situ stresses and the required percent increase in the factor of safety.

The integrity of an anchored geosynthetic system depends on the ability of the anchors to resist pullout and thereby maintain tension in the fabric. Although the ultimate pullout capacity of an anchor (T_{max}) can be computed by integrating the maximum shearing resistance along the length of the anchor, the combination of rigid translation and elastic axial deformation of the anchor may cause a loss of tension in the geosynthetic thereby reducing the system's effectiveness even at loads considerably below T_{max}. The pullout stiffness of the anchors, defined as the pullout force (T_o) divided by the displacement of

the top of the anchor (δ_o) thus becomes an important parameter in the design of such systems.

Each of the connection systems shown in Figure 1 imparts a different loading sequence to the anchor and geosynthetic. The spring steel collar (Fig. 1a) permits only unidirectional movement of the geosynthetic with respect to the anchor. The geosynthetic is tensioned by driving or pushing on the collar assembly. Once the installation force is removed, the collar fingers lock on the underside of the reinforcing rod ribs and the tensioned geosynthetic imparts an uplift to the anchor. The resulting rigid body translation and elastic extension of the anchor combine to produce the load-displacement curve for the anchor shown in Figure 2(a). The upward movement of the anchor connection in turn causes partial stress relaxation in the fabric. If the installation load is removed from the collar slowly enough so that oscillations of load between the anchor and geosynthetic do not occur, the system will come to equilibrium at point "E" in Figure 2(a).

A second possible tensioning system consists of a threaded anchor and nut as shown in Figure 1(b). A ball bearing plate may be used beneath the nut to prevent the transfer of torque to the geosynthetic. Since the tension in the geosynthetic and anchor develop simultaneously, as shown in Figure 2(b), the geosynthetic is never stretched beyond its designed tension. The critical design criteria for this type of connection is that the

incremental stiffness of the anchor ($dT_o/d\delta_o$) must be greater than the stiffness of the geosynthetic for loads up to the design T_o. Stated differently, for a unit increase in load, the geosynthetic connection must be able to move downward more than the anchor moves up. Otherwise the fabric cannot continue to be tensioned.

In anchored geosynthetic systems as described by Koerner (1986), the anchors are driven through reinforced openings in the fabric to approximately 90% of the required anchorage depth. The geosynthetic is then fastened to the anchor by a pin inserted through the anchor as shown in Figure 1(c) and driven or pushed to its final depth. The application of stress to the anchor causes, in addition to the rigid body displacement, an elastic shortening of the rod. Therefore, upon removal of the driving force, elastic rebound must precede the tensioning and stretching of the anchor (Fig. 2c). The resulting displacements of the anchor, δ_o, will be greater than in either the spring collar or threaded anchor and nut systems thereby rendering this system least attractive for maintaining tension in the fabric.

The present paper develops the theoretical solutions governing the pullout mechanics of single anchors in infinite slopes. Example problems will illustrate the use of pullout stiffness concepts to design. Although the practical application of the solutions presented in this paper will be to anchorage of surface loads for stabilization of slopes, the solutions presented are equally valid for any problem where long slender

elastic inclusions, including piles, are subject to tensioning and uplift.

THE GOVERNING DIFFERENTIAL EQUATION

The loads on an anchor element of length dz at a distance z from the anchor connection are shown in Figure 3. Lower case xyz will be used for a local coordinate system where the z direction is coincident with the anchor. Upper case (XYZ) coordinates will refer to the a system where the Z direction is down. Both coordinate systems have origin of axes at the anchor-geosynthetic connection. The displacement of the anchor in the z-direction is $\delta(z)$ and the axial force acting on a section of the anchor is $T(z)$. The difference between the tensile force at the top and bottom of the element is $dT/dz\ dz$. This difference must equal the force taken out by the soil along the element. If the shearing stress acting on the rod element is given by $\tau(z)$, then:

$$\tau(z) = \frac{1}{C} \frac{dT}{dz} \quad \text{.....(1)}$$

where C is the perimeter of the shearing surface. From Hooke's Law,

$$T = EA \frac{d\,\delta(z)}{dz} \quad \text{.....(2)}$$

where E=Young's modulus and A=cross sectional area of the anchor. Equation (2) may also be presented in differential form as:

$$\frac{dT}{dz} = EA \frac{d^2\delta(z)}{dz^2} \quad \text{.......................................} (3)$$

Combining eq. (1) and (3) produces the governing differential equation for the anchor pullout problem:

$$EA \frac{d^2\delta(z)}{dz^2} - C\,\tau(z) = 0 \quad \text{.................................} (4)$$

SOIL-ANCHOR INTERFACE FRICTION

Previous laboratory investigations (Hryciw, 1989; Hryciw and Irsyam, 1990; Hryciw and Vitton, 1991) have been performed to establish the interface friction characteristics between cohesionless soil and "ribbed inclusions" such as deformed reinforcing rod. In essence this is equivalent to development of t-z curves for piles.

A typical load versus displacement curve is shown in Figure 4. The first motion in the $+\delta$ direction represents the initial downward movement of the anchor during driving. The reverse motion then represents the resistance of the anchor to pullout. While the motion in the $+\delta$ direction is not needed for the present analysis, it is shown to emphasize that anchor driving preshears the soil and establishes a post-driving soil fabric that will control the mobilization of pullout resistance.

Peak stress upon pullout is developed at a displacement, δ_c. In several different soils and anchor rib spacings, δ_c was found to be approximately 0.25 in. (6.4 mm) (Hryciw, 1989, Vitton and

Hryciw, 1991). For $\delta \geq \delta_c$, a constant residual load (or stress) develops. Thus, we will idealize the shearing stress on a driven anchor as increasing linearly from 0 at $\delta=0$ to $\tau=\tau_{max}$ at $\delta=\delta_c$ and continuing at a constant $\tau=\tau_{max}$ when $\delta>\delta_c$.

In frictional soils the maximum shearing stress between soil and anchor, τ_{max} is given by:

$$\tau_{max}(z) = \sigma_n \nu^* \quad \ldots\ldots(5)$$

where ν^*=the apparent coefficient of friction and σ_n is the stress normal to the anchor. The following section develops the expressions for σ_n on an anchor installed at any orientation in an infinite homogeneous elastic slope.

NORMAL STRESS ON ANCHORS IN INFINITE SLOPES

Surface loading is most effective for stabilization of shallow failure surfaces. If the length of the failure surface is greater than approximately 20 times its depth, an infinit slope assumption is valid for stability analysis (Gonsior, 1974). Therefore, an infinite slope geometry is assumed for development of expressions for the in-situ stresses in a slope.

The stresses beneath level ground are given by:

$$\sigma_Z = \gamma Z \quad \ldots\ldots(6a)$$

$$\sigma_X = K_X \gamma Z \quad \ldots\ldots(6b)$$

$$\sigma_Y = K_Y \gamma Z \quad \ldots\ldots(6c)$$

$$\tau_{XZ} = \tau_{YX} = \tau_{YZ} = 0 \quad \ldots\ldots(6d)$$

where K_X and K_Y = coefficients of lateral earth pressure in the X and Y directions and γ= unit weight of soil. The slope may be modelled as a semi-infinite triangular surcharge load applied in compression to one half of the level surface as shown in Figure 5 and a semi-infinite triangular tensile load applied to the other half. The solutions for stresses in an elastic half-space due to semi-infinite triangular loads were presented by Gray (1936). Combining Gray's solutions with eqs. (6) yields the following equations for stresses in a an infinite slope.

$$\sigma_Z = \gamma Z + \gamma X \tan \beta, \quad \text{.....(7a)}$$

$$\sigma_X = K_X \gamma Z + \gamma X \tan \beta, \quad \text{.....(7b)}$$

$$\sigma_Y = K_Y \gamma Z + 2\gamma\nu X \tan \beta, \quad \text{.....(7c)}$$

$$\tau_{XZ} = \gamma Z \tan \beta \frac{(2\alpha-\pi)}{\pi} \quad \text{.....(7d)}$$

and

$$\tau_{YX} = \tau_{YZ} = 0 \quad \text{.....(7e)}$$

where β=slope angle and ν=Poisson's ratio.

For x=0 and y=0 (corresponding to the anchor axis), the following relationships between angles and the two coordinate systems can be invoked:

$$\alpha = \frac{\pi}{2} + \theta + \beta; \quad \text{.....(8a)}$$

$$X = z\sin(\theta+\beta) \quad \text{.....(8b)}$$

and

$$Z = z\cos(\theta+\beta) \quad \ldots\ldots(8c)$$

Combining eqs. 7 and 8 yields:

$$\sigma_Z = \gamma z\cos(\theta+\beta) + \gamma z\sin(\theta+\beta)\tan\beta, \quad \ldots\ldots(9a)$$

$$\sigma_X = K_X\gamma z\cos(\theta+\beta) + \gamma z\sin(\theta+\beta)\tan\beta, \quad \ldots\ldots(9b)$$

$$\sigma_Y = K_Y\gamma z\cos(\theta+\beta) + 2\gamma\nu z\sin(\theta+\beta)\tan\beta, \quad \ldots\ldots(9c)$$

and

$$\tau_{XZ} = 2\gamma z\cos(\theta+\beta)\tan\beta\,\frac{(\theta+\beta)}{\pi} \quad \ldots\ldots(9d)$$

The stress normal to the anchor in the XZ-plane is:

$$\sigma_x = \frac{\sigma_X + \sigma_Z}{2} + \frac{\sigma_X - \sigma_Z}{2}\cos 2(\theta+\beta) + \tau_{XZ}\sin 2(\theta+\beta) \quad \ldots\ldots(10a)$$

while the stress normal to the anchor and normal to the XZ-plane is

$$\sigma_y = \sigma_Y \quad \ldots\ldots(10b)$$

The average normal stress on the anchor is:

$$\sigma_n = \frac{\sigma_x+\sigma_y}{2} \quad \ldots\ldots(11)$$

Equations (9), (10) and (11) may be combined to give:

$$\sigma_n = F_n\gamma z \quad \ldots\ldots(12)$$

where F_n = a stress factor given by:

$$F_n = \frac{K_X+2K_Y+1}{4}\cos(\theta+\beta) + \frac{K_X-1}{4}\cos(\theta+\beta)\cos 2(\theta+\beta) + \frac{1+2\nu}{2}\sin(\theta+\beta)\tan\beta + \frac{\theta+\beta}{\pi}\cos(\theta+\beta)\sin 2(\theta+\beta)\tan\beta \quad \text{.....(13)}$$

Note that if $\theta=\beta=0$, $F_n=1/2(K_X+K_Y)$ and eq. (12) gives the stress normal to a vertical anchor (or pile) in level ground conditions.

SHEAR STRESS DISTRIBUTION

Because the shear stress, τ, increases linearly with δ for $\delta<\delta_c$ and is constant once $\delta\geq\delta_c$, the problem may be separated into two parts as shown in Figures 6a and 6c. The pullout load that causes a displacement of δ_c at the top of the anchor will be defined as the critical load, T_{cr} (Fig. 6b), while the load that causes a displacement of δ_c (and shear stress of τ_{max}) at the bottom of the anchor is the maximum load, T_{max} (Fig. 6d). If $T_o>T_{max}$, complete pullout will occur.

Assuming that δ_c is constant along the length of the anchor, when $T_o\leq T_{cr}$ the shear stress is:

$$\tau(z)=\tau_{max}\frac{\delta}{\delta_c} = \sigma_n\nu^* \frac{\delta}{\delta_c} = F_n\gamma\nu^* z \frac{\delta}{\delta_c} \quad \text{.....(14a)}$$

and when $T_o\geq T_{max}$, the shear stress becomes:

$$\tau(z)=\tau_{max} = \sigma_n \nu^* = F_n \gamma \nu^* z \quad \ldots\ldots\ldots\ldots\ldots\ldots\ldots\ldots\ldots\ldots (14b)$$

When $T_{cr}<T_o<T_{max}$, the shear stress from z=0 to a critical depth, $z=L_c$ (at which $\delta=\delta_c$) will be given by eq. (14b) while the shear stress on the remaining lower part of the anchor will be given by eq. (14a).

SOLUTIONS FOR TENSION AND DISPLACEMENT

The derivation of solutions presented in the remainder of this paper will contain lengthy series summation terms. To maintain brevity and conciseness, a set of constants that will appear frequently are presented in Table 1. The authors have found that n=6 to 8 must be used to provide stable values for the summation terms. Note should be taken that only Φ is a function of the anchor length while the Ψ's all contain L_c. The definition of λ follows immediately.

Condition I. $T_o \leq T_{cr}$

If $T_o \leq T_{cr}$, by definition $\delta \leq \delta_c$ for all z and $\tau(z)$ will be given by eq. (14a). Combining (14a) with the governing differential equation (4) gives:

$$\frac{d^2\delta(z)}{dz^2} - \lambda\delta(z)z = 0 \quad \ldots\ldots\ldots\ldots\ldots\ldots\ldots\ldots\ldots\ldots (15)$$

where:

$$\lambda = \frac{CF_n \gamma \nu^*}{EA\delta_c} \quad \text{.....(16)}$$

The solution to equation (15) is given by the Airy function:

$$\delta(z) = a_o \left[1 + \sum_{n=1}^{\alpha} \frac{\lambda^n z^{3n}}{P(n)}\right] + a_1 \left[z + \sum_{n=1}^{\alpha} \frac{\lambda^n z^{3n+1}}{Q(n)}\right] \quad \text{.....(17)}$$

where a_o and a_1 are constants to be determined from the boundary conditions. In consideration of equation (2), the corresponding expression for load is:

$$T(z) = AEa_o\left[\sum_{n=1}^{\infty} \frac{\lambda^n z^{3n-1}}{R(n)}\right] + AEa_1\left[1 + \sum_{n=1}^{\infty} \frac{\lambda^n z^{3n}}{S(n)}\right] \quad \text{.....(18)}$$

Invoking the boundary conditions:

$T = T_o$ at $z = 0$ .....(19a)

and

$T = 0$ at $z = L$ .....(19b)

where L=total anchor length, the following solutions are found for the constants:

$$a_1 = \frac{T_o}{AE} \quad \text{.....(20a)}$$

and

$$a_o = -\frac{T_o}{AE\Phi} \quad \text{.....(20b)}$$

Condition II. $T_{cr} \leq T_o \leq T_{max}$

At $T_o=T_{cr}$ full mobilization of shear strength develops at the top of the anchor. As the pullout load increases beyond T_{cr}, full mobilization propagates down the anchor. Figure 6c illustrates the condition when $T_{cr} \leq T \leq T_{max}$. For $z<L_c$, full shearing resistance has developed and $\tau(z)$ is given by eq. (14b) while for $z>L_c$, $\tau(z)$ is given by eq. (14a).

In the region $L_c \leq z \leq L$, the governing differential equation is still eq. (15). The solutions are once again given by eqs. (17) and (18) but since the boundary conditions will be different we ascribe new constants a_2 and a_3:

$$\delta(z) = a_2\left[1 + \sum_{n=1}^{\infty} \frac{\lambda^{n_z} 3n}{P(n)}\right] + a_3\left[z + \sum_{n=1}^{\infty} \frac{\lambda^{n_z} 3n+1}{Q(n)}\right] \quad \text{.....(21a)}$$

$$T(z) = AEa_2\left[\sum_{n=1}^{\infty} \frac{\lambda^{n_z} 3n-1}{R(n)}\right] + AEa_3\left[1 + \sum_{n=1}^{\infty} \frac{\lambda^{n_z} 3n}{S(n)}\right] \quad \text{.....(21b)}$$

The new boundary conditions are:

$T = 0$ at $z = L$ .....(22a)

and

$\delta = -\delta_c$ at $z = L_c$ .....(22b)

from which we find:

$$a_3 = \frac{\delta_c \Phi}{\Psi_1 - \Psi_2 \Phi} \quad \text{.....(23a)}$$

and

$$a_2 = \frac{-\delta_c}{\Psi_1 - \Psi_2\Phi} \quad \text{.....(23b)}$$

The displacement, tension and shear stress distributions for the region $0<z<L_c$ may now be determined. The governing differential equation (4) is recalled:

$$EA \frac{d^2\delta(z)}{dz^2} - C\tau(z) = 0 \quad \text{.....(4)}$$

Since shearing strength is fully mobilized, we combine with eq. (14b) to get:

$$\frac{d^2\delta(z)}{dz^2} - \kappa z = 0 \quad \text{.....(24)}$$

where

$$\kappa = \frac{-CF_n\gamma\nu^*}{EA} \quad \text{.....(25)}$$

The minus sign indicates that $\tau(z)$ must be numerically negative for upward displacement to be negative. The previously defined term, λ did not require such a stipulation because δ_c was always negative thereby making λ also numerically negative. Integrating eq.(24) produces:

$$\frac{d\delta(z)}{dz} = 1/2\ \kappa z^2 + G \quad \text{.....(26)}$$

and a second integration yields:

$$\delta(z) = 1/6\ \kappa z^3 + Gz + H \quad \text{.....(27)}$$

where G and H are constants of integration. If the boundary conditions

$$T = T_o \quad \text{at} \quad z = 0 \quad \text{.....(28a)}$$

and

$$\delta = -\delta_c \ \text{at}\ z = L_c \quad \text{.....(28b)}$$

are enforced, we obtain

$$G = \frac{T_o}{AE} \quad \text{.....(29a)}$$

and

$$H = -\left[\delta_c + 1/6\ \kappa L_c^3 + \frac{T_o L_c}{AE}\right] \quad \text{.....(29b)}$$

The expressions for displacement and tension in the section $0 \le z \le L_c$ are thus:

$$\delta(z) = 1/6\ \kappa z^3 + \frac{T_o}{AE} z - \left[\delta_c + \frac{1}{6}\ \kappa L_c^3 + \frac{T_o L_c}{AE}\right] \quad \text{.....(30a)}$$

and

$$T(z) = EA \frac{d\,\delta(z)}{dz} = EA \left[\frac{1}{2}\ \kappa z^2 + \frac{T_o}{AE}\right] \quad \text{.....(30b)}$$

Critical Load (T_{cr}) and Maximum Load (T_{max})

In order to apply the general solutions presented in the previous section to determination of anchor loads and displacements, an expression for T_{cr} must be derived. Equation

(17a) indicates that if $T_o \leq T_{cr}$ the displacement at the top of the anchor is:

$$\delta_o = a_o, \quad \ldots\ldots(31)$$

and when $T_o = T_{cr}$, we have $\delta_o = \delta_c = a_o$. Combining with eq. (20b), the critical load is found to be given by:

$$T_{cr} = AE\delta_c\Phi \quad \ldots\ldots(32)$$

The maximum load, T_{max} has previously been defined as the load at which $\delta(L) = -\delta_c$ and $\tau(L) = \tau_{max}$. Hence, the shear stress along the entire anchor length must also be τ_{max}. Thus, by equilibrium we must have:

$$T_{max} = C \int_0^L \tau_{max}(z)\, dz = CF_n\gamma\nu^* \int_0^L z\, dz \quad \ldots\ldots(33a)$$

or

$$T_{max} = \frac{1}{2} CF_n\gamma\nu^* L^2 \quad \ldots\ldots(33b)$$

which may also be written

$$T_{max} = \frac{1}{2} \lambda AE\delta_c L^2 \quad \ldots\ldots(33c)$$

A comparison of equations (32) and (33c) shows that the ratio T_{cr}/T_{max} is only a function of λ and L. This relationship is thus shown in Figure 7. Any consistent units for λ and L may be used.

Example 1. Solution for the Anchor Pullout Problem

At this point all of the requisite equations to perform an example problem are available. A list of typical soil and anchor parameters is provided in Table 2. For the given γ, K, ν, β and θ the normal stress factor, F_n, is computed by eq. (13) to be 0.875. By eq. (16), $\lambda=8.1\text{x}10^{-5}$ ft^{-3} ($2.9\text{x}10^{-3}$ m^{-3}) is found. For a 30 ft. (9.1 m) anchor T_{cr}/T_{max} = 0.64 from Figure 7. Thus, full mobilization of shear strength begins developing at approximately two-thirds of the maximum pullout resistance.

The tension, shear stress and displacement profiles are shown in Figure 8 for various T_o. The rigid body component of the displacement is equal to the motion of the bottom of the anchor, while displacement due to elastic elongation is given by the difference between displacements at the top and bottom. It is noteworthy that both rigid body motion and elastic elongation contribute significantly to the total displacement.

PULLOUT STIFFNESS AND INCREMENTAL PULLOUT STIFFNESS

While the complete solutions provide interesting insight into the load transfer between soil and anchors in tension, the only parameters truly relevant for anchored load systems are the previously defined pullout stiffness, T_o/δ_o and the incremental pullout stiffness, $\partial T_o/\partial \delta_o$. The pullout force versus displacement of the top of the anchor for example problem #1 is thus shown in Figure 9. As long as $T_o \leq T_{cr}$, the pullout stiffness and the incremental pullout stiffness are one and the same

constant. This constant is obtained by combining eqs. (20b) and (31) to give:

$$\frac{T_o}{\delta_o} = AE\Phi \quad \text{for } T_o \leq T_{cr} \quad \ldots\ldots\ldots\ldots\ldots\ldots\ldots\ldots\ldots\ldots\ldots (34)$$

For example problem #1 we find T_o/δ_o = 9696 lb/in (17 kN/cm).

Beyond T_{cr}, the load-displacement curve is no longer linear and both the pullout and the incremental pullout stiffnesses decrease. The expressions are naturally more complicated but may be developed as follows. The pullout force, T_o is computed by summing the shear stress along the two sections of the anchor:

$$T_o = C \int_0^{L_c} \tau(z)\, dz + C \int_{L_c}^{L} \tau(z)\, dz \quad \ldots\ldots\ldots\ldots\ldots\ldots\ldots\ldots\ldots\ldots (35)$$

The second term on the right side of eq. (35) is equal to the tension force in the anchor at $z=L_c$ and may be calculated by eq. (21b). In the first term, $\tau(z)$ is given by eq. (14b). Thus, combining eqs. (21b) and (14b) with (35), performing the integrations and simplifying yields:

$$T_o = \frac{1}{2} CF_n \gamma \nu^* L_c^2 + AE\delta_c \left[\frac{\Psi_6\Phi - \Psi_4}{\Psi_1 - \Psi_2\Phi}\right] \quad \ldots\ldots\ldots\ldots\ldots\ldots\ldots\ldots\ldots (36a)$$

which may also be written

$$T_o = AE\delta_c \left[\frac{1}{2} \lambda L_c^2 + \left[\frac{\Psi_6\Phi - \Psi_4}{\Psi_1 - \Psi_2\Phi}\right]\right] \quad \ldots\ldots\ldots\ldots\ldots\ldots\ldots\ldots\ldots (36b)$$

From equation (27) $\delta_o = H$ when $T_o > T_{cr}$. Combining with (29b) produces:

$$\delta_o = -\left[\delta_c + 1/6\ \kappa L_c^3 + \frac{T_o L_c}{AE}\right] \quad \text{.....(37a)}$$

Recognizing from eqs. (16) and (25) that $\kappa = -\lambda\delta_c$, eq. (37a) may also be written:

$$\delta_o = -\left[\delta_c - 1/6\ \lambda\delta_c L_c^3 + \frac{T_o L_c}{AE}\right] \quad \text{.....(37b)}$$

Combining eqs. (36b) into (37b) results in:

$$\delta_o = -\delta_c\left[1 + \frac{1}{3}\lambda L_c^3 + \frac{\Psi_6\Phi - \Psi_4}{\Psi_1 - \Psi_2\Phi} L_c\right] \quad \text{.....(38)}$$

Finally, dividing eq. (36b) by (38) produces the expression for pullout stiffness when $T_o > T_{cr}$:

$$\frac{T_o}{\delta_o} = \frac{-AE\left[\frac{1}{2}\lambda L_c^2 + \left[\frac{\Psi_6\Phi - \Psi_4}{\Psi_1 - \Psi_2\Phi}\right]\right]}{\left[1 + \frac{1}{3}\lambda L_c^3 + \frac{\Psi_6\Phi - \Psi_4}{\Psi_1 - \Psi_2\Phi} L_c\right]} \quad \text{.....(39)}$$

To determine the incremental pullout stiffness for $T_o > T_{cr}$, we note that both T_o and δ_o are functions of the variable L_c while all remaining terms are constants. Thus, by the chain rule of differentiation,

$$\frac{\partial T_o}{\partial \delta_o} = \frac{\partial T_o/\partial L_c}{\partial \delta_o/\partial L_c} \quad \text{...} (40)$$

Individually differentiating equations (36b) and (38) with respect to L_c and dividing the former result by the latter as required by equation (40) yields the expression for incremental pullout stiffness:

$$\frac{\partial T_o}{\partial \delta_o} = AE\delta_c \left[\lambda L_c - \left[\frac{(\Psi_1-\Psi_2\Phi)\Psi_3-(\Psi_4-\Psi_6\Phi)\Psi_4-[(\Psi_1-\Psi_2\Phi)\Psi_5-(\Psi_4-\Psi_6\Phi)\Psi_6]\Phi}{(\Psi_1-\Psi_2\Phi)^2} \right] \right.$$

$$\text{.......} (41)$$

The pullout stiffnesses and the incremental pullout stiffnesses were determined as a function of δ for example problem #1 and are shown in Figures 10 and 11. For comparison, the results for anchor lengths other than 30 ft. (9.1 m) as well as contours of L_c/L are also provided in the figures.

Example 2 Anchor Design

An example problem will illustrate the use of Figures 10 and 11 for design. The procedure for determining the required T_o to achieve a desired increase in a slope's factor of safety is given elsewhere (Hryciw, 1990). We will assume that T_o=0.8 kips (3.6 kN) is required.

A typical plot of load versus vertical displacement of an anchored geosynthetic is shown in Figure 12. Details of this figure are beyond the scope of the present work but several

relevant features must be addressed. First, during virgin loading the curve reflects the combined response of the geosynthetic as it is being stretched as well as compression of the soil beneath the fabric. Plastic yielding of the soil typically occurs and the soil bulges at some distance from the anchor. This bulging may actually help in developing the necessary curvature to transfer loads to the soil more uniformly with distance from the anchor.

a) Spring Steel Type Connection.

Both the plastic yielding of the soil and the geosynthetic strain are highly permanent. Upon release of installation loads, even a small upward movement of the connection point will greatly reduce the tension in the geosynthetic and T_o. It follows that a relatively stiff anchor as shown in Figure 13(a) will be required for this geosynthetic when a spring steel type connection is used.

A design chart such as shown in Figure 14 may be developed from Figure 12. The three curves correspond to unload cycles A, B and C. Thus, if the geosynthetic is unloaded and reloaded as shown by cycle C and T_o=0.8 kips (3.6 kN) is needed, the required pullout stiffness is approximately 9 kips/in. (15.8 kN/cm) We also note from Fig. 13(a) that the total displacement of the anchor connection will be less than δ_c=0.25 in. (6.4 mm) and thus L_c/L will be 0. If the soil and anchor properties, slope geometry, anchor dimensions and soil-anchor interface

characteristics given in Table 2 are assumed, the required anchor length is determined from Figure 10 to be approximately 28 ft. (8.5 m).

b) Threaded Anchor and Nut Connection

It was earlier stated that for threaded anchor and nut connections the incremental pullout stiffness of the anchor must be greater than that of the geosynthetic at least up to the design load, T_o. Koerner (1985) has indicated that following installation of an anchored geosynthetic system, the combination of stress relaxation in the fabric and soil creep may necessitate retensioning of the anchors. As such, it is important to recognize that the incremental stiffness criteria must hold for the reload cycles shown in Figures 12 and 13(b).

The maximum stiffness of the geosynthetic observed in Figure 13(b) is approximately 3.5 kips/in. (6.1 kN/cm). Since the anchor length is not known, we first assume that the anchor displacement will be less than δ_c. Referring to Figure 11, we see that the required anchor length would be 15 ft. (4.6 m) For a 15 ft. anchor and $\lambda=8.1\text{x}10^{-5}$ ft.$^{-3}$ ($2.9\text{x}10^{-3}$ m^{-3}) eq. 33(c) gives $T_{max}=0.95$ kips (4.2 kN) From Figure 7 we find for L=15 ft. and $\lambda=8.1\text{x}10^{-5}$ ft.$^{-3}$ that $T_{cr}/T_{max} = 0.93$. Since the design load of 0.8 kips is only 0.85 of T_{max}, the original assumption that $\delta_o<\delta_c$ was valid and L=15 ft. will be adequate.

By comparison to the 28 ft. (8.5 m) anchor length requirement for a spring steel type connection, the 15 ft. (4.6 m) length for

a threaded nut and anchor connection is a far better alternative. The required length for a driven anchor would be even greater. Although the anchorage requirements are controlled by the mechanical behavior of the geosynthetic and soil-fabric interaction, and are therefore fabric and site specific, the advantages of a threaded anchor and nut connection will generally hold.

SUMMARY AND CONCLUSIONS

The complete solutions for the pullout problem of linear elastic inclusions (anchors or piles) in soils has been presented. The mobilization of shearing resistance between soil and anchor was modelled as increasing linearly from 0 to τ_{max} at a critical displacement δ_c. Beyond δ_c, the shearing resistance remained constant at τ_{max}.

An application for the presented solutions is in anchored geosynthetic systems for stabilization of slopes. A procedure was presented for determining the normal stress distribution on anchors in slopes and an example problem illustrated that both elastic deformation and rigid body motion are significant components of the total upward displacement of anchors.

The pullout stiffness (T_o/δ_o) of anchors is an important design parameter for maintaining system tension when spring steel connections are used to fasten the fabric to the soil. When a threaded anchor and nut connection is used, the incremental stiffness ($dT_o/d\delta_o$) controls. An example problem

revealed that the threaded anchor and nut connection requires a significantly shorter anchor and is therefore preferred over spring steel connections or the current practice of tensioning by driving on the anchors.

ACKNOWLEDGEMENTS

This study was part of a research program supported and funded by the United States Air Force Office of Scientific Research under Grant No. AFOSR-88-0166. Financial support for Mr. Irsyam's graduate studies were provided by IUC-ITB/MUCIA-World Bank XVII.

TABLE 1. Terms Used in Series Solutions

$$\Phi = \frac{\sum_{n=1}^{\infty} \frac{\lambda^n L^{3n-1}}{R(n)}}{1 + \sum_{n=1}^{\infty} \frac{\lambda^{n_L 3n}}{S(n)}}$$

$$\Psi_1 = 1 + \sum_{n=1}^{\infty} \frac{\lambda^{n_{L_c} 3n}}{P(n)} \qquad \Psi_2 = L_c + \sum_{n=1}^{\infty} \frac{\lambda^{n_{L_c} 3n+1}}{Q(n)}$$

$$\Psi_3 = \sum_{n=2}^{\infty} \frac{\lambda^{n_{L_c} 3n-2}}{U(n)} \qquad \Psi_4 = \sum_{n=1}^{\infty} \frac{\lambda^{n_{L_c} 3n-1}}{R(n)}$$

$$\Psi_5 = \sum_{n=2}^{\infty} \frac{\lambda^{n_{L_c} 3n-1}}{V(n)} \qquad \Psi_6 = 1 + \sum_{n=1}^{\infty} \frac{\lambda^{n_{L_c} 3n}}{S(n)}$$

where $P(n) = (3n)(3n-1)(3n-3)(3n-4)\ldots(3)(2)$

$Q(n) = (3n+1)(3n)(3n-2)(3n-3)\ldots(4)(3)$

$R(n) = (3n-1)(3n-3)(3n-4)\ldots(3)(2)$

$S(n) = (3n)(3n-2)(3n-3)\ldots(4)(3)$

$U(n) = (3n-3)(3n-4)\ldots(3)(2)$

$V(n) = (3n-2)(3n-3)\ldots(4)(3)$

TABLE 2. Soil and Anchor Properties for Example Problems 1 and 2

Soil	Anchor	Soil/Anchor
γ = 115 lb/ft^3	E = 28,000 ksi	ν^* = 0.58
K = 0.5	r = 0.275 in.	δ_c = 0.25 in.
ν = 0.25	r_{in} = 0.238 in.	
β = 35°	C = 1.73 in.	
θ = 28°	A = 0.178 in^2	
	L = 30 ft	
	Computed: F_n = 0.875	
	λ = 8.1x10^{-5} ft^{-3}	
	T_{cr} = 2424 lbs	
	T_{max} = 3781 lbs	
	T_{cr}/T_{max} = 0.64	

note: 1 in. = 2.54 cm; 1 ft = 0.305 m; 1 lbf = 4.45 N

Appendix I. ——References

Gray, H. (1936) "Stress Distribution in Elastic Solids", Proc. of the First International Conference on Soil Mechanics and Foundation Engineering, Harvard University, Cambridge Mass., vol. II, 157-168.

Gonsior, M. J. Hartsog, W. S. and Martin, G. L. (1974) "Failure Surfaces in Infinite Slopes", USDA Forest Service Research Paper INT-150, 33 pp.

Greenwood, J. R. (1985) "Geogrids and Anchors for Slope Stabilization-Simple Method of Analysis," Discussion, Proceedings of the 11th International Conference on Soil Mechanics and Foundation Engineering, Vol. 5, pp. 2770-2771.

Hryciw, R. D. (1989) "Load Transfer Mechanisms in Anchored Geosynthetic Systems," Annual Report to the Air Force Office of Scientific Research on Project Number AFOSR-88-0166.

Hryciw, R. D. and Irsyam, M. (1990) "Shear Zone Characterization In Sands by Carbowax Impregnation," Geotechnical Testing Journal of ASTM, Vol. 13, No. 1, pp. 49-52.

Hryciw, R. D. (1990) "Anchor Design For Slope Stabilization by Surface Loading," Submitted to the Journal of Geotechnical Engineering of ASCE.

Koerner, R. M. (1984) "In-Situ Soil Slope Stabilization Using Anchored Nets," Low Cost & Energy Saving Construction Materials Conference Proceedings, Rio De Janiero, Brazil, 465-478.

Koerner, R. M. (1985) "Slope Stabilization Using Anchored Geotextiles and/or Geogrids," Proc. Special Geotechnical Engineering for Roads and Bridges, Harrisburg, PA.

Koerner, R. M. and Robins, J. C. (1986) "In-Situ Stabilization of Soil Slopes Using Nailed Geosynthetics," Proc. of the Third International Conference on Geotextiles, Vienna, Austria, 395-400.

Pearlman, S. (1990). Personal Communication, Nicholson Construction Co., Bridgeville, PA.

Vitton, S. J. and Hryciw, R. D. (1991) "Soil-Anchor Interaction in Anchored Geosynthetic Systems," Submitted to the Geotechnical Congress to be held at the University of Colorado at Boulder.

Weatherby, D. E. and Nicholson, P. J. (1982) "Tiebacks Used For Landslide Stabilization", Proc. of ASCE Sessions on Application of Walls to Landslide Control Problems, Las Vegas, NV. April 29, pp. 44-60.

Appendix II. ——Notation

A = cross sectional area of anchor
a_{0-3} = constants
C = perimeter of shearing surface
E = Young's modulus
F_n = normal stress factor
G = constant of integration
H = constant of integration
K = coefficient of lateral earth pressure
L = anchor length
L_c = critical anchor distance
r = radius of anchor shearing surface
r_{in} = radius of anchor excluding ribs
T_{cr} = critical pullout load
T_{max} = maximum pullout load
T_o = pullout load
X,Y,Z = cartesian coordinate system (Z=down)
x,y,z = cartesian coordinate system (z coincident with anchor)

α = angle used in solution for stresses in slopes
β = slope angle
γ = soil unit weight
δ = anchor displacement
δ_c = critical anchor displacement
Φ = summation term constant
ϕ = angle of internal friction of soil
κ = constant
λ = constant
ν = Poisson's ratio
ν^* = apparent coefficient of friction
θ = angle of anchor to slope normal
σ = stress
σ_n = average normal stress on the anchor
τ = shear stress
τ_{max} = maximum shearing resistance between soil and anchor
Ψ_{1-6} = summation constants

LIST OF FIGURES

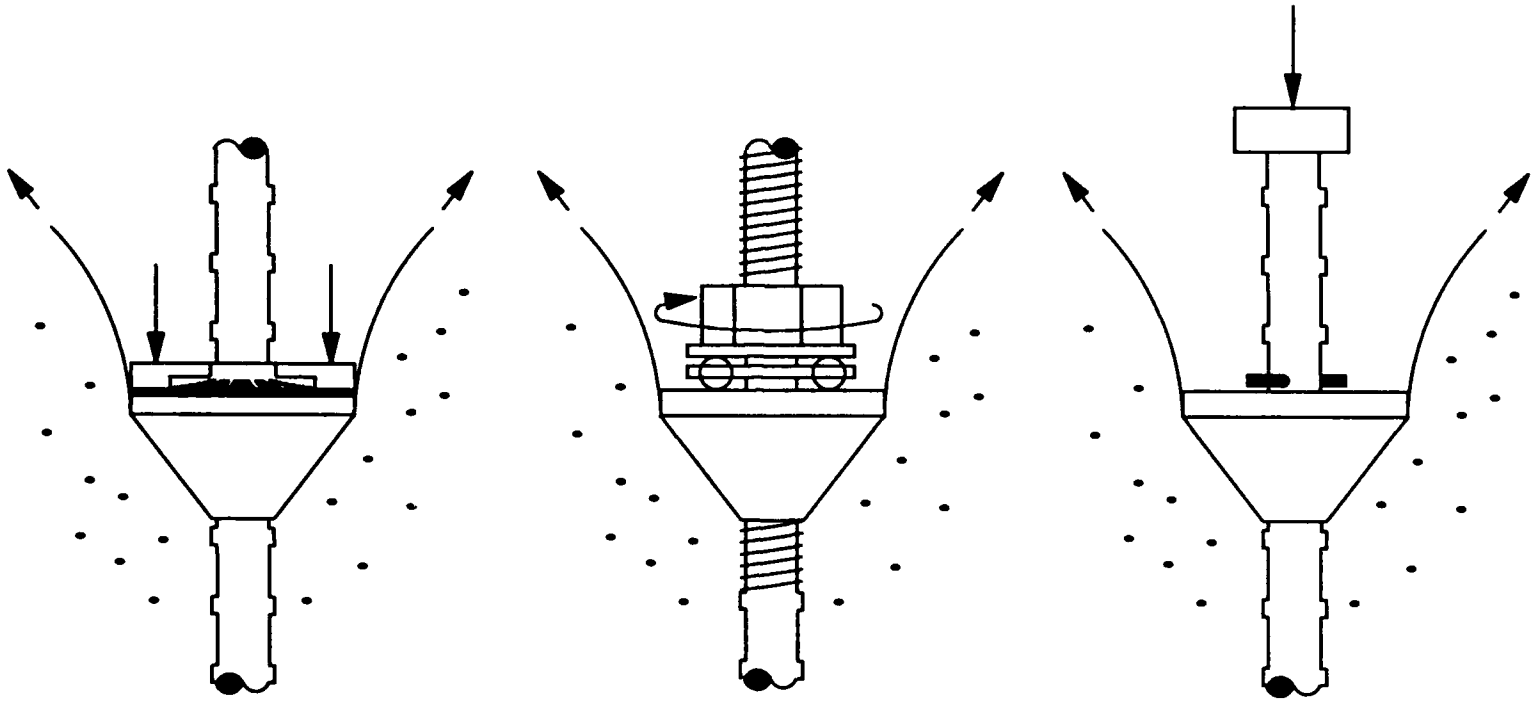

(a) Spring Steel Collar

(b) Threaded Anchor and Nut

(c) Pinned Anchor

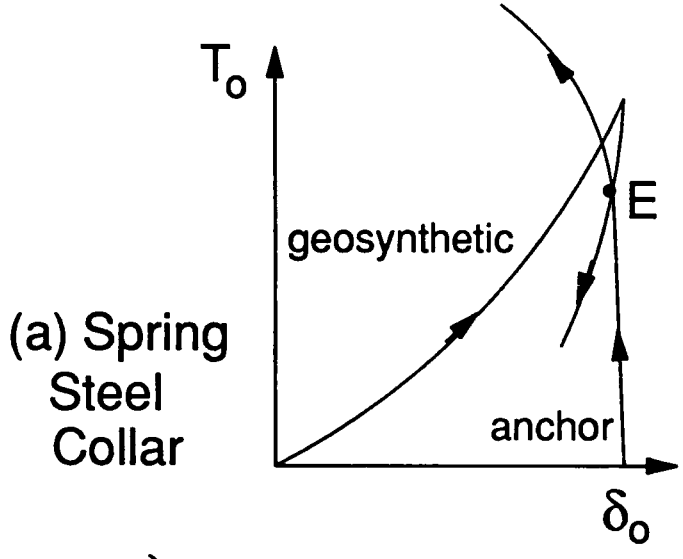

(a) Spring Steel Collar

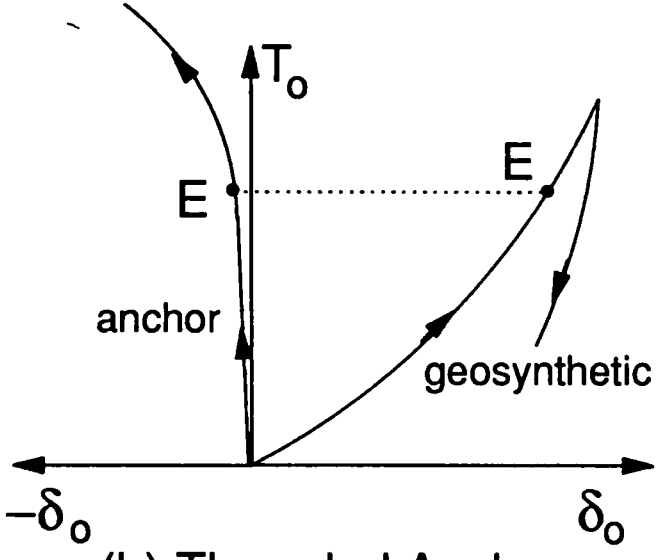

(b) Threaded Anchor and Nut

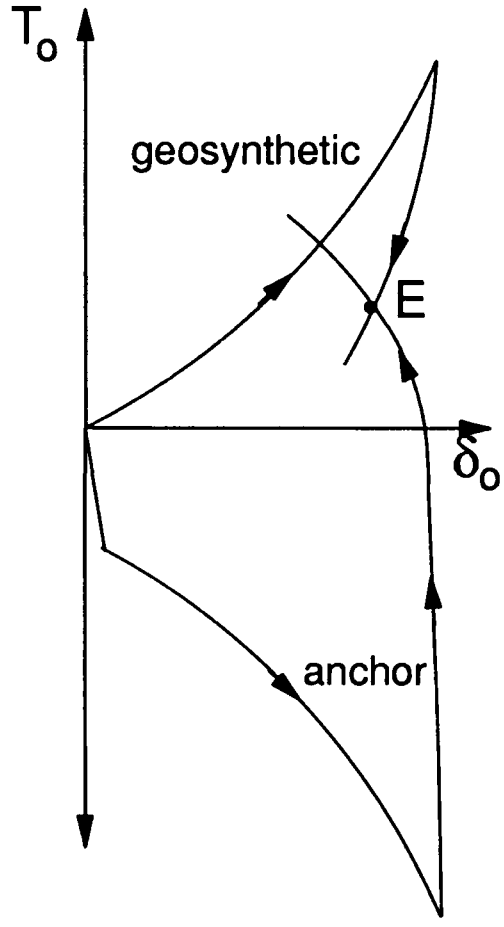

(c) Pinned Anchor

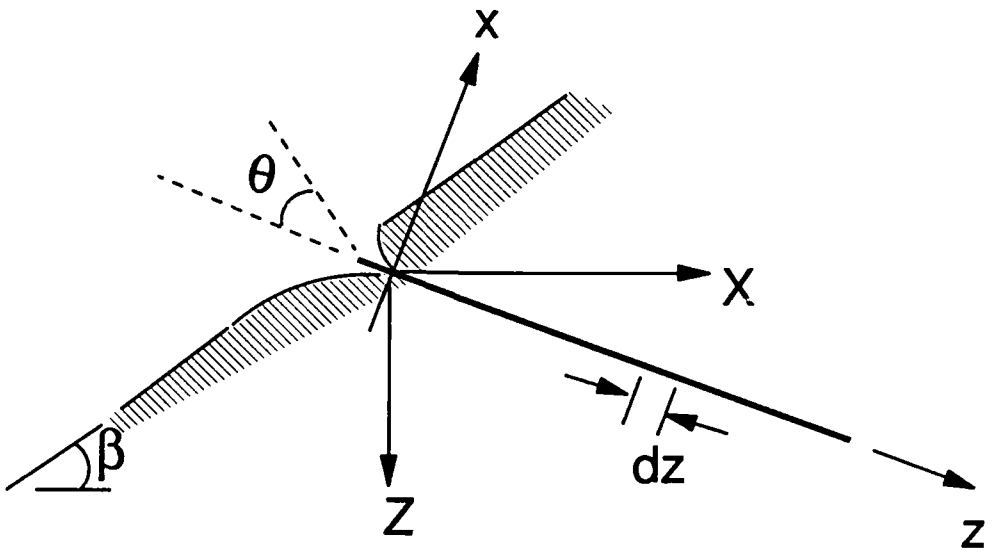
x
θ
X
β
dz
Z
z

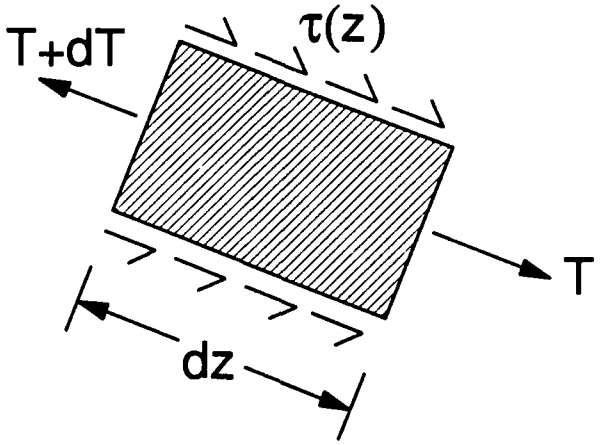
T+dT
τ(z)
T
dz

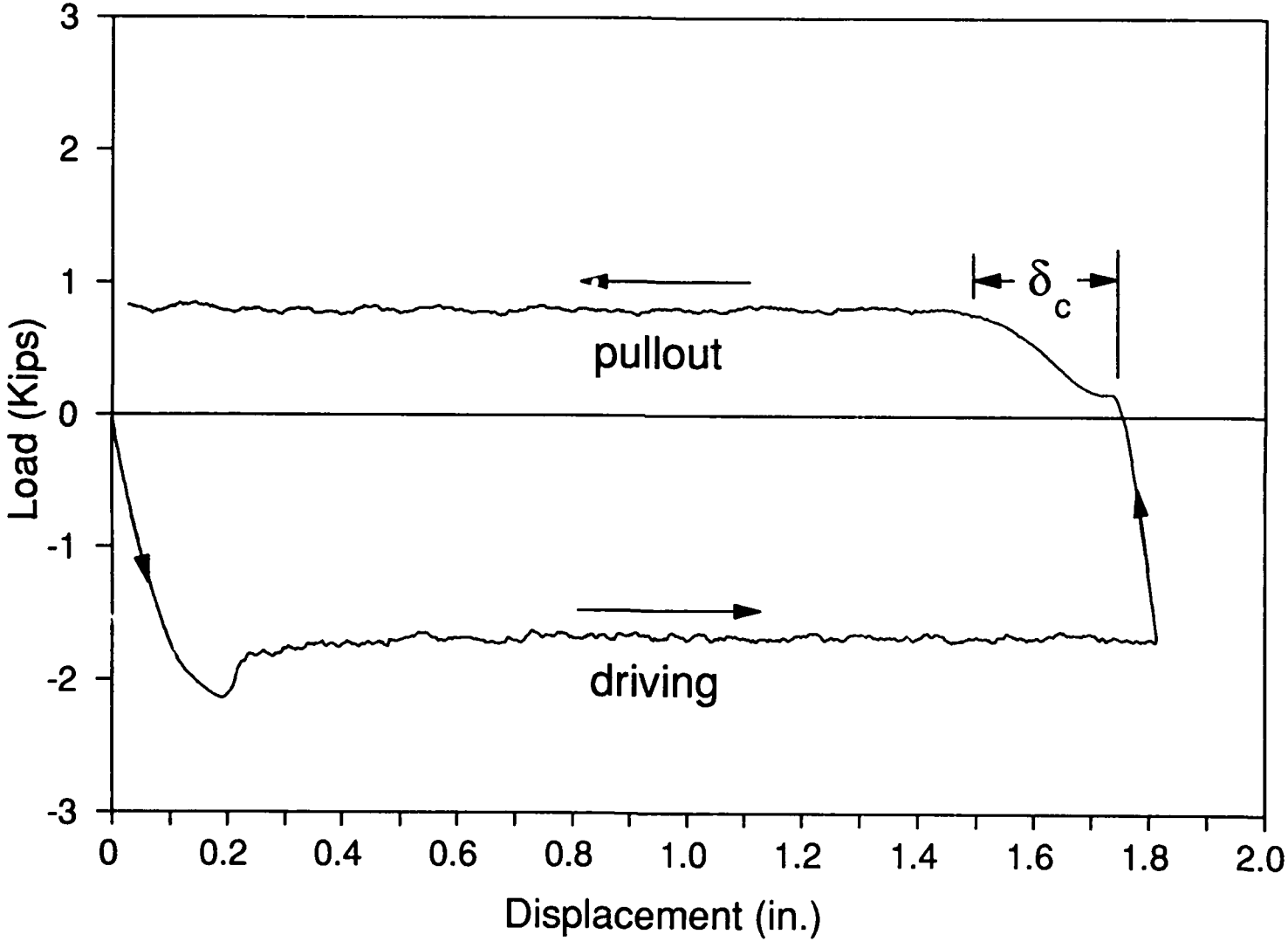
3
2
1
0
-1
-2
-3
Load (Kips)
pullout
δ_c
driving
0
0.2
0.4
0.6
0.8
1.0
1.2
1.4
1.6
1.8
2.0
Displacement (in.)

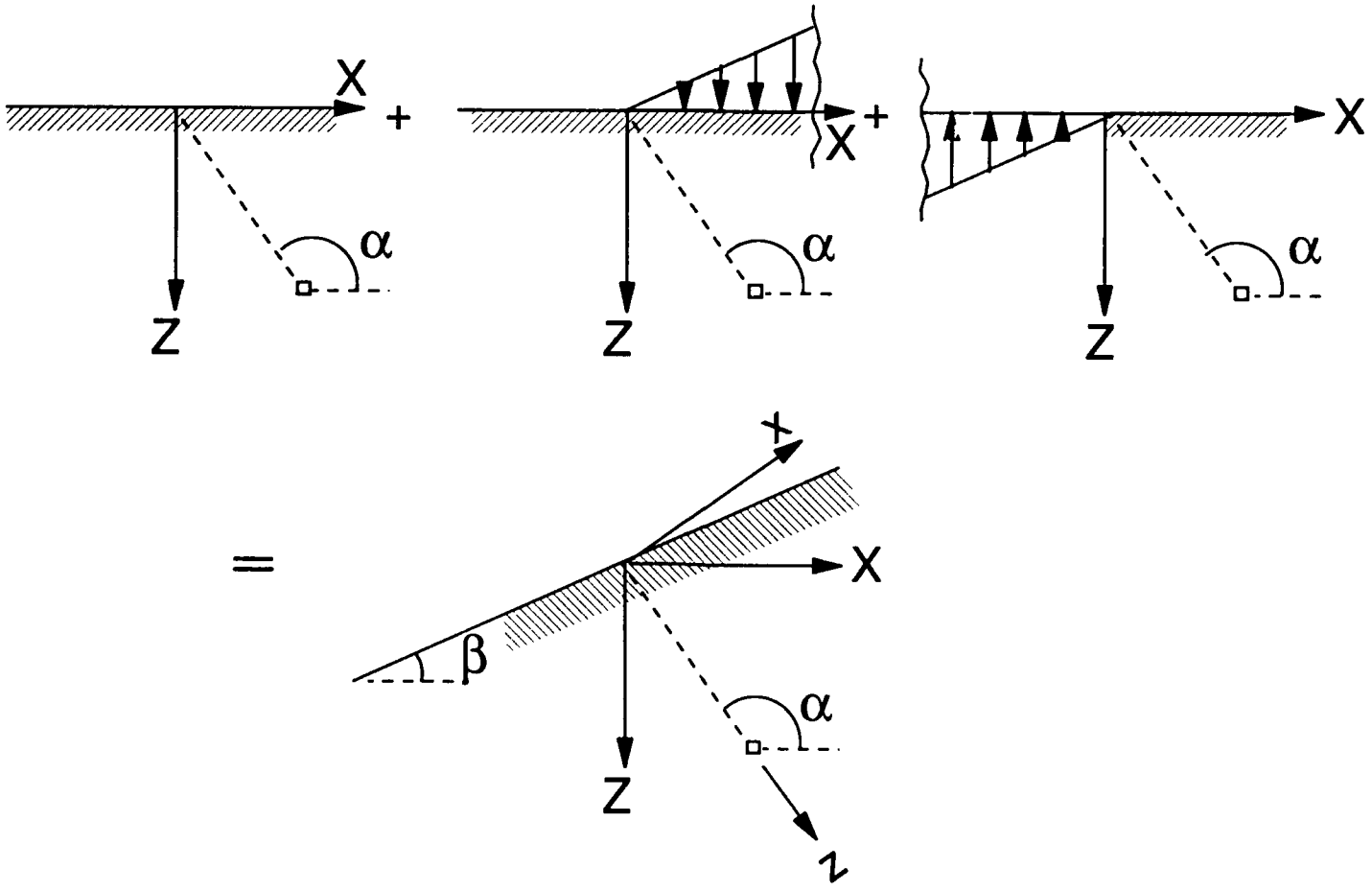
X
+
α
Z
X
+
α
Z
X
α
Z
=
Y
X
β
α
Z
z

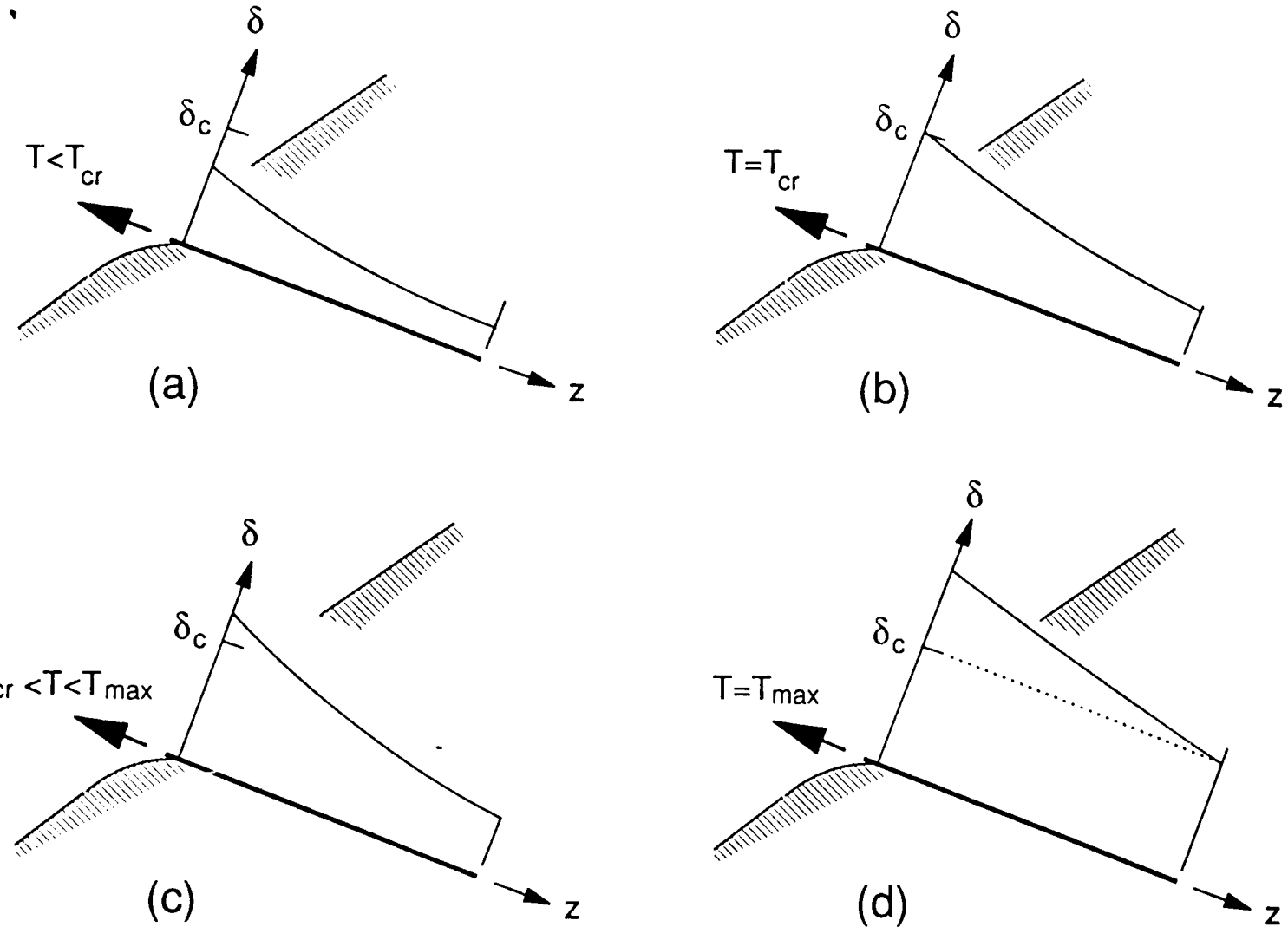
δ
δc
T<Tcr
z
(a)
δ
δc
T=Tcr
z
(b)
δ
δc
Tcr <T<Tmax
z
(c)
δ
δc
T=Tmax
z
(d)

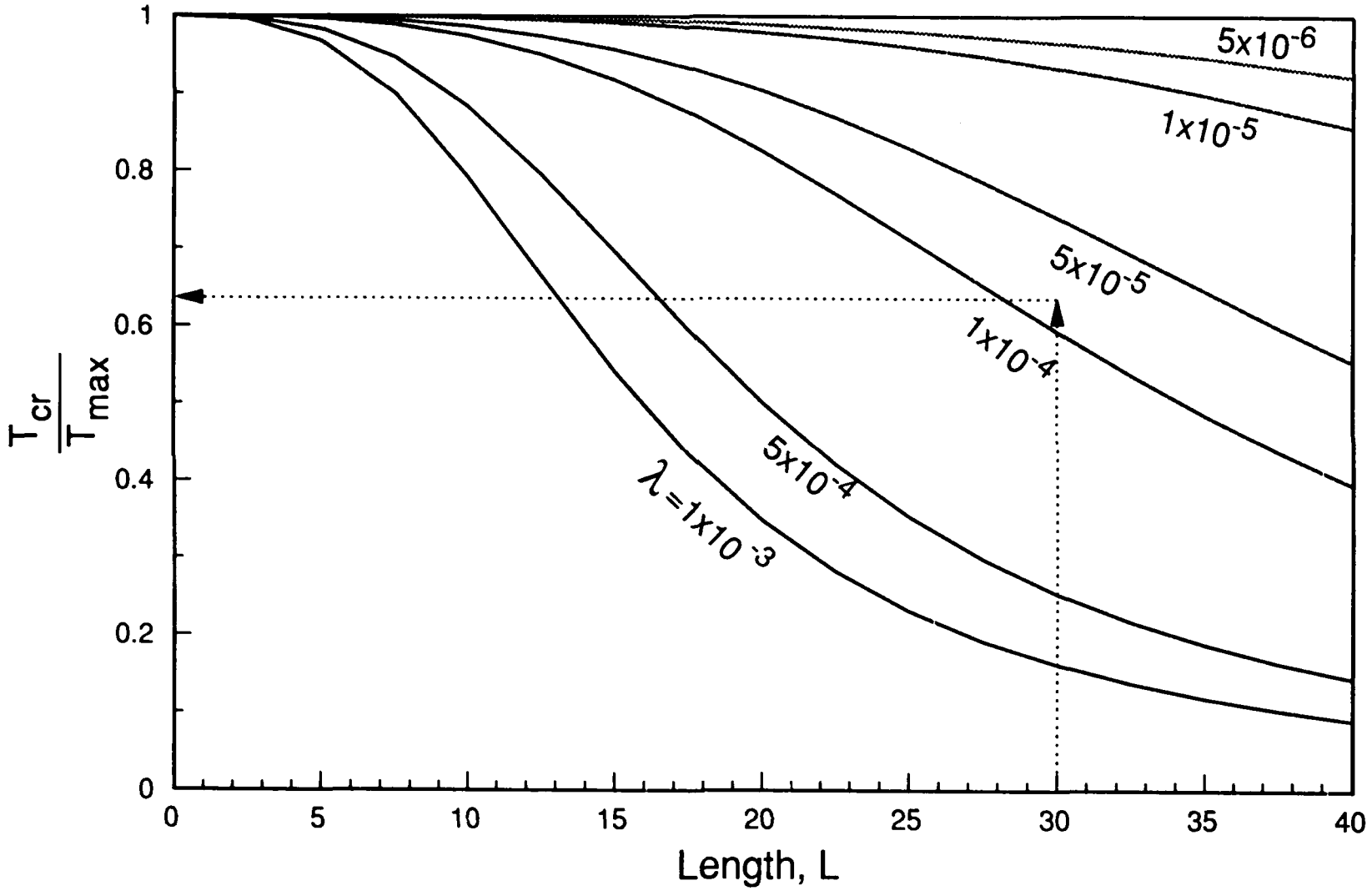
1
0.8
0.6
0.4
0.2
0
$\frac{T_{cr}}{T_{max}}$
0
5
10
15
20
25
30
35
40
Length, L
5x10-6
1x10-5
5x10-5
1x10-4
5x10-4
λ=1x10-3

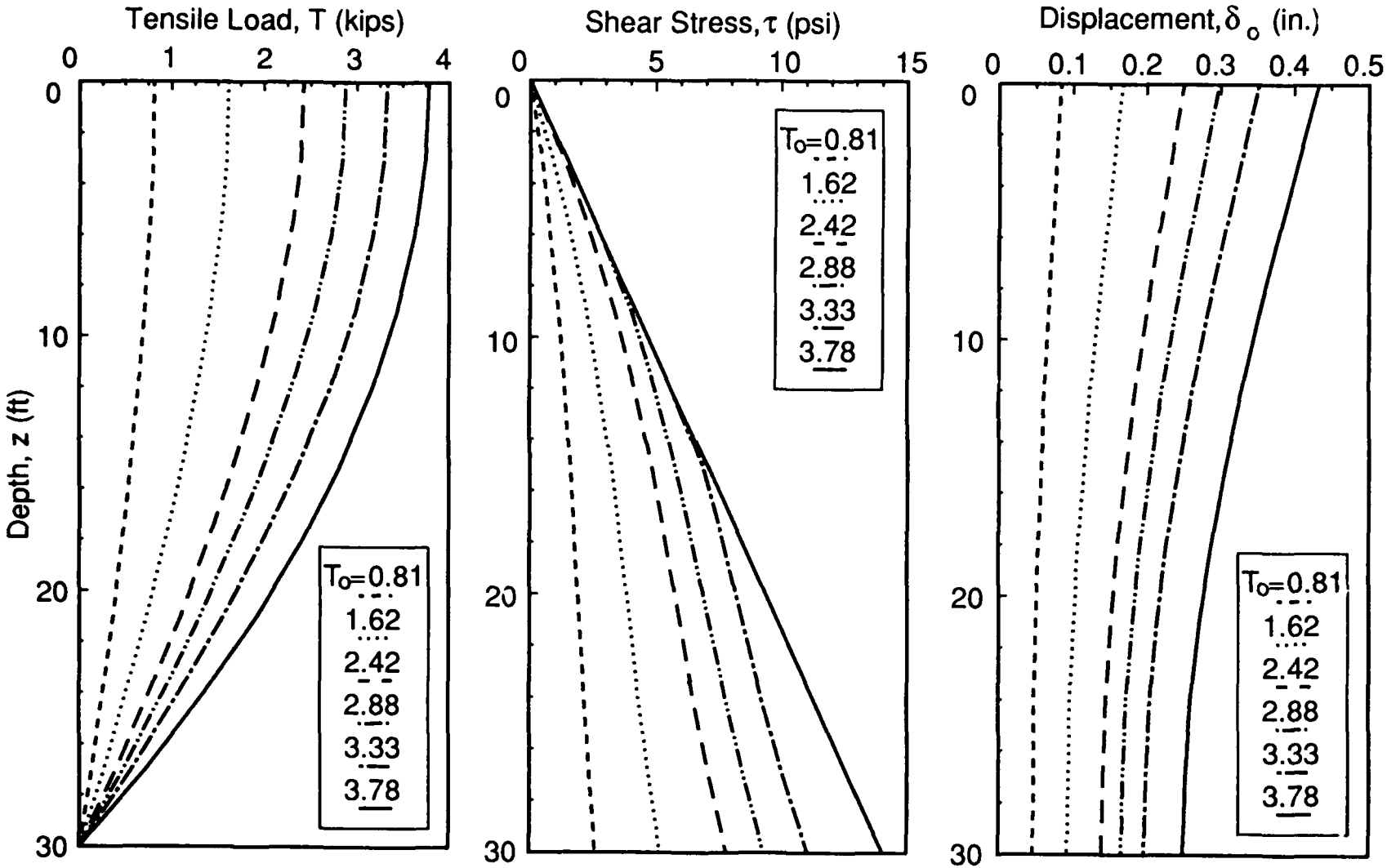
Tensile Load, T (kips)
0
1
2
3
4
Shear Stress, τ (psi)
0
5
10
15
Displacement, δ o (in.)
0
0.1
0.2
0.3
0.4
0.5
Depth, z (ft)
0
10
20
30
To=0.81
1.62
2.42
2.88
3.33
3.78

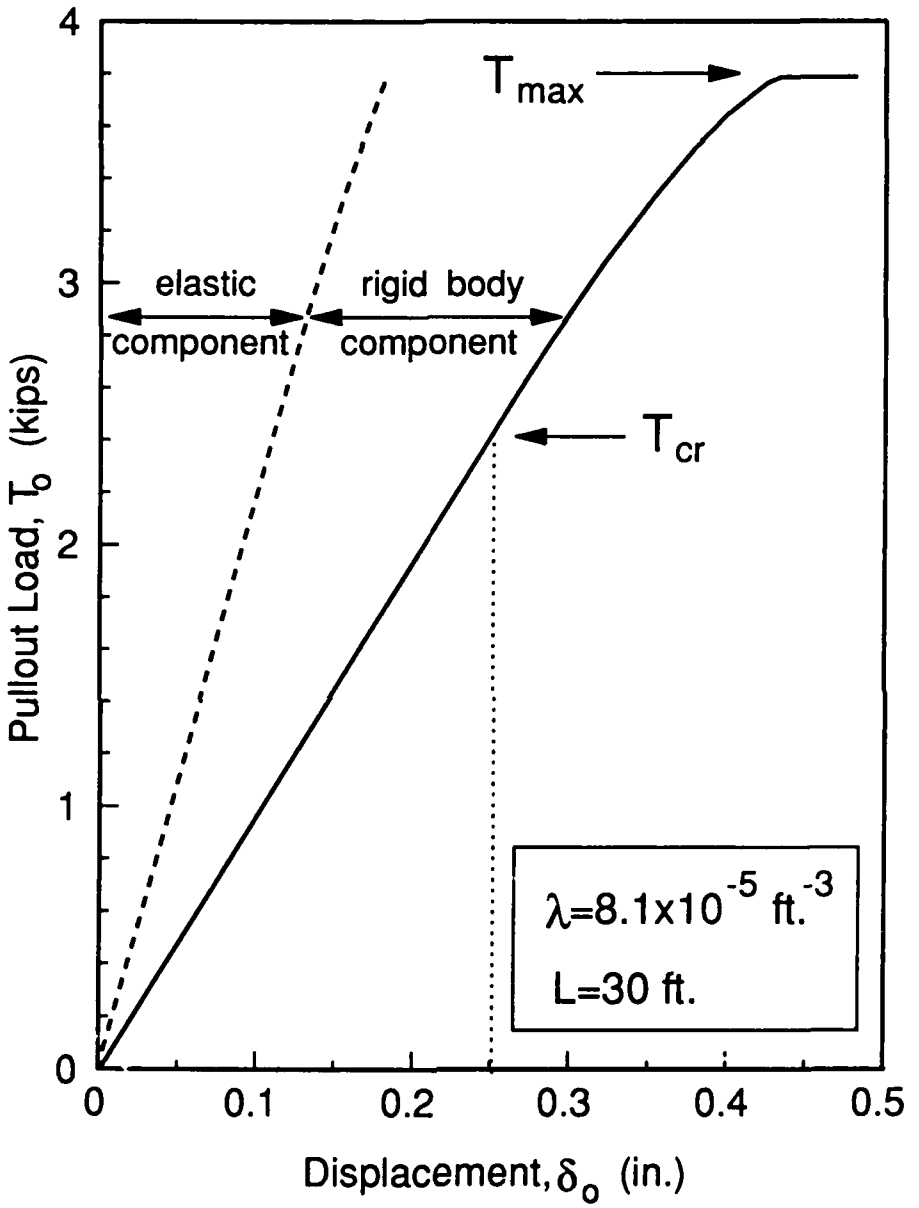
4
3
2
1
0
0
0.1
0.2
0.3
0.4
0.5
Pullout Load, T_o (kips)
Displacement, δ_o (in.)
T_{max}
T_{cr}
elastic component
rigid body component
λ=8.1x10^{-5} ft.$^{-3}$
L=30 ft.

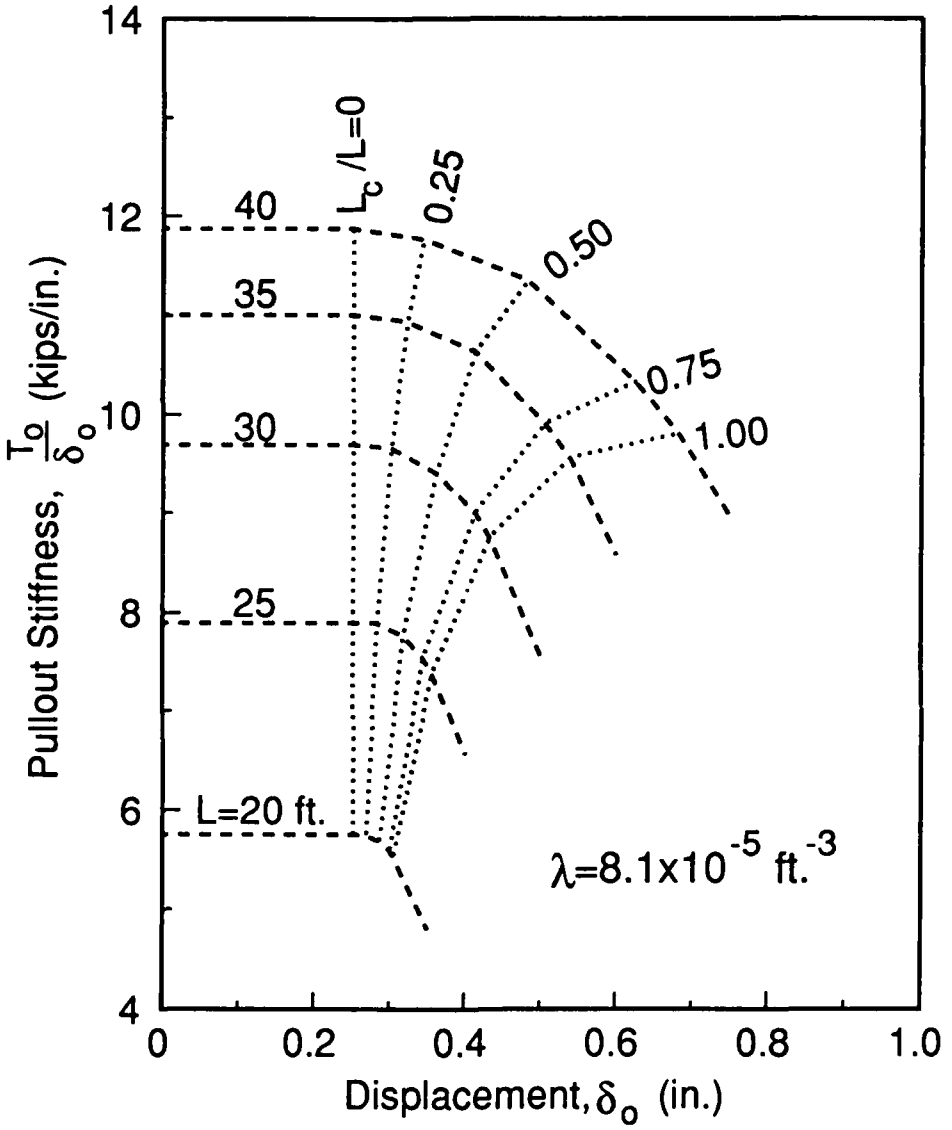
14
12
10
8
6
4
0
0.2
0.4
0.6
0.8
1.0
40
35
30
25
L=20 ft.
$L_c/L=0$
0.25
0.50
0.75
1.00
$\lambda=8.1\times10^{-5}$ ft.$^{-3}$
Pullout Stiffness, $\frac{T_o}{\delta_o}$ (kips/in.)
Displacement, δ_o (in.)

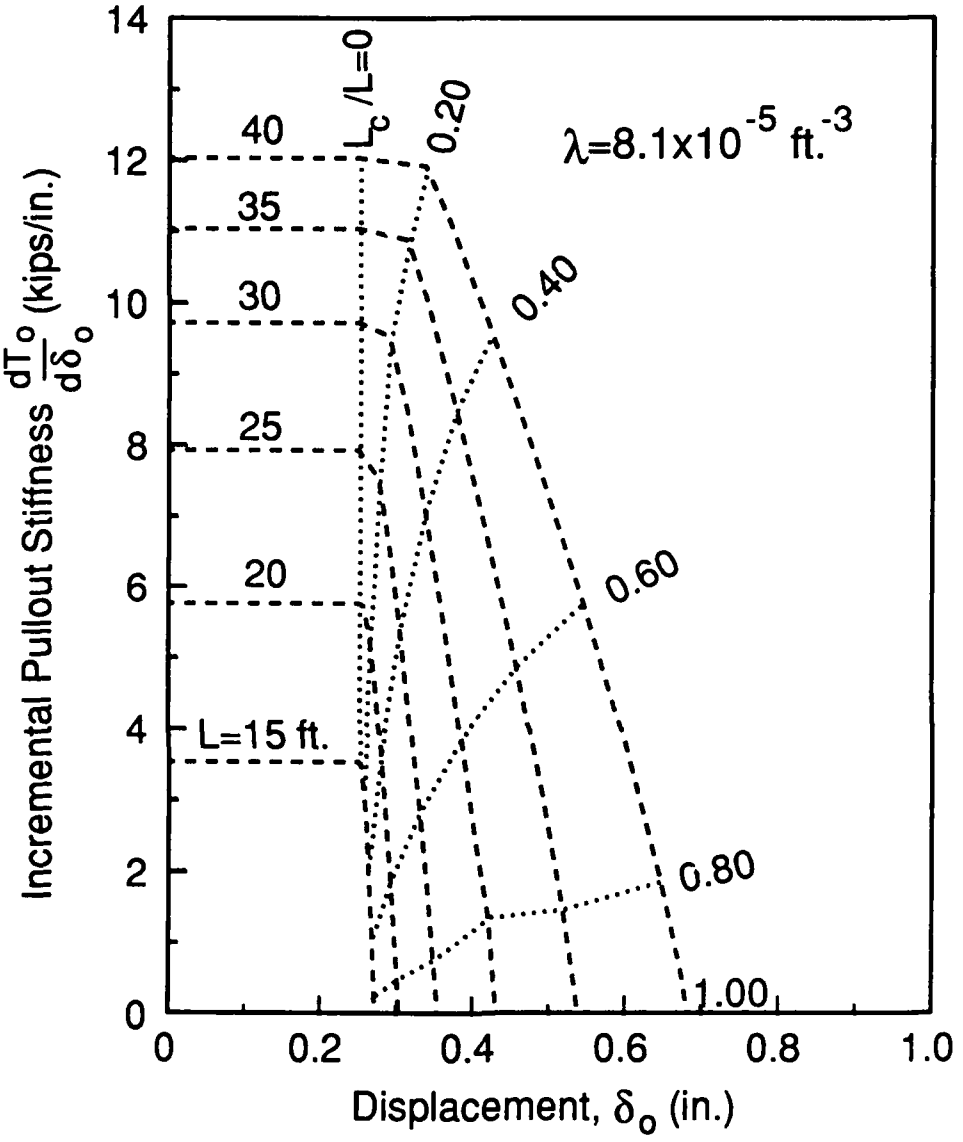
Incremental Pullout Stiffness $\frac{dT_o}{d\delta_o}$ (kips/in.)
Displacement, δ_o (in.)
λ=8.1x10^{-5} ft.$^{-3}$
L_c/L=0
0.20
0.40
0.60
0.80
1.00
40
35
30
25
20
L=15 ft.
0
2
4
6
8
10
12
14
0
0.2
0.4
0.6
0.8
1.0

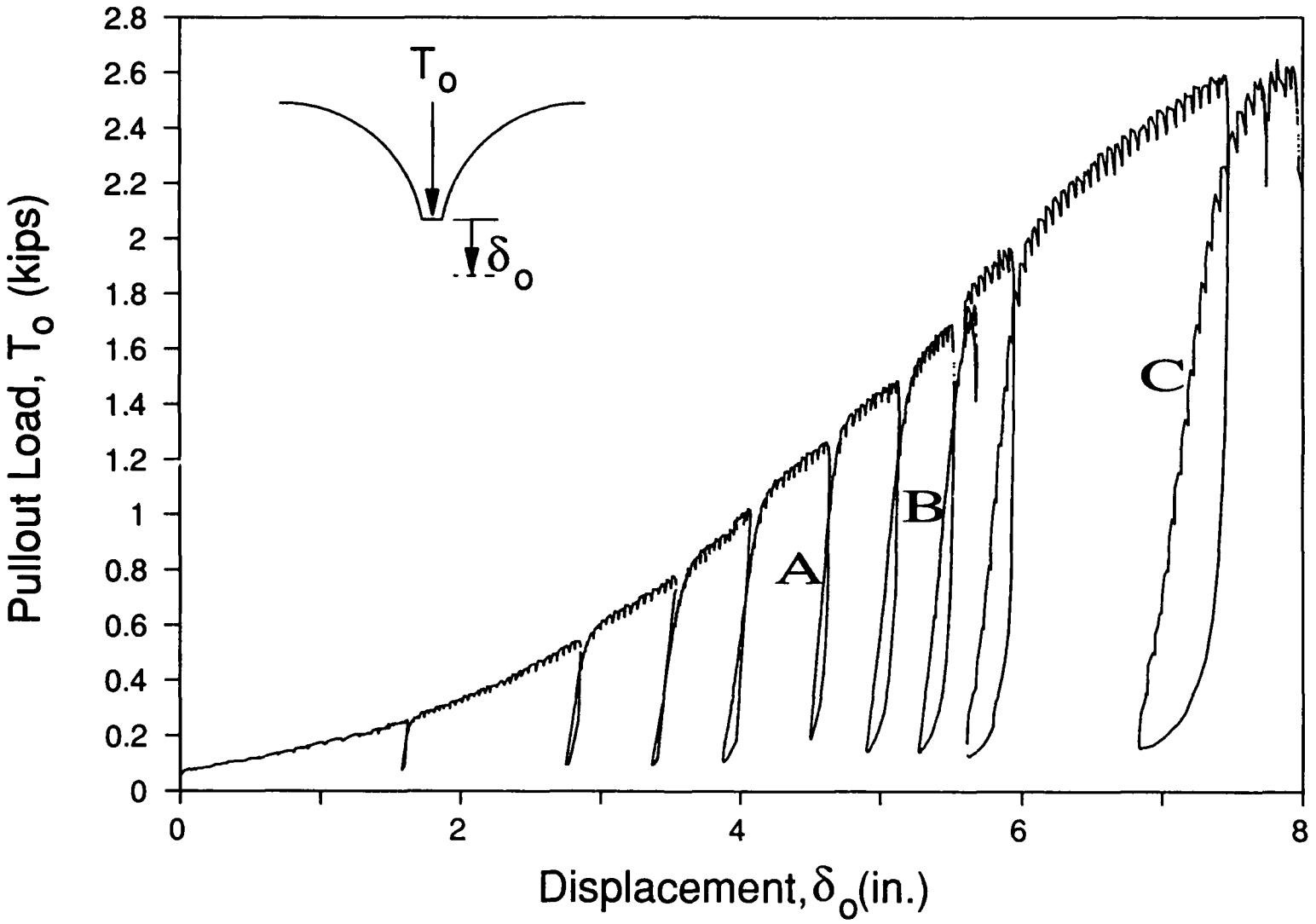
Pullout Load, T_o (kips)
2.8
2.6
2.4
2.2
2
1.8
1.6
1.4
1.2
1
0.8
0.6
0.4
0.2
0
T_o
δ_o
A
B
C
0
2
4
6
8
Displacement, δ_o(in.)

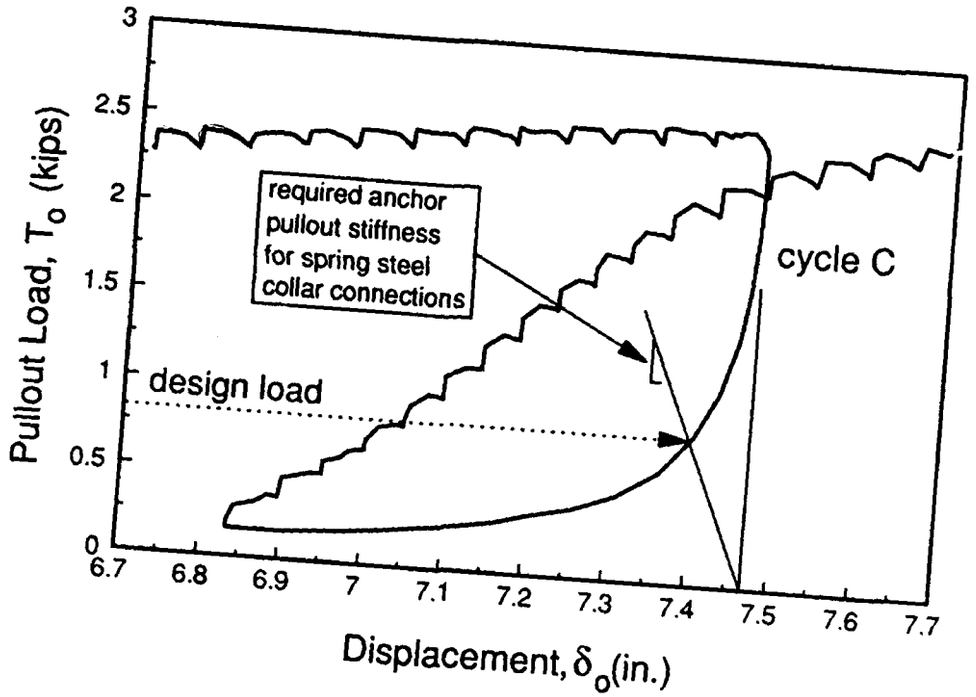
Pullout Load, T_o (kips)
3
2.5
2
1.5
1
0.5
0
required anchor pullout stiffness for spring steel collar connections
cycle C
design load
6.7
6.8
6.9
7
7.1
7.2
7.3
7.4
7.5
7.6
7.7
Displacement, δ_o(in.)

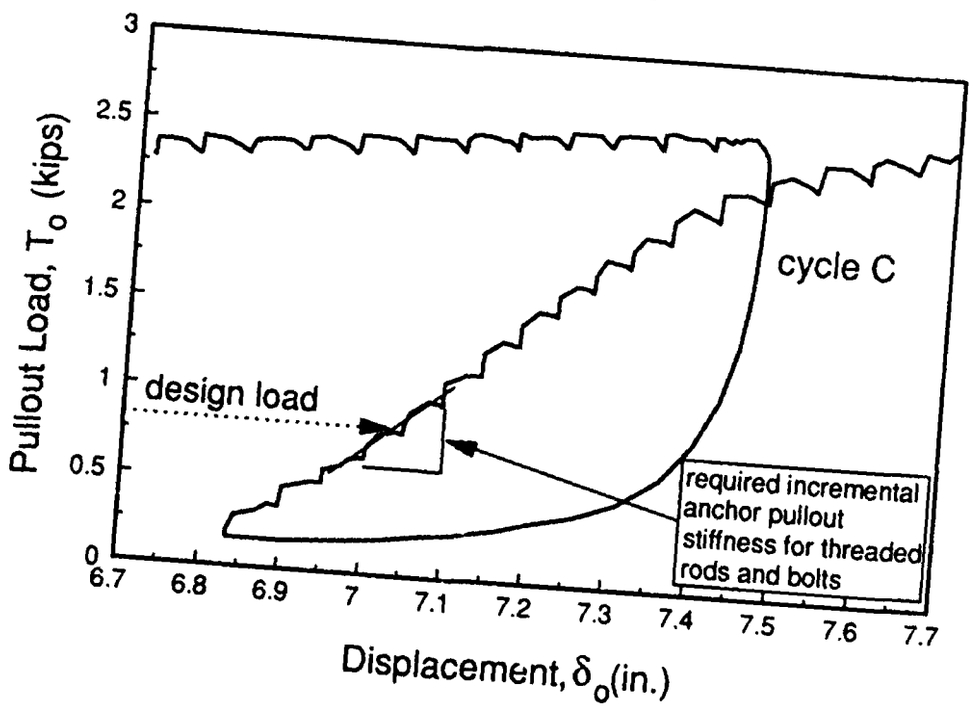
Pullout Load, T_o (kips)
3
2.5
2
1.5
1
0.5
0
cycle C
design load
required incremental anchor pullout stiffness for threaded rods and bolts
6.7
6.8
6.9
7
7.1
7.2
7.3
7.4
7.5
7.6
7.7
Displacement, δ_o(in.)

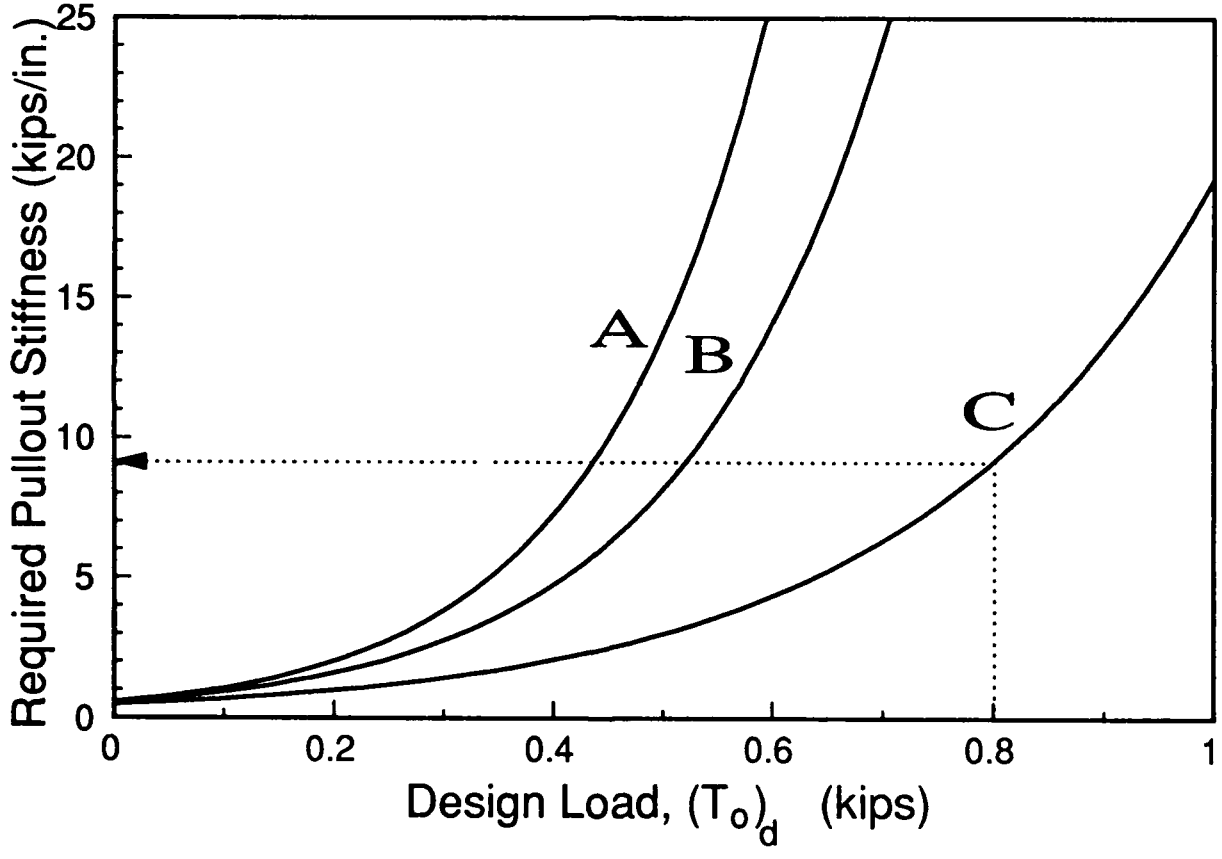
Required Pullout Stiffness (kips/in.)
25
20
15
10
5
0
A
B
C
0
0.2
0.4
0.6
0.8
1
Design Load, $(T_o)_d$ (kips)

APPENDIX B

Results of Carbowax Solidification

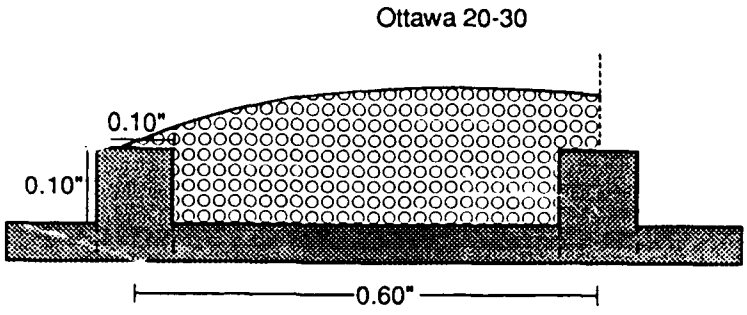

SPACING: 0.60"

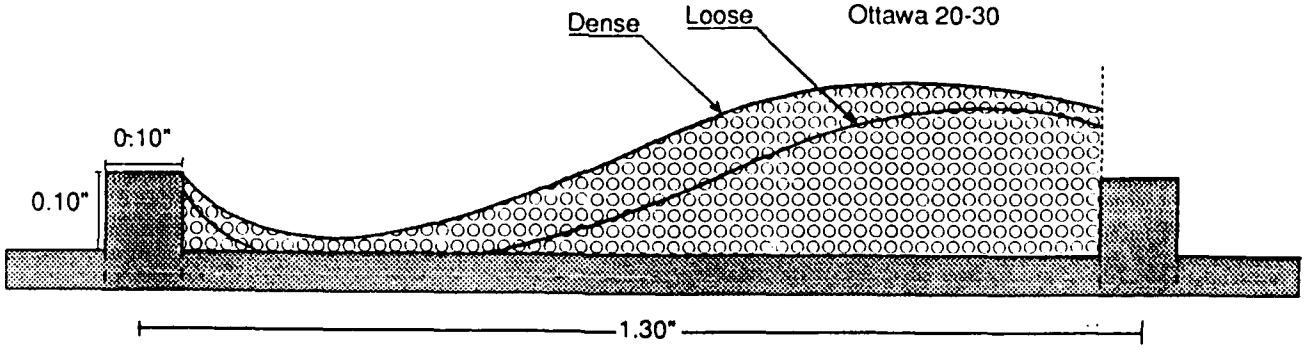

SPACING: 1.30"

EFFECT OF SPACING

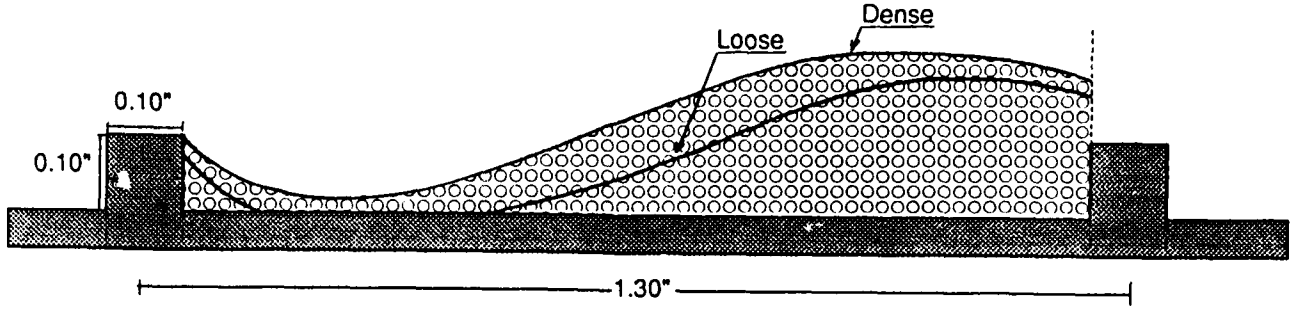

OTTAWA 20-30

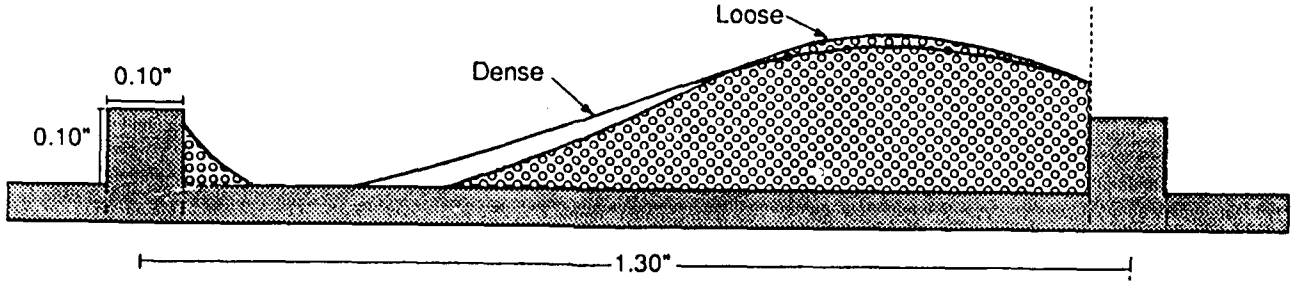

OTTAWA 40-50

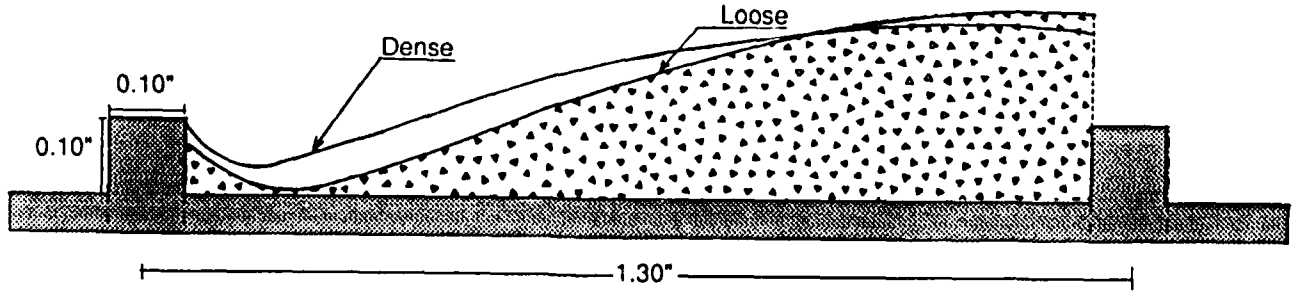

GLAZIER WAY 20-30

EFFECT INITIAL VOID RATIO

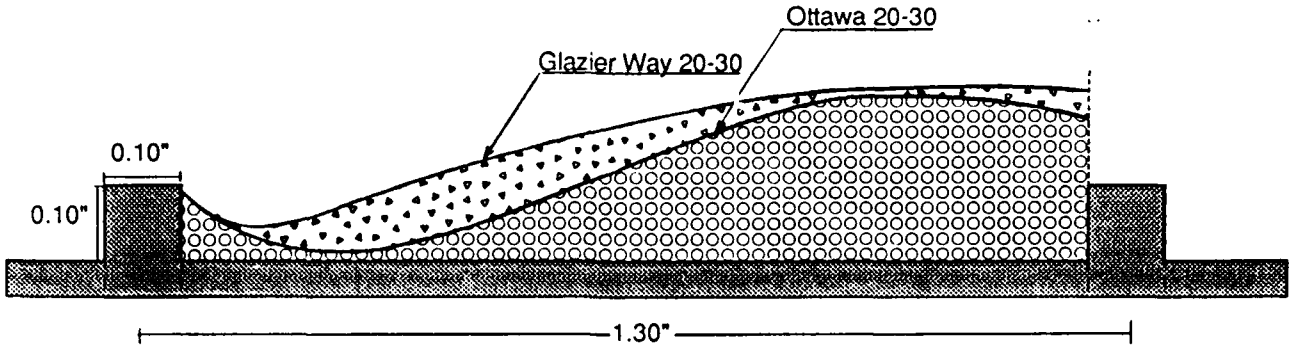

DENSE

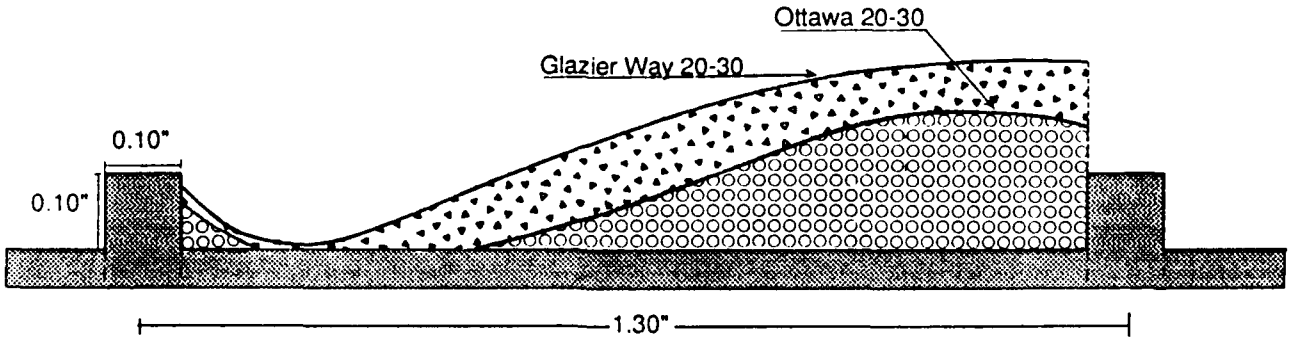

LOOSE

EFFECT OF GRAIN SHAPE

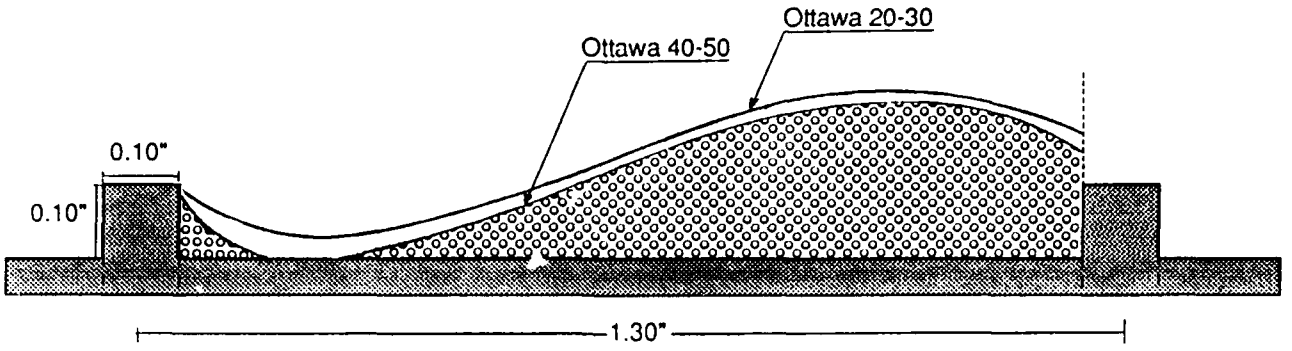

DENSE

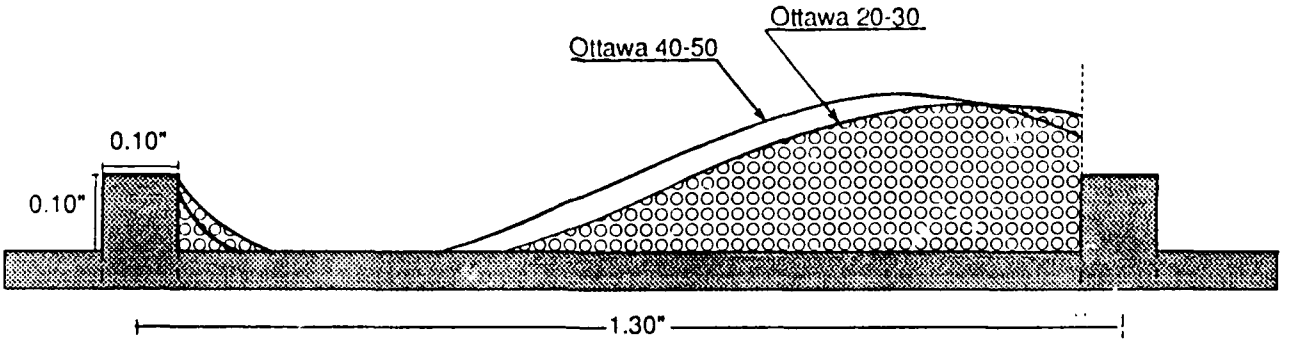

LOOSE

EFFECT OF GRAIN SIZE

APPENDIX C

Direct Shear Test Results of Plane Ribbed Inclusions

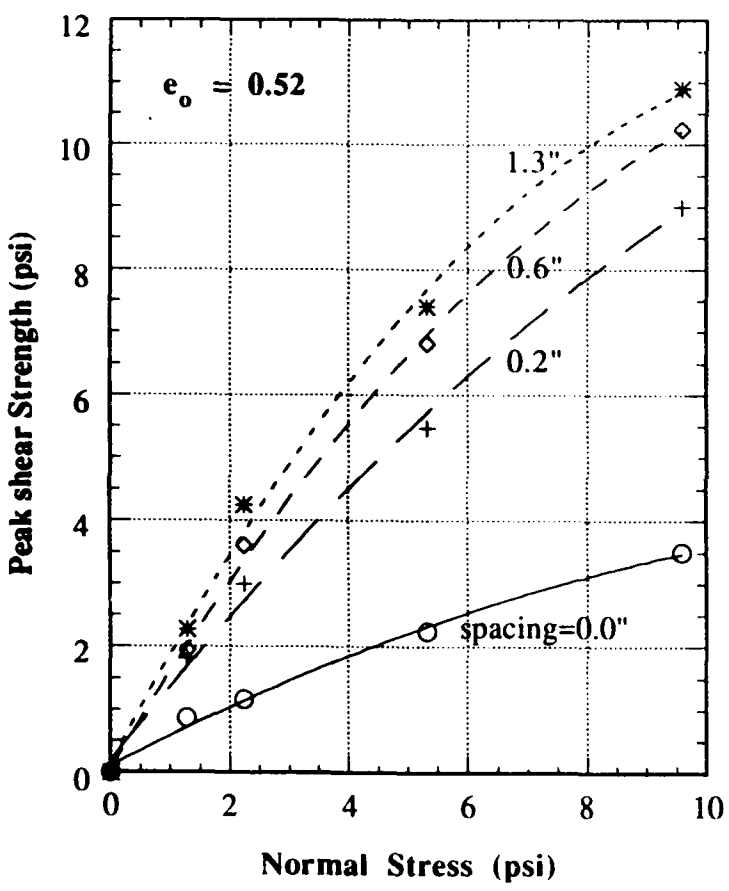

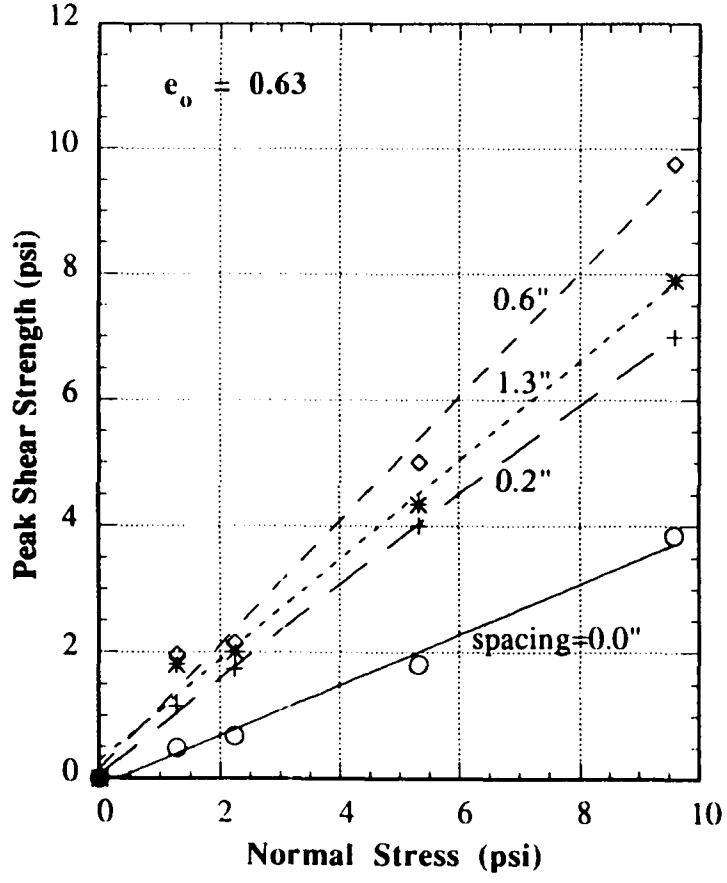

Effect of Normal Stress on Peak Shear Strength

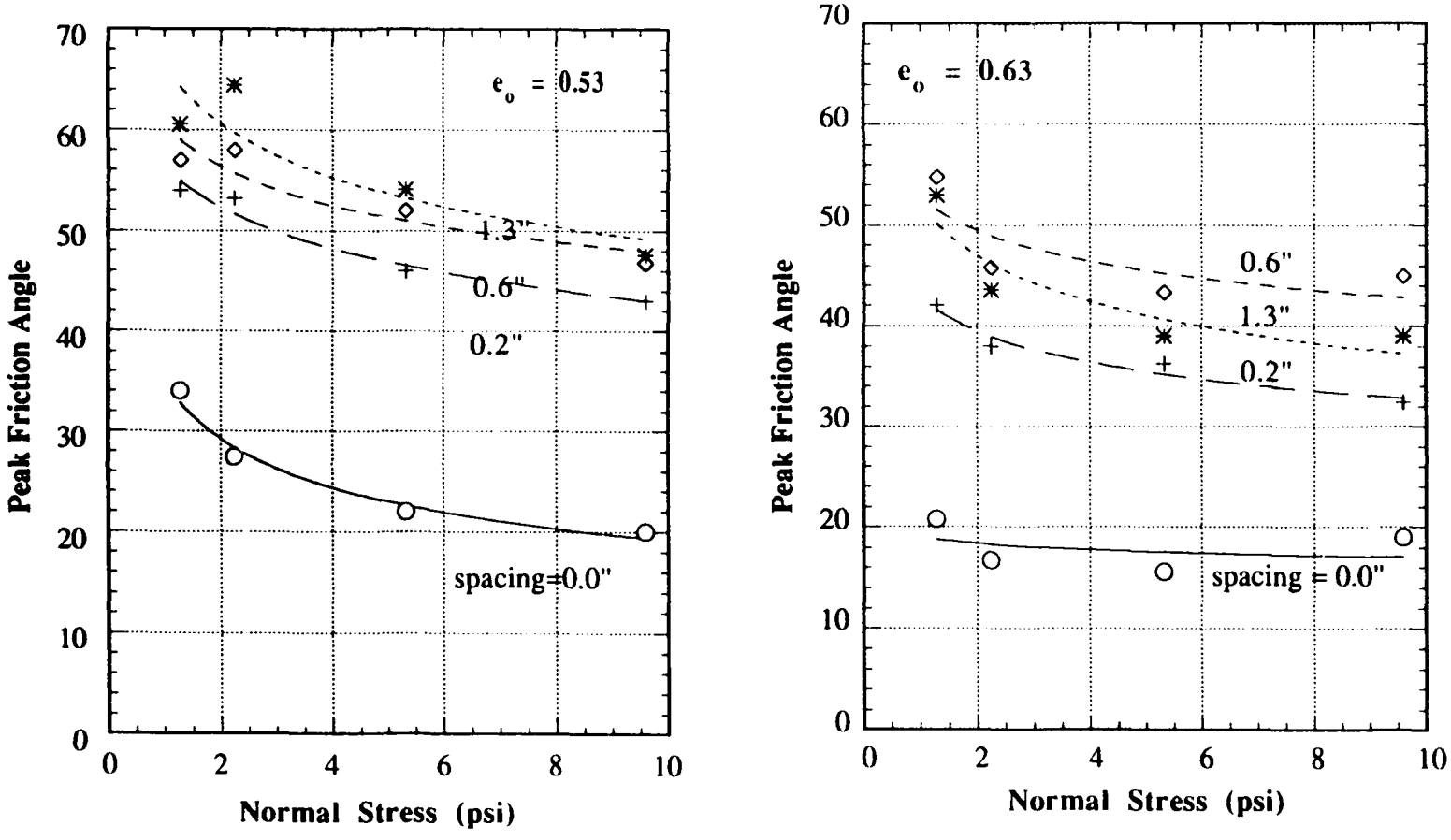

Effect of Normal Stress on Peak Friction Angle

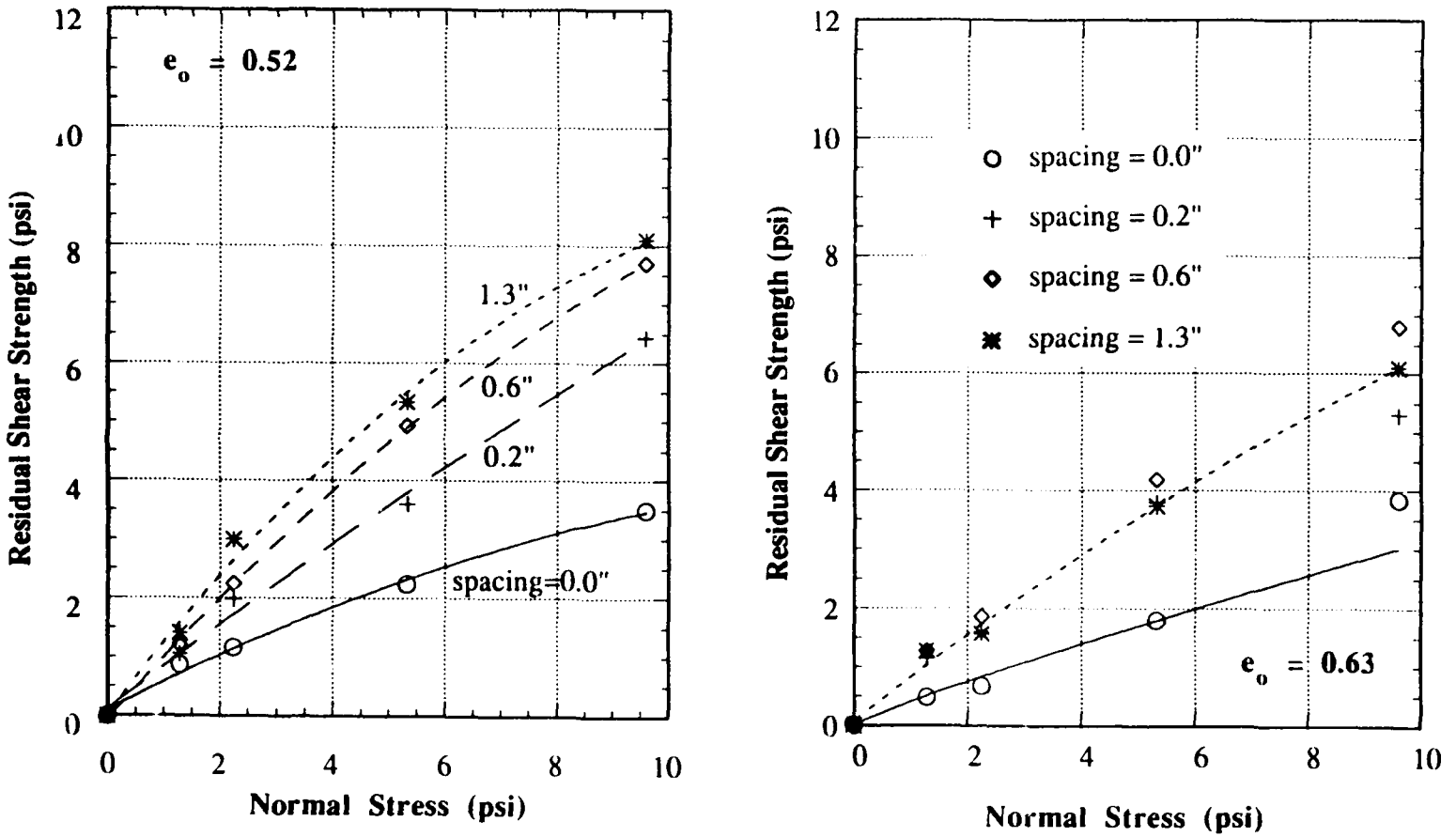

Effect of Normal Stress on Residual Shear Strength

C=4

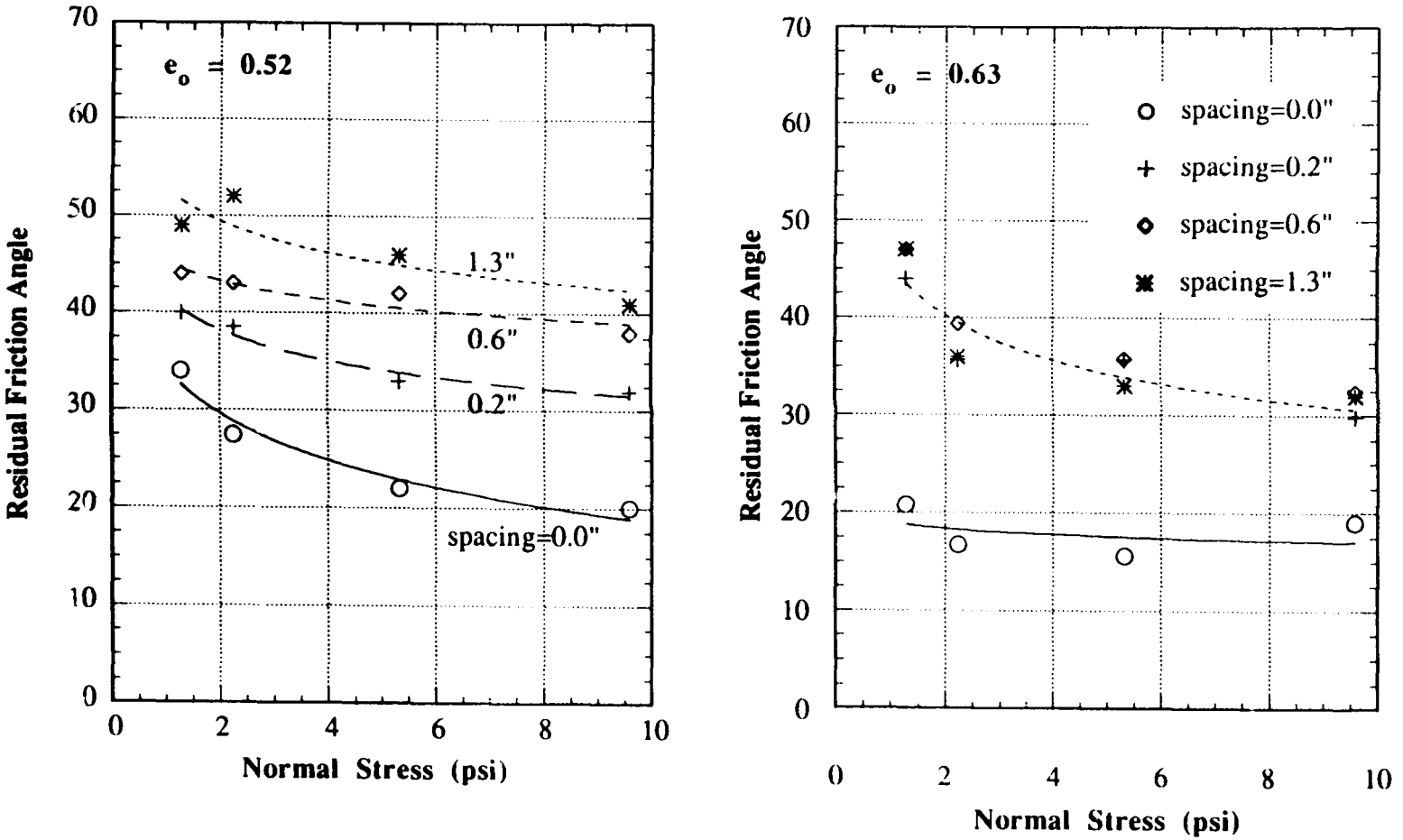

Effect of Normal Stress on Residual Friction Angle

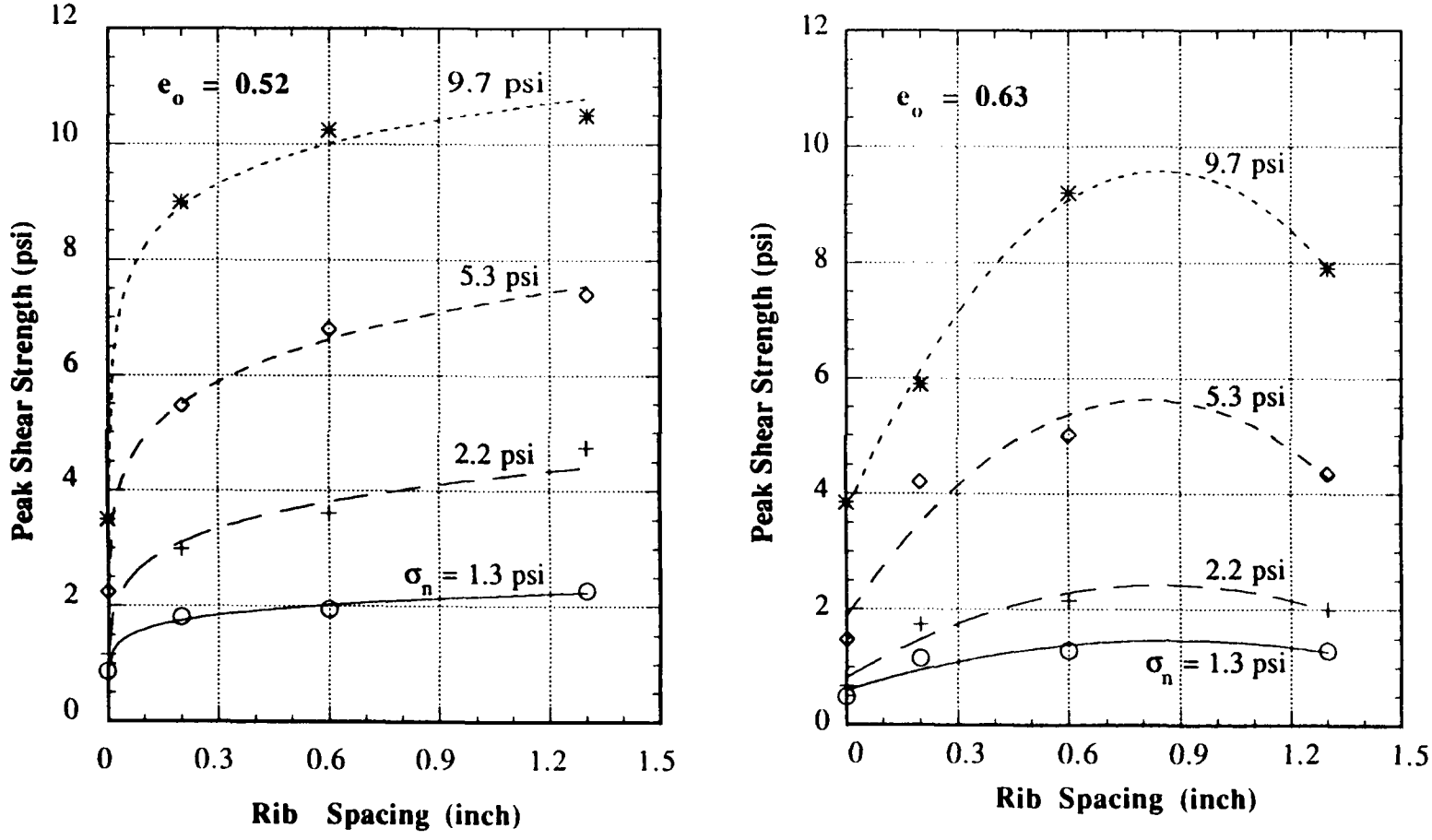

Effect of Rib Spacing on Peak Shear Strength

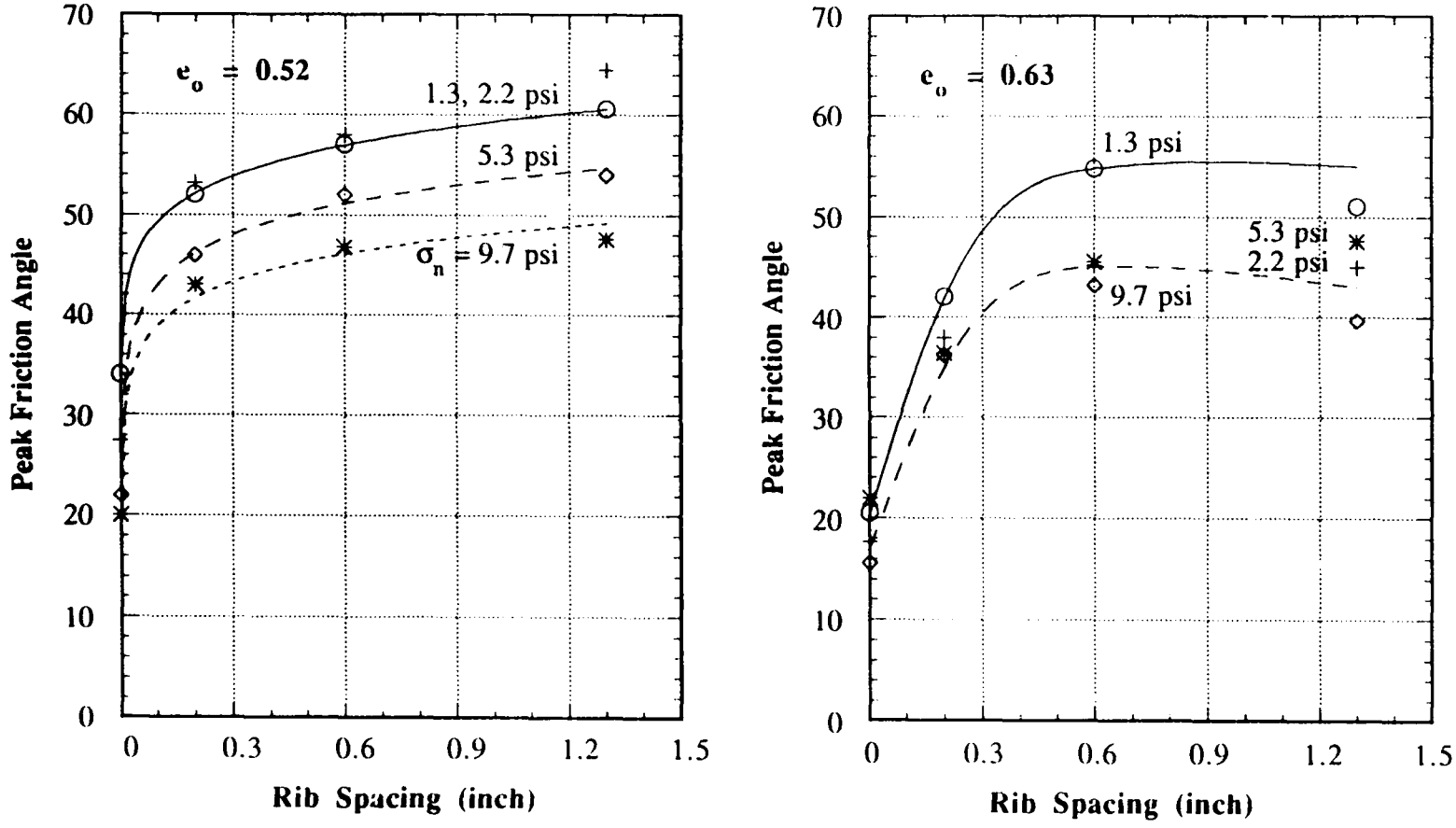

Effect of Rib Spacing on Peak Friction Angle

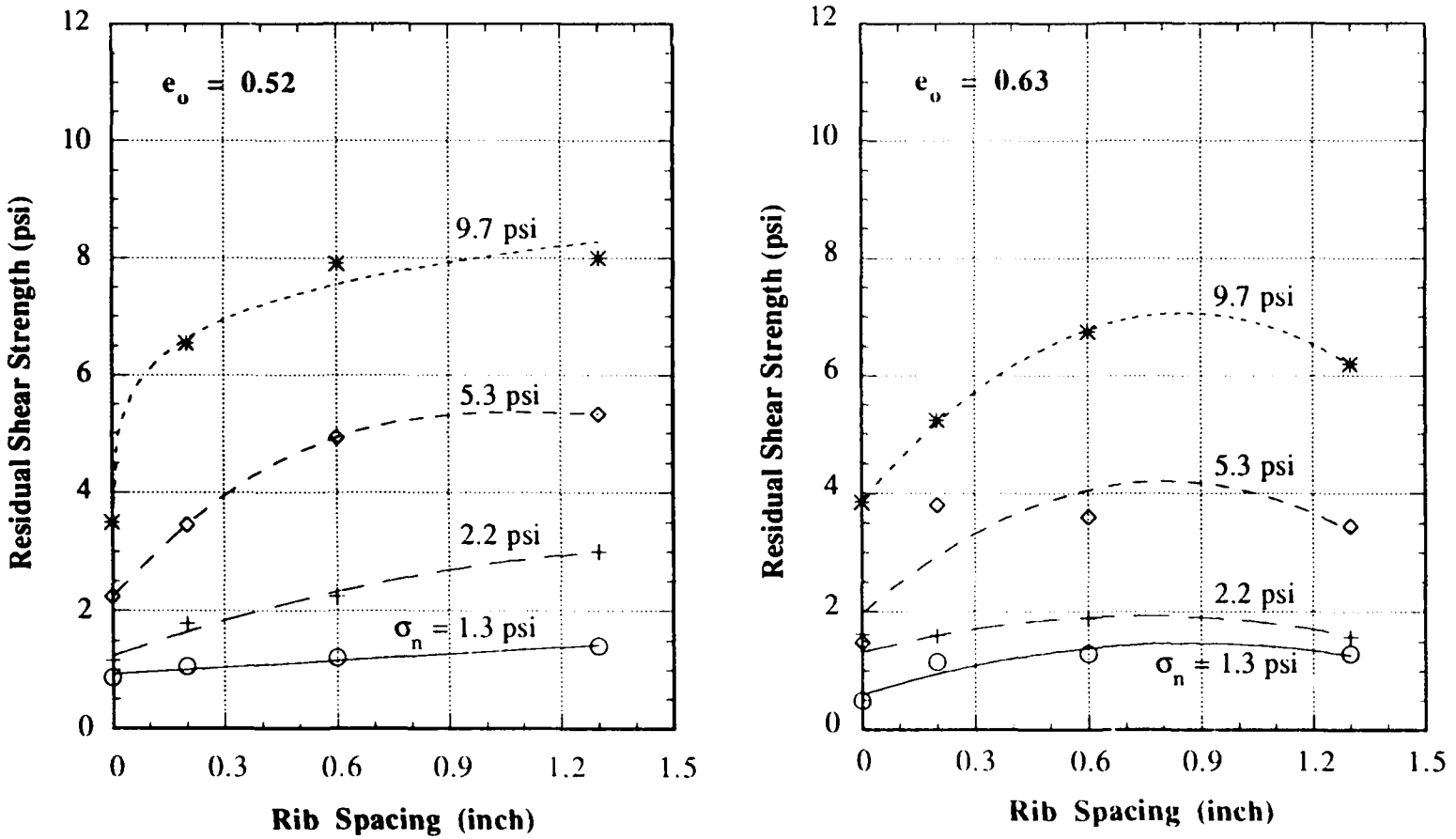

Effect of Rib Spacing on Residual Shear Strength

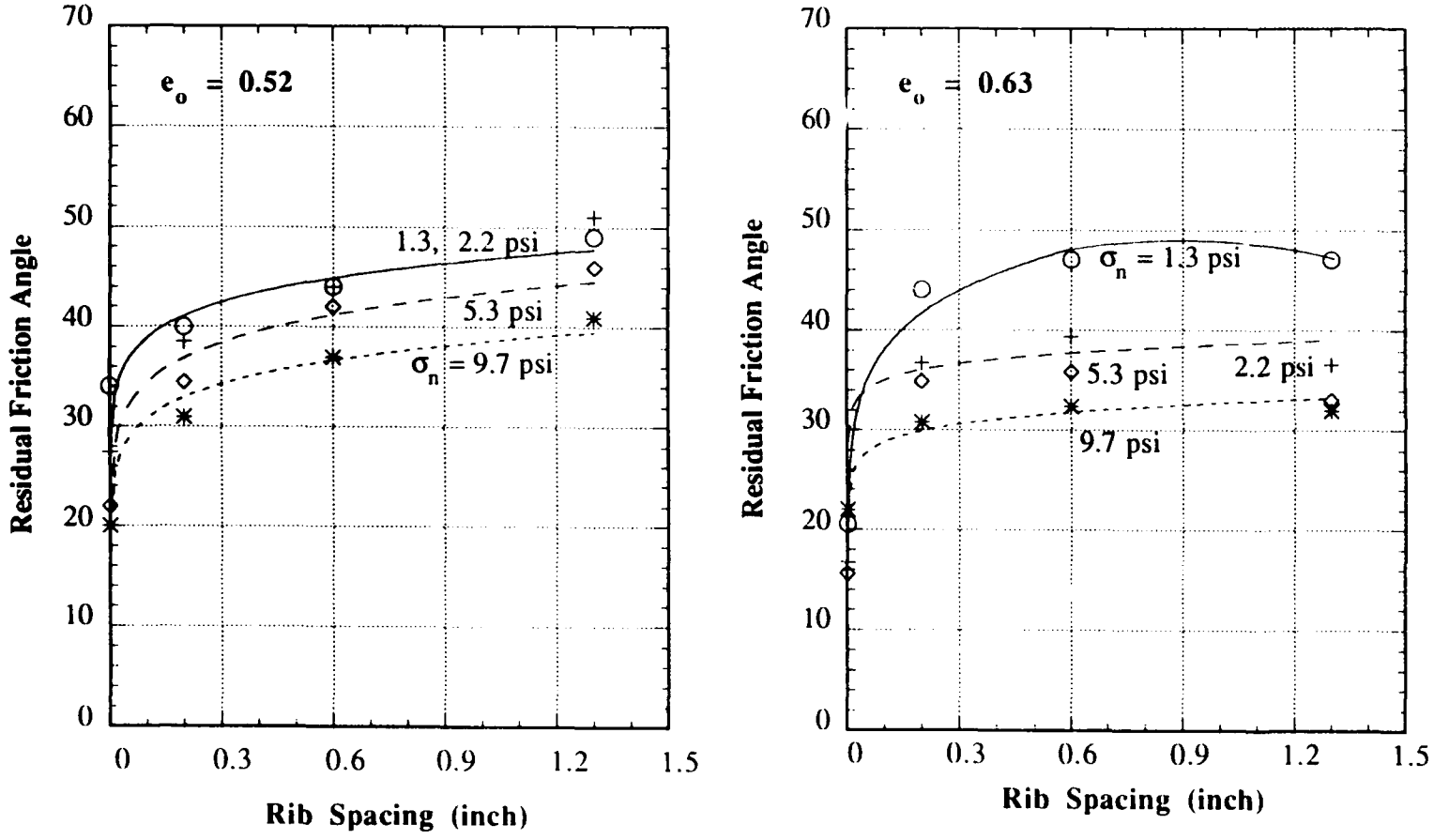

Effect of Rib Spacing on Residual Friction Angle

APPENDIX D

Parametric Study of Passive Resistance Based On Plane Ribbed Inclusion Model.

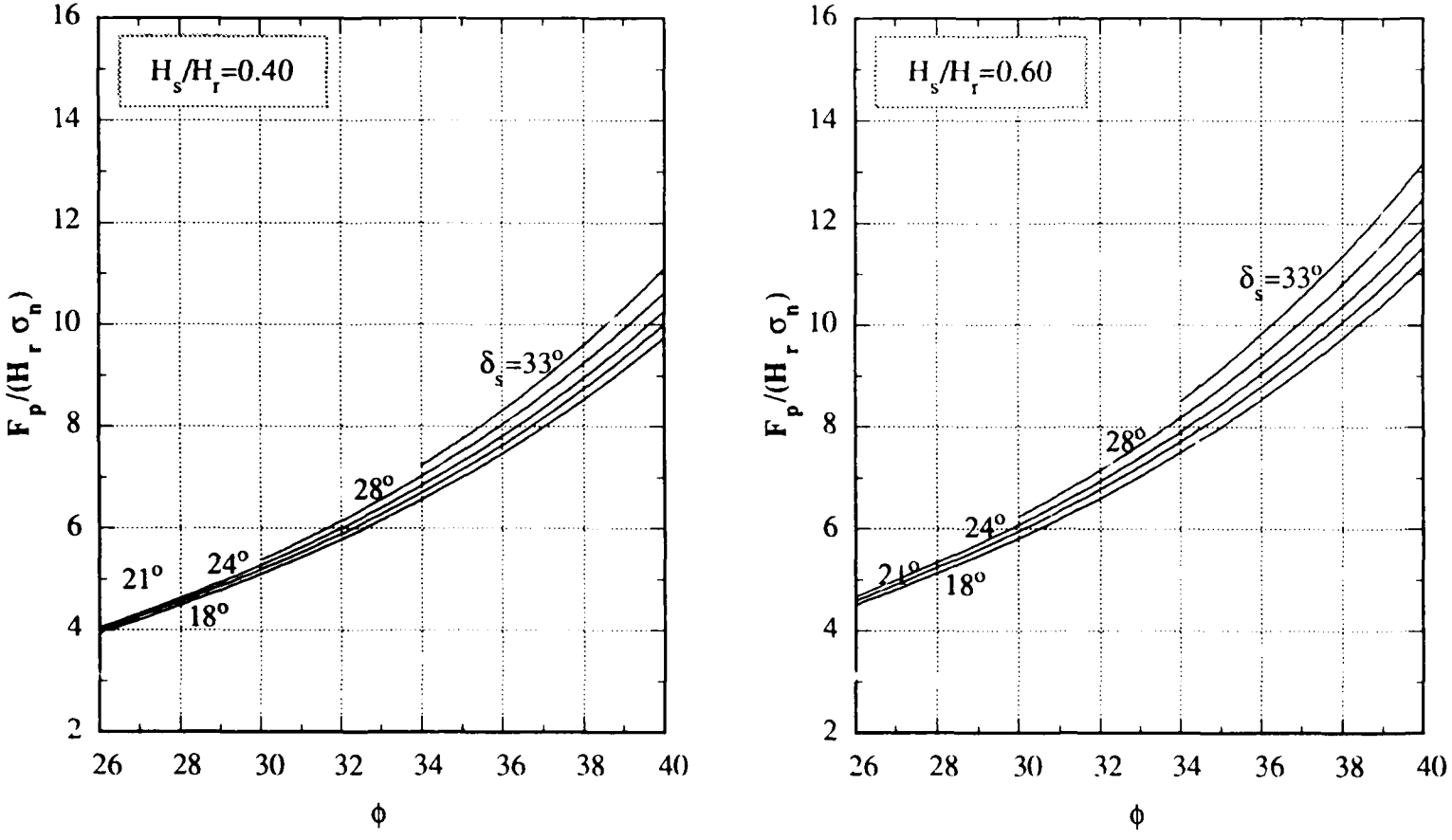

$\delta_r = \delta_b = 18^o$

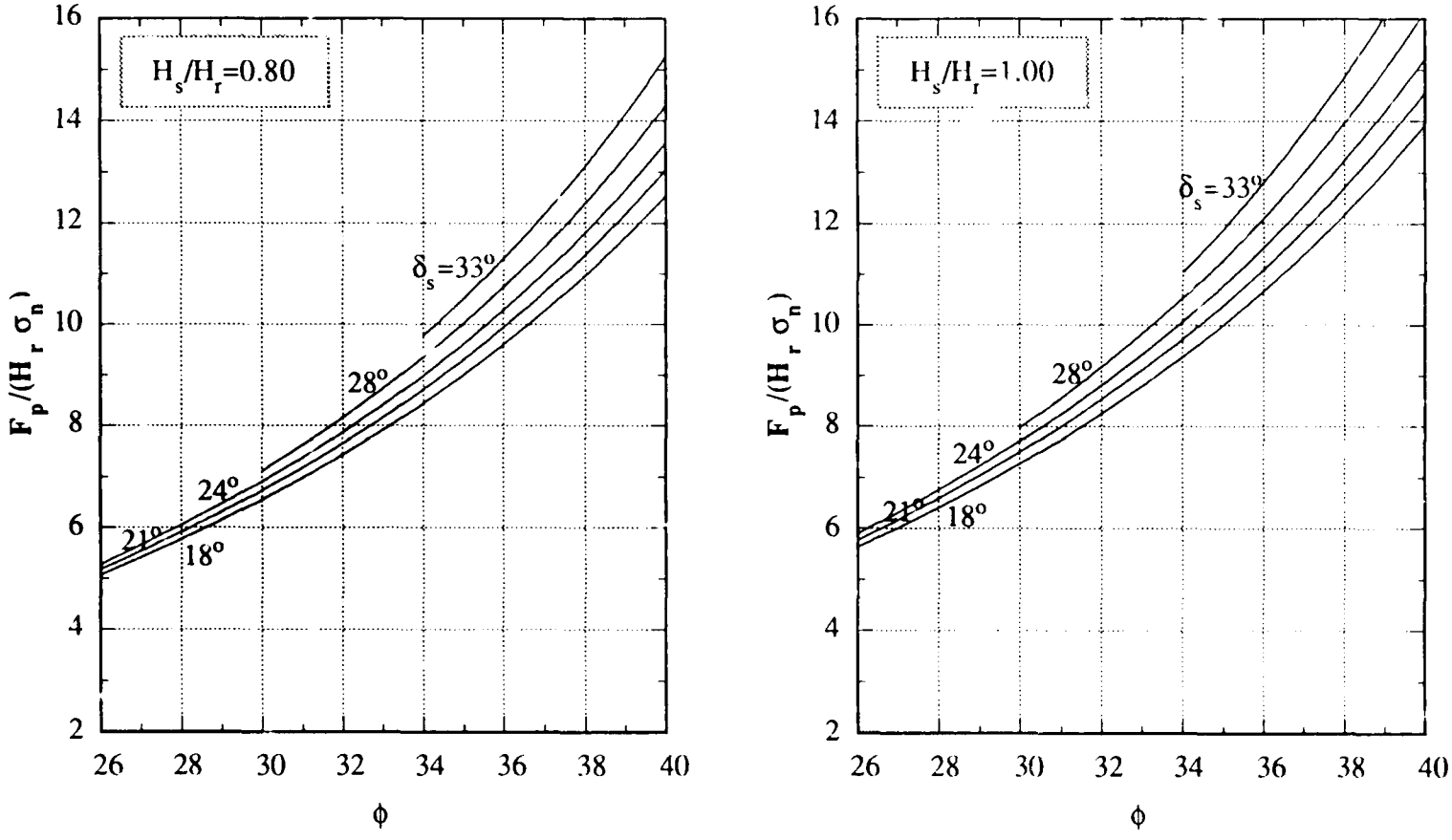

$\delta_r = \delta_b = 18^o$

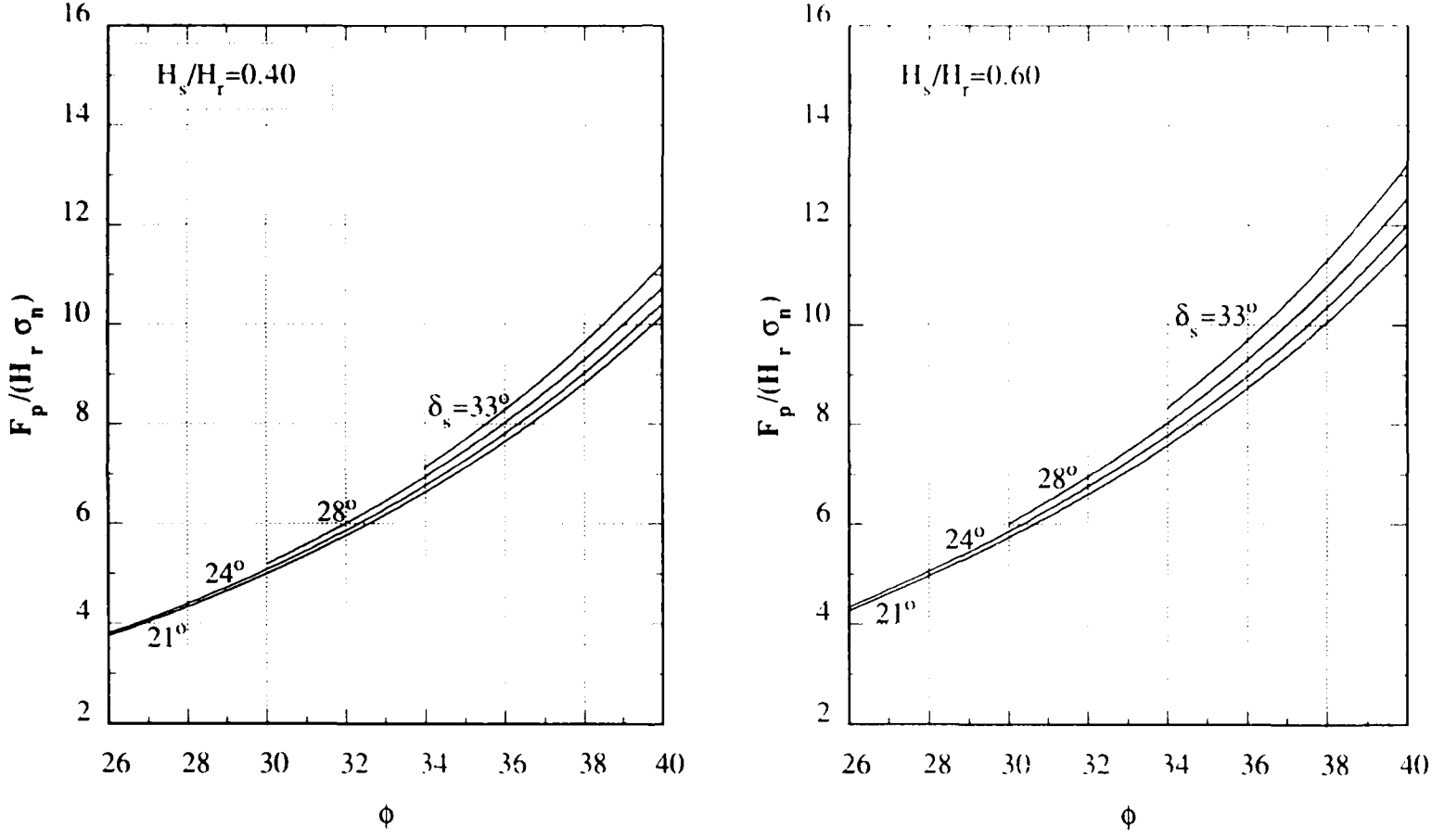

$\delta_r = \delta_b = 21^o$

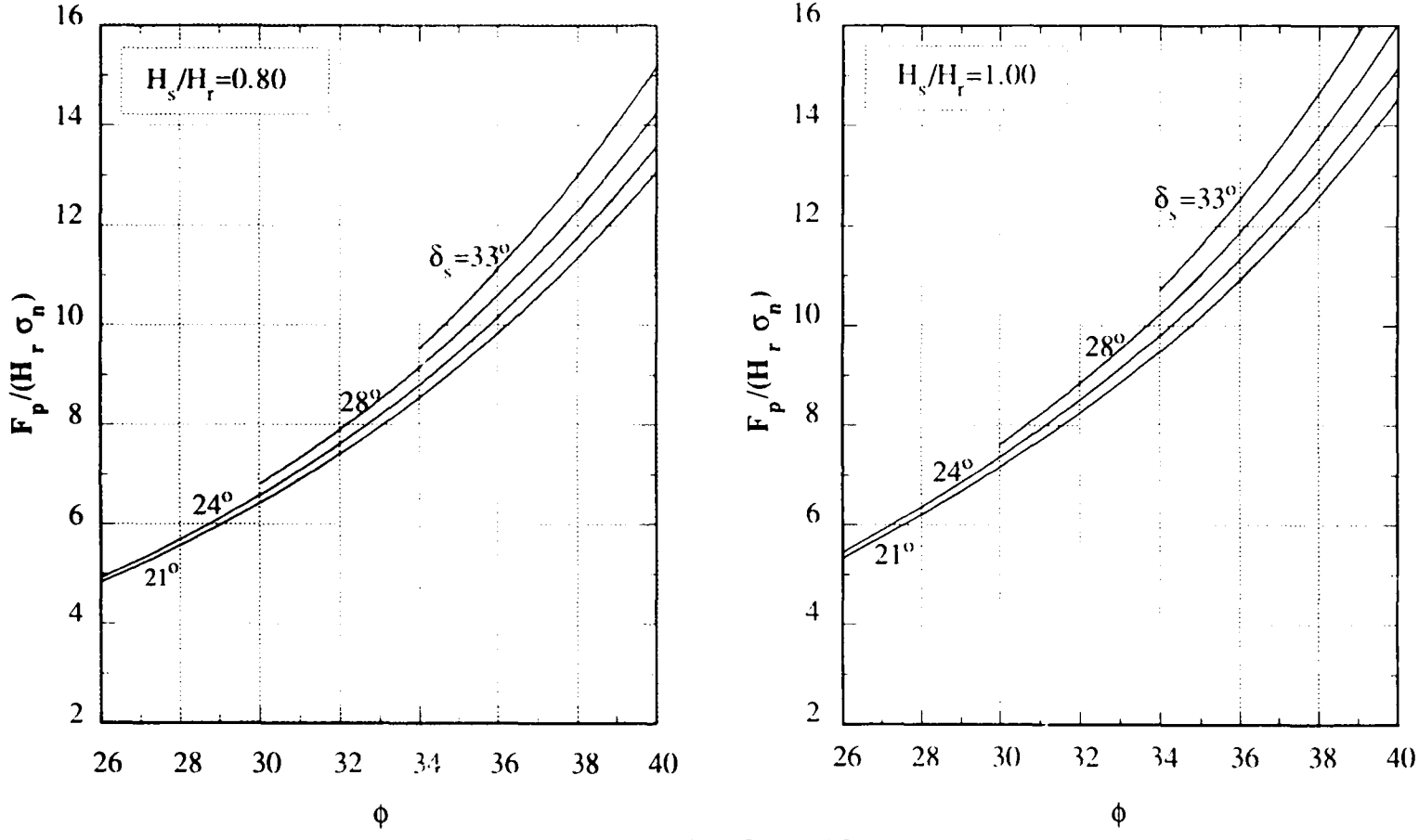

$\delta_r=\delta_b=21^o$

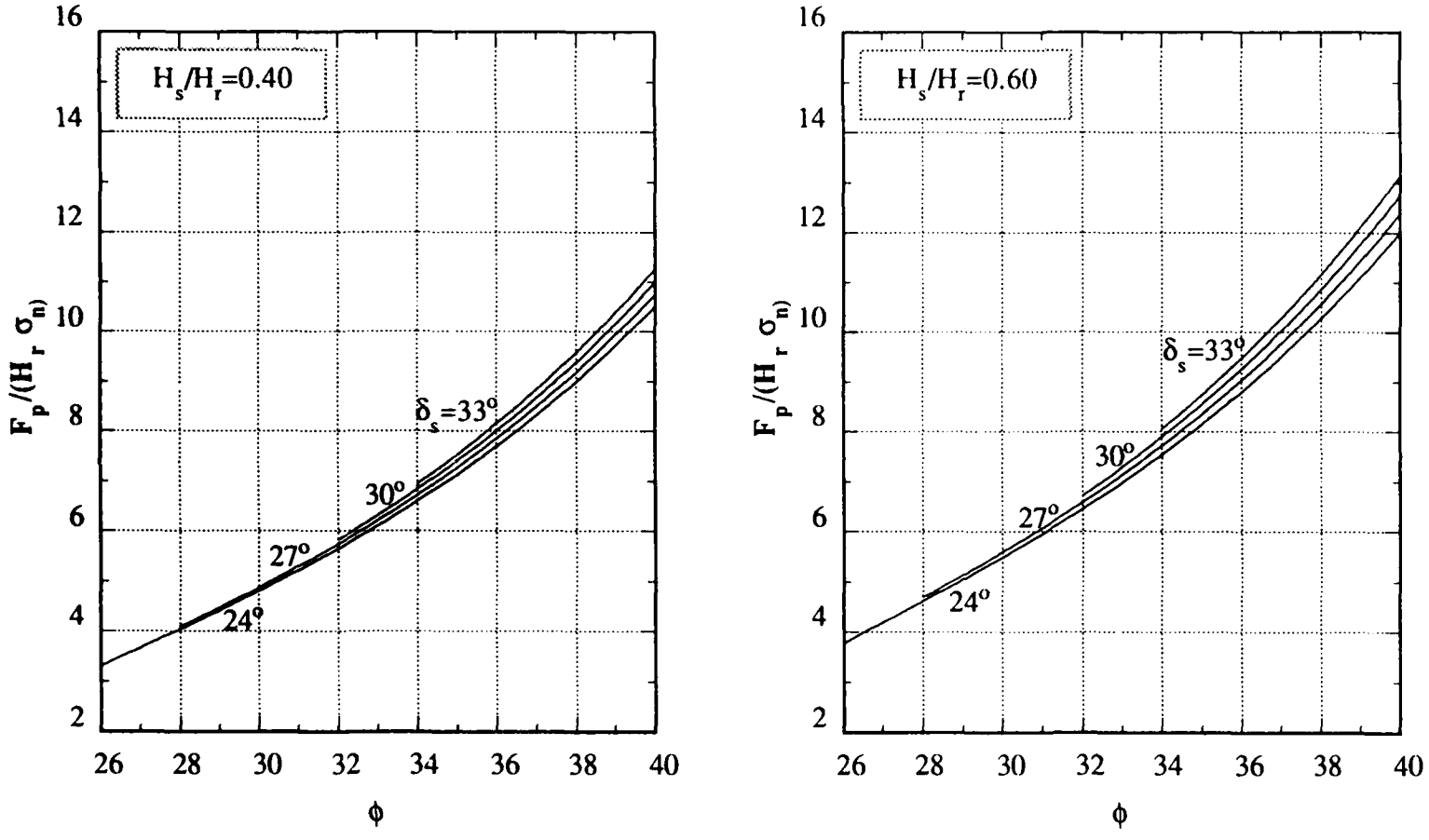

$\delta_r = \delta_b = 24^o$

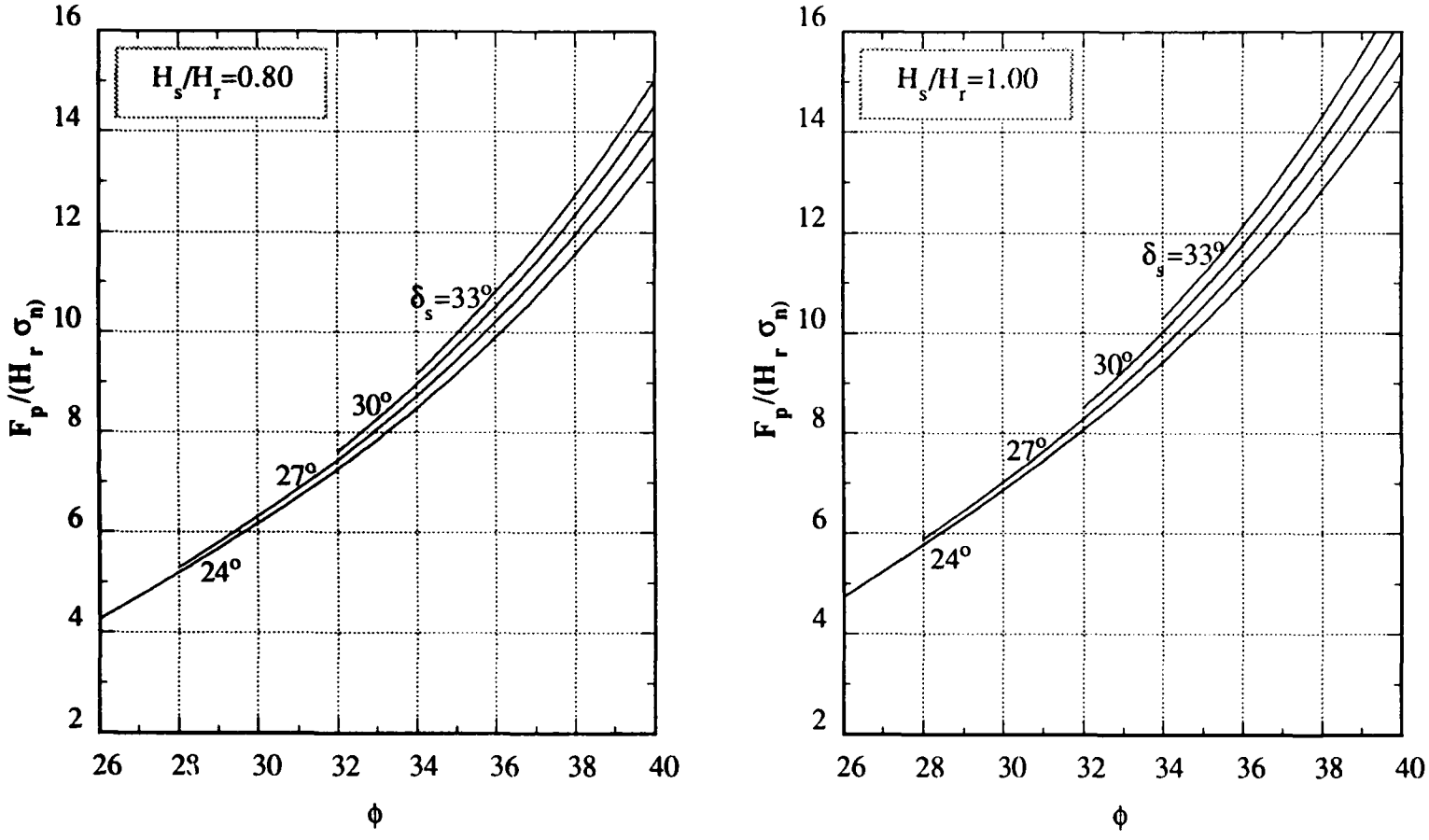

$\delta_r = \delta_b = 24^o$

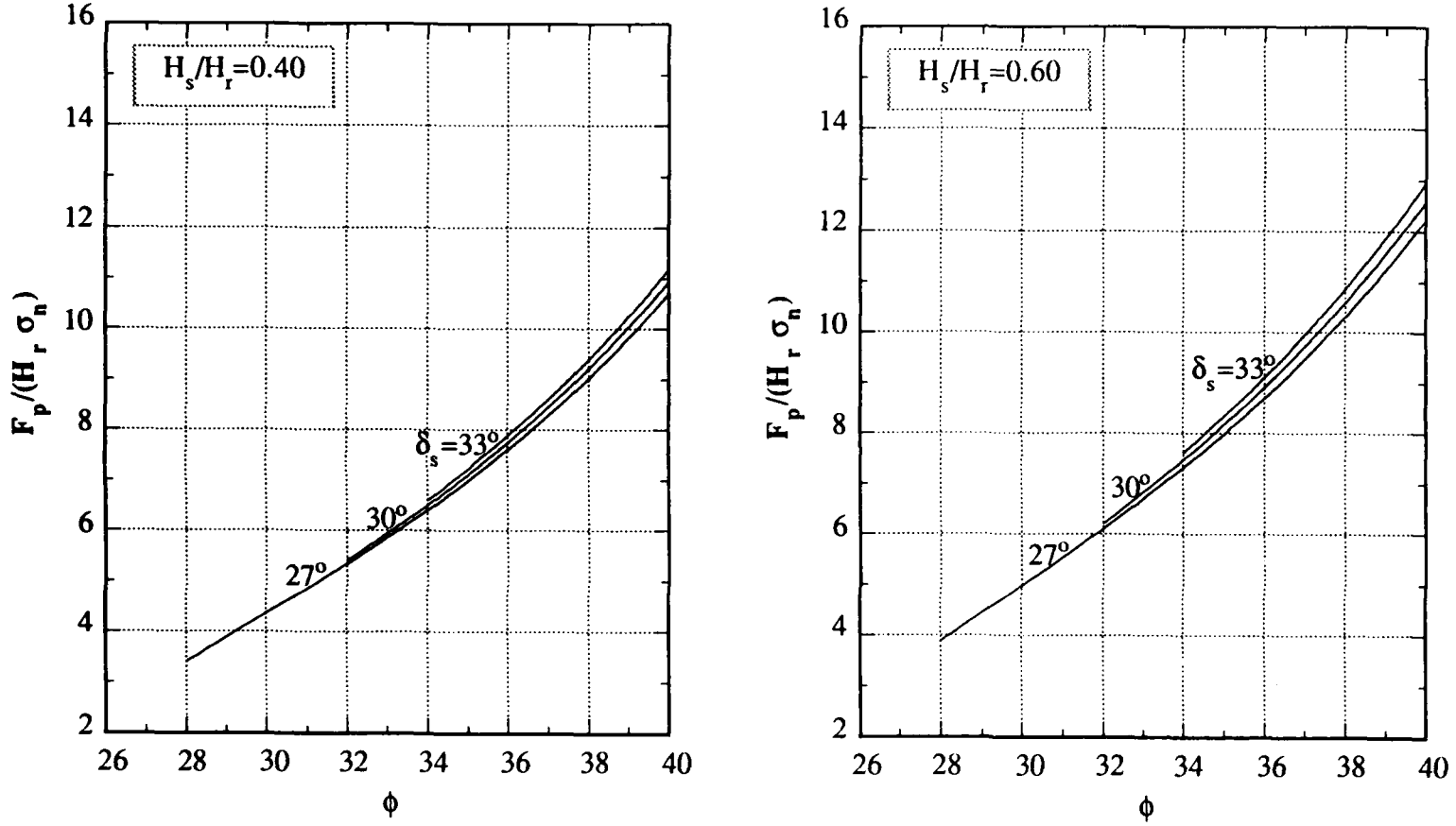

$\delta_r=\delta_b=27°$

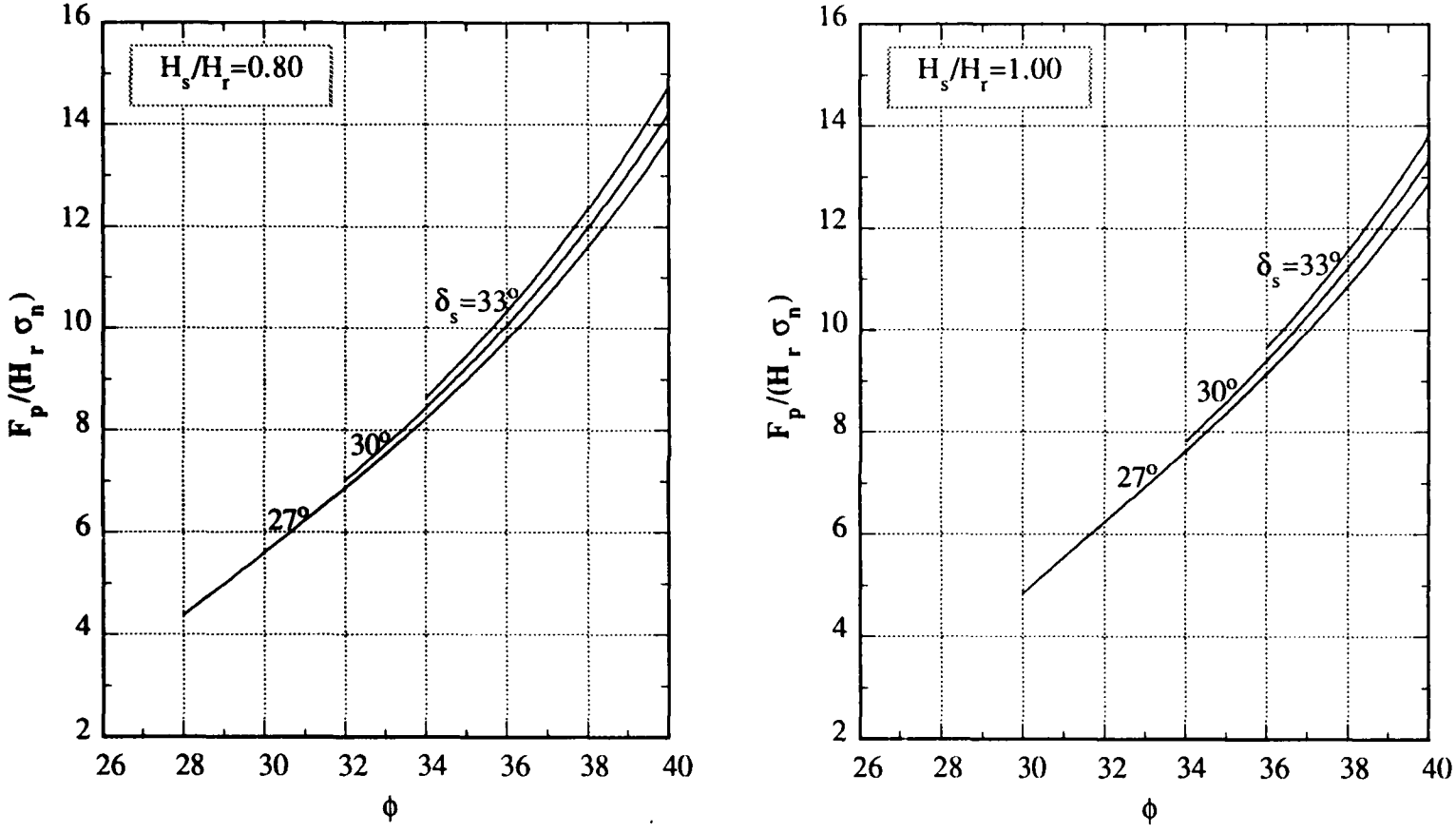

$\delta_r=\delta_b=27^o$

APPENDIX E

Parametric Study of Optimum Rib Spacing Based On Plane Ribbed Inclusion Model.

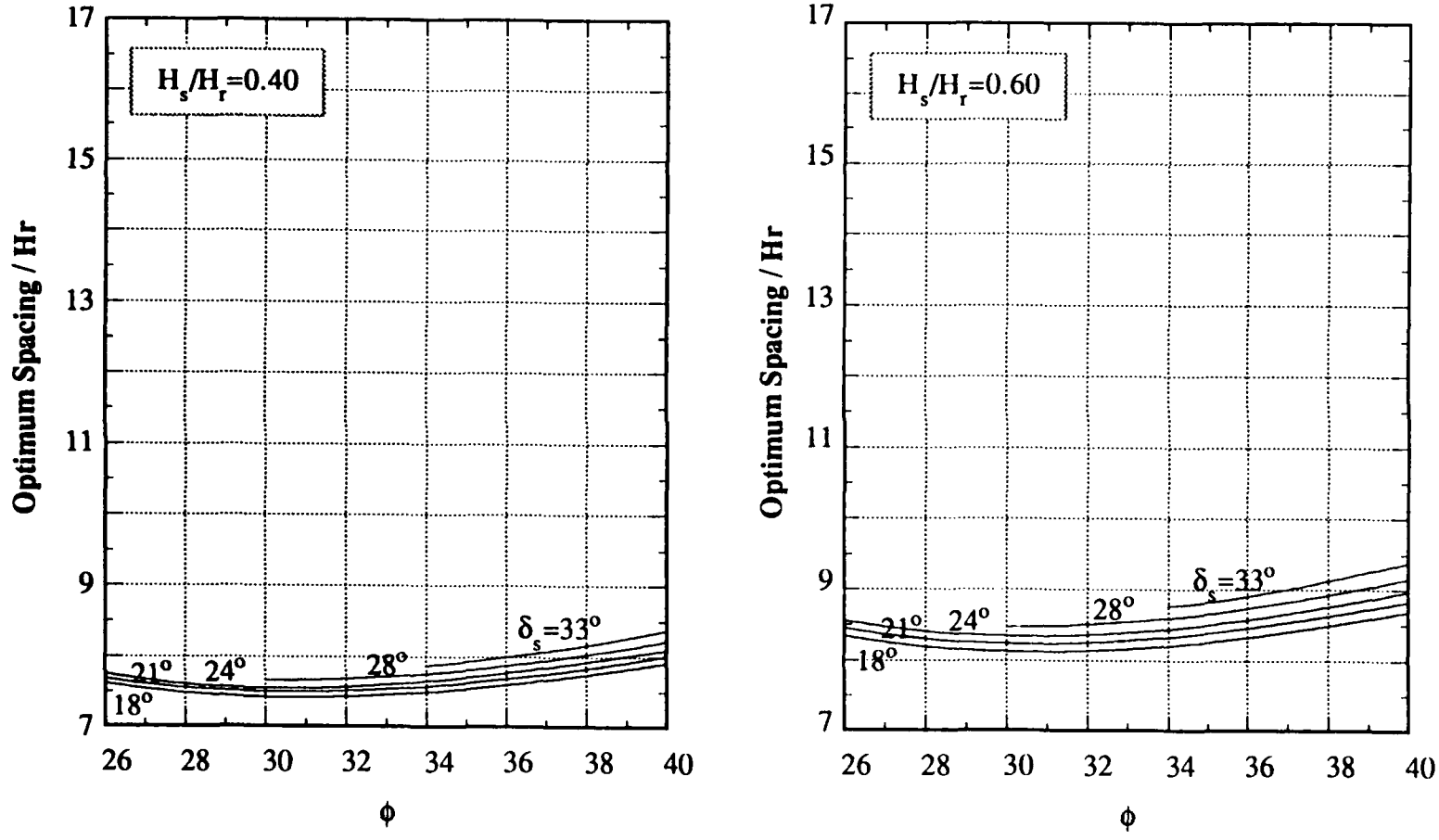

$\delta_r=\delta_b=18^o$

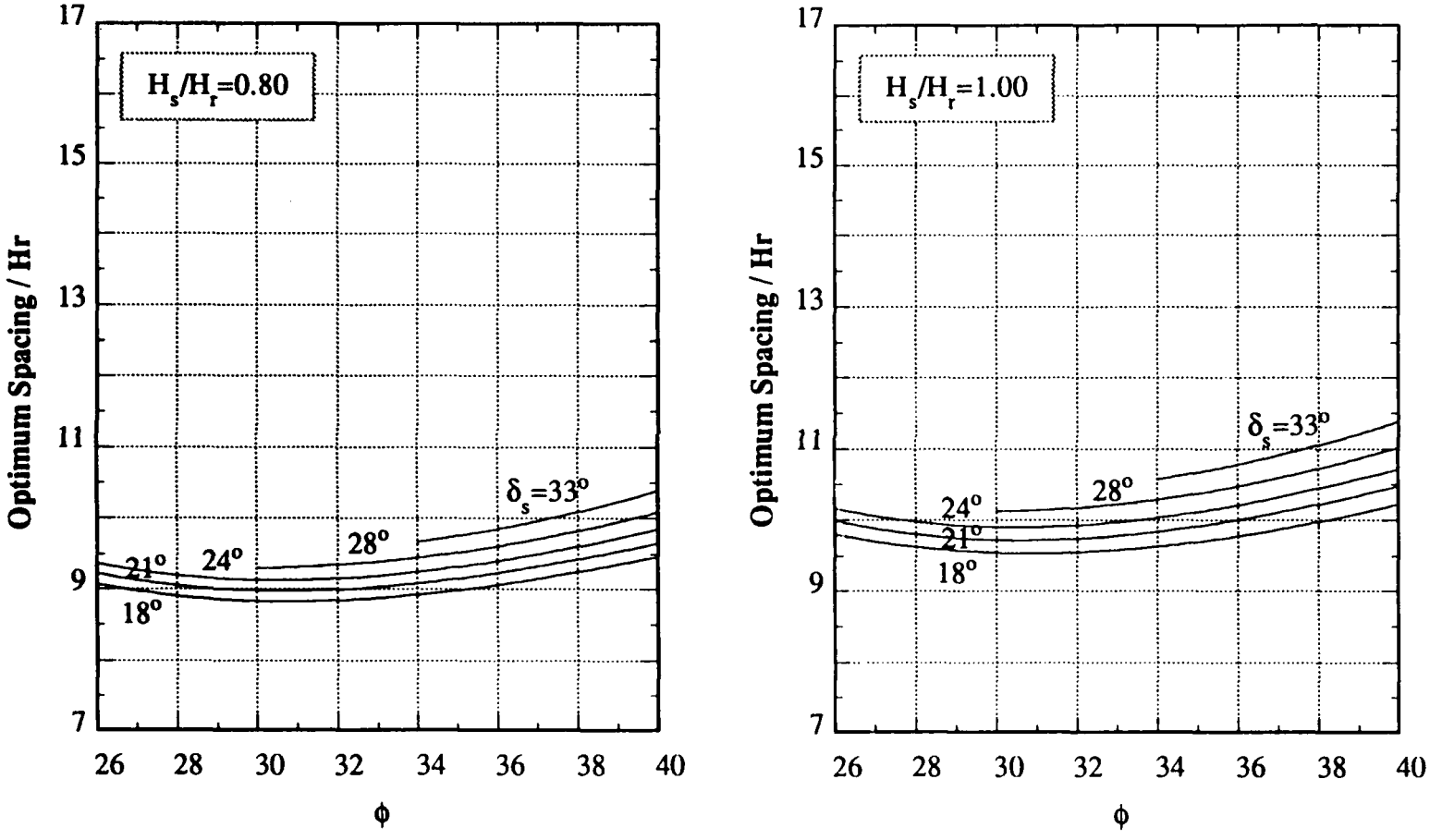

$\delta_r=\delta_b=18^o$

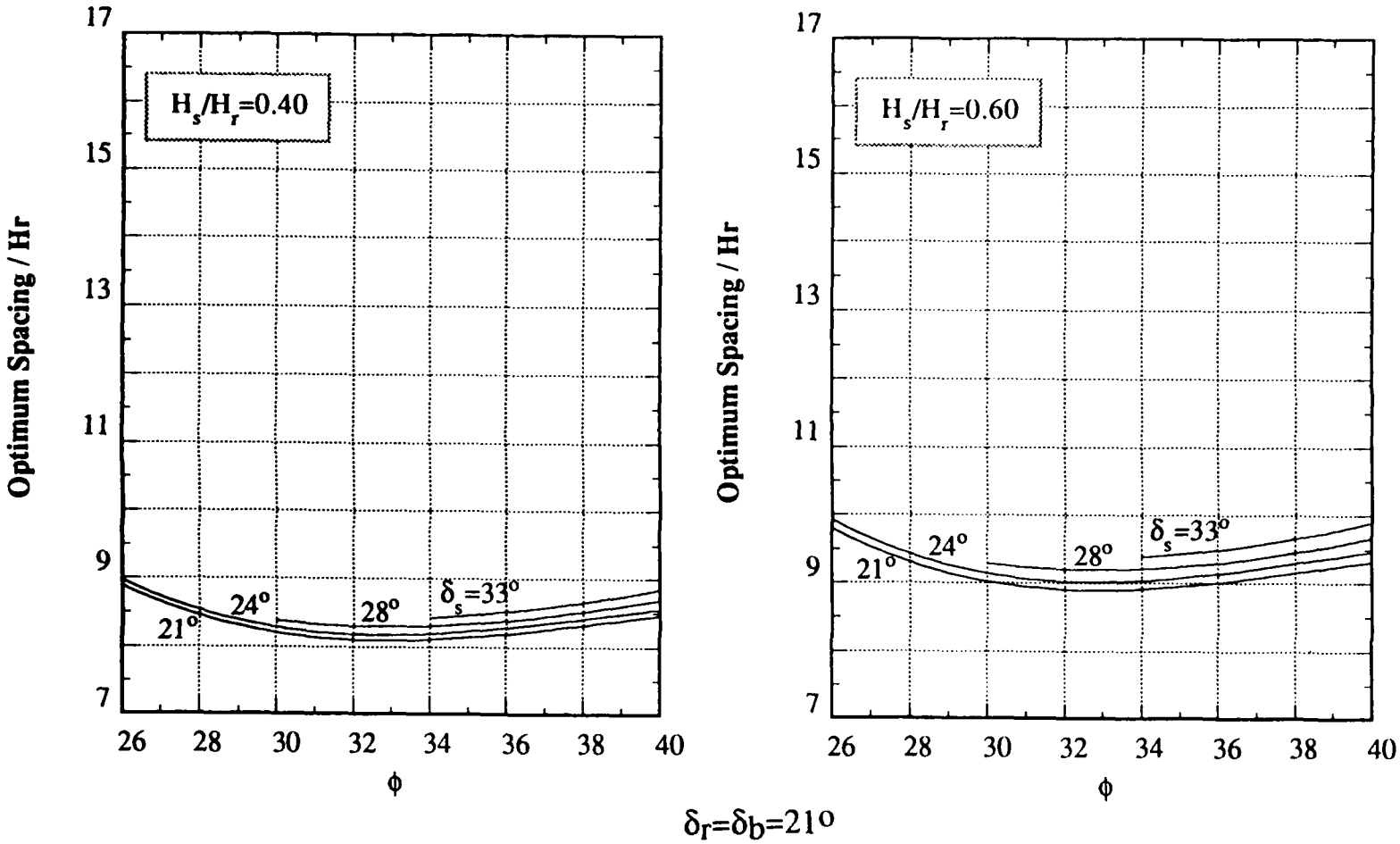

$\delta_r=\delta_b=21^o$

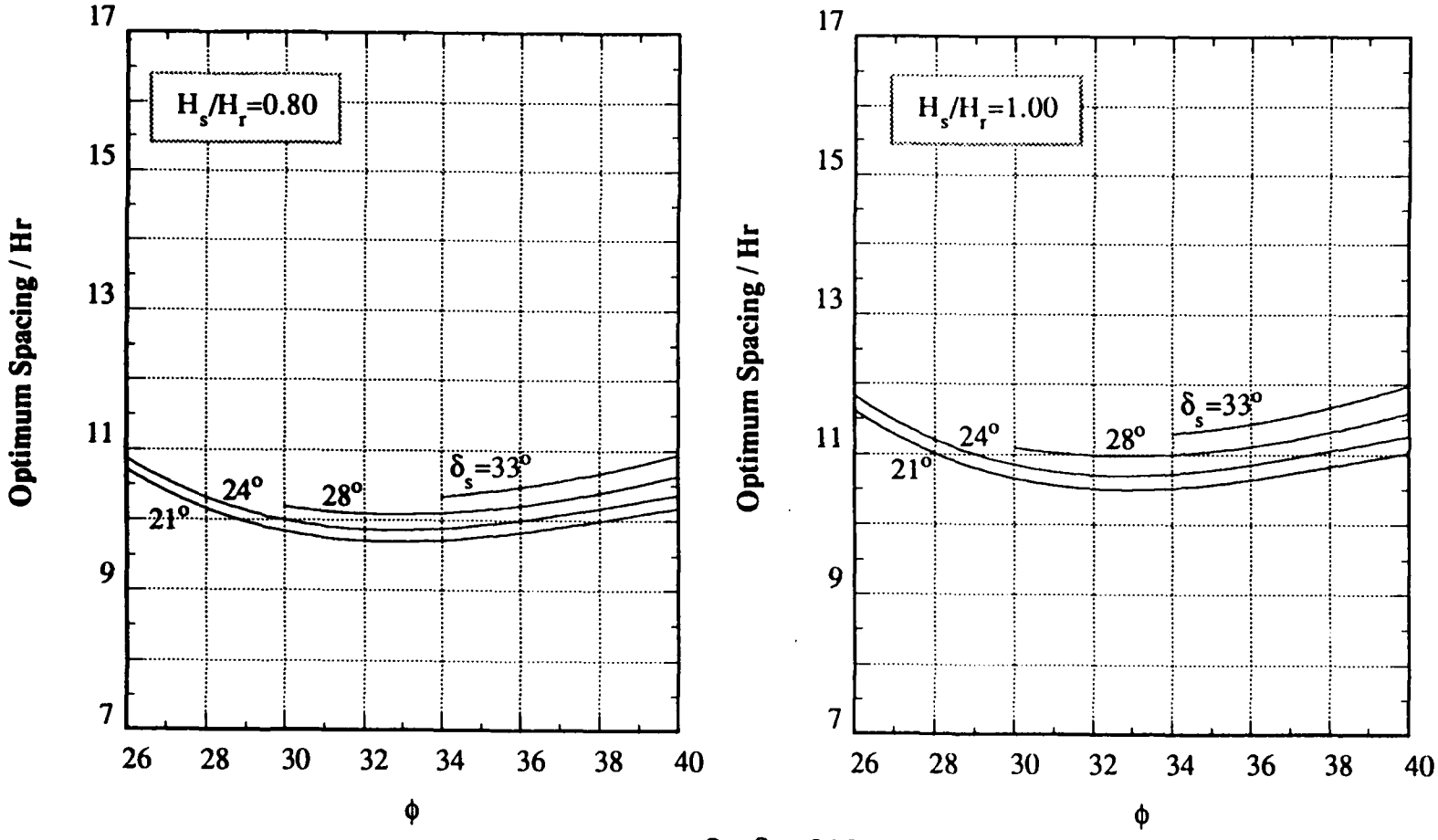

$\delta_r=\delta_b=21^o$

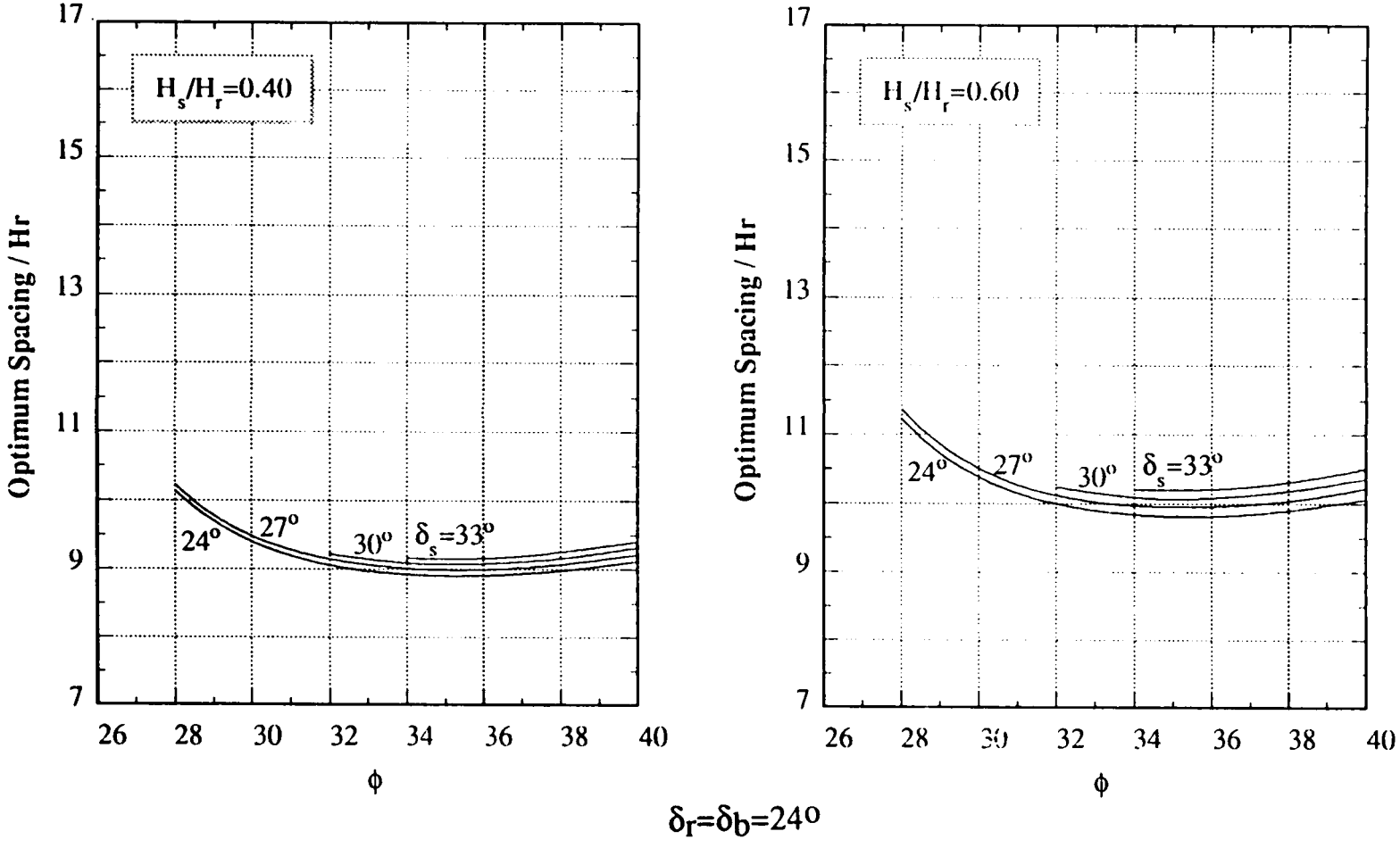

$\delta_r=\delta_b=24^o$

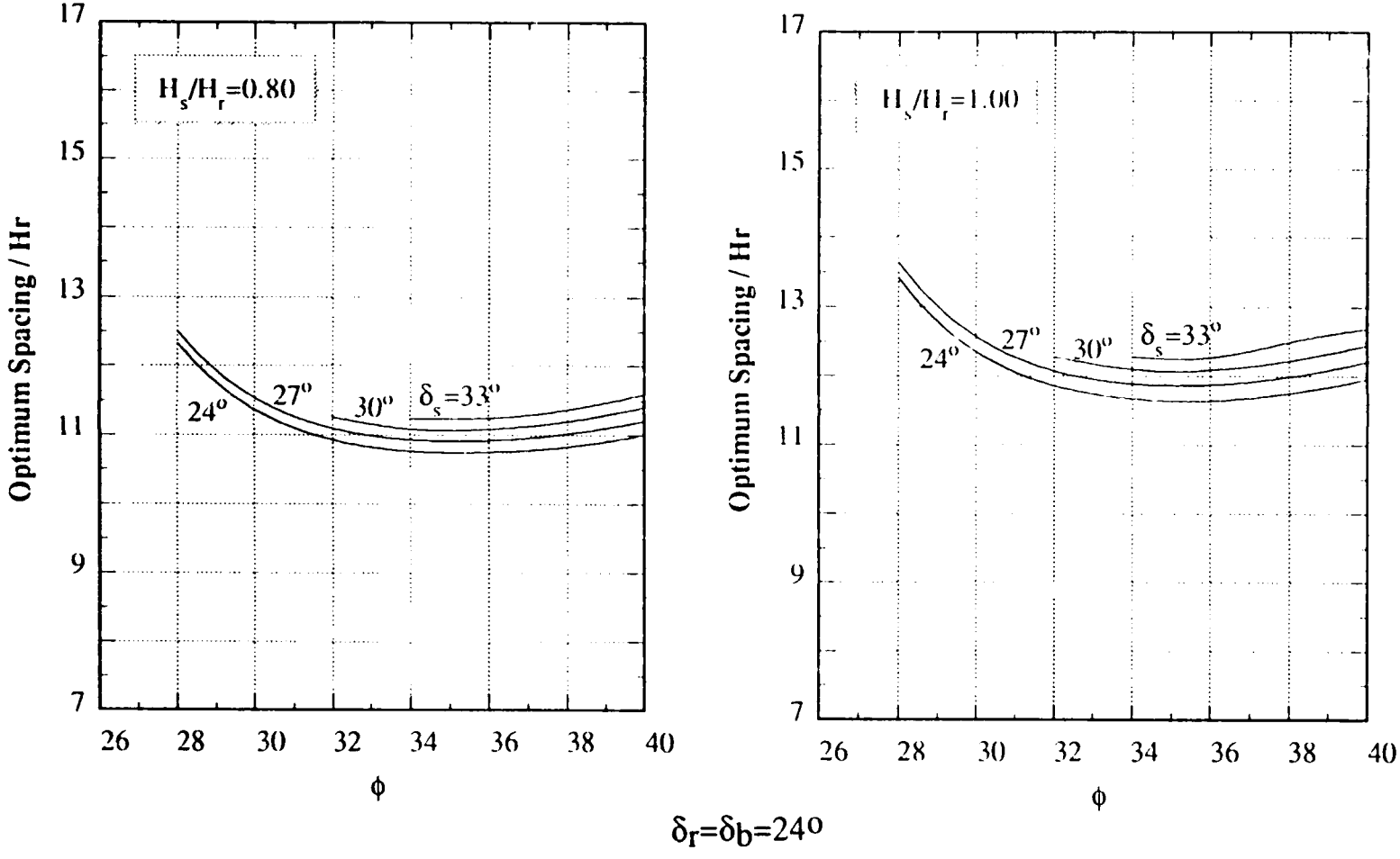

$\delta_r=\delta_b=24^o$

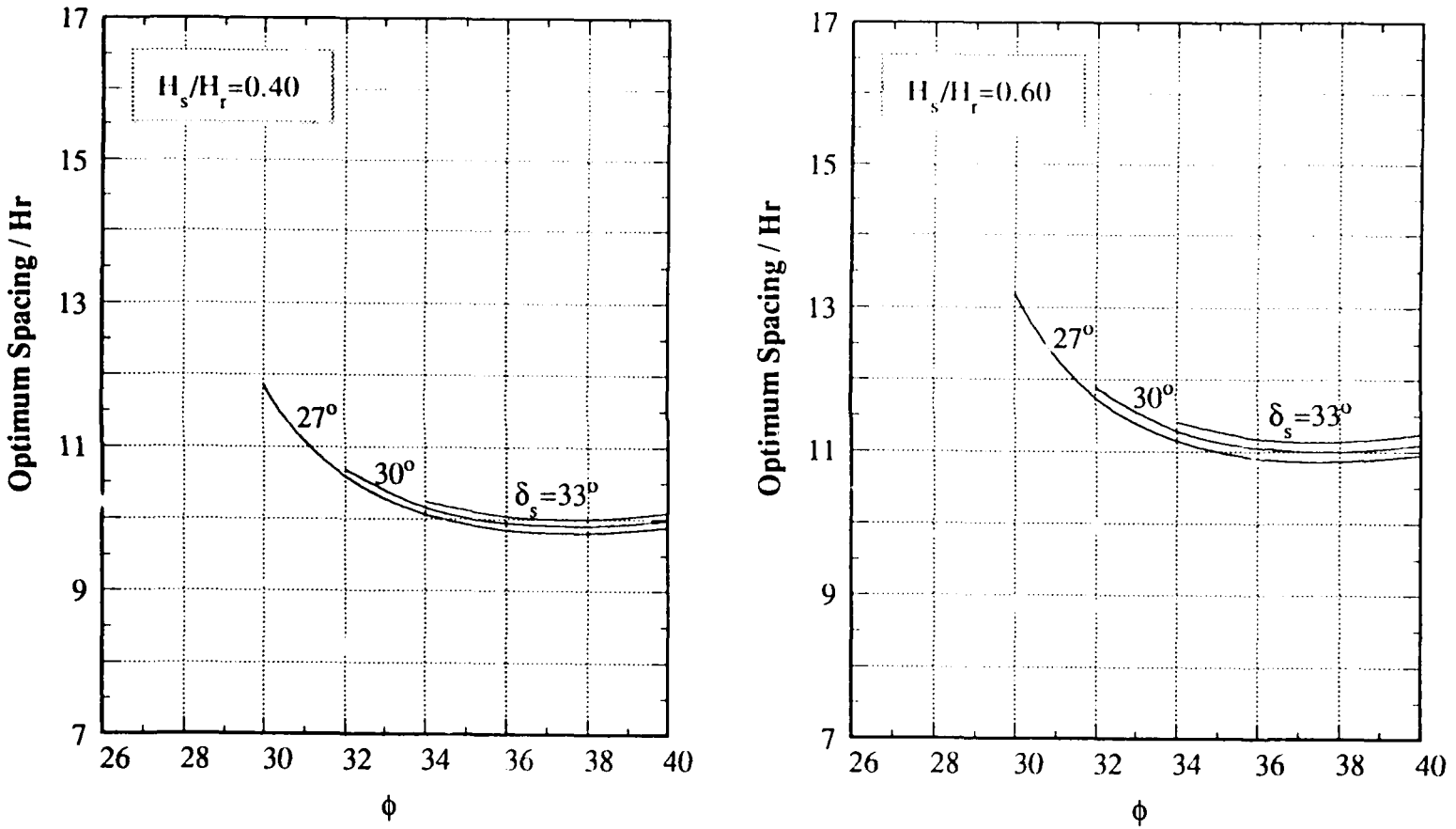

$\delta_r=\delta_b=27°$

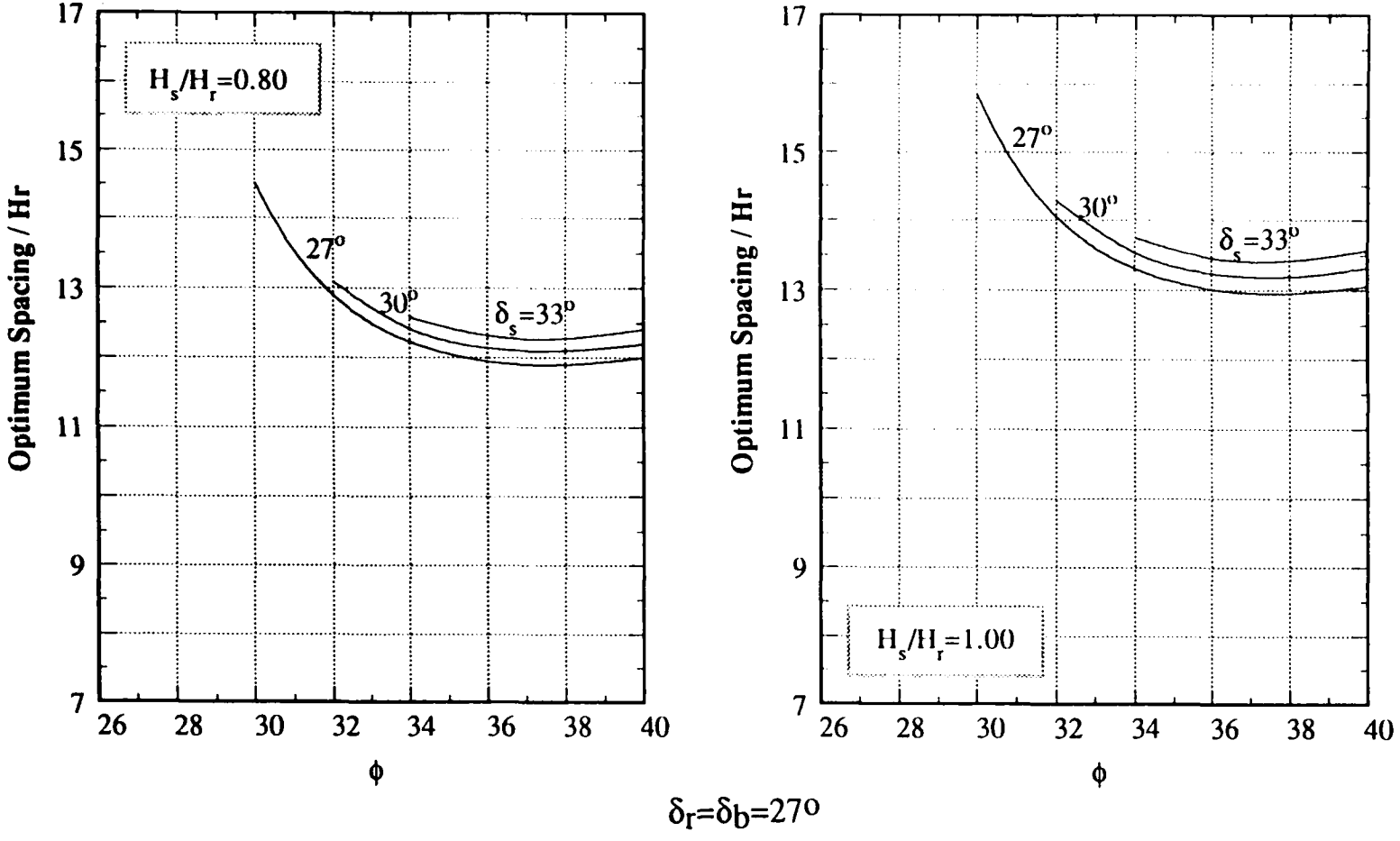

$\delta_r=\delta_b=27^o$